

# Milestone 3.4 Report (In-Situ Measurement of Stress)

Project Title: A Multi-Component Approach to Characterizing In-Situ Stress at the U.S. DOE FORGE EGS Site: Laboratory, Modeling and Field Measurement

## UNIVERSITY OF UTAH SUBAWARD AGREEMENT NO. 10039612-Battelle-2-2439-AF1

Prepared by:  
Battelle  
505 King Avenue  
Columbus, OH 43201-2696

Submitted to:  
University of Utah  
201 Presidents Circle  
Salt Lake City, UT 84112

February 22, 2024

**Technical Point of Contact:**  
Mark Kelley Research Leader  
Battelle, Columbus, OH 43201  
Email: [kelleym@battelle.org](mailto:kelleym@battelle.org)  
Phone: 614-424-3704

**Contractual Point of Contact:**  
Courtney Brooks, Contracts Manager  
Battelle, Columbus, OH 43201  
Email: [brooksc1@battelle.org](mailto:brooksc1@battelle.org)  
Phone: 614-424-5623

### Team Members:

University of Pittsburgh

Authors:

Mark Kelley (Battelle), Samin Raziperchikolaee (Battelle), Fatmir Likrama (Baker Hughes)

Technical Contributors:

Stuart Skopec, Jorge Barrios (Battelle)  
Steve Smith, Greg Schlachter, Umesh Prasad, Agus Tjengdrawira, Javier Franquet, Merouan Foudi, Richard Alt, Sy Rex, Oluwaseun Savage (Baker Hughes)  
Andy Bunger, Guanyi Lu, Ayyaz Mustafa (University of Pittsburgh)

## EXECUTIVE SUMMARY

This report describes the use of minifrac tests conducted in the 16B(78)-32 well at the Utah FORGE site, together with logging data from the well, to characterize subsurface stresses, including the magnitude and orientation of the minimum and maximum horizontal stresses and the magnitude of the vertical stress. This work was conducted under FORGE Research and Development Project 2439 “A Multi-Component Approach to Characterizing In-Situ Stress at the U.S DOE FORGE Enhanced Geothermal System (EGS) Site: Laboratory, Modeling and Field Measurement”.

A minifrac test was conducted at seven different depths in the 9-5/8-inch diameter open (uncased) borehole from June 22 to July 2, 2023. The minifrac tests are described in Section 1 of this document and in a summary report on the field testing which is provided in Appendix A. Geophysical logs, including a resistivity and acoustic image log as well as a dipole-sonic log, were obtained before and after the minifrac tests to provide data to help characterize the stresses. Minifrac tests were conducted using Baker Hughes’ Reservoir Characterization (RCX) straddle-packer tool and logs were obtained using Baker Hughes’ STAR tool (resistivity image log), UXPL tool (formerly CBIL – acoustic image log), and XMAC tool (dipole sonic). Although the aim was to conduct minifrac tests in the vertical section (above the kick-off point at 5,638 ft MD) and also in the deviated section of the uncased borehole, between 5,638 ft and a maximum depth of 9,000 ft MD, using pipe-conveyance (rather than wireline conveyance) to mitigate the risk of stuck tools, all seven minifrac tests were completed in the interval from 5202 ft MD (5201.15 ft TVD) to 5980 ft MD (5966.18 TVD). Furthermore, due to equipment problems encountered in the field, only the baseline logging run (i.e., pre minifrac tests) and the first three minifrac tests (MF-1, MF-2, and MF-3) were conducted using pipe conveyance; all other logging and minifrac testing was conducted using wireline conveyance.

In Section 2 of this document, vertical stress ( $V_s$ ) is estimated from a combination of density-log data obtained from the 16B(78)-32 well (below a depth of ~3900 ft) and density measurements on cutting samples from nearby well 58-32 (for the shallow interval above the density-log). Based on this approach,  $V_s$  was estimated to be ~1.08 psi/ft across the depth interval where the seven minifrac tests were conducted.

A minifrac test provides pressure versus injection-rate data for a series of short-duration injection/shut-in cycles; these data can be analyzed to determine several fracture-related parameters, including breakdown pressure (first cycle only), propagation pressure, instantaneous shut-in pressure, re-opening pressure, and fracture closure pressure. Generally, the minimum horizontal stress ( $Sh_{min}$ ) magnitude is assumed to be equal to the fracture closure pressure. The orientation of an induced fracture observed on an image log obtained after the minifrac test corresponds to the orientation of  $SH_{max}$  and the orientation of  $Sh_{min}$  is assumed to be perpendicular to the orientation of  $SH_{max}$ . Of the seven minifrac tests performed, breakdown was observed in only three tests (MF-2, MF-4, and MF-5) based on the pressure response, and an induced fracture was observed on image logs after the test for only minifrac test MF-2. As described in Section 3 of this document, multiple methods were used to estimate fracture closure pressure, including G-Function analysis, square root of time (SRT) analysis, log-log pressure derivative analysis, instantaneous shut-in pressure, and bi-linear inflection analysis. The ISIP from minifrac test MF-2 (0.6 psi/ft) is considered to be the most representative value of  $Sh_{min}$  magnitude. An “adjustment” to  $Sh_{min}$  magnitude for cooling performed immediately prior to the minifrac tests (necessitated to protect the logging/testing tools from exposure to excessively high temperatures) was estimated to be as large as 0.34 psi/ft with a “mid-range” value of 0.2 psi/ft. If these adjustment factors are added to the unadjusted  $Sh_{min}$  “best” value of 0.6 psi/ft, the resulting  $Sh_{min}$

estimate ranges from 0.6 psi/ft (no adjustment) to 0.94 psi/ft (high adjustment), with a middle value of 0.8 psi/ft.

In Section 4 of this document, the orientation of SHmax is estimated to be approximately 30° based on the orientation of the fracture in the MF-2 test interval and 27° based on the orientation of multiple drilling induced fractures (DIFs) observed on the image logs. In addition, Section 4 describes how the magnitude of SHmax was estimated using the stress polygon method. A range of SHmax values was calculated based on input properties for minifrac tests MF-2 and MF-4 for two tensile strength (T<sub>0</sub>) scenarios (T<sub>0</sub>=0 and T<sub>0</sub>=unconfined compressive strength [UCS] divided by 10) and each of the three derived Shmin values (0.6 psi/ft, 0.8 psi/ft, and 0.94 psi/ft). This analysis provides a broad range of SHmax values. For example, for the Shmin value of 0.6 psi/ft and the two tensile strength scenarios, the range of resulting SHmax values is ~0.6 psi/ft to 0.92 psi/ft for MF-2 and MF-4 combined. For the Shmin value of 0.8 psi/ft, the range of SHmax values is 1.0 psi/ft to 1.5 psi/ft for MF-2 and MF-4 combined, and, for the Shmin value of 0.94 psi/ft, the range of SHmax values is 1.37 psi/ft to 1.9 psi/ft for MF-2 and MF-4 combined. It was possible to constrain this range using estimated value(s) of T<sub>0</sub> from the MF-2 and MF-4 test data. Specifically, the difference between breakdown pressure in the first cycle and re-opening pressure in second cycle is an estimate of T<sub>0</sub>. This value is small (less than 200 psi in MF-2 and less than 50 psi in MF-4). As a result, the tensile scenario of T<sub>0</sub>=0 is probably more appropriate than T<sub>0</sub>=UCS/10. Taking advantage of a known T<sub>0</sub> leads to a better constrained SHmax. The SHmax value, assuming T<sub>0</sub>=0, is ~0.6 psi/ft for MF-2 and MF-4 combined. For the Shmin of 0.8 psi/ft, the range of SHmax values is 1.0 psi/ft to 1.11 psi/ft for MF-2 and MF-4 combined. For the Shmin of 0.94 psi/ft, the range of SHmax values is 1.37 psi/ft to 1.5 psi/ft for MF-2 and MF-4 combined.

A similar analysis of SHmax was done based on DIFs in the vertical section of the borehole rather than properties of MF-2 and MF-4. The analysis provides a similar broad range of SHmax values. For Shmin of 0.6 psi/ft., SHmax ranges from 0.68 psi/ft to 1.47 psi/ft. For Shmin of 0.8 psi/ft., SHmax ranges from 1.15 to 1.99 psi/ft. And, for Shmin of 0.94 psi/ft, SHmax ranges from 1.45 to 2.43 psi/ft. The SHmax values estimated from the DIFs using the polygon method are likely to have greater uncertainty compared to the SHmax values estimated from the minifrac tests (MF-2 and MF-4) because of uncertainty in the amount of cooling during drilling, the tensile strength of the rock, and uncertainty in the Shmin magnitude.

Another objective of this study was to assess the stresses as a function of depth. In Section 5 of this document, Shmin and SHmax calculated at discrete depths where DIFs were observed were used to develop a “continuous” depth profile (i.e., curves) of Shmin and SHmax values for the 16B(78)-32 well using two methods: an effective stress ratio (ESR) method and a poroelastic (stress contrast) method. Based on the relative magnitude of the Shmin, SHmax, and Sv curves, the stress regime could be Normal (Sv>SHmax>Shmin) or strike-slip (SHmax>Sv>Shmin).

In Section 6 of this document, four topics are discussed in more detail, including (1) stress regime, (2) analysis of flowback data, (3) re-opening pressure, and (4) pressure response during the minifrac tests. All four subjects are directly related to the primary objective(s) of this study (i.e., characterizing stresses and stress regime, and finding the best method and station to estimate Shmin). The analysis of stress regime attempts to determine the stress regime by predicting (using stress modeling) the location around the wellbore (i.e., top, bottom, sides) where tensile fractures and shear fractures along weak planes are most likely to form in a normal stress regime and a strike slip stress regime and comparing these predictions to the actual location of induced tensile and shear fractures observed on image logs to infer the stress regime. This analysis indicates that the strike slip regime is more likely than the normal stress. It should be noted that this analysis is only valid in deviated sections of wellbore.

An analysis of flowback data was performed for three minifrac tests to estimate fracture closure pressure. The estimated fracture closure pressure determined with the flowback analysis method for the three tests (MF-1 cycle 1, MF-5 cycle 1, and MF-6 cycle 1) was lower than the fracture closure pressure estimated during the fall-off period (specifically ISIP).

Determining fracture re-opening pressure is essential to ensure an induced fracture is opened after first cycle and fracture closure estimated after re-opening is reliable. Plotting pressure versus cumulative injected fluid volume was done to ensure fracture re-opening occurred and for estimating fracture re-opening pressure for minifrac tests MF-2, MF-4, MF-5, and MF-6.

The discussion of pressure response identifies challenges during the minifrac tests for the 16B(78)-32. It also explains why the ISIP from minifrac test MF-2 is considered to be the most reliable estimate of  $Sh_{min}$ . In addition, a comparison of  $Sh_{min}$  values estimated in this study and previous studies for the FORGE site is provided.

## ACRONYM LIST

BH	Baker Hughes
DFIT	diagnostic fracture injection test
DIF	drilling induced tensile fracture
EGS	enhanced geothermal system
ESR	effective stress ratio
FBP	fracture breakdown pressure
FCP	fracture closure pressure
FORGE	Frontier Observatory for Research in Geothermal Energy
FPP	fracture propagation pressure
FRP	fracture re-opening pressure
GR	gamma ray
HF	hydraulic fracturing
ISIP	instantaneous shut-in pressure
MD	measured depth
ORIT	orientation tool
PCL	pipe-conveyed logging
RCI/RCX	Baker Hughes Reservoir Characterization Instrument/ Reservoir Characterization Explorer (straddle packer tool)
SFIB	Baker Hughes Stress and Failure of Inclined Boreholes software
SHmax	maximum horizontal stress
Shmin	minimum horizontal stress
SLV/ SLVP	Baker Hughes Sleeve Fracture Packer
SRT	square root of time
STAR	Baker Hughes resistivity imaging tool
Sv	vertical stress
TUV	triaxial stress ultrasonic velocity
TVD	total vertical depth
UCS	unconfined compressive strength

# TABLE OF CONTENTS

Executive Summary.....	i
Acronym List .....	iv
Table of Contents.....	v
1 Introduction .....	1-1
1.1 Objective .....	1-1
1.2 Scope.....	1-1
1.3 Methods.....	1-1
1.3.1 Minifrac Method for Determining Minimum Horizontal Stress (Shmin) .....	1-1
1.3.2 Minifrac Testing Program .....	1-4
2 Vertical Stress .....	2-1
3 Minimum Horizontal Stress (Shmin) Determined from Minifrac Tests.....	3-1
3.1 MF-1.....	3-1
3.2 MF-2.....	3-6
3.3 MF-3.....	3-11
3.4 MF-4.....	3-16
3.5 MF-5.....	3-22
3.6 MF-6.....	3-26
3.7 MF-7.....	3-30
3.8 Summary of Shmin Magnitude .....	3-34
3.8.1 Summary of Mini-frac Test Results .....	3-34
(a). cycles 3 and 4 of MF-3 were rebound tests.....	3-37
3.8.2 Shmin Magnitude Adjusted for Cooling during Minifrac Testing.....	3-38
3.8.3 Shmin Results with Temperature Adjustment for Cooling prior to Testing .....	3-44
4 Maximum Horizontal Stress.....	4-1
4.1 SHmax Azimuth from Minifrac Tests .....	4-1
4.2 SHmax Azimuth from Drilling Induced Fractures.....	4-2
4.3 SHmax Magnitude from Minifrac Tests MF-2 and MF-4 .....	4-3
4.4 SHmax Magnitude from Drilling Induced Fractures Using the Stress Polygon Method .....	4-10
4.5 Summary SHmax Magnitude Calculated from Drilling Induced Fractures .....	4-18
4.6 Verification of SHmax Magnitude Values from Stress Polygon .....	4-18
5 Calculating Shmin and SHMAX depth profiles .....	5-1

6	Discussion (Supplemental Analyses).....	6-1
6.1	Stress Regime.....	6-1
6.1.1	Tensile Failure Modeling .....	6-1
6.1.2	Shear Failure Modeling .....	6-7
6.1.3	Stress Regime Summary .....	6-12
6.2	Flowback Analysis for Estimating Fracture Closure Pressure .....	6-12
6.2.1	Flowback Analysis for Minifrac Tests Conducted in This Study.....	6-14
6.2.2	Flowback Summary.....	6-19
6.3	Re-opening Pressure Estimation with Pressure versus Injected Volume Plots .....	6-19
6.3.1	Re-Opening Pressure Results .....	6-20
6.3.2	Re-Opening Pressure Summary .....	6-23
6.4	Observations Regarding Pressure Behavior during Minifrac Tests.....	6-23
7	REFERENCES.....	7-1

## FIGURES

Figure 1-1	Example minifrac test for a permeable limestone; from Baker Hughes. Fracture closure pressure (not labeled) will occur along the fall-off pressure curve. ....	1-2
Figure 1-2.	Example minifrac test in an impermeable shale formation. Fracture closure pressure (not labeled) will occur along the fall-off pressure curve. Note flowback pumping technique was used to close the fracture due to very slow pressure fall-off after shut-in. ....	1-3
Figure 2-1.	Overburden (Vertical) Stress Gradient (Track 4) estimated using two methods: one method (pink curve in track 4) uses a combination of density log data for the 16B(78)-32 well (below 3890 ft) and matrix measurements made on cuttings from the 58-32 well (above 3890 ft); the other method (green curve in track 4) uses density-log data from 16B(78)-32 well below 3890 ft and extrapolation of the density-log curve above 3890 ft. ....	2-2
Figure 2-2.	Calculated bulk density of cuttings samples for the 58-32 well. Points above 3890.5 ft were used to construct the Sv curve.....	2-2
Figure 3-1.	Pressure and injection rate for both cycles of MF-1.....	3-2
Figure 3-2.	Data analysis plots for cycle 1 of MF-1. ....	3-3
Figure 3-3.	Data analysis plots for cycle 2 of MF-1. ....	3-4
Figure 3-4.	Bi-linear analysis for cycles 1 and 2 of MF-1, which yielded a FCP (ISIP) of 4526 psi (0.8 psi/ft) and 4423 psi (0.78 psi/ft), respectively. ....	3-5
Figure 3-5.	Pressure and injection rate plot for the three cycles of MF-2. ....	3-6
Figure 3-6.	G-Function plot (top left), SRT analysis (top right), ISIP (bottom left), derivative plot (bottom right) for MF-2 cycle 1.....	3-7
Figure 3-7.	G-Function plot (top left), SRT analysis (top right), ISIP (bottom left), derivative plot (bottom right) for MF-2 cycle 2.....	3-8
Figure 3-8.	G-Function plot (top left), SRT plot (top right), ISIP (bottom left), derivative plot (bottom right) for MF-2 cycle 3.....	3-9

Figure 3-9.	Bi-linear plots for cycles 1, 2 and 3 for MF-2, which yielded a FCP (ISIP) of 3288 psi (0.6 psi/ft), 3237 psi (0.59 psi/ft), and 3323 psi (0.6 psi/ft), respectively.....	3-10
Figure 3-10.	Pressure rate plot for the four cycles of Station MF-4.....	3-12
Figure 3-11.	G-Function plot (top left), SRT analysis (top right), ISIP (bottom left), derivative plot (bottom right) for cycle 1.....	3-13
Figure 3-12.	G-Function plot (top left), SRT analysis (top right), ISIP (bottom left), derivative plot (bottom right) for cycle 2 OF MF-3.....	3-14
Figure 3-13.	Bi-linear analysis for cycle 1 (top) and cycle 2 (bottom) of MF-3, which yielded a FCP (ISIP) of 2745 psi (0.5 psi/ft) and 2853 psi (0.53 psi/ft) for cycles 1 and 2, respectively.....	3-15
Figure 3-14.	Pressure rate plot for the 3 cycles of MF-4.....	3-17
Figure 3-15.	G-Function plot (top left), SRT analysis (top right), ISIP (bottom left), derivative plot (bottom right) for MF-4 cycle 1.....	3-18
Figure 3-16.	G-Function plot (top left), SRT analysis (top right), ISIP (bottom left), derivative plot (bottom right) for MF-4 cycle 2.....	3-19
Figure 3-17.	G-Function plot (top left), SRT analysis (top right), ISIP (bottom left), derivative plot (bottom right) for MF-4 cycle 3.....	3-20
Figure 3-18.	Bi-linear analysis for cycle 1 (top left), cycle 2 (top right), and cycle 3 (bottom) of MF-4, which yielded a FCP (ISIP) of 3315 psi (0.56 psi/ft), 3568 psi (0.6 psi/ft), and 3556 psi (0.6 psi/ft), respectively.....	3-21
Figure 3-19.	Pressure rate plot for the four cycles of Station MF-5.....	3-22
Figure 3-20.	G-Function plot (top left), SRT analysis (top right), ISIP (bottom left), derivative plot (bottom right) for MF-5 cycle 1.....	3-23
Figure 3-21.	G-Function plot (top left), SRT analysis (top right), ISIP (bottom left), derivative plot (bottom right) for MF-5 cycle 2.....	3-24
Figure 3-22.	Bi-linear analysis for cycle 1 (top) and cycle 2 (bottom) of MF-5, which yielded a FCP (ISIP) of 3250 psi (0.55 psi/ft) for cycle 1. A FCP could not be determined for cycle 2 using the bi-linear method.....	3-25
Figure 3-23.	Pressure rate plot for the three cycles of MF-6.....	3-26
Figure 3-24.	G-Function plot (top left), SRT analysis (top right), ISIP (bottom left), derivative plot (bottom right) for cycle 1 of MF-6.....	3-27
Figure 3-25.	G-Function plot (top left), SRT analysis (top right), ISIP (bottom left), derivative plot (bottom right) for cycle 3 of MF-6.....	3-28
Figure 3-26.	Bi-linear analysis for cycle 1 (top) and cycle 3 (bottom) of MF-6, which yielded a FCP (ISIP) of 3473 psi (0.62 psi/ft) and 3405 psi (0.6 psi/ft) for cycle 2.....	3-29
Figure 3-27.	Pressure rate plot for the three cycles of MF-7.....	3-30
Figure 3-28.	G-Function plot (top left), SRT analysis (top right), ISIP (bottom left), derivative plot (bottom right) for cycle 1 of MF-7.....	3-31
Figure 3-29.	G-Function plot (top left), SRT analysis (top right), ISIP (bottom left), derivative plot (bottom right) for cycle 2 of MF-7.....	3-32
Figure 3-30.	G-Function plot (top left), SRT analysis (top right), ISIP (bottom left), derivative plot (bottom right) for cycle 3 of MF-7.....	3-33
Figure 3-31.	Bi-linear analysis for cycle 1 (top left), cycle 2 (top right), and cycle 3 (bottom) of MF-7.....	3-34
Figure 3-32.	Modeled temperature profile at multiple depths in run 1 (top) and run 2 (bottom). Note that 0.4 ft is distance from borehole center to borehole wall.....	3-40

Figure 3-33.	Gamma ray profile, dynamic and static Young's modulus, Poisson ratio, Internal friction coefficient, unconfined compressive strength profile for well 16B(78)-32. ....	3-41
Figure 3-34.	Image log after hydraulic fracture in Station MF-2 showing induced fractures, and presence of foliations in the test interval. ....	3-44
Figure 4-1.	Image logs of minifrac test Station MF-2 before and after minifrac test (STAR and CBIL[UXPL] are Baker image logs; FMI and UBI are Schlumberger image logs. The STAR image after the minifrac test shows a stick and pull; therefore, affected portion of STAR image has limited usefulness for interpreting features. ....	4-1
Figure 4-2.	Image log for interval 4844 to 6155 ft showing orientation of DIFs, foliation features, and natural fractures. ....	4-2
Figure 4-3.	Image log for interval 6155 to 8200 ft showing several DIFs (indicated by blue horizontal lines/rectangles in track 5 from the left). ....	4-3
Figure 4-4.	Stress Polygon for Determining SHmax magnitude for MF-2 at 5966 ft TVD for Shmin=0.6 psi/ft and two tensile strength scenarios ( $T_0=0$ and $T_0=UCS/10=2000$ psi). This analysis assumes differential drilling mud temperature of $-70^\circ\text{F}$ relative to the ambient formation temperature).....	4-4
Figure 4-5.	Stress Polygon for Determining SHmax magnitude for MF-2 at 5495 ft TVD for Shmin=0.8 psi/ft and two tensile strength scenarios ( $T_0=0$ and $T_0=UCS/10=2000$ psi). This analysis assumes a differential drilling mud temperature of $-70^\circ\text{F}$ relative to the ambient formation temperature).....	4-5
Figure 4-6.	Stress Polygon for Determining SHmax magnitude for MF-2 at 5495 ft TVD for Shmin=0.94 psi/ft and two tensile strength scenarios ( $T_0=0$ and $T_0=UCS/10=2000$ psi). This analysis assumes a differential drilling mud temperature of $-70^\circ\text{F}$ relative to the ambient formation temperature). ....	4-6
Figure 4-7.	Stress Polygon for Determining SHmax magnitude for MF-4 at 5966 ft TVD for Shmin=0.6 psi/ft and two tensile strength scenarios ( $T_0=0$ and $T_0=UCS/10=2000$ psi). This analysis assumes a differential drilling mud temperature of $-59^\circ\text{F}$ relative to the ambient formation temperature).....	4-7
Figure 4-8.	Stress Polygon for Determining SHmax magnitude for MF-4 at 5966 ft TVD for Shmin=0.8 psi/ft and two tensile strength scenarios ( $T_0=0$ and $T_0=UCS/10=2000$ psi). This analysis assumes a differential drilling mud temperature of $-59^\circ\text{F}$ relative to the ambient formation temperature).....	4-8
Figure 4-9.	Stress Polygon for Determining SHmax magnitude for MF-4 at 5966 ft TVD for Shmin=0.94 psi/ft and two tensile strength scenarios ( $T_0=0$ and $T_0=UCS/10=2000$ psi). This analysis assumes a differential drilling mud temperature of $-59^\circ\text{F}$ relative to the ambient formation temperature). ....	4-9
Figure 4-10.	Bottom hole pressure (red) during MF-2 showing tensile strength estimate. ....	4-9
Figure 4-11.	Bottom hole pressure (red) during MF-4 showing tensile strength estimate. ....	4-10
Figure 4-12.	DIFs identified on STAR and CBIL (UXPL) image logs (highlighted with blue rectangles).....	4-11
Figure 4-13.	Calculated SHmax values (shown as green and blue diamonds in track 8) for Shmin=0.8 psi/ft and the two tensile strength scenarios and values of key input parameters used to calculate SHmax. In track 8, the blue diamonds assume the tensile strength is equal to the UCS/10; whereas, the green diamonds assume the tensile strength is equal to zero. ....	4-12

Figure 4-14.	Calculated SHmax values (shown as green and blue diamonds in track 8) for Shmin=0.6 psi/ft and the two Tensile strength scenarios and values of key input parameters used to calculate SHmax. In track 8, the blue diamonds assume the tensile strength is equal to the UCS/10; whereas, the green diamonds assume the tensile strength is equal to zero. ....4-13	4-13
Figure 4-15.	Calculated SHmax values (shown as green and blue diamonds in track 8) for Shmin=0.94 psi/ft and the two Tensile strength scenarios and values of key input parameters used to calculate SHmax. In track 8, the blue diamonds assume the tensile strength is equal to the UCS/10; whereas, the green diamonds assume the tensile strength is equal to zero .....4-14	4-14
Figure 5-1.	A set of Shmin and SHmax curves are presented with Shmin calibrated to the non-temp adjusted closure pressures from the P-inflection method for Stations MF-2 and MF-4. The continuous blue Shmin curve was constructed using an ESR of 0.3 in the shallower section and 0.43 in the deeper section to match the trend of the Poroelastic (green) curve and to honor the DFIT closure pressures from well 58-32 (shown by red dots). The black dots indicate the SHmax magnitudes calculated from DIFs given an Shmin magnitude of 0.6 psi/ft and assuming cooling during drilling. ....5-2	5-2
Figure 5-2.	A different set of Shmin and SHmax depth curves are presented with Shmin being calibrated to only the temp adjusted (using the high end temperature adjustment) closure pressure from P-inflection method in Stations MF-2 and MF-4. The black dots indicate the SHmax magnitudes from the stress polygon analysis of DIFs given an Shmin magnitude of 0.94 psi/ft and assuming cooling during drilling. The resultant stress regime is strike slip. This scenario is considered less likely as the modeled wellbore failures do not match observations. ....5-3	5-3
Figure 5-3.	Shmin and SHmax depth curves with Shmin being calibrated to only the temp adjusted (using the mid value temperature adjustment) to closure pressure from P-inflection method in Stations MF-2 and MF-4. The black dots indicate the SHmax magnitudes from the stress polygon analysis of DIFs given an Shmin magnitude of 0.8 psi/ft and assuming cooling during drilling. ....5-3	5-3
Figure 6-1.	Predicted DIF location in deviated borehole for normal stress regime. White lines represent the DIF. DIF is likely to occur predominantly at the top and bottom (0 and 180°).....6-2	6-2
Figure 6-2.	Predicted DIF location in deviated borehole for strike slip stress regime. White lines represent the DIFs. DIF are likely to occur predominantly on the sides (90 and 270°) of the borehole. ....6-3	6-3
Figure 6-3.	Image log for depth interval 7086 to 7101 ft of well 16B(78)-32, which is in the deviated section (inclination = 68°). Blue boxes show DIFs. All blue boxes are located on sides of the borehole. ....6-4	6-4
Figure 6-4.	Image log for depth interval 7141 to 7155 ft of well 16B(78)-32, which is in the deviated section (inclination = 68°). Blue boxes show DIFs. All blue boxes are located on sides of the borehole. ....6-5	6-5
Figure 6-5.	Image log for depth interval 7729 to 7741 ft of well 16B(78)-32, which is in the deviated section (inclination = 69°). Blue boxes show DIFs. All blue boxes are located on sides of the borehole. ....6-6	6-6

Figure 6-6.	Predicted location of shear failure of a weak plane in a normal stress regime. Shear failure of a weak plane is likely to occur on the sides (90 and 270°) of the borehole in a normal regime.....	6-8
Figure 6-7.	Predicted location of shear failure of a weak plane in a strike slip stress regime. Shear failure of a weak plane is likely to occur closer to the top and bottom) of the borehole in a strike slip regime. ....	6-9
Figure 6-8.	Image log of depth interval 7047 to 7062 ft in the 16B(78)-32 well. Blue boxes show rock shear failure along weak plane. Blue boxes are located on top/bottom of borehole. Pink curves show foliation locations. Note: additional foliations probably existed above/below two examples in image log ones (which is not depicted,) and weak bedding plane shear failure above two example foliations overlaying on them.....	6-10
Figure 6-9.	Image log of depth interval 6967 to 6981 f ft in the 16B(78)-32 borehole. Blue boxes show rock shear failure along weak plane. Blue boxes are located on top/bottom of borehole. Pink curves show foliation locations. ....	6-11
Figure 6-10.	A diagnostic plot of the flowback test showing characteristic increasingly negative slope (Savitski and Dudley, 2011). ....	6-13
Figure 6-11.	Pressure versus flowback volume curve for cycle 1 of Station MF-1.....	6-15
Figure 6-12.	Pressure and flowback rate versus time for cycle 1 of Station MF-1.....	6-15
Figure 6-13.	Pressure versus flowback volume curve for cycle 1 of Station MF-5.....	6-16
Figure 6-14.	Pressure and flowback rate versus time for cycle 1 of Station MF-5.....	6-17
Figure 6-15.	Pressure versus flowback volume curve for cycle 1 of Station MF-6.....	6-18
Figure 6-16.	Pressure and flowback rate versus time for cycle 1 of Station MF-6.....	6-18
Figure 6-17.	Pressure versus injected volume for repeat cycle 2 of Station MF-1.....	6-20
Figure 6-18.	Pressure versus injected volume for repeat cycles 2 and 3 of Station MF-2. ....	6-20
Figure 6-19.	Pressure versus injected volume for repeat cycle 2 of Station MF-3.....	6-21
Figure 6-20.	Pressure versus injected volume for recycles of Station MF-4. ....	6-21
Figure 6-21.	Pressure versus injected volume for repeat cycle 2 of Station MF-5.....	6-22
Figure 6-22.	Pressure versus injected volume for cycle 2 of Station MF-6. ....	6-22
Figure 6-23.	Pressure versus injected volume for recycles of Station MF-7. ....	6-23
Figure 6-24.	Constant injection rate in multiple cycles of Station MF-2. ....	6-24
Figure 6-25.	Example of pressure increase in cycle 2 compared to cycle 1 of Station MF- 3. ....	6-25
Figure 6-26.	Possible conductive natural fracture in the Station MF-1 test interval (shown by blue line at ~5655 to 5657 ft). ....	6-27
Figure 6-27.	Station MF-1 pressure time record (no indication of breakdown), possibly due to the presence of fractures. ....	6-28
Figure 6-28.	Presence of foliations in Station MF-3 interval (shown by square symbol on a stick in Track 5).....	6-29
Figure 6-29.	G-Function plot showing multiple humps for cycle 2 of Station MF-2. ....	6-30
Figure 6-30.	G-Function plot showing multiple humps for cycle 1 of Station MF-3). ....	6-30
Figure 6-31.	Comparison of the Tangent and Compliance methods for estimating fracture closure pressure on a G-Function plot (Broker and Ma, 2022). ....	6-31
Figure 6-32.	G-Function plot for MF-2 cycle 3. ....	6-32
Figure 6-33.	G-Function plot for MF-1 cycle 1. ....	6-32
Figure 6-34.	G-Function plot for MF-3 cycle 1. ....	6-33

## TABLES

Table 1-1.	Baker Hughes Logging tool strings used to conduct the minifrac testing program. ....	1-4
Table 1-2.	Minifrac test depths in the 16B(78)-32 well .....	1-5
Table 1-3.	Summary of circulation (cooling) events, logging runs, and minifrac (RCX) tool string deployments. ....	1-5
Table 1-4.	Summary of minifrac test parameters .....	1-6
Table 3-1.	Summary table for MF-1 analyses. ....	3-5
Table 3-2.	Summary table for MF-2 analyses. ....	3-11
Table 3-3.	Summary of MF-3 analyses. ....	3-16
Table 3-4.	Summary of MF-4 analyses. ....	3-21
Table 3-5.	Summary of MF-5 analyses. ....	3-25
Table 3-6.	Summary of MF-6 analyses. ....	3-29
Table 3-7.	Summary of MF-7 analyses. ....	3-34
Table 3-8.	Summary of mini-frac test analysis parameters. ....	3-36
Table 3-9.	Average measured temperature for each station during the mini-frac tests. ....	3-39
Table 3-10.	Input data for calculating thermal stress correction for $S_{hmin}$ . ....	3-43
Table 3-11.	Calculated thermal stress correction for $S_{hmin}$ using Equation 3-4. ....	3-43
Table 4-1.	$S_{Hmax}$ magnitude determined for MF-2 and MF-4. ....	4-10
Table 4-2.	Calculated Values of $S_{Hmax}$ from DIFs at 33 depths. ....	4-15
Table 4-3.	Summary of $S_{Hmax}$ values determined with stress polygon method for 33 DIFs for two tensile strength scenarios and three values of $S_{hmin}$ (all 33 DIFs included). ....	4-18
Table 4-4.	Summary of $S_{Hmax}$ values determined with stress polygon method for 12 DIFs for two tensile strength scenarios and three values of $S_{hmin}$ (only DIFs in vertical section of borehole included [ depth less than 5638 ft]). ....	4-18
Table 5-1.	Effective Stress Ratios and Tectonic Strains used to calculate $S_{hmin}$ and $S_{Hmax}$ Depth Profiles .....	5-2
Table 6-1.	Parameters used for modeling DIFs. ....	6-1
Table 6-2.	Parameters used for modeling shear failure of a weak plane. ....	6-7
Table 6-3.	Comparison of fracture closure pressure from analysis of flowback data and analysis of fall-off data. ....	6-19

## LIST OF APPENDICES

Appendix A	Minifrac Field-Testing Summary Report. ....	A-1
------------	---	-----

# 1 INTRODUCTION

## 1.1 Objective

This report documents research conducted as part of Utah Frontier Observatory for Research in Geothermal Energy (FORGE) Research and Development Project 2439, “A Multi-Component Approach to Characterizing In-Situ Stress at the U.S DOE FORGE Enhanced Geothermal System (EGS) Site: Laboratory, Modeling and Field Measurement”. The overall objective of Project 2439 is to collaborate with the Utah FORGE operations team to characterize stress in the EGS reservoir using methods that are similar to the methods used by the FORGE team in prior phases as well as those methods that are complementary to the methods utilized in prior phases by the Utah FORGE team. Specifically, the project entails implementation of three distinct methods of estimating stress (Methods 1 and 3 are complementary approaches; Method 2 is similar to stress testing conducted previously in the Utah FORGE 58-32 well).

- Method 1 is focused on estimating stresses in FORGE wellbore(s) based on the relationship between applied stresses and ultrasonic wave velocities (from triaxial [polyaxial] stress ultrasonic velocity [TUV] rock physics experiments) and sonic well-log data for the well(s), enabled by machine learning methods.
- Method 2 is focused on measuring stresses at multiple depths in FORGE 16B(78)32 wellbore(s) by conducting a series of in-situ open borehole minifrac stress tests.
- Method 3 is focused on developing and applying a numerical model(s) to estimate a far-field (reservoir) stress from near-field stress determined in Method 1. This method will also use numerical modeling to assimilate currently existing and new stress data to derive an improved stress estimate for the site.

This report documents the work performed and results obtained from Method 2 (field testing), which is Task 3.4 of the project, and is a requirement to achieve Milestone 3.4.

## 1.2 Scope

This report describes the approach and results of minifrac testing conducted in the 16B(78)-32 well and analysis of the minifrac test data to determine the subsurface stresses at the DOE Utah FORGE site, including minimum and maximum horizontal stress magnitude and azimuth and vertical stress magnitude.

## 1.3 Methods

### 1.3.1 Minifrac Method for Determining Minimum Horizontal Stress ( $S_{hmin}$ )

The minifrac tests entailed conducting a series of short duration, low volume, hydraulic fracturing (HF) tests (HF is a borehole field-test method designed to assess the state of in-situ stress in the earth crust; this method is also referred to as a minifrac test [Haimson and Cornet, 2003]<sup>1</sup>) at multiple depth stations to determine magnitude of minimum horizontal stress ( $S_{hmin}$ ). De Bree and Walters (1989) provide a conceptual illustration of a minifrac test that shows the typical pressure response. Examples of actual minifrac tests are shown in

---

<sup>1</sup> The term minifrac test is used in this document.

Figure 1-1 (permeable limestone) and Figure 1-2 (impermeable shale) from Baker Hughes. As shown in these examples, a minifrac test involves performing a number of short pumping (injection) cycles to pressurize a preselected, usually short (~3 to 5 ft) interval of the borehole that is isolated with a straddle packer or similar device. Injection continues until pressure builds and fracturing occurs at the fracture breakdown pressure (FBP) (initial cycle only) and then stabilizes at the fracture propagation pressure. Pumping continues for a short time after reaching FPP. After injection is stopped (shut-in), the fracture closes as the pressure declines due to borehole fluid leak-off into the formation. For permeable rocks, pressure fall-off occurs relatively quickly. In low permeability rocks, however, pressure fall-off may occur very slowly and may need to be accelerated by pumping (withdrawing) fluid from the test interval (Figure 1-2). Typically, two more injection cycles of fracture re-opening, propagation and closure are performed to measure the minimum horizontal stress away from the influence of the borehole induced stresses. In subsequent cycles performed after achieving breakdown, FBP is not observed again and pressure just increases until reaching FPP. FRP occurs at a pressure less than FPP. Each cycle is followed by a shut-in period of several minutes until pressure declines to below fracture closure pressure (FCP). Typically, the FCP is determined from analysis of the decline curve of the various cycles and is used to define the total (far-field) minimum in-situ stress (Shmin). Fracture re-opening pressure (FRP), observable on repeat injection cycles after the initial cycle, is sometimes used to define Shmin.

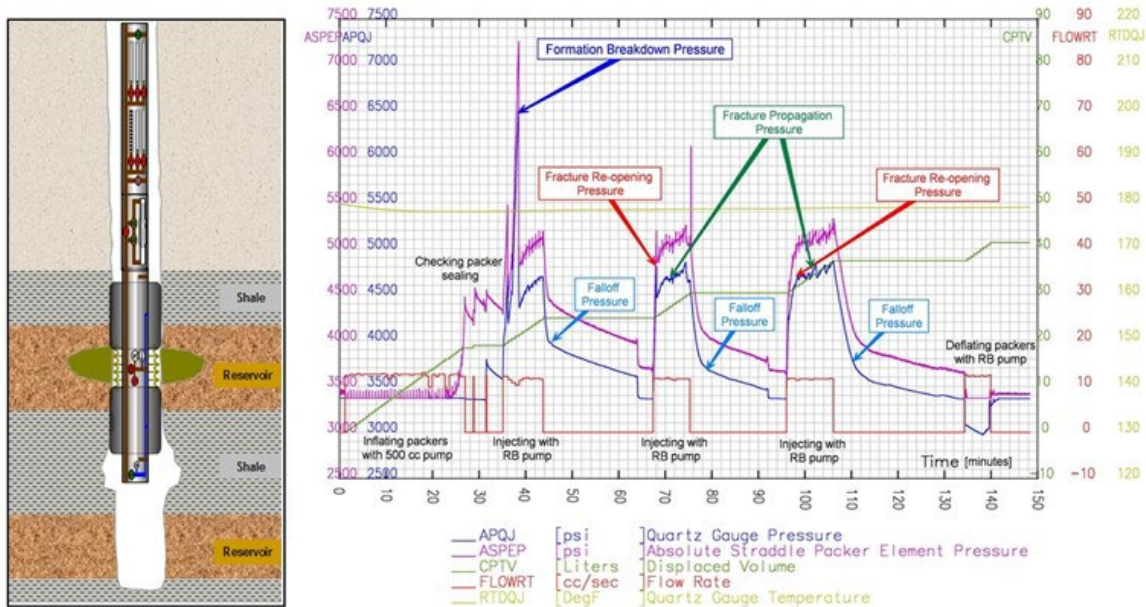
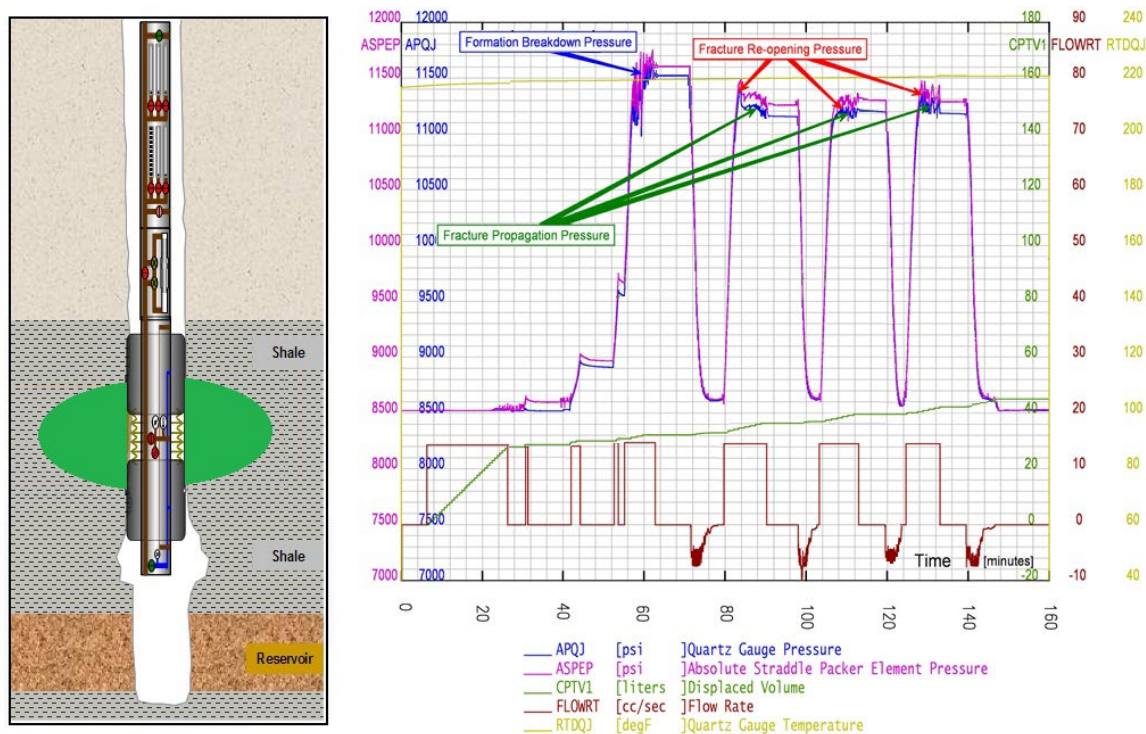


Figure 1-1 Example minifrac test for a permeable limestone; from Baker Hughes. Fracture closure pressure (not labeled) will occur along the fall-off pressure curve.



**Figure 1-2. Example minifrac test in an impermeable shale formation. Fracture closure pressure (not labeled) will occur along the fall-off pressure curve. Note flowback pumping technique was used to close the fracture due to very slow pressure fall-off after shut-in.**

FCP can be determined by multiple techniques, including:

- P-inflection analysis can be used to detect the FCP using a simple graphical approach to find the first inflection point (ISIP) from the linear trend during pressure decline after shut-in during natural fall-off only (i.e., not during flowback, if performed). The P-inflection method assumes the ISIP equals FCP.
- Bi-linear pressure decay analysis can be used to identify an inflection point by interpreting two linear regressions of P versus  $dP/dt$  after shut-in during natural fall-off only (i.e., not during flowback, if performed). The bi-linear decay method assumes the inflection point equals FCP.
- Square root of time (SRT) pressure decline analysis uses the borehole fluid pressure versus square-root of shut-in time. Depending upon flow characteristics, if the flow is linear, the FCP is identified when pressure profile deviates from linearity.
- Log-log pressure decline analysis uses the pressure derivative of the delta pressure and delta time in log-log plot. The plot also shows the flow regime, for linear flow, the slope equals half ( $1/2$ ), beyond which radial flow starts and the slope becomes one (1). If bi-linear flow exists with pre-existing fractures feeding into the fracture, then the slope is one-quarter ( $1/4$ ).
- G-function analysis uses plotting of the G-function derivative  $GdP/dG$  on a pressure versus Nolte G-time plot. G function is a dimensionless function representing elapse time after shut-in duly normalized to duration of fracture extension period. G-function also indicates type of leak-off

taking place. Deviation of G-function from the straight line in  $GdP/dG$ , or just before the inflection point indicates FCP.

In this project, all of the above techniques were applied to interpret the minifrac tests; the results of these analyses are presented in [Section 3](#).

### 1.3.2 Minifrac Testing Program

Battelle collaborated with Baker Hughes (BH) to conduct the minifrac tests using BH’s RCX (Reservoir characterization) tool. The RCX tool is a sophisticated testing tool for conducting injection-fall-off tests and drawdown-buildup pumping tests for reservoir-property characterization. The RCX tool can also be used to conduct minifrac tests because it is equipped with a dual (straddle) packer with vertical spacing on the order of 3 feet for zonal isolation, a pump for injecting or withdrawing fluid from the test interval; sensors for pumping rate, pressure and temperature in test interval, packer pressure, and diagnostics; and real-time readout (display) and data-logging/recording capabilities.

In addition to running the RCX tool, two types of image logs were obtained before and after the minifrac tests to identify the induced fracture (if created) to aid in determining the stress regime. The image logging tools included the STAR log (a resistivity-based image log) and the CBIL (UXPL) log (an acoustic image log). The orientation (azimuth) of the induced fracture corresponds to the direction of maximum horizontal stress (SHmax) in vertical section of the well, the minimum horizontal stress being orthogonal to this. In addition, a multi-pole sonic log (XMAC) for deep shear-wave processing was also acquired before and after the minifrac tests to aid in determining fracture orientation away from the borehole.

Two separate tool strings were required to conduct the minifrac tests and acquire the necessary logs. The RCX minifrac tool and the logging tools were run as shown in Table 1-1. One string contained the two image logging tools (STAR and UXPL [CBIL]) and the sonic (XMAC) tool, plus gamma ray, and an orientation tool (ORIT). The second tool string included the RCX tool, a sleeve frac packer (SLVP), 3-arm caliper, hole finder, plus gamma ray.

**Table 1-1. Baker Hughes Logging tool strings used to conduct the minifrac testing program.**

Tool String	Tool/Service
Tool string #1	PCL-GR-STAR-ORIT-XMAC-UXPL
Tool string #2	PCL-GR-RCX-SP-SLVP-3CAL-HFIND

PCL (Pipe Conveyed Logging); GR (Gamma Ray); STAR (acoustic borehole imager); ORIT (Orientation Tool); XMAC (dipole sonic log); UXPL (Acoustic borehole Imager); RCX (Microfrac Tool); SP (Straddle Packer); SLVP (SleeveFrac Packer); 3CAL (3-arm caliper); HFIND (Hole Finder).

The minifrac testing program included three deployments of the RCX tool and two deployments of the logging tools, including one before the minifrac tests and one after. A total of seven minifrac tests were conducted, all in the vertical or nearly vertical section of the borehole (the kick-off point [depth where deviated borehole begins] is 5,638 ft; so any tests above this depth are in the vertical section of the borehole ([Table 1-2](#)). Multiple minifrac tests were performed during each RCX deployment. Three tests (MF-1, MF-2, and MF-3) were conducted during the first deployment, three tests (MF-4, MF-5 and MF-6 [cycle 1 only] were conducted during the second deployment, and two tests (MF-6 [cycles 2 and 3] and MF-7) were conducted during the third deployment. A more detailed summary of the field program is provided in [Appendix A](#). Due to the anticipated high downhole temperatures above the working limit of the BH min-frac and logging tools (350° F or 400° F), it was necessary to cool the borehole by circulating fluid to depth and through drill pipe and two chillers at the surface before and intermittently during the minifrac testing program. Three circulation/cooling events were conducted, including one

before the first RCX deployment (MF-1, MF-2, MF-3), another before the second RCX deployment (MF-4, MF-5, and MF-6 [partial]), and another before the third RCX deployment (MF-4, MF-5, MF-6) (Table 1-3).

**Table 1-2. Minifrac test depths in the 16B(78)-32 well.**

MF Test #	Date	MD/TVD <sup>a</sup> (ft)	Lithology	Comments
MF-1	6-28-23	5657 /5655.2	Rhyolite	
MF-2	6-28-23	5495/5494	Granodiorite	
MF-3	6-28-23	5202/5201.1	Rhyolite	
MF-4	7-1-23	5980/5966.18	Granodiorite	
MF-5	7-1-23	5919/5909.23	Granodiorite	
MF-6	7-1-23 7-2-23	5639.2/5637.64	Granodiorite/ Rhyolite	Cycles 1 and 2 on 7-1-23; cycle 3 on 7-2-23 (SP removed and replaced after cycles 1 and 2)
MF-7	7-2-23	5616/5614.67	Granodiorite/ Rhyolite	

a. MD (measured depth); TVD (total vertical depth); the kick-off point [depth where deviated borehole begins] is 5,638 ft

**Table 1-3. Summary of circulation (cooling) events, logging runs, and minifrac (RCX) tool string deployments.**

First circulation/cooling event (depth 9,000 ft MD); 16.1 hrs
Baseline logging run (PC) (depth 9,000 ft MD)
2nd circulation/cooling event (depth 6,000 ft); 39.75 hrs
First (PC) deployment of minifrac (RCX) tool string (depth 6,000 ft MD); completed MF-1, MF-2, MF-3
3 <sup>rd</sup> circulation/cooling event (depth 9,000 ft MD); 16 hrs
2 <sup>nd</sup> (WL) deployment of minifrac (RCX) tool string (6,000 ft MD); completed MF-4, MF-5, MF-6 [cycle 1]
3 <sup>rd</sup> (WL) deployment of minifrac (RCX) tool string (6,000 ft MD); completed MF-6 [cycles 2 and 3] and MF-7
Repeat logging run (WL) (depth 9,000 ft MD)

PC (pipe conveyed); WL (wireline conveyed)

Table 1-4 summarizes key test parameters for the seven minifrac tests (depth/measured depth [MD], depth/total vertical depth [TVD], hydrostatic pressure, temperature, injected fluid volume, flowback fluid volume, flowback pumping rate, and time).

**Table 1-4. Summary of minifrac test parameters.**

Station	Cycle	Depth MD	Depth TVD	Hydrostatic Before	Hydrostatic After	Average Temperature during test	Inject Volume	Injection Rate	Flowback Volume	Flowback Rate	Station Time
				psi	psi	degF	L	cc/s	L	cc/s	Min
Station MF-1	1	5657.00	5655.20	2431	2430	230	5.40	5.00	4.50	21.90	
	2	5657.00	5655.20	2431	2430	230	4.30	5.20	3.02	2.60	110
Station MF-2	1	5495.00	5494.00	2358	2359	230	2.95	5.20	1.27	2.10	
	2	5495.00	5494.00	2358	2359	230	5.44	5.45	2.59	2.30	
	3	5495.00	5494.00	2358	2359	231	7.77	5.47	5.27	2.33	260
Station MF-3	1	5202.00	5201.10	2229	2228	230	2.68	5.47	3.80	7.00	
	2	5202.00	5201.10	2229	2228	230	8.85	18.00	4.29	5.70	
	3	5202.00	5201.10	2229	2228	230	9.73	18.00	1.88	3.10	
	4	5202.00	5201.10	2229	2228	230	13.27	18.00	4.29	5.50	240
Station MF-4	1	5980.00	5966.18	2546	2245	263	2.95	5.10	0.43	3.60	
	2	5980.00	5966.18	2546	2245	264	11.51	20.00	0.06	3.00	
	3	5980.00	5966.18	2546	2245	264	9.73	26.80	0.32	3.00	150
Station MF-5	1	5919.00	5909.23	2521	2521	265	4.02	5.20	0.88	2.30	
	2	5919.00	5909.23	2521	2521	266	10.61	26.00	3.37	2.30	
	3	5919.00	5909.23	2521	2521	266	8.84	SRT	2.37	2.30	
	4	5919.00	5909.23	2521	2521	266	22.44	5.30	NA	NA	190
Station MF-6	1	5639.20	5637.64	2407	2407	260	11.50	24.00	1.80	5.23	
	2	5639.20	5637.64	2407	2407	260	30.40	40.00	NA	NA	80
	3	5639.20	5637.64	2406	2407	259	7.00	33.00	2.68	NA	70
Station MF-7	1	5616.00	5614.67	2396	2395	262	22.87	36.00	14.75	4.94	
	2	5616.00	5614.67	2396	2395	262	28.32	34.00	21.15	4.94	
	3	5616.00	5614.67	2396	2395	262	30.00	31.00	13.00	4.92	310

## 2 VERTICAL STRESS

As shown by Zoback et al. (2003), the magnitude of vertical stress ( $S_v$ ) can be calculated by integration of rock density from the surface to the depth of interest,  $z$ :

$$S_v = \int_0^z \rho(z)gdz \quad \text{Equation 2-1}$$

where:

$\rho(z)$  is the density as a function of depth, and  $g$  is the gravitational acceleration constant.

A density log for the 16B(78)-32 well, acquired by Schlumberger (June 19, 2023), is available below a depth of 3890.5 ft. The density-log data are shown by the pink curve in track 2 of [Figure 2-1](#). Because the log does not extend to land surface, bulk density for the missing shallow interval was estimated in two ways. The first way is simply an extrapolation of the density log for the 16B(78)-32 well; this extrapolated density log is shown by the red curve in track 3 of [Figure 2-1](#). The second way calculated bulk density for the missing section (above 3890.5 ft) by converting matrix density measured on cutting samples from the 58-32 well and porosity-log data ([Figure 2-2](#)). Point values of cutting density are shown by the black dots in track 2 of [Figure 2-1](#) and also in [Figure 2-2](#). Density was calculated for the cutting samples as follows:

$$\rho_b = \rho_m(1 - \theta) + (\rho_f * \theta) \quad \text{Equation 2-2}$$

where:

$\rho_b$  is the bulk density of the formation ( $\text{gm/cm}^3$ ),

$\rho_m$  is the matrix density of the formation ( $\text{g/cm}^3$ ),

$\rho_f$  is the fluid density ( $\text{g/cm}^3$ ), and

$\theta$  is the porosity calculated or measured.

The resulting vertical stress gradient curves are shown in Track 4 of [Figure 2-1](#). The pink  $S_v$  curve has a magnitude from 1.05 to 1.10 psi/ft across the minifrac test interval, whereas the green  $S_v$  curve has a magnitude from 1.10 to 1.15 psi/ft across the minifrac test interval.

Previous investigators estimated  $S_v$  at the Utah FORGE site. Aljubran et al. (2021) and Nadimi et al. (2020) estimated  $S_v$  to be 1.13 psi/ft based on rock-cutting density data and other previous density measurements from nearby wells for shallow depths and density-log data for well 58-32 for deeper depths. Xing et al. (2020) reported a  $S_v$  for 16A(78)-32 between 1.1 to 1.16 psi/ft.

## Overburden Stress

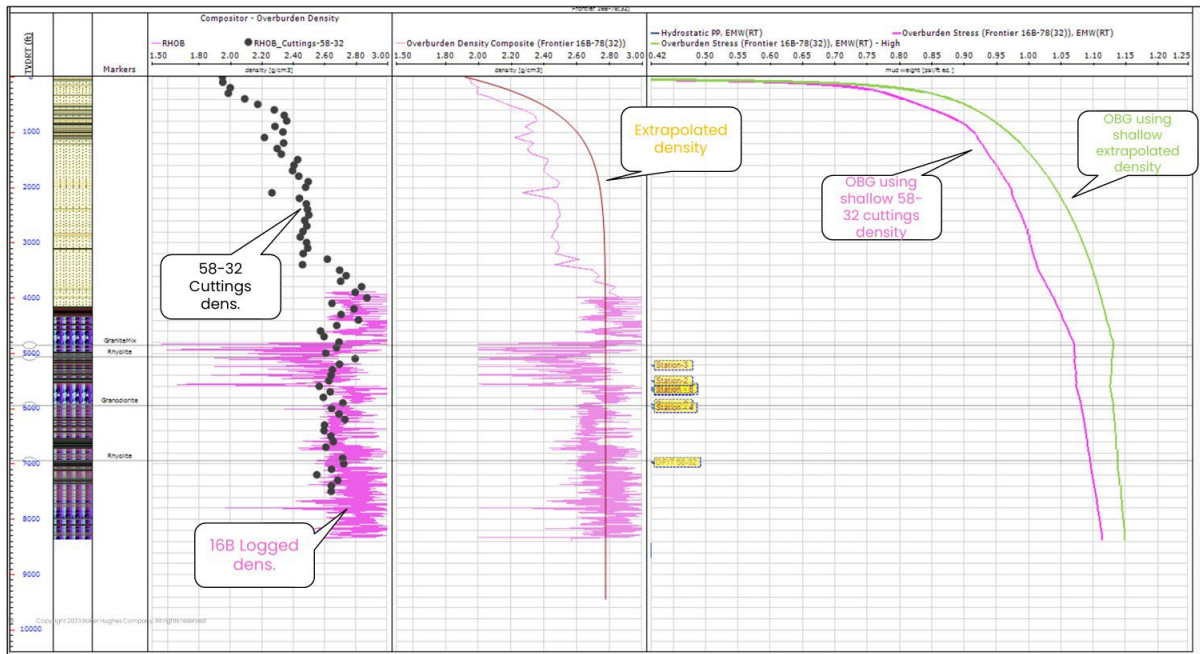


Figure 2-1. Overburden (Vertical) Stress Gradient (Track 4) estimated using two methods: one method (pink curve in track 4) uses a combination of density log data for the 16B(78)-32 well (below 3890 ft) and matrix measurements made on cuttings from the 58-32 well (above 3890 ft); the other method (green curve in track 4) uses density-log data from 16B(78)-32 well below 3890 ft and extrapolation of the density-log curve above 3890 ft.

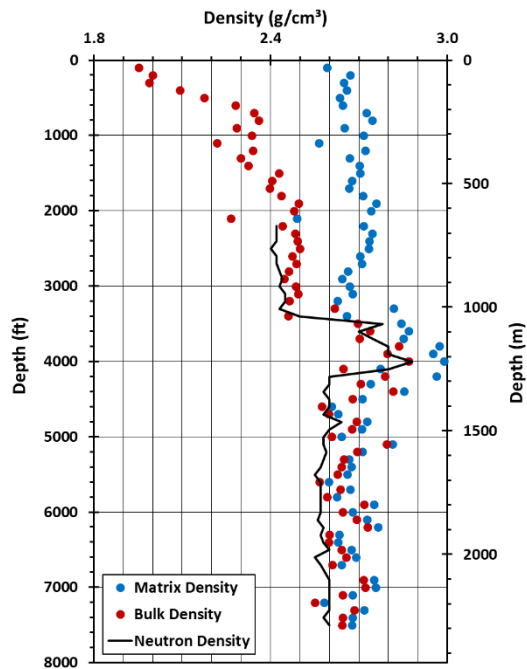


Figure 2-2. Calculated bulk density of cuttings samples for the 58-32 well. Points above 3890.5 ft were used to construct the Sv curve.

### 3 MINIMUM HORIZONTAL STRESS (SHMIN) DETERMINED FROM MINIFRAC TESTS

This section describes each of the seven minifrac tests and the results of analyses performed to estimate Shmin.

#### 3.1 MF-1

Minifrac test MF-1 was conducted with the Baker Hughes RCX straddle packer tool centered on a depth of 5657 ft (5655.2 ft TVD) in the 16B(78)-32 9-5/8 inch diameter open borehole. The test included two injection cycles, as shown in [Figure 3-1](#). During both cycles, the injection rate was nearly constant at approximately 5.0 and 5.2 cc/sec (0.3 to 0.31 L/min), respectively. A total water volume of 5.4 L and 4.3 L was injected during cycle 1 and cycle 2, respectively. The duration of each injection cycle was approximately 20 minutes. The duration of the entire test, including both cycles, was 110 minutes.

Following each injection period, there is a short fall-off period during which pressure declined naturally; however, due to the slow rate of pressure decline during the fall-off period, flowback (withdrawal pumping) was implemented to increase the rate of pressure decline. During the flowback period, water was pumped from the test interval using the pump in BH's RCX tool. Injection rates were variable (decreasing), ranging from ~2 L/min to zero.

The MF-1 test data were analyzed to determine FCP using the following techniques: G-function analysis, SRT pressure decline analysis, log-log pressure decline analysis, and P-inflection analysis. A plot for each of these four techniques is shown in [Figure 3-2](#) (cycle 1) and [Figure 3-3](#) (cycle 2). There is no indication, based on the pressure data from cycles 1 and 2, that breakdown occurred during the injection period of either cycle (see [Figure 3-2](#) and [Figure 3-3](#)).

Similarly, no evidence of fracture closure is indicated by the G-function analysis plot, SRT pressure decline analysis plot, or the log-log pressure decline analysis plot; therefore, the ISIP was assumed to be representative of FCP. ISIP was determined using the P-inflection plots shown in [Figure 3-2](#) and [Figure 3-3](#). In addition, the test data were analyzed using the bi-linear pressure decay method as an additional method to identify FCP ([Figure 3-4](#)). Results (FCP) of the pressure-data analysis are summarized in [Table 3-1](#). The P-inflection plot indicates a FCP of 4536 psi (0.8 psi/ft) and 4421 psi (0.78 psi/ft) for cycles 1 and 2, respectively. The bi-linear pressure decay method yielded a FCP (ISIP) of 4526 psi (0.8 psi/ft) and 4423 psi (0.78 psi/ft) for cycles 1 and 2, respectively. [Table 3-2](#) summarizes parameters estimated from the analysis of the MF-1 test data.

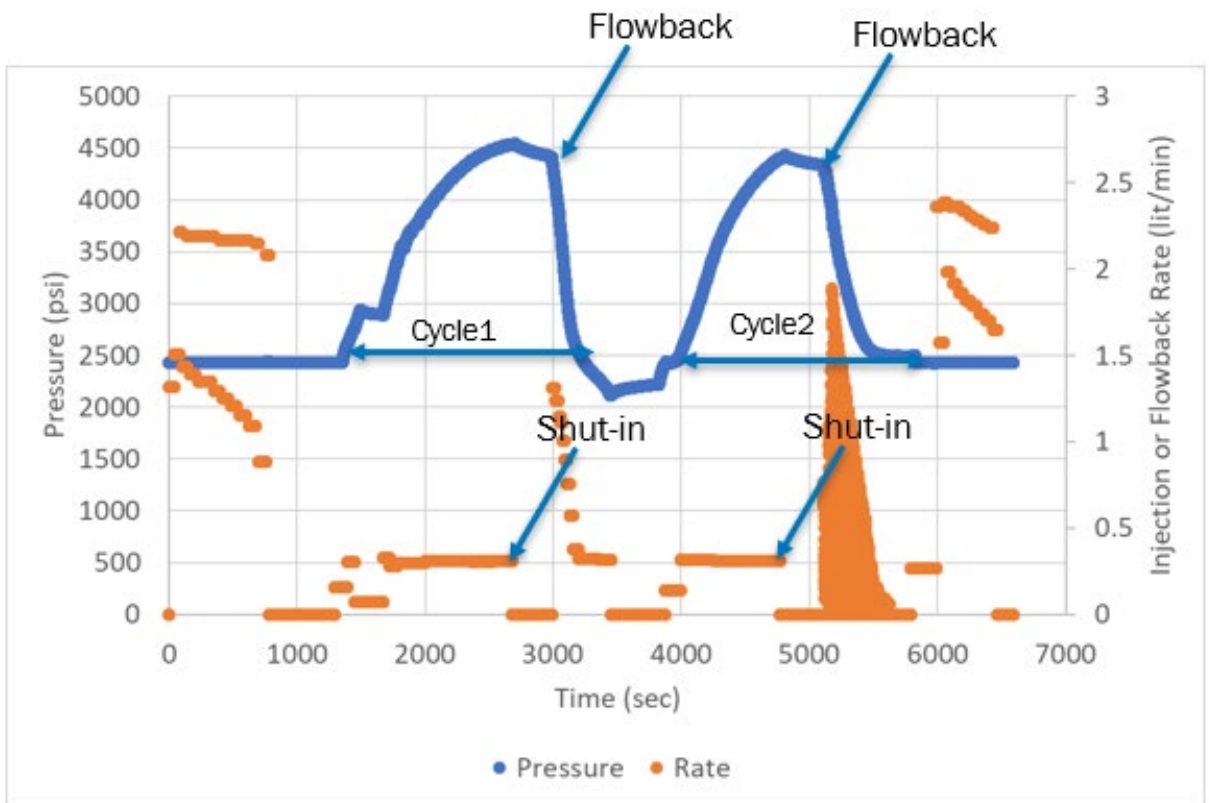


Figure 3-1. Pressure and injection rate for both cycles of MF-1.

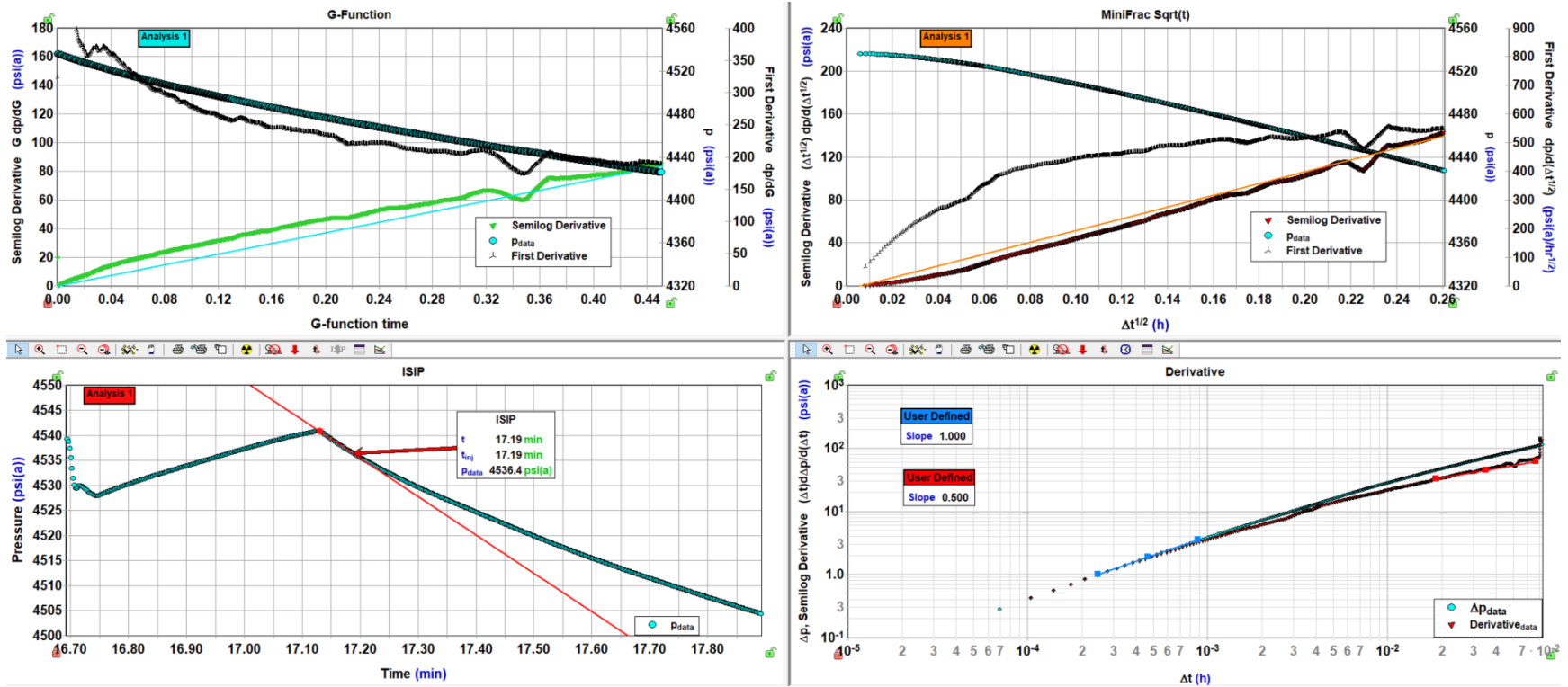


Figure 3-2. Data analysis plots for cycle 1 of MF-1.

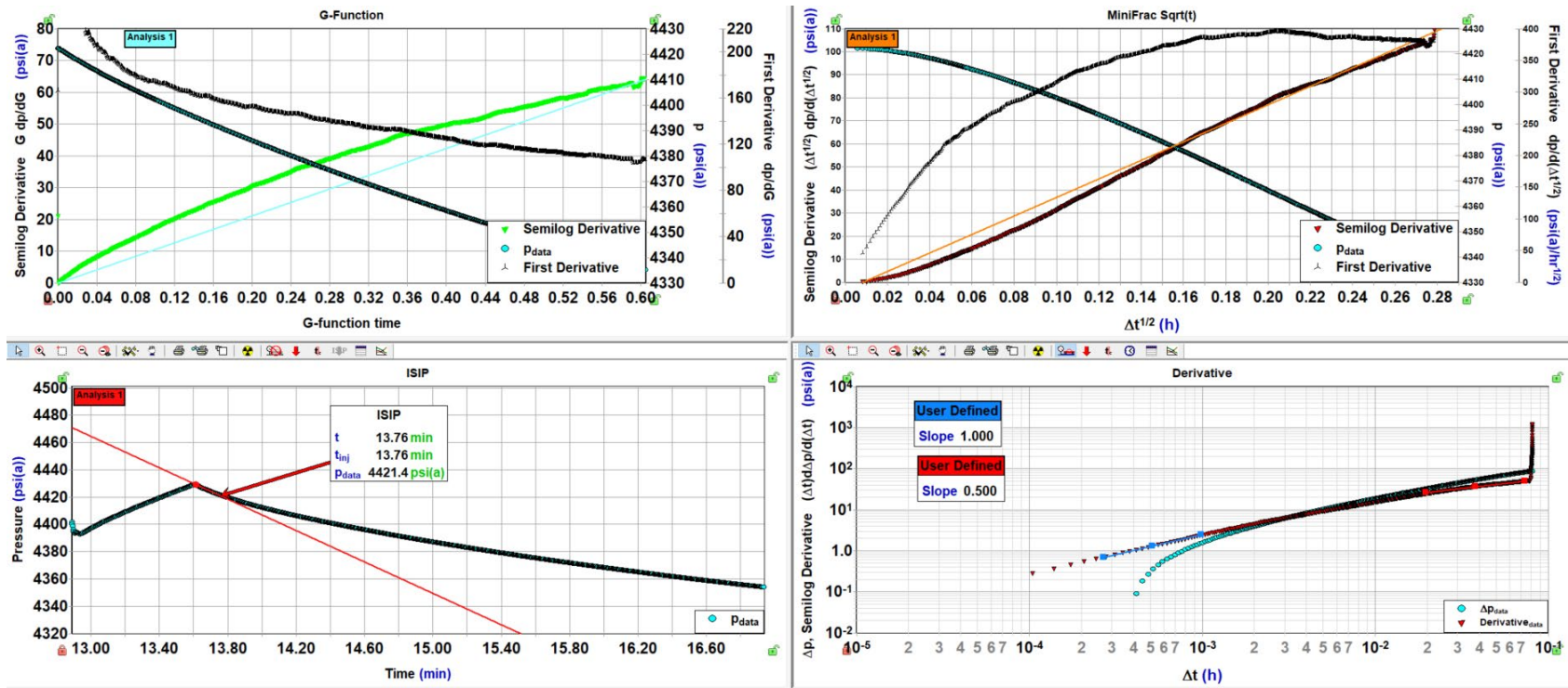


Figure 3-3. Data analysis plots for cycle 2 of MF-1.

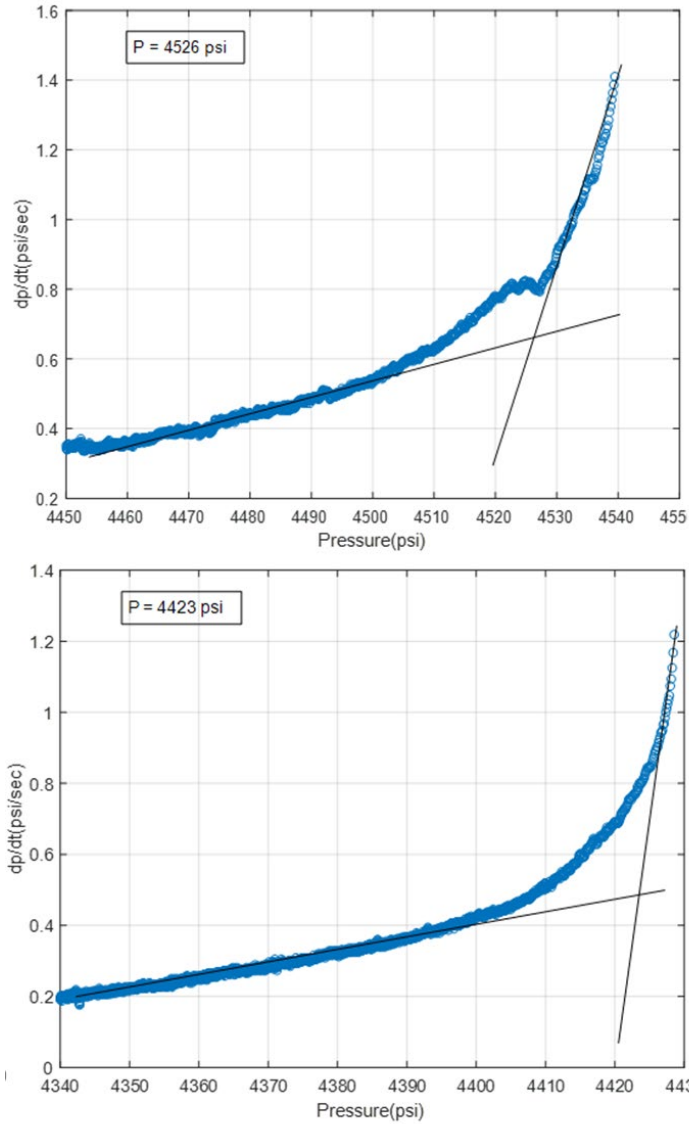


Figure 3-4. Bi-linear analysis for cycles 1 and 2 of MF-1, which yielded a FCP (ISIP) of 4526 psi (0.8 psi/ft) and 4423 psi (0.78 psi/ft), respectively.

Table 3-1. Summary table for MF-1 analyses.

Station	Cycle	Depth MD (ft)	Depth TVD (ft)	Breakdown / Re-opening Pressure (psi) and Gradient (psi/ft)		Propagation pressure (psi) and Gradient (psi/ft)		Instantaneous Shut-in (psi) and Gradient (psi/ft)		Bi-linear Pressure (psi) and Gradient (psi/ft)	
MF-1	1	5657	5655.2	NA	NA	NA	NA	4536	0.8	4526	0.8
MF-1	2	5657	5655.2	3751	0.66	NA	NA	4421	0.78	4423	0.78
Station	Cycle	Depth MD (ft)	Depth TVD (ft)	SRT Closure (psi) and Gradient (psi/ft)		Derivative Pressure (psi) and Gradient (psi/ft)		G-Function plot 1 Closure (psi) and Gradient (psi/ft)		G-Function plot 2 Closure (psi) and Gradient (psi/ft)	
MF-1	1	5657	5655.2	NA		NA		NA		NA	
MF-1	2	5657	5655.2	NA		NA		NA		NA	

### 3.2 MF-2

Minifrac test 2 (MF-2) was conducted with the straddle packer centered on a depth of 5495 ft (5494 ft TVD) in the 16B(78)-32 9-5/8 inch diameter open borehole. The test included three injection cycles, as shown in Figure 3-5. During all three cycles, the injection rate was nearly constant at approximately 6.75 cc/sec (0.4 L/min). A total water volume of 2.95 L, 5.44 L, and 7.77 L was injected during cycles 1, 2, and 3, respectively. Each injection period was followed by a fall-off period, during which pressure declined naturally. Each fall-off period was followed by a flowback event during which water was actively withdrawn (pumped) from the test interval using the pump included in the RCX straddle packer tool. Withdrawal rates during the flowback periods were variable (decreasing), ranging from ~1.5 L/m to zero. The duration of the entire test, including all three cycles, was 260 minutes.

Breakdown appears to have occurred in cycle 1, as indicated by the abrupt pressure drop (at ~3531 psi) in this cycle (see Figure 3-5). The resulting breakdown pressure gradient is 0.64 psi/ft based on a breakdown pressure of 3531 psi.

The MF-2 test data were analyzed to determine FCP using: G-function analysis, SRT pressure decline analysis, log-log pressure decline analysis, and P-inflection analysis. A plot for each of these four techniques is shown in Figure 3-6 for cycle 1, Figure 3-7 for cycle 2, and Figure 3-8 for cycle 3. Multiple fracture-closure events are visible in the G-function plot for all three cycles. In addition, the data were analyzed using the bi-linear pressure decay method to identify FCP (Figure 3-9). Results (FCP) of the pressure-data analysis are summarized in Table 3-2. Taking into account the multiple methods used to determine FCP, the results indicate a range for FCP from 0.56 psi/ft to 0.61 psi/ft.

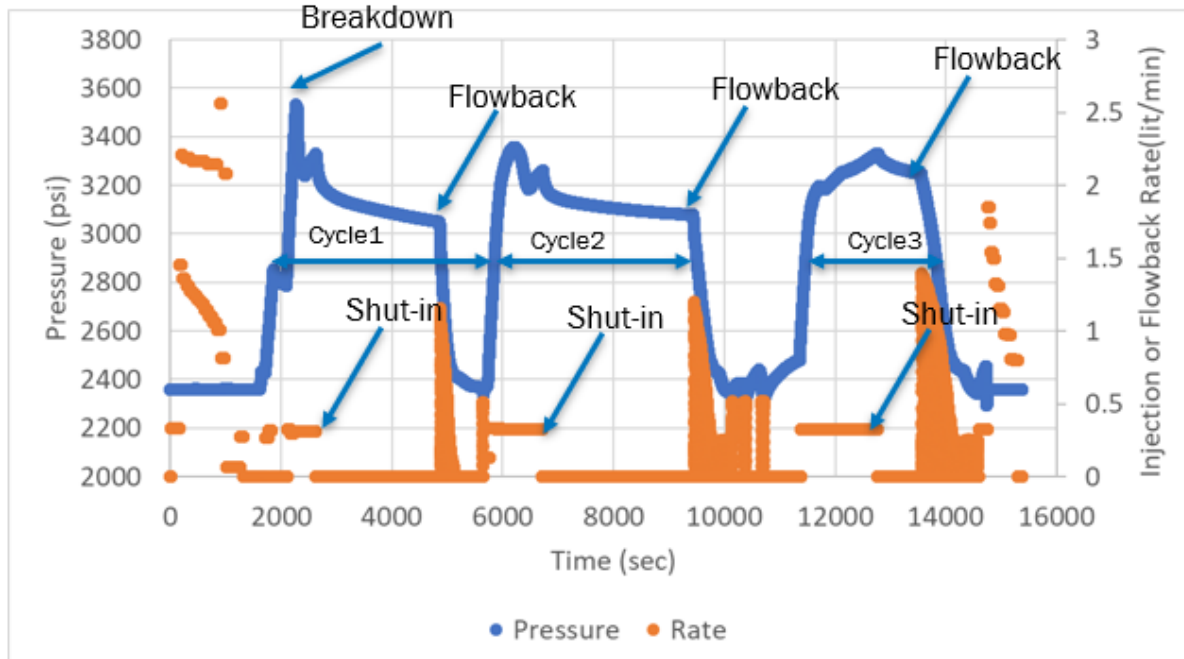


Figure 3-5. Pressure and injection rate plot for the three cycles of MF-2.

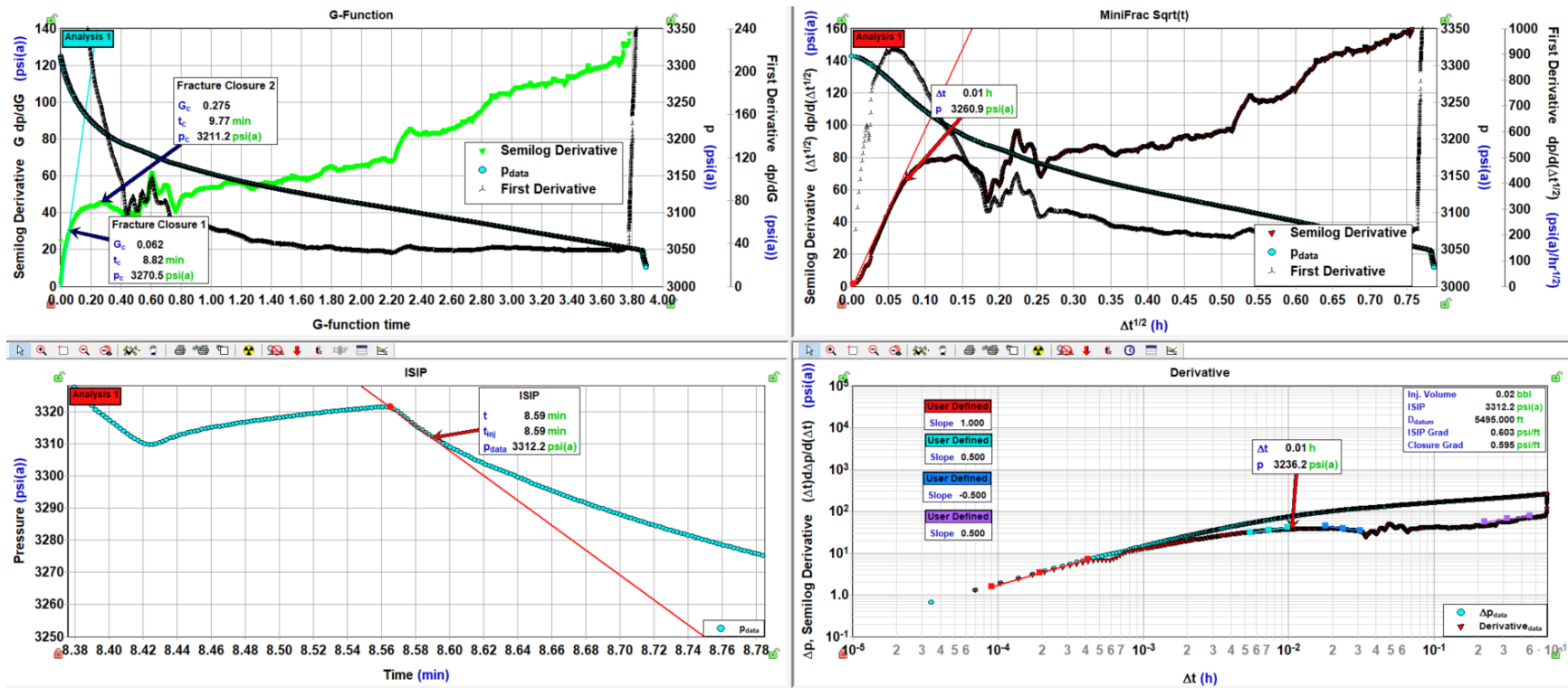


Figure 3-6. G-Function plot (top left), SRT analysis (top right), ISIP (bottom left), derivative plot (bottom right) for MF-2 cycle 1.

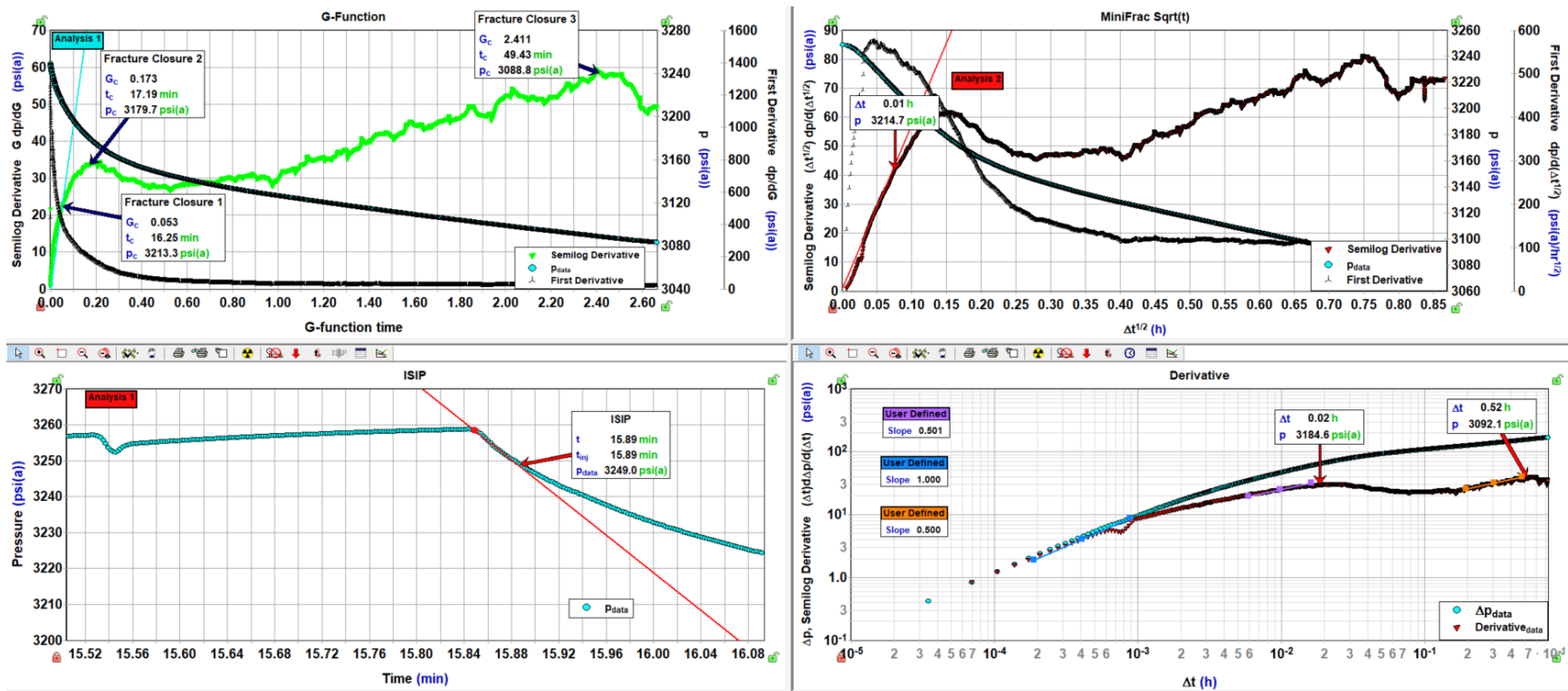


Figure 3-7. G-Function plot (top left), SRT analysis (top right), ISIP (bottom left), derivative plot (bottom right) for MF-2 cycle 2.

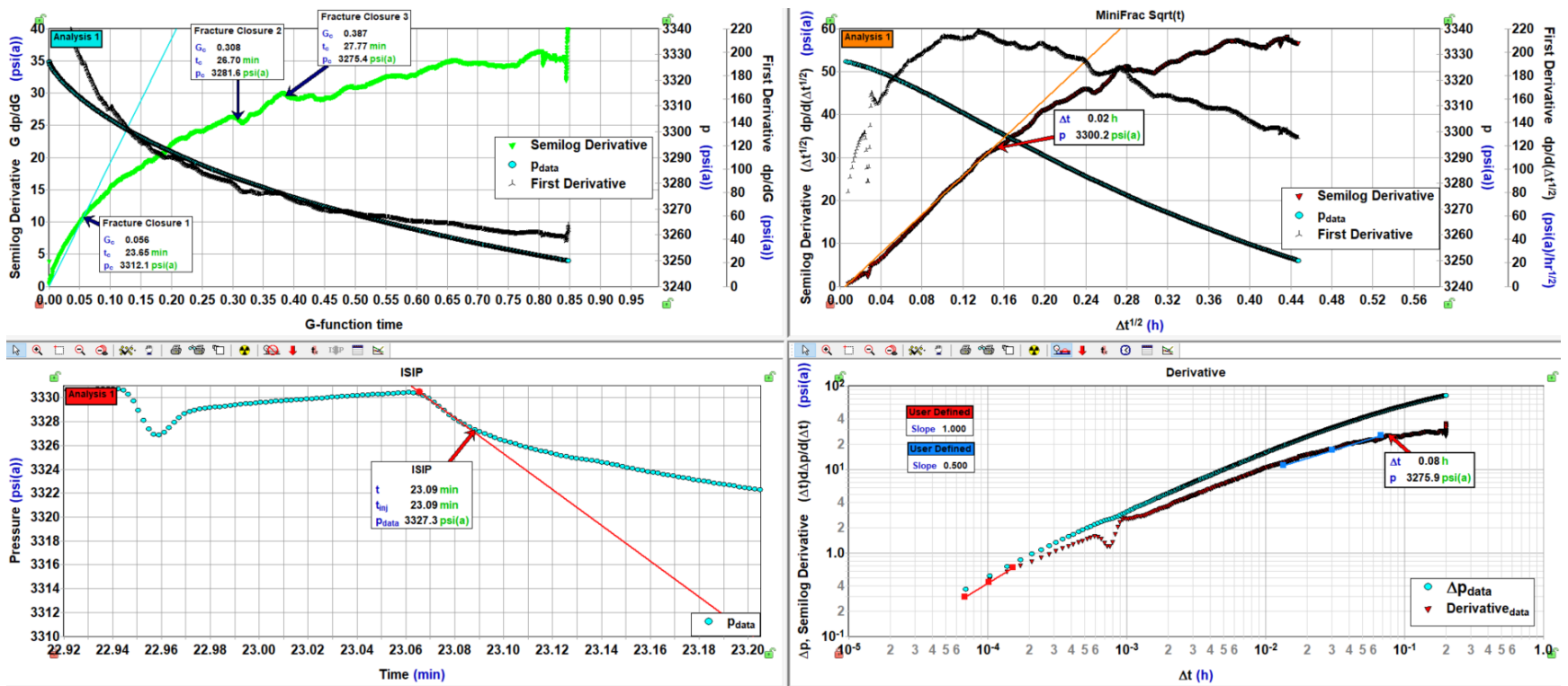
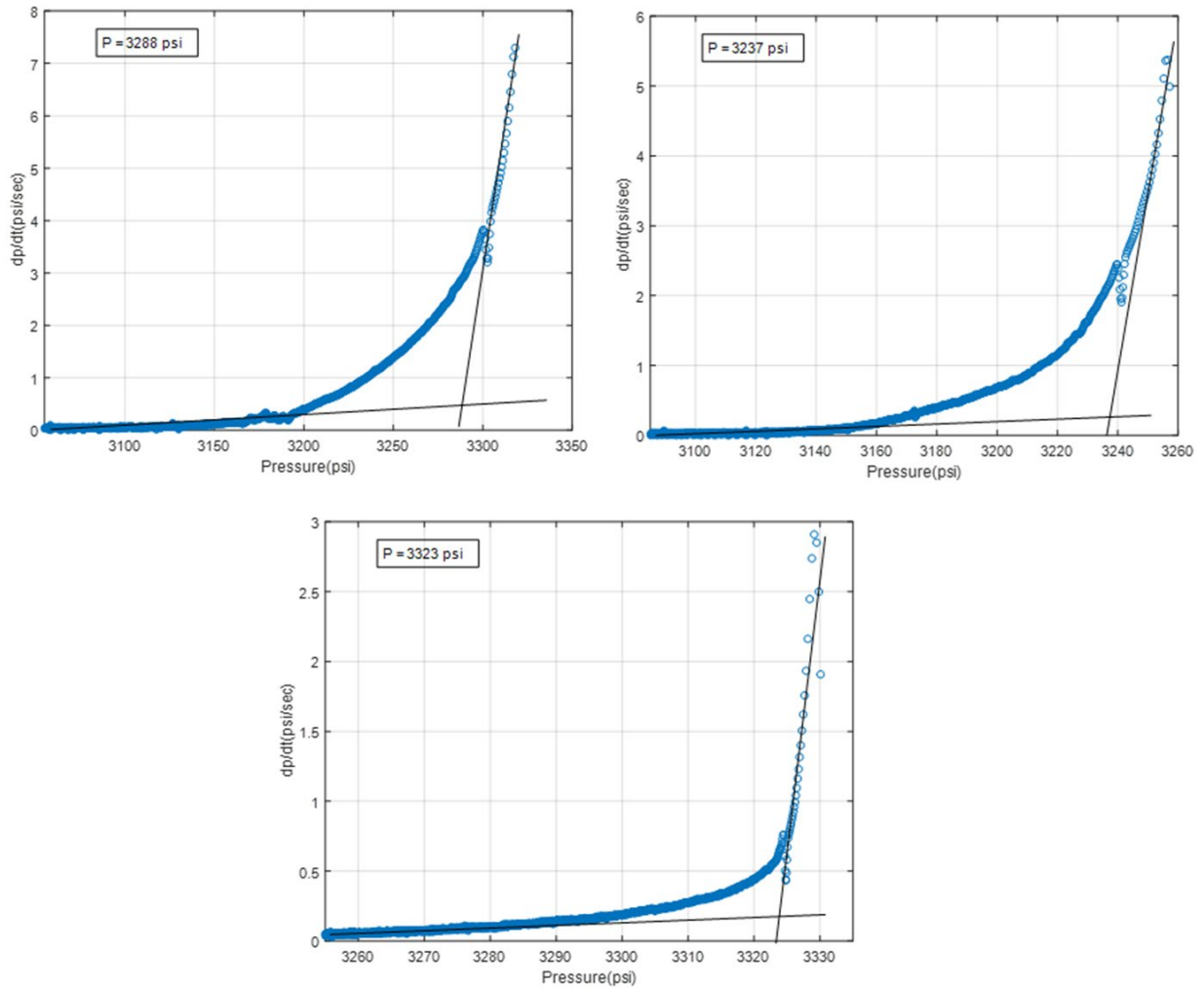


Figure 3-8. G-Function plot (top left), SRT plot (top right), ISIP (bottom left), derivative plot (bottom right) for MF-2 cycle 3.



**Figure 3-9. Bi-linear plots for cycles 1, 2 and 3 for MF-2, which yielded a FCP (ISIP) of 3288 psi (0.6 psi/ft), 3237 psi (0.59 psi/ft), and 3323 psi (0.6 psi/ft), respectively.**

**Table 3-2. Summary table for MF-2 analyses.**

Station	Cycle	Depth MD (ft)	Depth TVD (ft)	Breakdown / Re-opening Pressure (psi) and Gradient (psi/ft)				Propagation pressure (psi) and Gradient (psi/ft)				Instantaneous Shut-in (psi) and Gradient (psi/ft)		Bi-linear Pressure (psi) and Gradient (psi/ft)	
				SRT Closure (psi) and Gradient (psi/ft)		Derivative Pressure (psi) and Gradient (psi/ft)		Derivative Pressure 2 (psi) and Gradient (psi/ft)		G-Function plot 1 Closure (psi) and Gradient (psi/ft)		G-Function plot 2 Closure (psi) and Gradient (psi/ft)		G-Function plot 3 Closure (psi) and Gradient (psi/ft)	
MF-2	1	5495	5494	3531	0.64	3328	0.61	3312	0.60	3288	0.60				
MF-2	2	5495	5494	3194V	0.58	3258	0.59	3249	0.59	3237	0.59				
MF-2	3	5495	5494	3116V	0.57	3330	0.61	3327	0.61	3323	0.60				
Station	Cycle	Depth MD (ft)	Depth TVD (ft)	SRT Closure (psi) and Gradient (psi/ft)		Derivative Pressure (psi) and Gradient (psi/ft)		Derivative Pressure 2 (psi) and Gradient (psi/ft)		G-Function plot 1 Closure (psi) and Gradient (psi/ft)		G-Function plot 2 Closure (psi) and Gradient (psi/ft)		G-Function plot 3 Closure (psi) and Gradient (psi/ft)	
MF-2	1	5495	5494	3260	0.59	3235	0.59	NA	NA	3270	0.60	3211	0.58	NA	NA
MF-2	2	5495	5494	3214	0.59	3184	0.58	3092	0.56	3179	0.58	3088	0.56	NA	NA
MF-2	3	5495	5494	3300	0.60	3275	0.60	NA	NA	3312	0.60	3281	0.60	3275	0.60

### 3.3 MF-3

Minifrac test 3 (MF-3) was conducted with the straddle packer centered on a depth of 5202 ft (5201.1 ft TVD) in the 16B(78)-32 open borehole. The test included four injection cycles, as shown in [Figure 3-10](#). Cycles 3 and 4 were conducted as rebound tests so these are not analyzable for FCP. The average injection rate was variable during the four injection cycles, at 5.47 cc/sec for cycle 1 and 18 cc/sec for cycles 2, 3 and 4. A total of 2.68 L, 8.85 L, 9.73 L, and 13.27 L of water were injected during the four cycles. The duration of the MF-3 test, including all four cycles, was approximately 4.5 hours.

For cycles 1 and 2, a flowback event was performed using the pump out module on the RCX tool to increase the rate of pressure decline during the fall-off period (see [Figure 3-10](#)). For cycles 3 and 4, flowback was not performed after natural fall-off but instead multiple flowback/rebound cycles were performed by valve opening to help determine FCP; however, this technique did not reveal any fracture closure events. In cycle 1, there is no clear indication that breakdown (i.e., fracturing) occurred.

Nevertheless, the MF-3 test data were analyzed to determine FCP using the G-function analysis, SRT pressure decline analysis, Log-Log pressure decline analysis, and P-inflection analysis. A plot for each of these four techniques is shown in [Figure 3-11](#) (cycle 1) and [Figure 3-12](#) (cycle 2). Indications of fracture closure are present in all plots for both cycles (the G-Function plot for cycle 1 suggests three closure events occurred). These closure events are likely related to pre-existing fractures (natural or drilling induced fracture [DIF]) that were present before the minifrac tests were conducted. In addition, the MF-3 test data were analyzed using the bi-linear pressure decay method ([Figure 3-13](#)). Interpreted FCP values for all of these methods are summarized in [Table 3-3](#) and range from 0.52 to 0.56 psi/ft. Of these, the ISIP, determined from the P-inflection method (0.53 to 0.56 psi/ft), and the FCP determined from the bi-linear method (0.53 to 0.55 psi/ft) are considered to be the most reliable indicator of FCP.

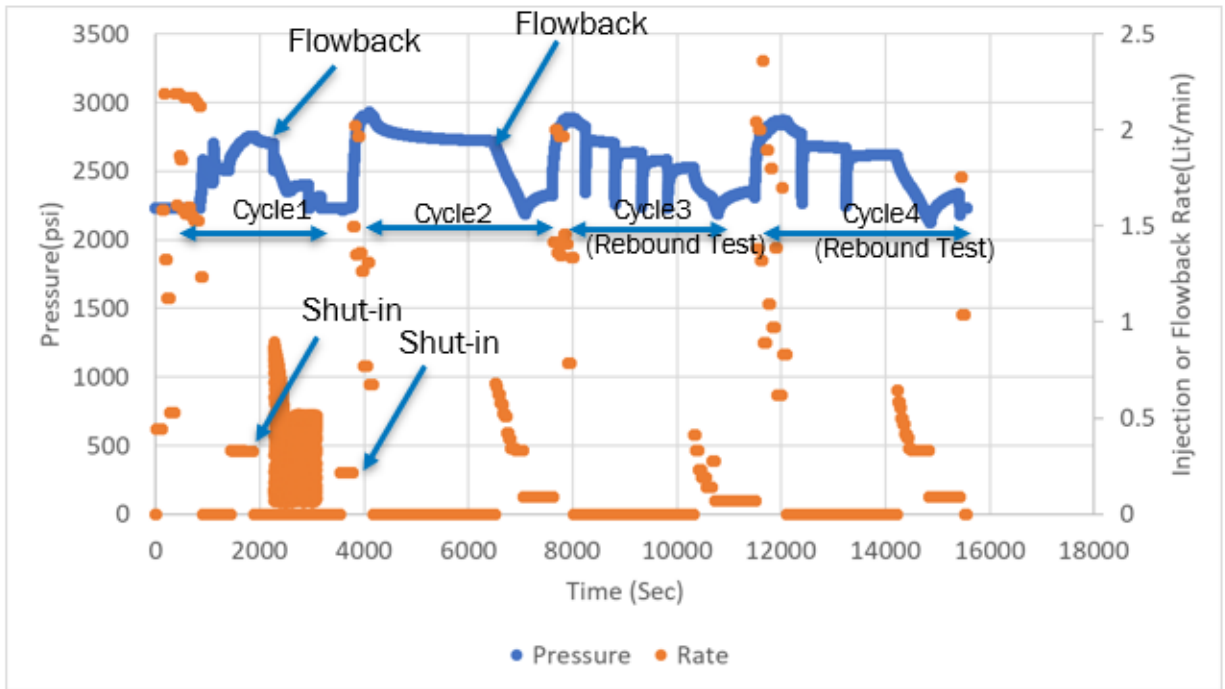


Figure 3-10. Pressure rate plot for the four cycles of Station MF-4.

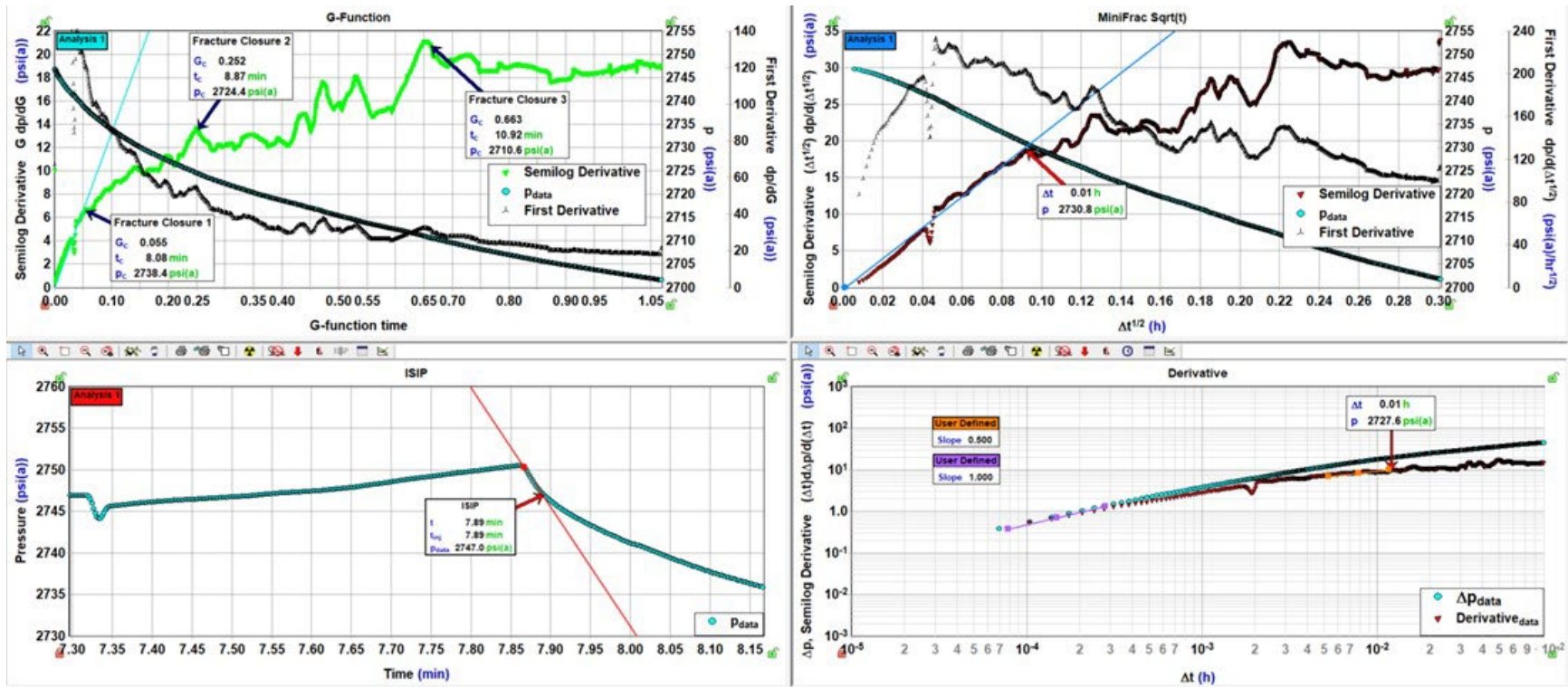


Figure 3-11.G-Function plot (top left), SRT analysis (top right), ISIP (bottom left), derivative plot (bottom right) for cycle 1.

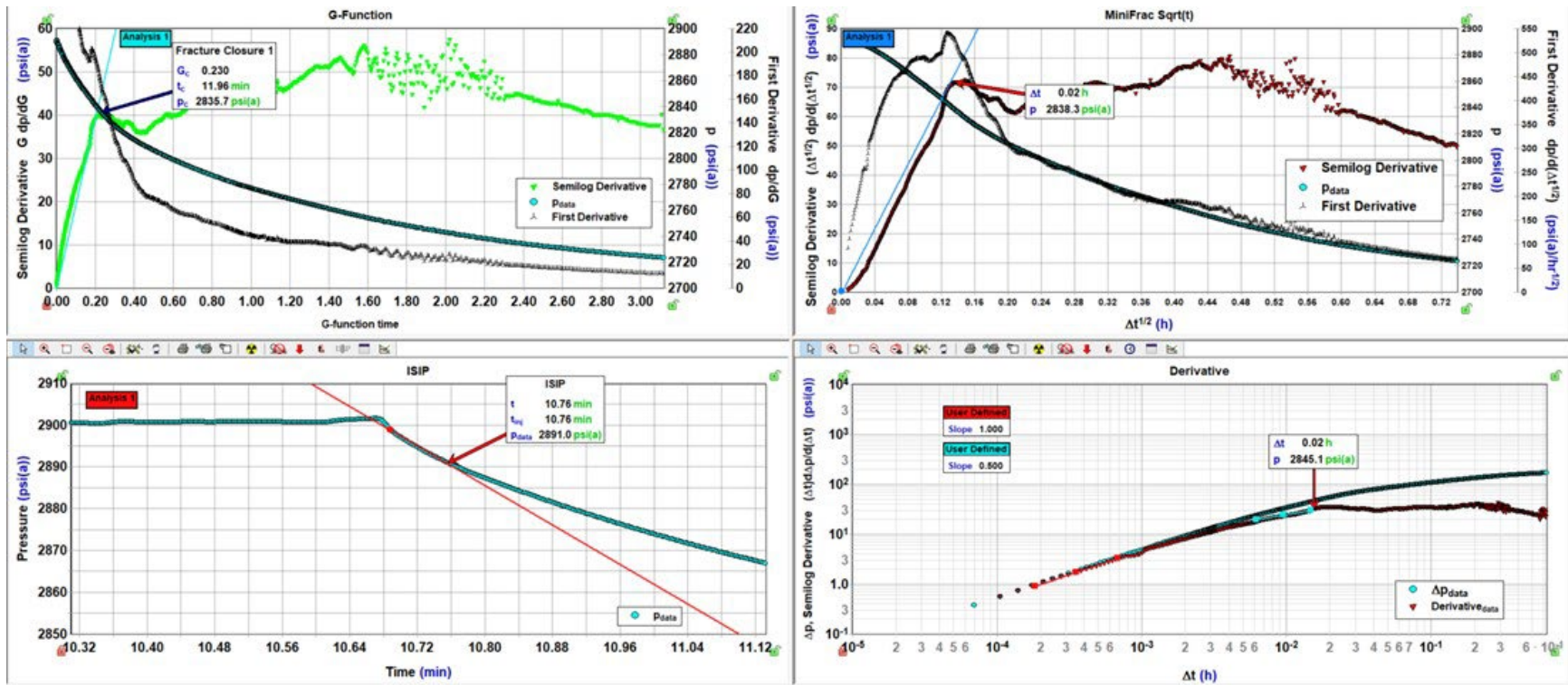
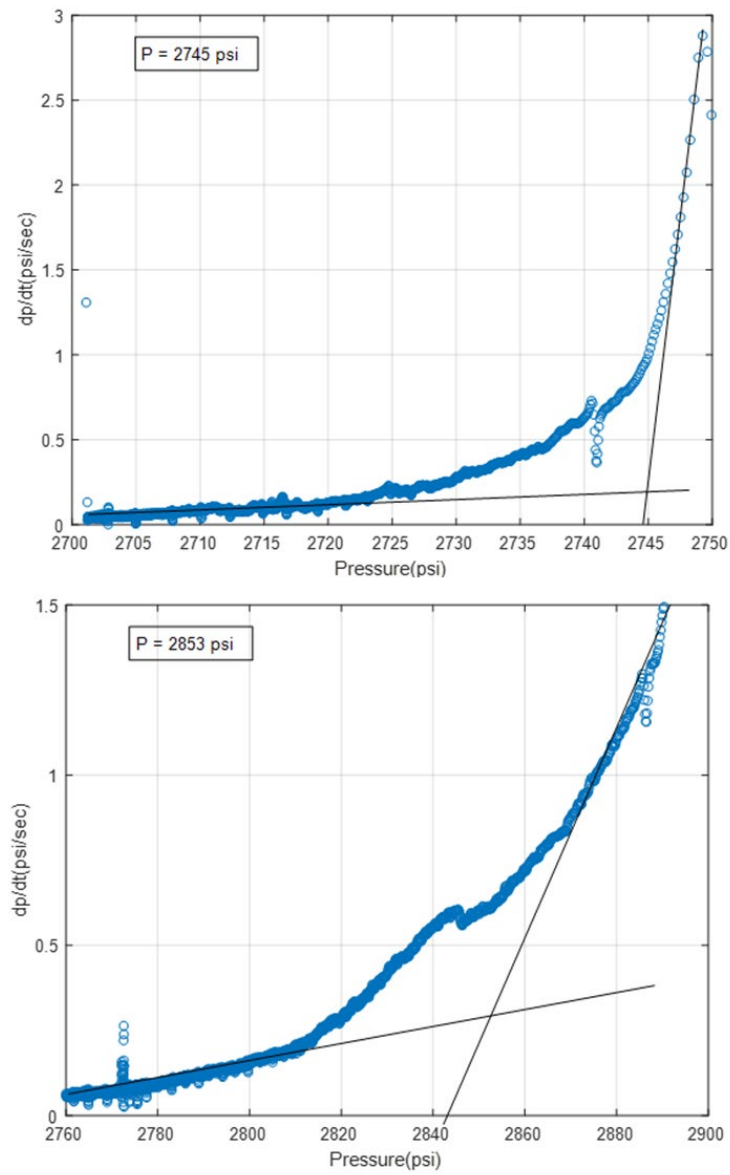


Figure 3-12.G-Function plot (top left), SRT analysis (top right), ISIP (bottom left), derivative plot (bottom right) for cycle 2 OF MF-3.



**Figure 3-13. Bi-linear analysis for cycle 1 (top) and cycle 2 (bottom) of MF-3, which yielded a FCP (ISIP) of 2745 psi (0.5 psi/ft) and 2853 psi (0.53 psi/ft) for cycles 1 and 2, respectively.**

**Table 3-3. Summary of MF-3 analyses.**

Station	Cycle	Depth MD (ft)	Depth TVD (ft)	Breakdown / Re-opening Pressure (psi) and Gradient (psi/ft)		Propagation pressure (psi) and Gradient (psi/ft)		Instantaneous Shut-in (psi) and Gradient (psi/ft)		Bi-linear Pressure (psi) and Gradient (psi/ft)			
MF-3	1	5202	5201.1	NA	NA	2750	0.53	2747	0.53	2745	0.53		
MF-3	2	5202	5201.1	2625v	0.5	2898	0.56	2891	0.56	2853	0.55		
Station	Cycle	Depth MD (ft)	Depth TVD (ft)	SRT Closure (psi) and Gradient (psi/ft)		Derivative Pressure (psi) and Gradient (psi/ft)		G-Function plot 1 Closure (psi) and Gradient (psi/ft)		G-Function plot 2 Closure (psi) and Gradient (psi/ft)		G-Function plot 3 Closure (psi) and Gradient (psi/ft)	
MF-3	1	5202	5201.1	2731	0.53	2728	0.52	2738	0.53	2724	0.52	2711	0.52
MF-3	2	5202	5201.1	2838	0.55	2845	0.55	2836	0.55	NA	NA	NA	NA

### 3.4 MF-4

Minifrac test 4 (MF-4) was conducted with the straddle packer centered on a depth of 5980 ft (5966.18 ft TVD) ± in the 16B(78)-32 open borehole. The test included three injection cycles, as shown in [Figure 3-14](#). The average injection rate was variable during the three injection cycles, at 5.10 cc/sec for cycle 1, 20 cc/sec for cycle 2, and 26.8 cc/sec for cycle 3. A total of 2.95 L, 11.51 L, and 9.73 L of water were injected during the three cycles. In cycle 1, there is an indication that breakdown (i.e., fracturing) occurred at 3645 psi. The duration of the MF-4 test, including all three cycles, was approximately 2.5 hours.

Flowback was performed during all three cycles using the pump out module on the RCX tool to increase the rate of pressure decline during the fall-off period (see [Figure 3-14](#)). Flowback was performed for all three cycles after a decline was observed in the pressure recovery rate during natural fall-off. The MF-4 test data were analyzed to determine FCP using the G-function analysis, SRT pressure decline analysis, log-log pressure decline analysis, and P-inflection analysis; all four plots were made using fall-off data. A plot for each of these four techniques is shown in [Figure 3-15](#) (cycle 1), [Figure 3-16](#) (cycle 2), and [Figure 3-17](#) (cycle 3). Indications of fracture closure are present in one or more plots for cycles 2 and 3. In addition, the MF-4 test data were analyzed using the bi-linear pressure decay method ([Figure 3-18](#)). Interpreted FCP values for all these methods are summarized in [Table 3-4](#) and range from 0.52 to 0.60 psi/ft. Of these, the ISIP, determined from the P-inflection method (0.56 to 0.60 psi/ft), are considered to be the most reliable indicator of FCP as discussed in Section 6.4.

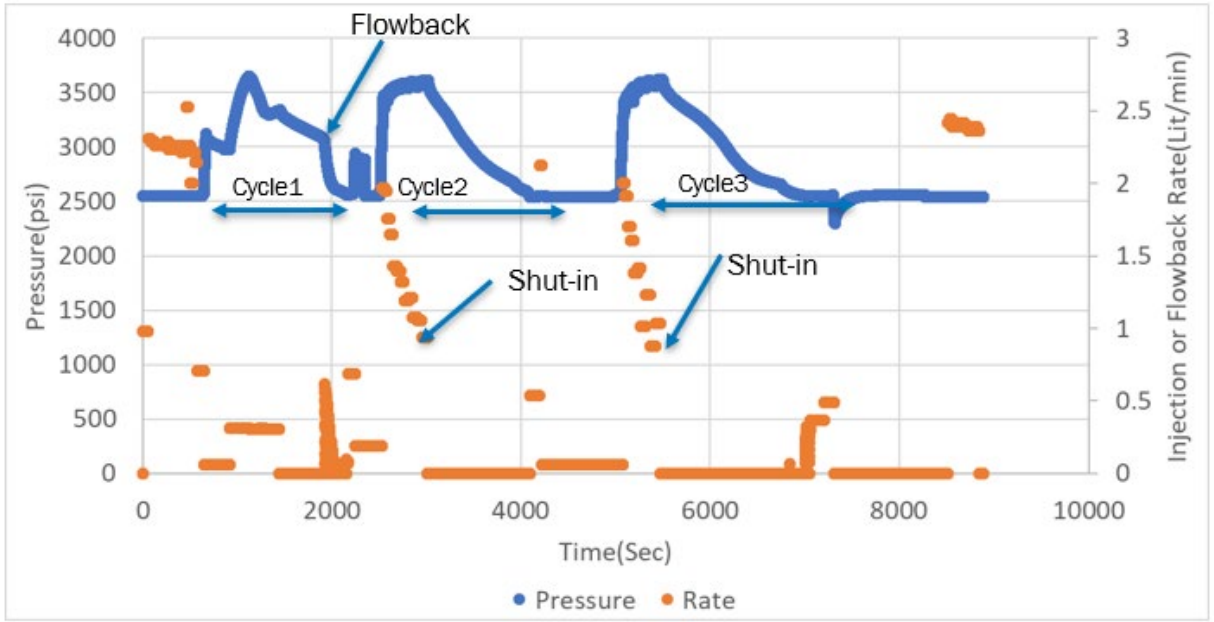


Figure 3-14. Pressure rate plot for the 3 cycles of MF-4.

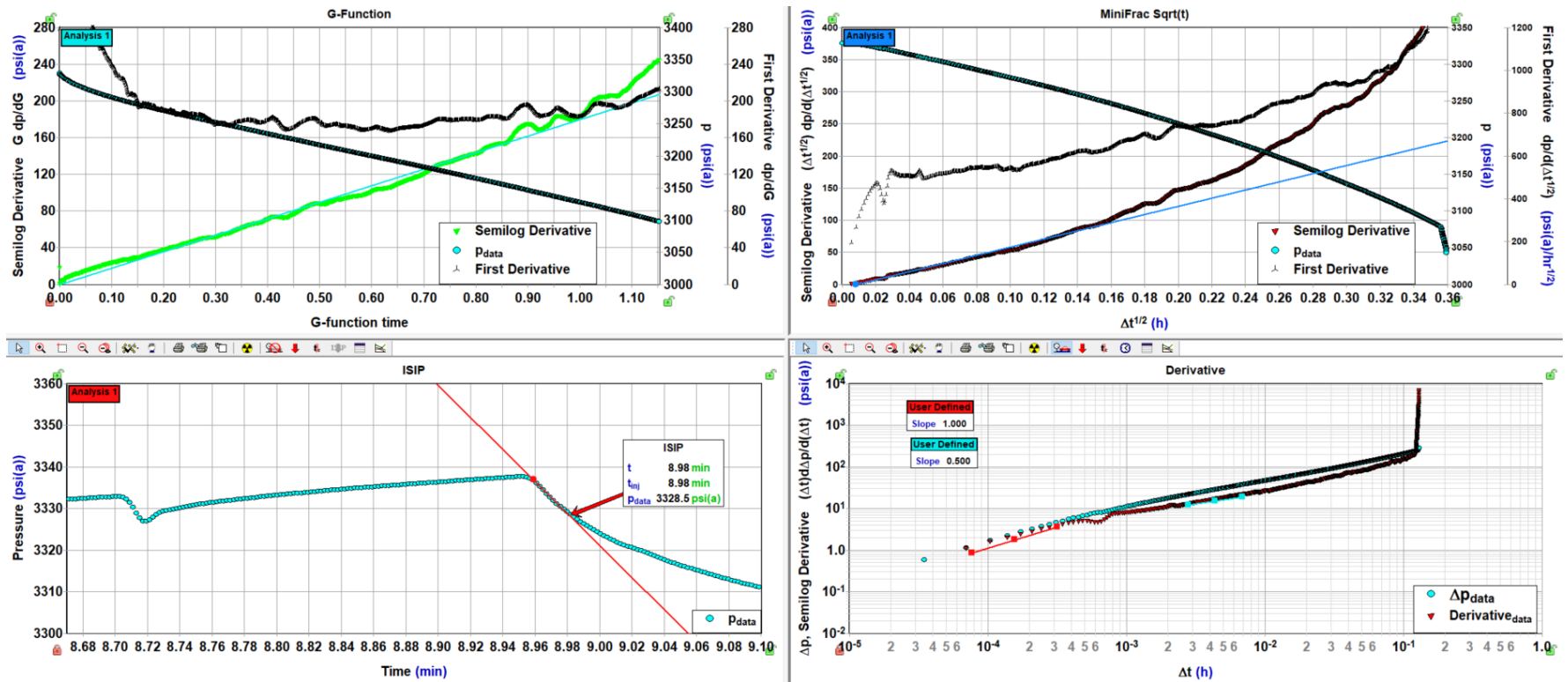


Figure 3-15.G-Function plot (top left), SRT analysis (top right), ISIP (bottom left), derivative plot (bottom right) for MF-4 cycle 1.

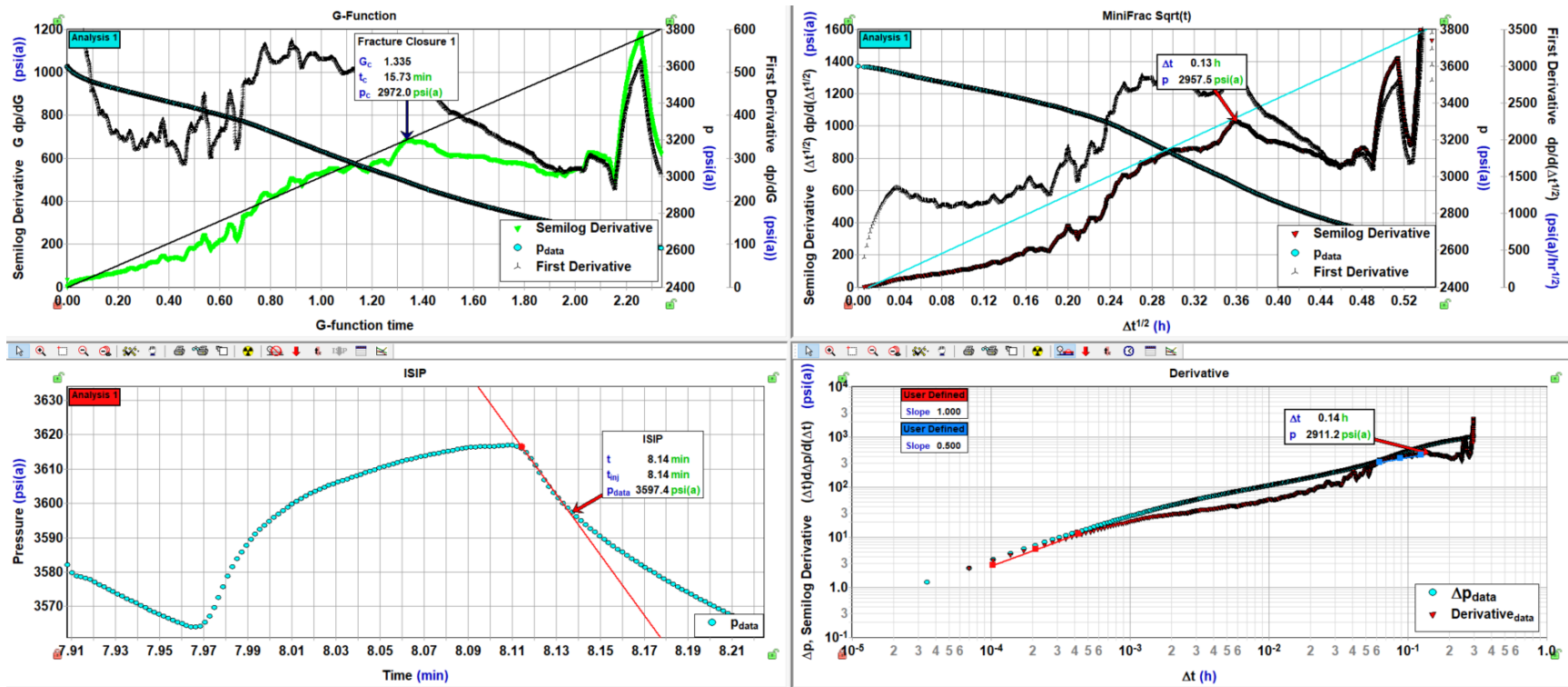


Figure 3-16. G-Function plot (top left), SRT analysis (top right), ISIP (bottom left), derivative plot (bottom right) for MF-4 cycle 2.

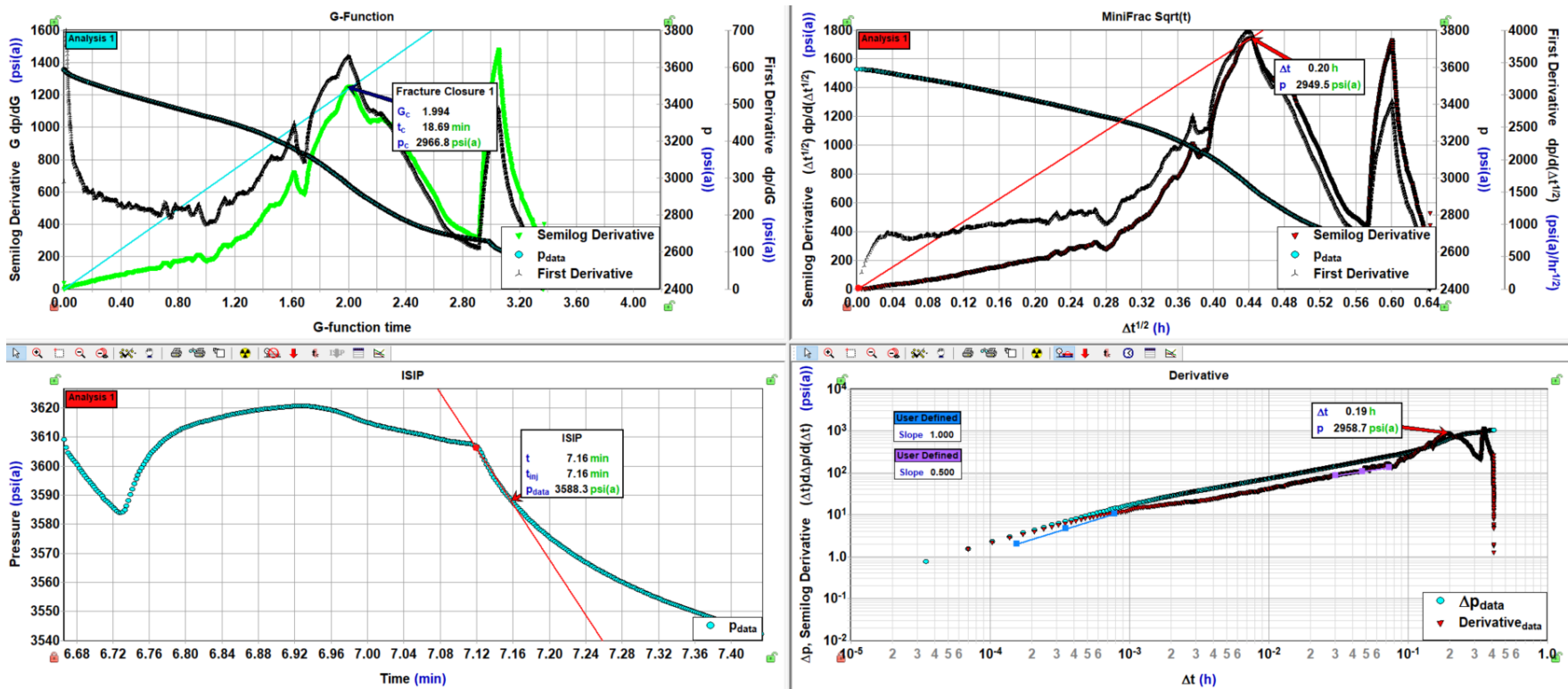


Figure 3-17.G-Function plot (top left), SRT analysis (top right), ISIP (bottom left), derivative plot (bottom right) for MF-4 cycle 3.

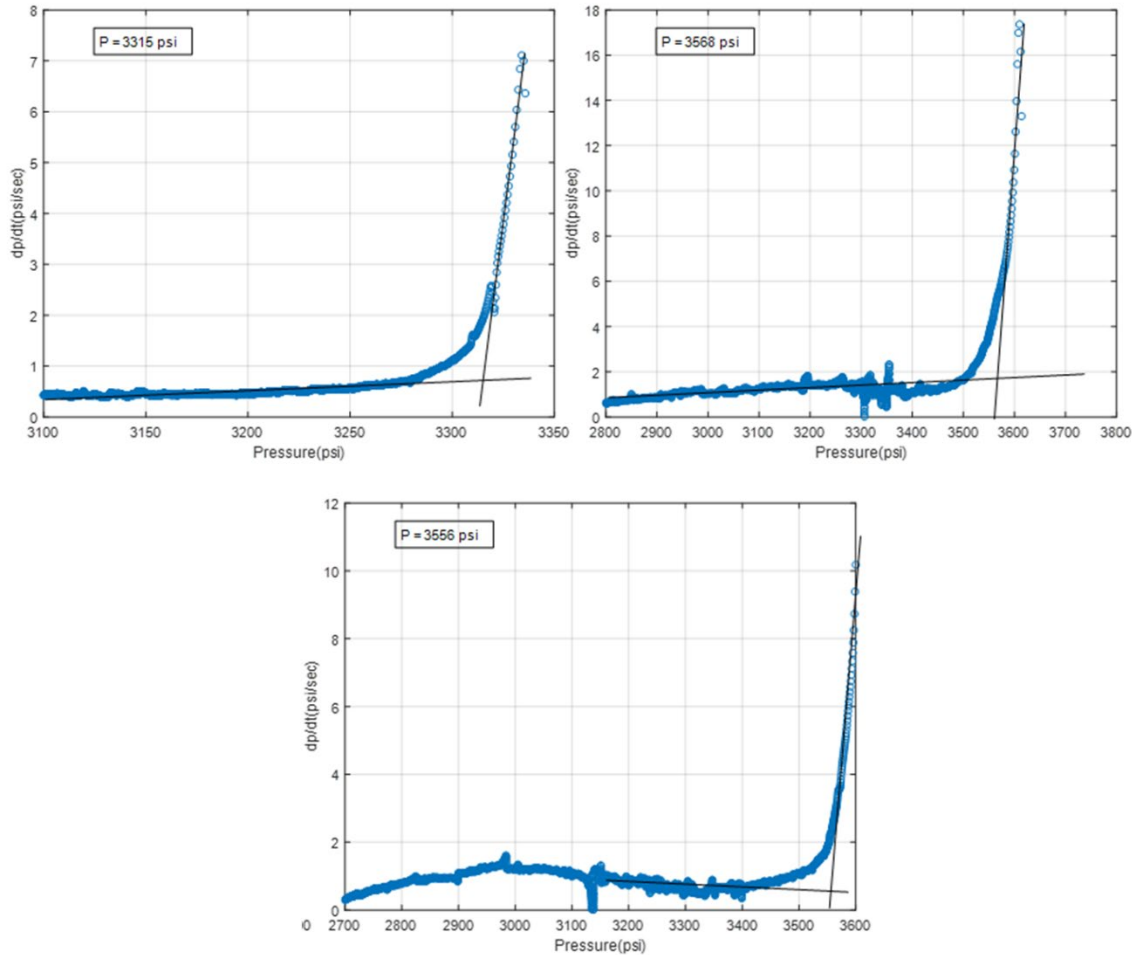


Figure 3-18. Bi-linear analysis for cycle 1 (top left), cycle 2 (top right), and cycle 3 (bottom) of MF-4, which yielded a FCP (ISIP) of 3315 psi (0.56 psi/ft), 3568 psi (0.6 psi/ft), and 3556 psi (0.6 psi/ft), respectively.

Table 3-4. Summary of MF-4 analyses.

Station	Cycle	Depth MD (ft)	Depth TVD (ft)	Breakdown / Re-opening Pressure (psi) and Gradient (psi/ft)		Propagation pressure (psi) and Gradient (psi/ft)		Instantaneous Shut-in (psi) and Gradient (psi/ft)		Bi-linear Pressure (psi) and Gradient (psi/ft)	
MF-4	1	5980	5966.18	3645	0.61	3337	0.56	3328	0.56	3315	0.56
MF-4	2	5980	5966.18	3475V	0.58	3616	0.61	3597	0.60	3568	0.60
MF-4	3	5980	5966.18	3432V	0.58	3619	0.61	3588	0.60	3556	0.60
Station	Cycle	Depth MD (ft)	Depth TVD (ft)	SRT Closure (psi) and Gradient (psi/ft)		Derivative Pressure (psi) and Gradient (psi/ft)		G-Function plot 1 Closure (psi) and Gradient (psi/ft)		G-Function plot 2 Closure (psi) and Gradient (psi/ft)	
MF-4	1	5980	5966.18	NA	NA	NA	NA	NA	NA	NA	NA
MF-4	2	5980	5966.18	2957	0.50	2911	0.49	2972	0.50	NA	NA
MF-4	3	5980	5966.18	2949	0.49	NA	NA	2967	0.50	NA	NA

### 3.5 MF-5

Minifrac test 5 (MF-5) was conducted with the straddle packer centered on a depth of 5919 ft MD (5909.23 ft TVD) in the 16B(78)-32 open borehole. The test included four injection cycles, as shown in Figure 3-19. Cycle 3 was a step-rate test. During cycle 4, the packer seal was lost, so no fracture closure analysis was possible from this cycle. The average injection rate was variable during the injection cycles, at 5.2 cc/sec for cycle 1, 26 cc/sec for cycle 2, 0.33 to 28.33 cc/sec for cycle 3, and 5.3 cc/sec for cycle 4 (cycle 3 was a step-rate test, with five stepped pump rates). A total water volume of 4.02 L, 10.61 L, 8.84 L and 22.44 L were injected into the test interval during the four cycles. In cycle 1, there is an indication that breakdown (i.e., fracturing) occurred at approximately 3915 psi. The duration of the MF-5 test, including all three cycles, was approximately 3 hours.

Flowback was performed during cycles 1 through 3 using the pump out module on BH's RCX tool to speed up pressure decline during the post-injection period (see Figure 3-19). Flowback volumes were 0.88 L (cycle 1), 3.37 L (cycle 2), and 2.37 L (cycle 3).

The MF-5 test data were analyzed to determine FCP using the G-function analysis, SRT pressure decline analysis, log-log pressure decline analysis, and P-inflection (ISIP) analysis; all four plots were made using pressure data from the fall-off period (i.e., before flowback). A plot for each of these four techniques is shown in Figure 3-20 (cycle 1) and Figure 3-21 (cycle 2). Plots are not presented for cycle 3, which was conducted as a step-rate test, and cycle 4, because the packer seal was lost during the fall-off period. In addition, the MF-5 test data (cycles 1 and 2) were analyzed using the bi-linear pressure decay method (Figure 3-22). Clear indications of fracture closure are not present in the G-function plot, SRT plot, or the log-log pressure derivative plot for cycle 1 or cycle 2. Therefore, the ISIP plot and the bi-linear pressure plot are used to estimate FCP. Interpreted FCP values for these methods range from 0.55 to 0.61 psi/ft Table 3-5.

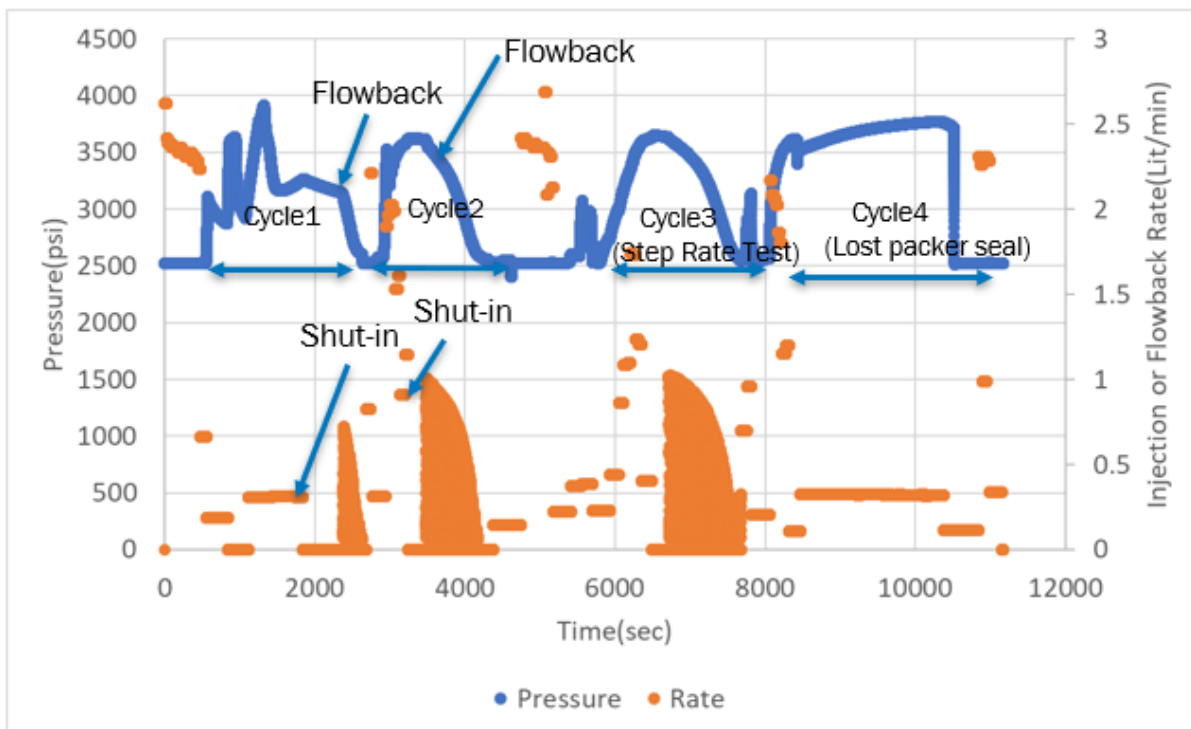


Figure 3-19. Pressure rate plot for the four cycles of Station MF-5.

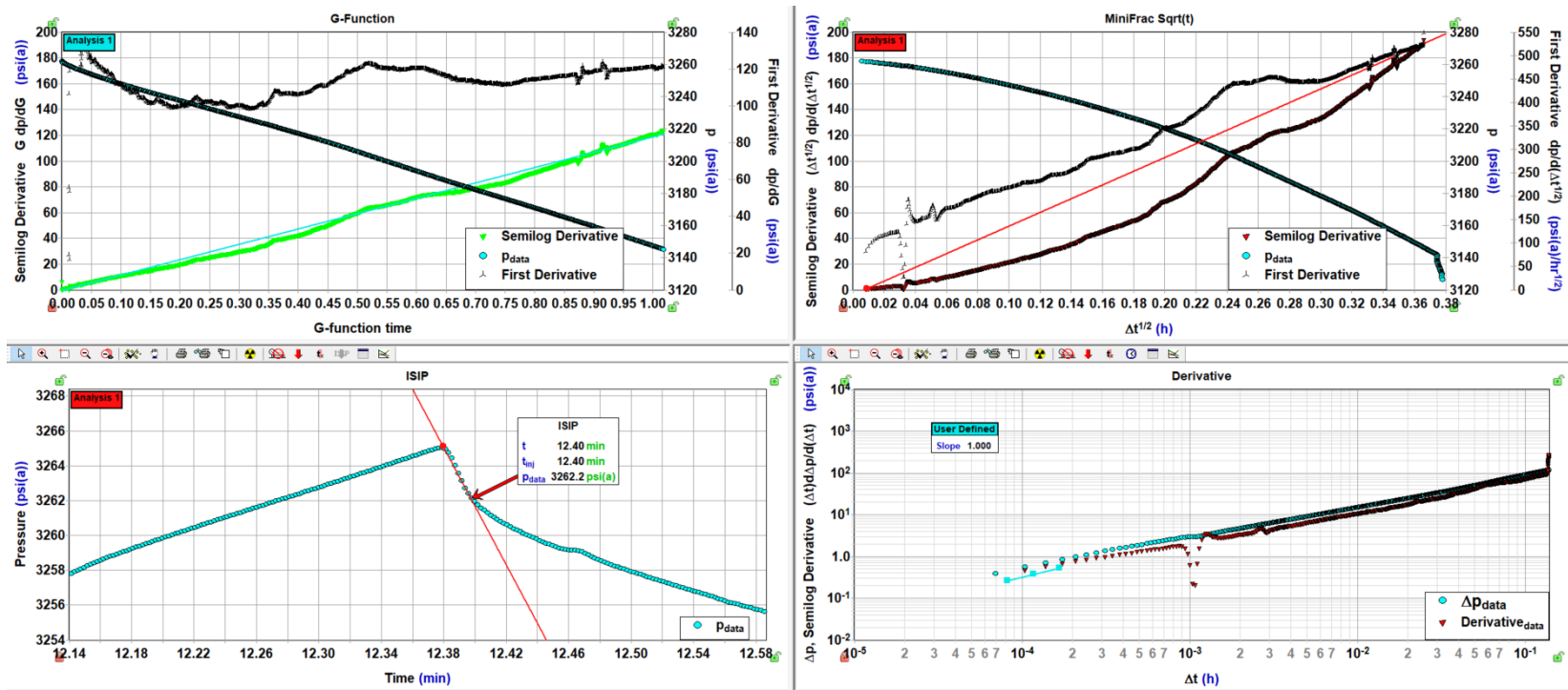


Figure 3-20.G-Function plot (top left), SRT analysis (top right), ISIP (bottom left), derivative plot (bottom right) for MF-5 cycle 1.

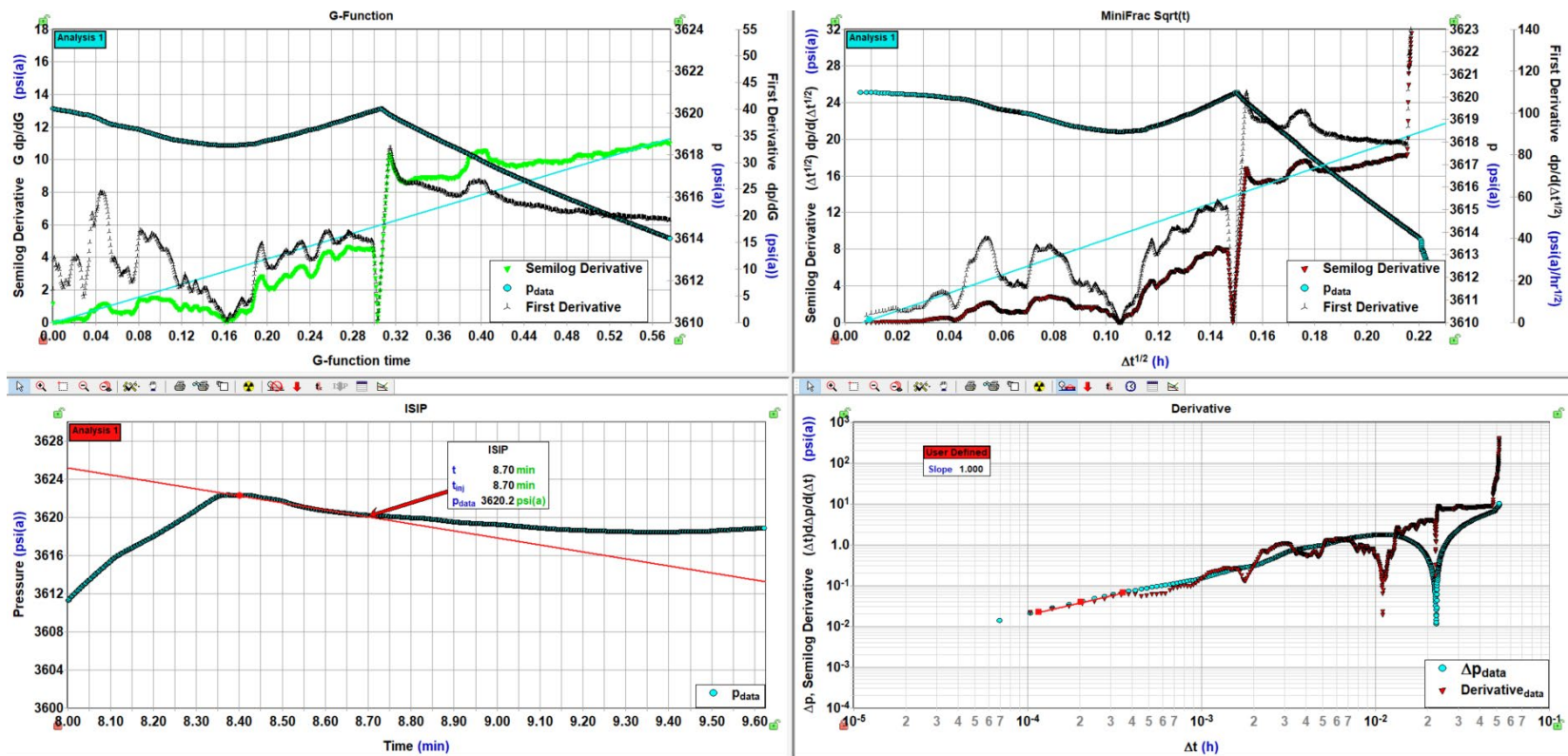


Figure 3-21.G-Function plot (top left), SRT analysis (top right), ISIP (bottom left), derivative plot (bottom right) for MF-5 cycle 2.

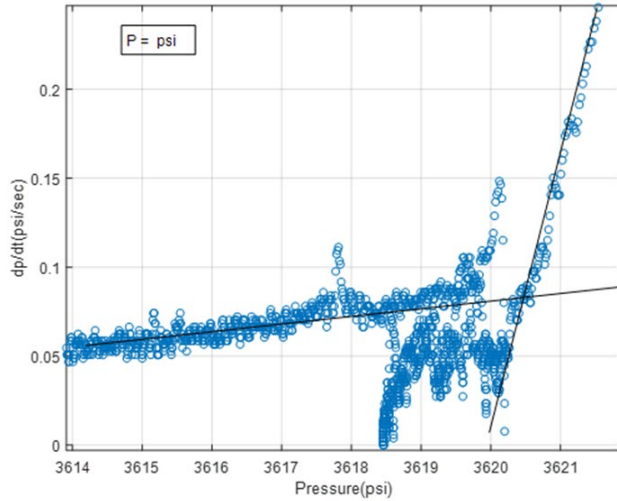
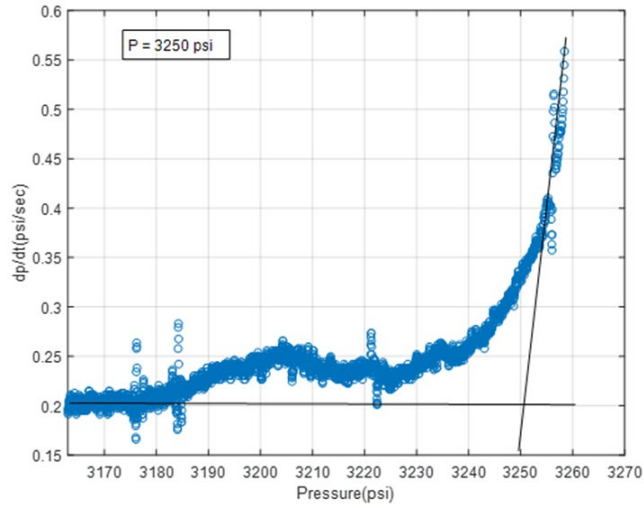


Figure 3-22. Bi-linear analysis for cycle 1 (top) and cycle 2 (bottom) of MF-5, which yielded a FCP (ISIP) of 3250 psi (0.55 psi/ft) for cycle 1. A FCP could not be determined for cycle 2 using the bi-linear method.

Table 3-5. Summary of MF-5 analyses.

Station	Cycle	Depth MD (ft)	Depth TVD (ft)	Breakdown / Re-opening Pressure (psi) and Gradient (psi/ft)		Propagation pressure (psi) and Gradient (psi/ft)		Instantaneous Shut-in (psi) and Gradient (psi/ft)		Bi-linear Pressure (psi) and Gradient (psi/ft)	
MF-5	1	5919	5909	3915	0.66	3265	0.55	3262	0.55	3250	0.55
MF-5	2	5919	5909	3527	0.60	3610	0.61	3620	0.61	ND	ND
Station	Cycle	Depth MD (ft)	Depth TVD (ft)	SRT Closure (psi) and Gradient (psi/ft)		Derivative Pressure (psi) and Gradient (psi/ft)		G-Function plot 1 Closure (psi) and Gradient (psi/ft)		G-Function plot 2 Closure (psi) and Gradient (psi/ft)	
MF-5	1	5919	5909	NA		NA		NA		NA	
MF-5	2	5919	5909	NA		NA		NA		NA	

### 3.6 MF-6

Minifrac test 6 (MF-6) was conducted with the straddle packer centered on a depth of 5639.2 ft MD (5637.64 ft TVD) in the 16B(78)-32 open borehole. The test included three attempted injection cycles, as shown in Figure 3-23, however, only cycles 1 and 3 are valid tests. During cycle 2, the packer failed (lost pressure) and isolation of the test interval was lost. This necessitated pulling out the tool string and replacing the straddle packer with an unused straddle packer before conducting cycle 3. The average injection rate during the injection cycles was 24 cc/sec for cycle 1 and 33 cc/sec for cycle 3. A total water volume of 11.5 L and 7 L were injected into the test interval during cycles 1 and 3, respectively. There is no clear indication that breakdown (i.e., fracturing) occurred in any cycle. Pressure in the test interval increased during injection but then the rate of pressure increase slowed (due in part to a decreasing injection rate) and never resulted in breakdown. Following a short fall-off period, flowback was performed during both cycles 1 and 3 using the pump out module on BH's RCX tool to speed up pressure decline (see Figure 3-23). This resulted in the removal of 1.8 L (cycle 1) and 2.68 L (cycle 3). The duration of the MF-6 test was approximately 1.5 hours.

The MF-6 test data were analyzed to determine FCP using the G-function analysis, SRT pressure decline analysis, log-log pressure decline analysis, and P-inflection (ISIP) analysis; all four plots were made using pressure data from the fall-off period (i.e., before flowback). A plot for each of these four analysis techniques is shown in Figure 3-24 (cycle 1) and Figure 3-25 (cycle 3). Plots are not presented for cycle 2 due to packer failure during the fall-off period. In addition, the MF-6 test data (cycles 1 and 3) were analyzed using the bi-linear pressure decay method (Figure 3-26). Indications of fracture closure are visible in the cycle 1 G-function plot (three events), SRT plot (1 event), and the log-log pressure derivative plot (three events). The pressure gradient for these events ranges from 0.61 to 0.62 psi/ft. However, no indication of fracture closure is observed cycle 2. The ISIP plot and the bi-linear pressure plot suggest a FCP for cycle 2 of 0.60 to 0.61 psi/ft. Interpreted FCP values for these methods are summarized in Table 3-6.

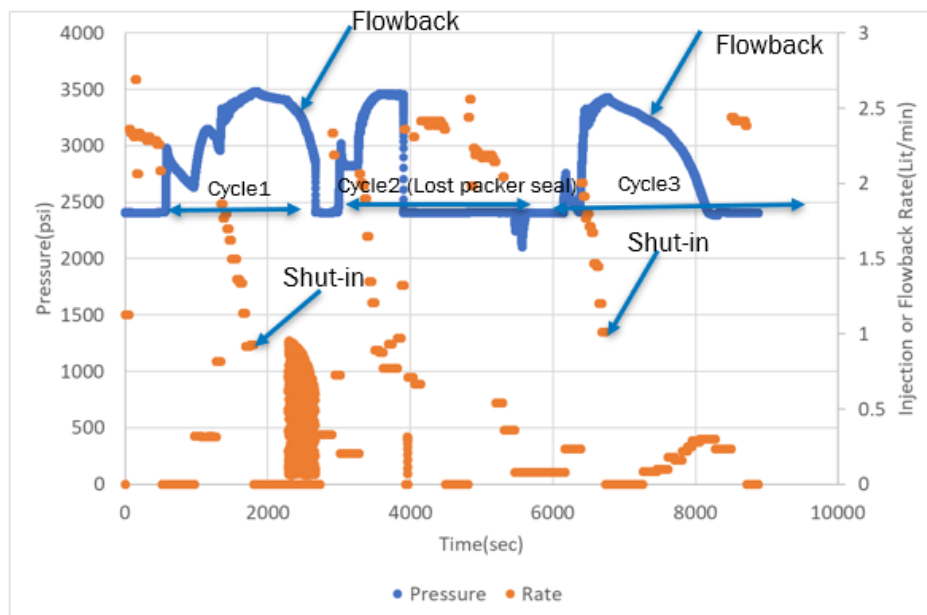


Figure 3-23. Pressure rate plot for the three cycles of MF-6.

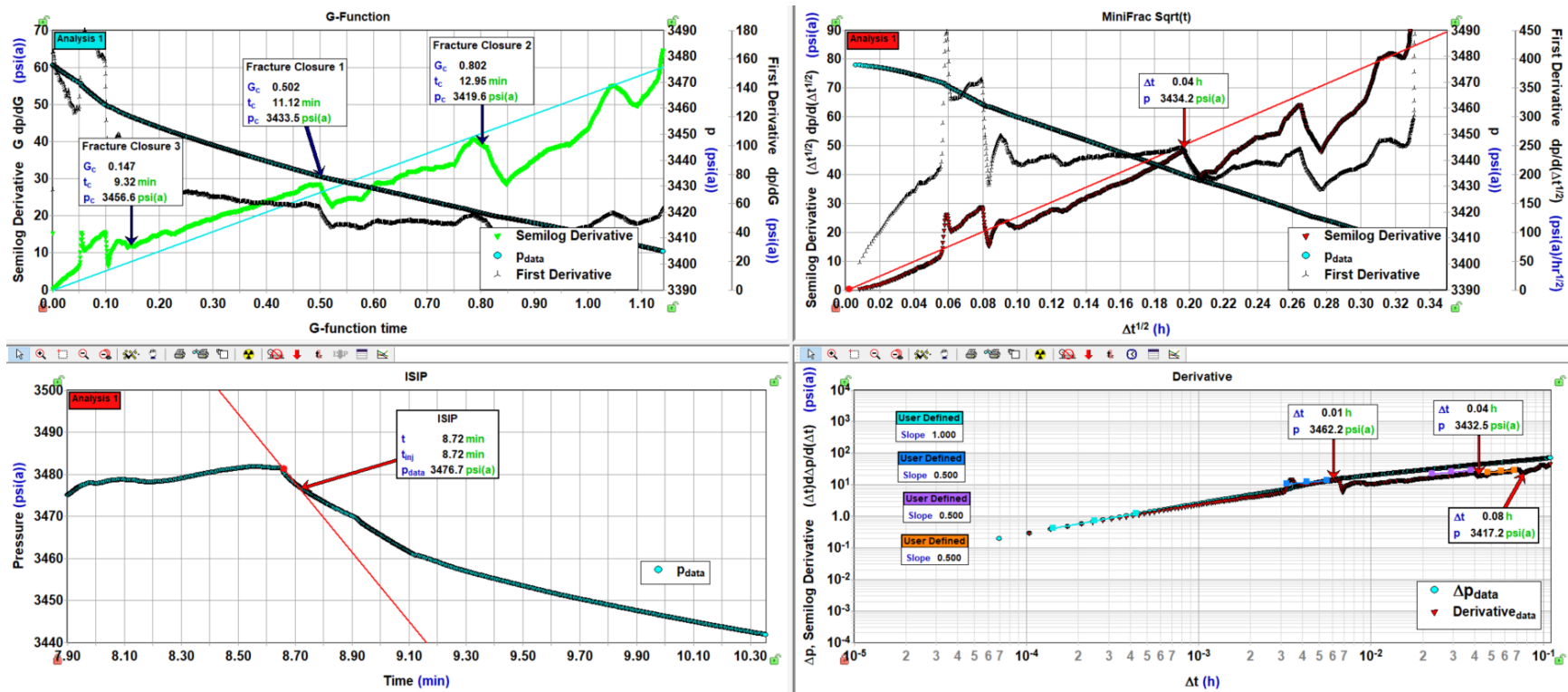


Figure 3-24. G-Function plot (top left), SRT analysis (top right), ISIP (bottom left), derivative plot (bottom right) for cycle 1 of MF-6.

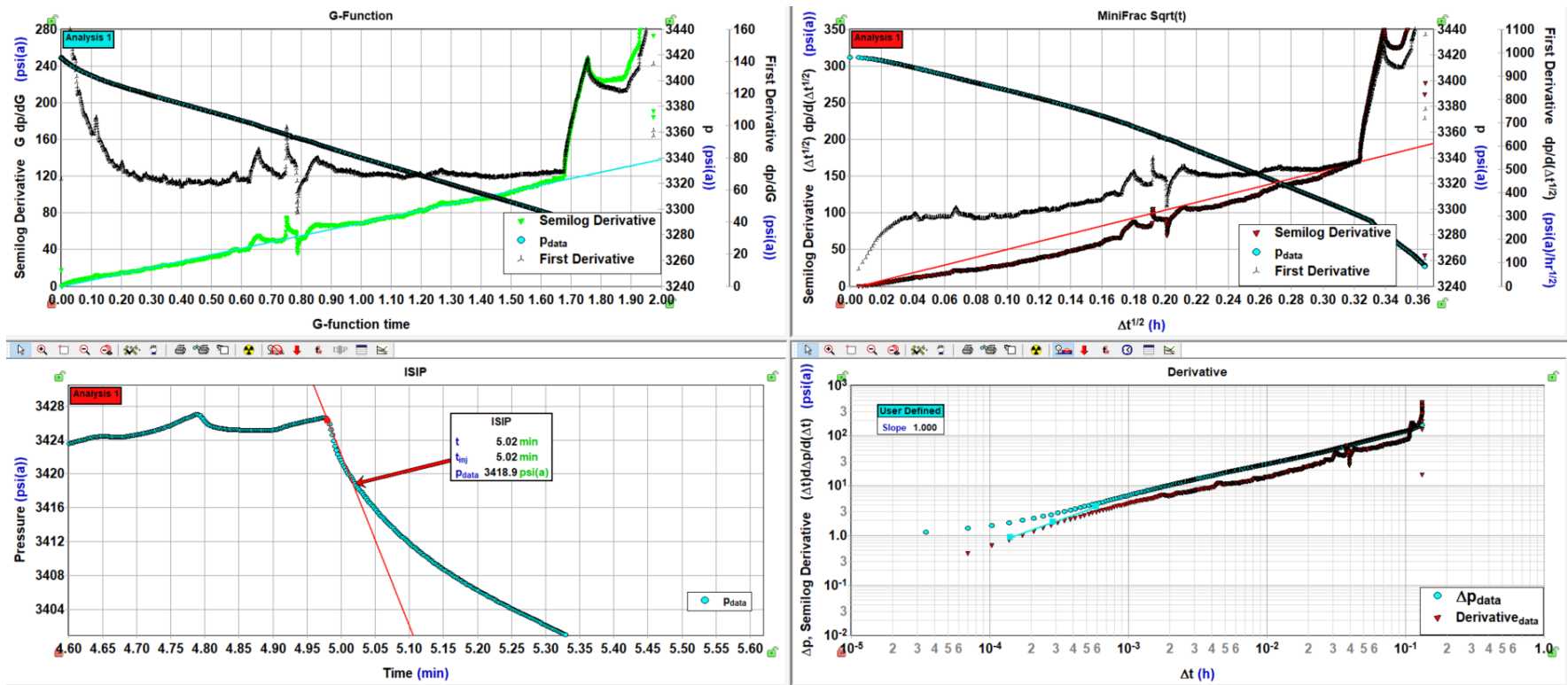


Figure 3-25.G-Function plot (top left), SRT analysis (top right), ISIP (bottom left), derivative plot (bottom right) for cycle 3 of MF-6.

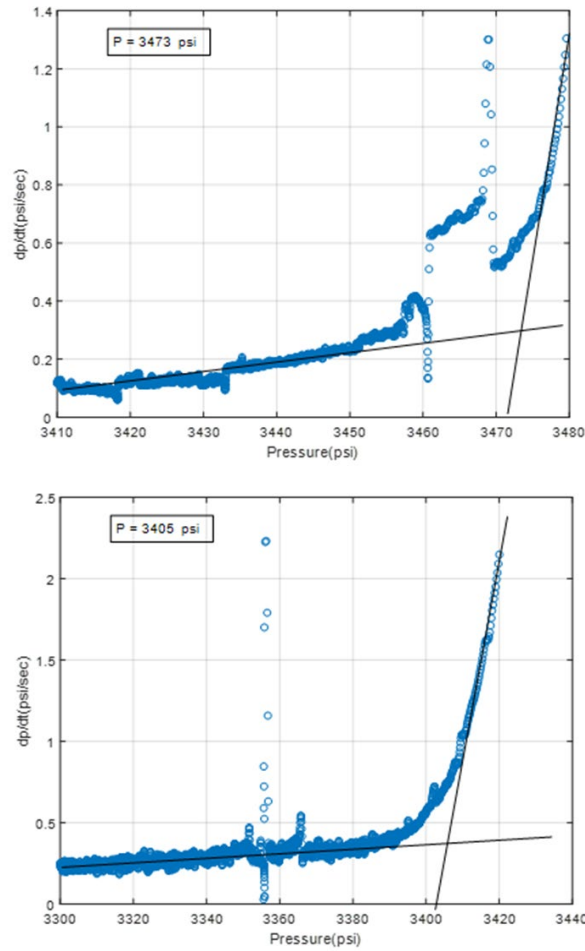


Figure 3-26. Bi-linear analysis for cycle 1 (top) and cycle 3 (bottom) of MF-6, which yielded a FCP (ISIP) of 3473 psi (0.62 psi/ft) and 3405 psi (0.6 psi/ft) for cycle 2.

Table 3-6. Summary of MF-6 analyses.

Station	Cycle	Depth MD (ft)	Depth TVD (ft)	Breakdown / Re-opening Pressure (psi) and Gradient (psi/ft)		Propagation pressure (psi) and Gradient (psi/ft)		Instantaneous Shut-in (psi) and Gradient (psi/ft)		Bi-linear Pressure (psi) and Gradient (psi/ft)							
				NA	NA	3481	0.62	3476	0.62	3473	0.62						
MF-6	1	5639	5637	NA	NA	3481	0.62	3476	0.62	3473	0.62						
MF-6	3	5639	5637	3313V	0.59	3426	0.61	3418	0.61	3405	0.60						
Station	Cycle	Depth MD (ft)	Depth TVD (ft)	SRT Closure (psi) and Gradient (psi/ft)		Derivative Pressure 2 (psi) and Gradient (psi/ft)		Derivative Pressure 3 (psi) and Gradient (psi/ft)		G-Function plot 1 Closure (psi) and Gradient (psi/ft)		G-Function plot 2 Closure (psi) and Gradient (psi/ft)		G-Function plot 3 Closure (psi) and Gradient (psi/ft)			
				3434	0.61	3462	0.61	3432	0.61	3417	0.61	3456	0.61	3433	0.61	3419	0.61
MF-6	1	5639	5637	3434	0.61	3462	0.61	3432	0.61	3417	0.61	3456	0.61	3433	0.61	3419	0.61
MF-6	3	5639	5637	NA		NA	NA	NA	NA	NA	NA	NA	NA	NA	NA	NA	NA

### 3.7 MF-7

Minifrac test 7 (MF-7) was conducted with the straddle packer centered on a depth of 5616 ft MD (5614.67 ft TVD) in the 16B(78)-32 open borehole. The test included three attempted injection cycles, as shown in Figure 3-27. The average injection rate during the injection cycles was 36 cc/sec for cycle 1, 34 cc/sec for cycle 2, and 31 cc/sec for cycle 3. A total water volume of 22.87 L, 28.32 L, and 30 L was injected into the test interval during cycles 1, 2 and 3, respectively. Similar to MF-6, there is no clear indication that breakdown (i.e., fracturing) occurred in any cycle. Pressure in the test interval increased during injection but then the rate of pressure increase slowed (due in part to a decreasing injection rate) and never resulted in breakdown. Following a short fall-off period, flowback was performed during all three cycles to speed up pressure decline (see Figure 3-27). This resulted in the removal of 14.75 L (cycle 1), 21.15 L (cycle 2), and 13 L (cycle 3). The duration of the MF-7 test was approximately 5 hours.

The MF-7 test data were analyzed to determine FCP using the G-function analysis, SRT pressure decline analysis, log-log pressure decline analysis, and P-inflection (ISIP) analysis; all four plots were made using pressure data from the fall-off period (i.e., before flowback). A plot for each of these four techniques is shown in Figure 3-28 (cycle 1), Figure 3-29 (cycle 2), and Figure 3-30 (cycle 3). In addition, the MF-7 test data were analyzed using the bi-linear pressure decay method (Figure 3-31). Indications of fracture closure are visible in the G-function plot, SRT plot, and the log-log pressure derivative plot for cycle 1 and cycle 3, but not for cycle 2. Pressure gradient values for these interpreted closure events range from 0.61 to 0.62 psi/ft. The ISIP plot and the bi-linear pressure plot suggest a FCP for all three cycles of 0.59 to 0.62 psi/ft. Interpreted FCP values for these methods are summarized in Table 3-7.

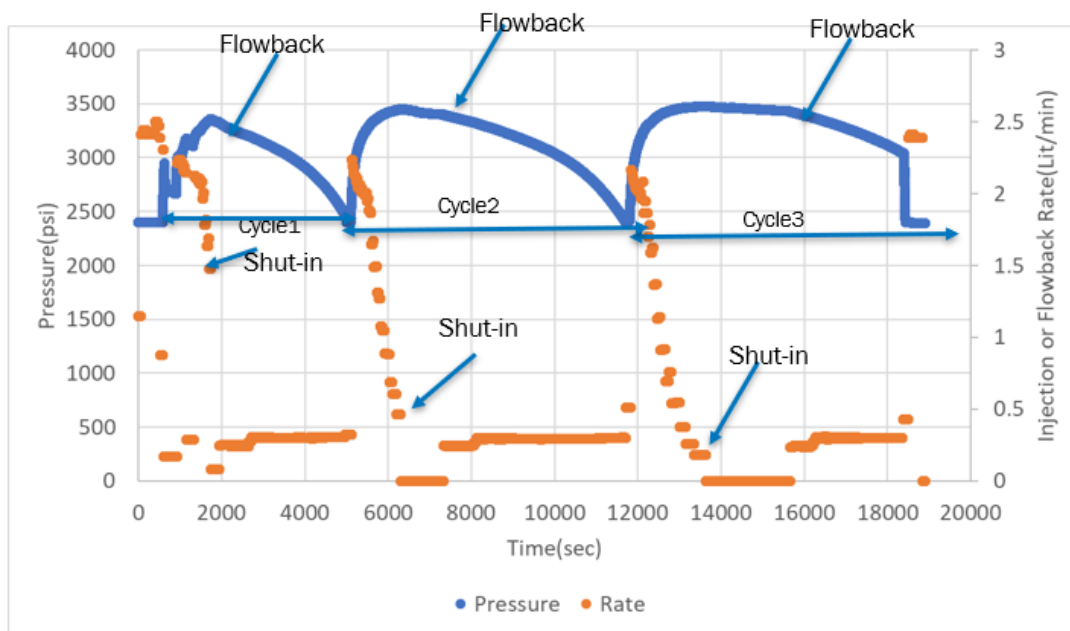


Figure 3-27. Pressure rate plot for the three cycles of MF-7.

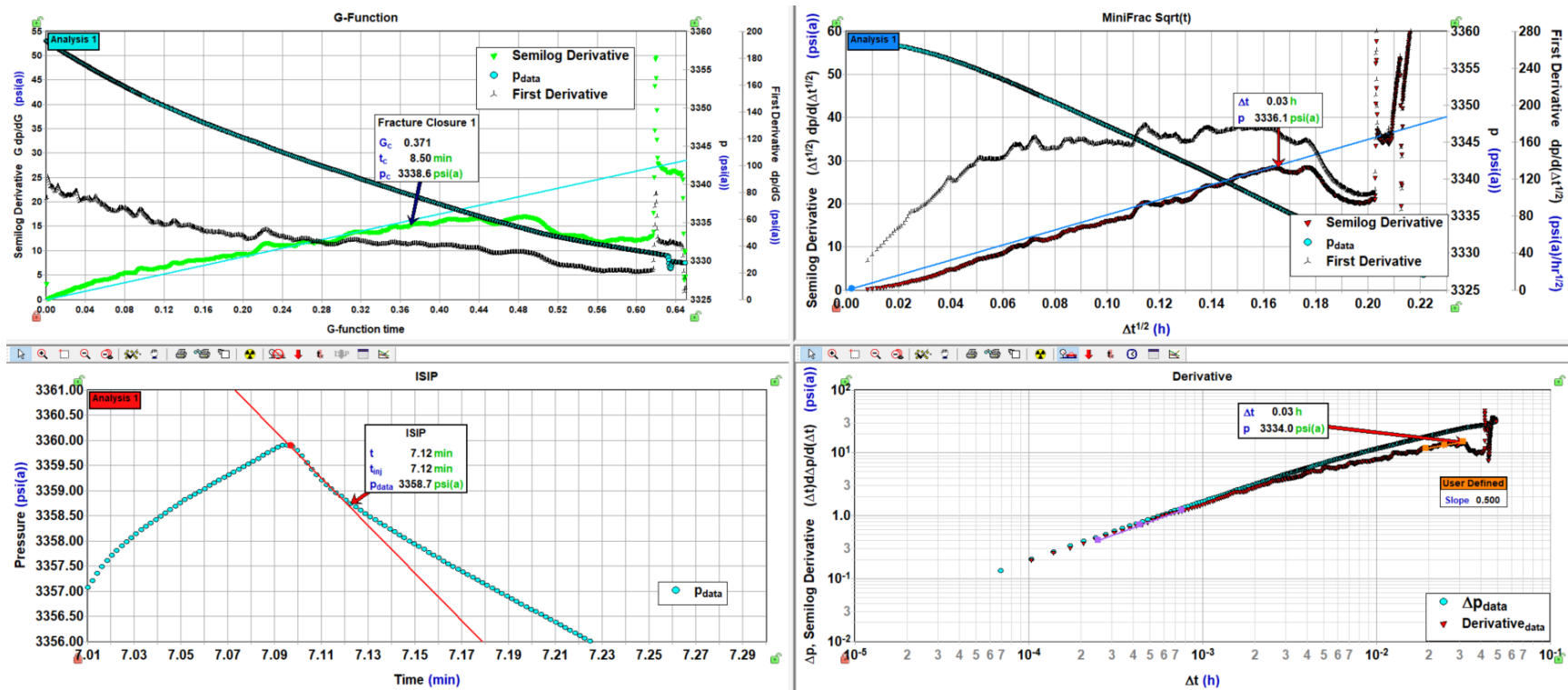


Figure 3-28.G-Function plot (top left), SRT analysis (top right), ISIP (bottom left), derivative plot (bottom right) for cycle 1 of MF-7.

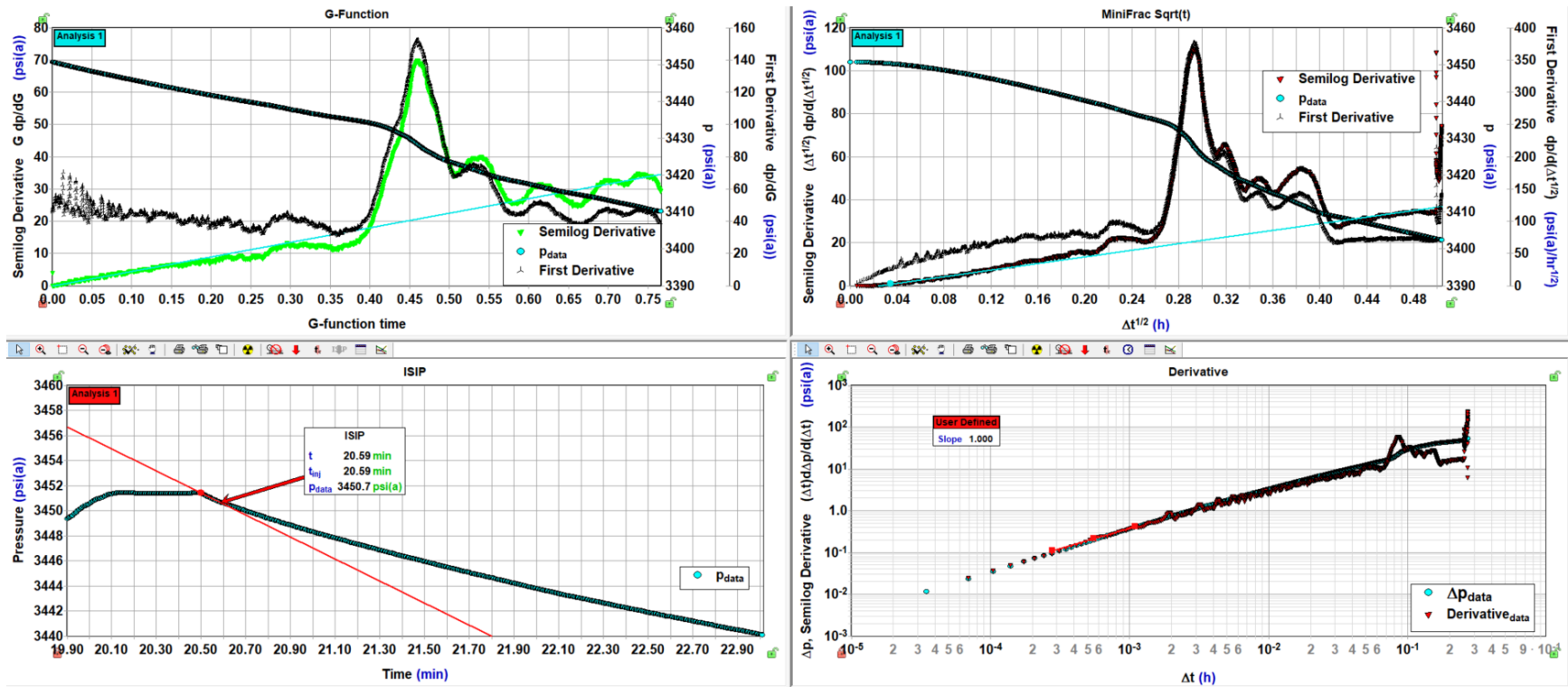


Figure 3-29. G-Function plot (top left), SRT analysis (top right), ISIP (bottom left), derivative plot (bottom right) for cycle 2 of MF-7.

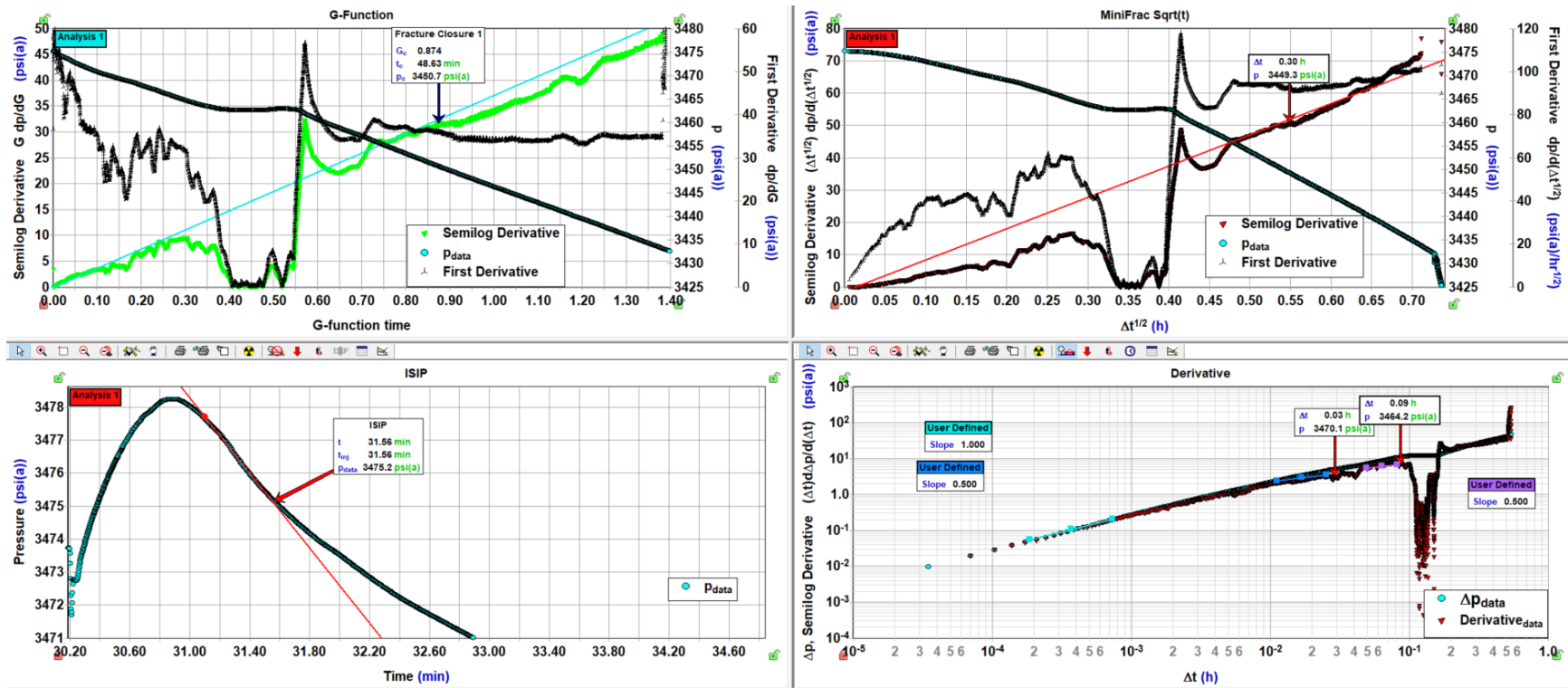


Figure 3-30. G-Function plot (top left), SRT analysis (top right), ISIP (bottom left), derivative plot (bottom right) for cycle 3 of MF-7.

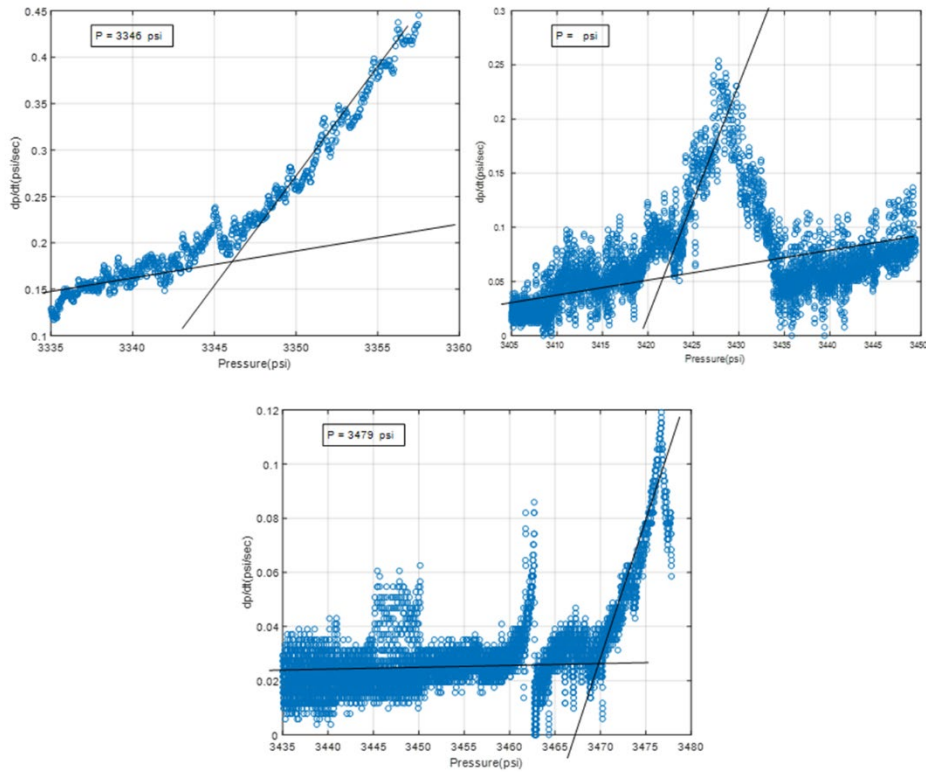


Figure 3-31. Bi-linear analysis for cycle 1 (top left), cycle 2 (top right), and cycle 3 (bottom) of MF-7.

Table 3-7. Summary of MF-7 analyses.

Station	Cycle	Depth MD (ft)	Depth TVD (ft)	Breakdown / Re-opening Pressure (psi) and Gradient (psi/ft)		Propagation pressure (psi) and Gradient (psi/ft)		Instantaneous Shut-in (psi) and Gradient (psi/ft)		Bi-linear Pressure (psi) and Gradient (psi/ft)	
MF-7	1	5616	5614	NA	NA	3359	0.60	3359	0.60	3346	0.6
MF-7	2	5616	5614	2933v	0.52	3451	0.61	3450	0.61	NA	NA
MF-7	3	5616	5614	2933v	0.52	3478	0.62	3475	0.62	3479	0.62
Station	Cycle	Depth MD (ft)	Depth TVD (ft)	SRT Closure (psi) and Gradient (psi/ft)		Derivative Pressure (psi) and Gradient (psi/ft)		G-Function plot 1 Closure (psi) and Gradient (psi/ft)		G-Function plot 2 Closure (psi) and Gradient (psi/ft)	
MF-7	1	5616	5614	3361	0.6	3334	0.59	3339	0.59	NA	
MF-7	2	5616	5614	NA	NA	NA	NA	NA	NA	NA	
MF-7	3	5616	5614	3449	0.61	3470	0.62	3451	0.61	NA	

### 3.8 Summary of Shmin Magnitude

#### 3.8.1 Summary of Mini-frac Test Results

Parameters determined from analysis of the seven minifrac tests are summarized in Table 3-8. This is the same information that was previously presented in Table 3-1 (MF-1) through Table 3-7 (MF-7).

Results include breakdown pressure, re-opening pressure, propagation pressure, and multiple estimates of closure pressure (i.e., from SRT analysis, pressure-derivative analysis, G-function analysis, inflection point [ISIP] analysis, and bi-linear inflection analysis).

Of the seven minifrac tests conducted, MF-2 had a pressure response that most closely mimics a typical minifrac test. The pressure response for MF-2 strongly indicates that breakdown occurred, analysis of the test data yielded multiple estimates of closure pressure that are in close agreement, and image logs obtained after the minifrac test show a fracture that is not present in the pre-test image logs. Estimated closure pressure for MF-2, considering all methods of analysis and all test cycles, range from 0.56 psi/ft to 0.6 psi/ft.

The pressure response for MF-4 also indicates breakdown occurred during this test, although the image logs do not reveal a newly created fracture. Estimated closure pressure for MF-4, considering all methods of analysis and all test cycles, range from 0.49 psi/ft to 0.6 psi/ft. Of these, the ISIP and the FCP determined from the bi-linear method (0.56 to 0.60 psi/ft) are considered to be the most reliable estimates of FCP for MF-4.

Based on the pressure response during MF-5, breakdown may also have occurred during this test. However, similar to MF-4, the image logs do not provide evidence that a fracture was created during the test. Furthermore, clear indications of fracture closure are not present in the G-function plot, SRT plot, or the log-log pressure derivative plot (for the two cycles analyzed, cycle 1 and cycle 2). Therefore, the ISIP plot and the bi-linear pressure plot are used to estimate FCP. Interpreted FCP values for these methods are summarized in [Table 3-8](#) and range from 0.55 to 0.61 psi/ft.

**Table 3-8. Summary of mini-frac test analysis parameters.**

MF Test #/ Cycle #	Breakdown Press (psi); gradient (psi/ft)	Re-opening (psi); gradient (psi/ft)	Propagation (psi); gradient (psi/ft)	Closure Pressure Estimates (psi and psi/ft)						
				ISIP	Bi	SRT	P-Der1	P-Der2, P-Der3	G1	G2, G3
MF-1/1	---	---	---	4536 (0.8)	4526 (0.8)	--	--	--	--	--
MF-1/2	---	3751 (0.66)	---	4421 (0.78)	4423 (0.78)	--	--	--	--	--
MF-2/1	3531 (0.64)	---	3328 (0.61)	3312 (0.6)	3288 (0.6)	3260 (0.59)	3235 (0.59)	--	3270 (0.6)	3211 (0.58)
MF-2/2	---	3194 (0.58)	3258 (0.59)	3249 (0.59)	3237 (0.59)	3214 (0.59)	3184 (0.58)	3092 (0.6)	3179 (0.58)	3088 (0.56)
MF-2/3	---	3116 (0.57)	3330 (0.61)	3327 (0.61)	3323 (0.6)	3300 (0.6)	3275 (0.6)	--	3312 (0.6)	3281 (0.6) 3275 (0.6)
MF-3/1	---	---	2750 (0.53)	2747 (0.53)	2745 (0.53)	2731 (0.53)	2728 (0.52)	--	2738 (0.53)	2724 (0.52) 2711 (0.52)
MF-3/2	---	2625 (0.5)	2898 (0.56)	2891 (0.56)	2853 (0.55)	2838 (0.55)	2845 (0.55)	--	2836 (0.55)	--
MF-3/3	Footnote (a)									
MF-3/4	Footnote (a)									
MF-4/1	3645 (0.61)	---	3337 (0.56)	3328 (0.56)	3315 (0.56)	---	--	--	--	--
MF-4/2	---	3475 (0.58)	3616 (0.61)	3597 (0.6)	3568 (0.6)	2957 (0.5)	2911 (0.49)	--	2972 (0.5)	--
MF-4/3	---	3432 (0.58)	3619 (0.61)	3588 (0.6)	3556 (0.6)	2949 (0.49)	--	--	2967 (0.5)	--
MF-5/1	3915 (0.66)	---	3265 (0.55)	3262 (0.55)	3250 (0.55)	--	--	--	--	--
MF-5/2	---	3527 (0.60)	3610 (0.61)	3620 (0.61)	---	--	--	--	--	--
MF-5/3	Footnote (b)									
MF-5/4	Footnote (c)									

**Table 3-8. Summary of minifrac test analysis parameters. (Continued)**

MF Test #/ Cycle #	Breakdown Press (psi); gradient (psi/ft)	Re-opening (psi); gradient (psi/ft)	Propagation (psi); gradient (psi/ft)	Closure Pressure Estimates (psi and psi/ft)						
				ISIP	Bi	SRT	P-Der1	P-Der2, P-Der3	G1	G2, G3
MF-6/1	---	---	3481 (0.62)	3476 (0.62)	3473 (0.62)	3434 (0.61)	3462 (0.61)	3432 (0.61) 3417 (0.61)	3456 (0.61)	3433 (0.61) 3419 (0.61)
MF-6/2	Footnote (d)									
MF-6/3	---	3313 (0.59)	3426 (0.61)	3418 (0.61)	3405 (0.60)	--	--	--	--	--
MF-7/1	---	---	3359 (0.6)	3359 (0.6)	3346 (0.6)	3361 (0.6)	3334 (0.59)	---	3339 (0.59)	---
MF-7/2	---	2933 (0.52)	3451 (0.61)	3450 (0.61)	---	---	---	---	---	---
MF-7/3	---	2933 (0.52)	3478 (0.62)	3475 (0.62)	3479 (0.62)	3449 (0.61)	3470 (0.62)	---	3451 (0.61)	---

- (a). cycles 3 and 4 of MF-3 were rebound tests.
- (b). cycle 3 of MF-5 was a step-rate test.
- (c). cycle 4 of MF-5 was not analyzed because packer lost seal during test.
- (d). cycle 2 of MF-6 was not analyzed because packer lost seal during test.

### 3.8.2 Shmin Magnitude Adjusted for Cooling during Minifrac Testing

In order to protect the minifrac test equipment from exposure to potentially-damaging temperatures, the borehole was cooled prior to conducting minifrac tests by circulating borehole fluid through chillers at the surface. This reduced the temperature of the rock and may have resulted in a corresponding reduction in the breakdown pressure and closure pressure. Consequently, an adjustment to the estimated closure pressure(s) may be warranted to account for the effect of cooling.

The following procedure was used to estimate the impact of cooling on fracture closure pressure:

- (1) estimate induced fracture radius due to minifrac test;
- (2) estimate the difference between rock temperature at fracture half radius and far field ambient formation temperature; and,
- (3) estimate stress changes due to cooling using a linear thermoelastic model.

Two scenarios were considered, including a non-leaky fracture (no leakoff scenario) and a leaky fracture (high leakoff scenario).

#### 3.8.2.1 No Leakoff Scenario

To estimate the potential impact of temperature on fracture closure pressure, the fracture extension into the formation (fracture radius) needs to be determined first. Two simple models were used to estimate the extension of fracture into formation. The first model assumes a radial (penny shaped) fracture developed as a result of the minifrac test. The radial fracture grows from a point source assuming there is no barrier constraining height growth. Also, there is no fluid leakoff into the formation in this model. Equation 3-1 was used to estimate fracture radius using the no leakoff assumption (Economides and Nolte, 1989):

$$R = 0.52 * \left( \frac{E' * q^3}{\mu} \right)^{\frac{1}{9}} * t^{\frac{4}{9}} \quad \text{Equation 3-1}$$

$$E' = \frac{E}{1-\nu^2} \quad \text{Equation 3-2}$$

where:

$R$  is fracture radius (m),

$E'$  is plane stress modulus (Pa),

$E$  is Young's modulus (Pa),

$\nu$  is Poisson ratio,

$q$  is injection rate (m<sup>3</sup>/sec),

$t$  is injection time (sec), and

$\mu$  is fluid viscosity (Pa-sec).

Station MF-2 minifrac test data were used to estimate fracture radius because the post minifrac test image log detected a fracture in this test interval created by the minifrac test. The longest injection interval during the MF-2 test (1320 sec [22 minutes] in cycle 3 of Station MF-2) was used as injection time. Injection rate during the test cycle was 5 cc/sec (5e-6 m<sup>3</sup>/sec). Additional parameters include an average Young's Modulus of 55 GPa (55e+9 Pa), a Poisson ratio of 0.3, and a fluid viscosity of 10e-3 Pa-s. The estimated fracture radius using the above-mentioned equation and assumptions is 7.3 m (~24 ft).

### 3.8.2.2 High Leakoff Scenario

The second model assumes again a radial (penny shaped) fracture development as a result of a minifrac test, but there is a large amount of fluid leakoff into the formation in this scenario. Equation 3-3 was used to estimate fracture radius using the high leakoff assumption (Economides and Nolte, 1989):

$$R = \frac{1}{\pi} \left( \frac{q^2 * t}{C_L^2} \right)^{1/4} \quad \text{Equation 3-3}$$

where:

$C_L$  is leak-off coefficient (m/srt(sec)).

Station MF-2 minifrac test data were again used to estimate fracture radius. The total injection time including all three cycles of Station MF-2 (2400 sec [40 minutes]) was used as the injection time assuming all injection contributes to generating a fracture. An injection rate of 5 cc/sec (5e-6 m<sup>3</sup>/sec) was used based on test data. A leakoff coefficient of 10e-4 m/srt(sec) was assumed. The estimated fracture radius using Equation 3-2 and assumptions for the high leakoff scenario is 0.5 m (1.6 ft).

The no leakoff scenario (Equation 3-1) assumes that all injected fluid went into the fracture and contributed to making a larger fracture radius. Conversely, the leakoff dominating fracture model (Equation 3-2) assumes that (depending on leakoff coefficient value) a portion of the injected fluid enters the formation when injecting. This might be due to the presence of natural fractures or other features capable of transmitting fluid (e.g., foliations). As a result, the fracture radius is much smaller when leakoff is high compared to when there is no leakoff (1.6 ft radius compared to 24 ft radius).

Next, the temperature change in the formation due to cooling in the borehole was estimated using thermal simulations conducted by DrillCool. Due to the fluid circulation before the minifrac tests, the well and corresponding rock at the wellbore wall have a lower temperature compared to the formation further away from the wellbore. Table 3-9 shows the average temperature at each of the seven minifrac test stations during the test as measured by the downhole temperature sensor in BH's RCX straddle packer test tool.

**Table 3-9. Average measured temperature for each station during the mini-frac tests.**

Station	Depth (ft)	Temperature (F)	RCX Deployment (Run) # and Date
MF-1	5657	231.6	1 <sup>st</sup> Run June 28
MF-2	5495	232.1	1 <sup>st</sup> Run June 28
MF-3	5202	229.7	1 <sup>st</sup> Run June 28
MF-4	5980	263	2 <sup>nd</sup> Run July 1 -2
MF-5	5919	265	2 <sup>nd</sup> Run July 1 -2
MF-6	5639	260	2 <sup>nd</sup> Run July 1 -2
MF-7	5616	262	2 <sup>nd</sup> Run July 1 -2

The modeled temperature profile extending away from the wellbore was estimated using formation thermal properties, measured borehole temperatures at the injection intervals during the minifrac tests, and far field (ambient) temperature at each test depth using available regional temperature gradient measured in wells drilled at the Utah FORGE site (Allis et al., 2018).

Figure 3-32 shows modeled temperature profile extending into the formation for run 1 (Stations MF-1, MF-2, MF-3), and run 2 (Stations MF-3, MF-5, MF-6, MF-7) using thermal simulation results.

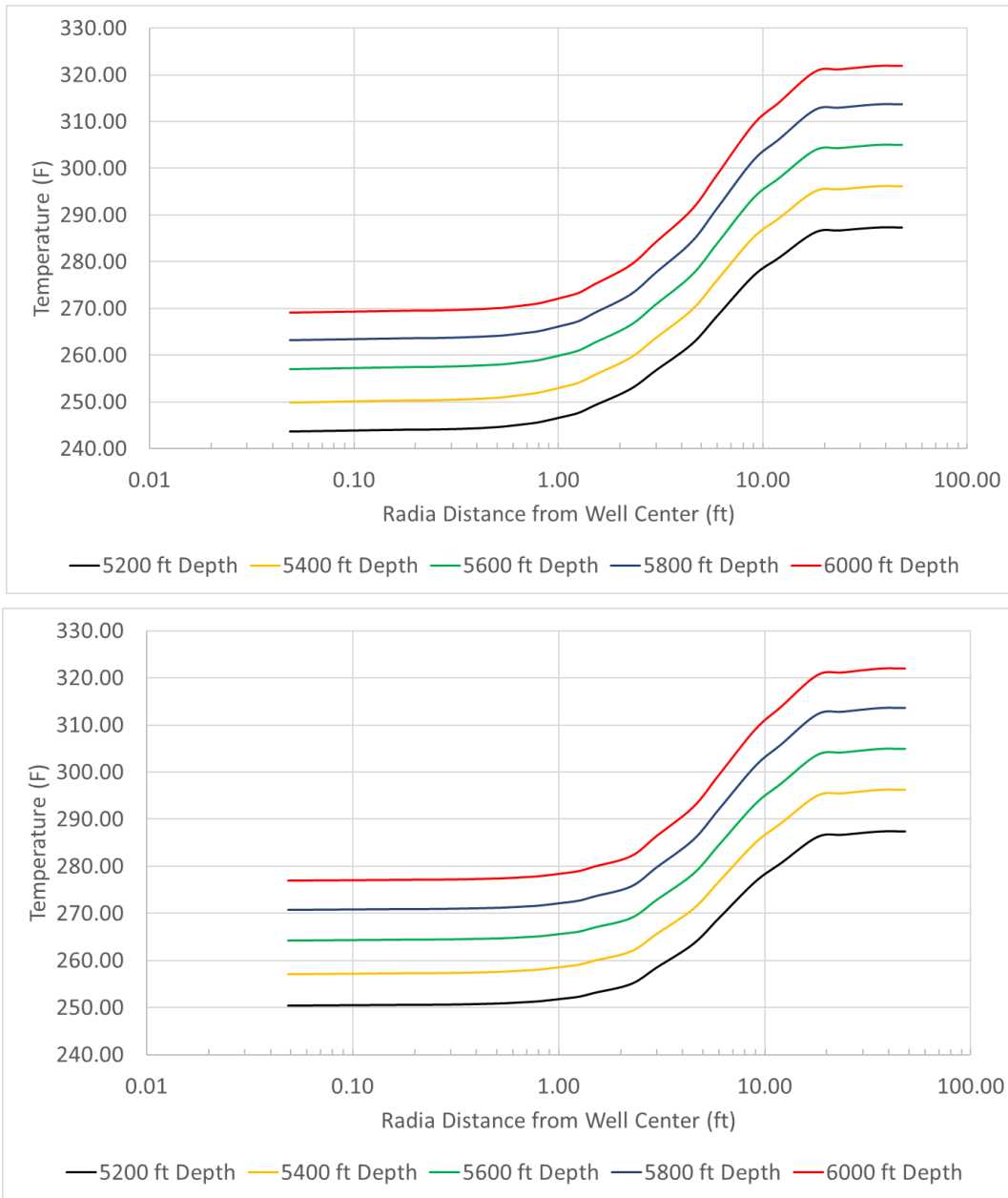


**Figure 3-32. Modeled temperature profile at multiple depths in run 1 (top) and run 2 (bottom). Note that 0.4 ft is distance from borehole center to borehole wall.**

As Figure 3-32 shows, temperature starts to increase ~0.8 ft from wellbore center, and rapidly reaches the ambient temperature for intact formation temperature ~20 to 30 ft away from the wellbore. The expected fracture radius using no leakoff and high leakoff assumptions will be in this region. Using the estimated fracture radius from the previous step, the amount of temperature cooling in the fracture (at a distance of half fracture radius) can be determined for both the high leakoff scenario ( $R=1.6$  ft) and the no leakoff scenario ( $R=24$  ft). To illustrate, for a depth of 5200 ft (similar to MF-3 depth), Figure 3-32 (top plot) indicates that ~40 °F cooling (285-245 °F) would be expected at the fracture half radius  $R/2=0.8$  ft ( $R=1.6$  ft) assuming high leakoff, whereas only ~6 °F (285-279 °F) of cooling would be expected

at the fracture radius of R/2=12 ft (R=24 ft) assuming no leakoff. Note that the fracture R values calculated with Equation 3-1 and Equation 3-3 describe the length of the fracture from the borehole wall; therefore, 0.4 ft needs to be added to the R/2 values to determine the half-radius distance from borehole center in Figure 3-32. The temperature difference between fracture half radius and ambient formation temperature for run 2 was obtained in a similar manner to the run 1 example using modeled temperature profiles shown in the bottom plot in Figure 3-32.

The last step involves calculating a temperature correction to closure pressure and corresponding Shmin using the estimated fracture radius and temperature difference. A linear thermoelastic model (Equation 3-4) was used to estimate thermal effect on stress (Zoback, 2010):

$$\Delta\sigma = \frac{E \cdot \alpha \cdot \Delta T}{1 - \nu} \quad \text{Equation 3-4}$$

where:

$\Delta\sigma$  is stress correction (psi),

$\alpha$  is linear coefficient of thermal expansion (1/°F), and

$\Delta T$  is temperature difference between intact rock and fracture half radius (°F).

Poisson ratio ( $\nu$ ) and Young’s modulus (E) were obtained from the mechanical property depth profiles for well 16B(78)-32 as input (Figure 3-33). Density and sonic slowness from well 16B(78)-32 were used to estimate dynamic Young’s modulus and Poisson ratio. Then, experimental data from well 58-32 were used to calibrate and convert to static elastic Young’s modulus (static Young’s modulus =0.75\* Dynamic Young’s modulus). Static Poisson ratio was assumed to be equal to the dynamic value. A linear coefficient of thermal expansion of 7.4e-6 1/°C (4.11e-6 1/°F) was obtained from thermal expansion laboratory experiment data using core from well 58-32. Table 3-10 summarizes input data used to estimate the closure pressure thermal correction.

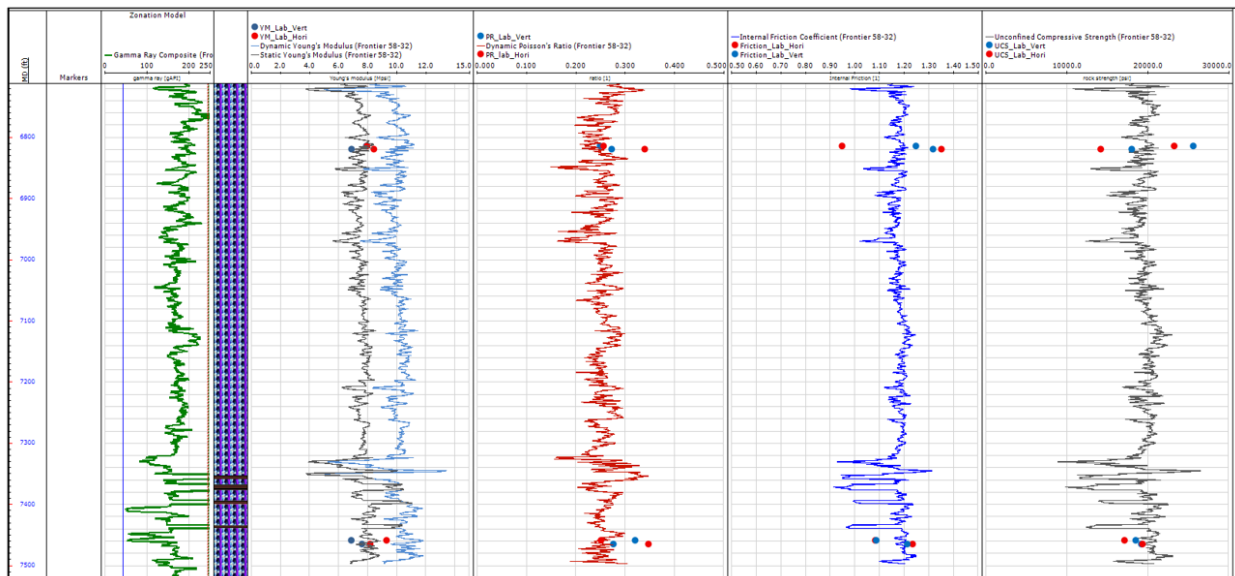


Figure 3-33. Gamma ray profile, dynamic and static Young’s modulus, Poisson ratio, Internal friction coefficient, unconfined compressive strength profile for well 16B(78)-32.



**Table 3-10. Input data for calculating thermal stress correction for Shmin.**

Station	Young's Modulus (1e+6 psi)	Poisson ratio	Thermal coefficient (1e-6 1/°F)	Temperature difference in fracture at half radius using high leakoff assumption (°F)	Temperature difference in fracture at half radius using no leakoff assumption (°F)
MF-1	8.7	0.24	4.11	44	7
MF-2	8.1	0.24	4.11	43	7
MF-3	8.6	0.23	4.11	39.7	6.5
MF-4	8	0.26	4.11	43	8.15
MF-5	7.5	0.29	4.11	42	8
MF-6	8.5	0.24	4.11	39	7.4
MF-7	7.6	0.28	4.11	39	7.4

Table 3-11 shows the calculated thermal correction values to closure stress for the no leakoff and the high leakoff fracture scenarios. Assuming no leakoff from the fracture results in very small thermal correction of (0.06 psi/ft). Conversely, assuming a high leakoff fracture results in a much larger stress correction (0.3 to 0.37 psi/ft). Both the high leakoff and no leakoff scenarios include uncertainty in model assumptions (e.g., injection time, leakoff coefficient, choosing half fracture radius to estimate fracture temperature). As a result, the true value of thermal impact on stress is also uncertain.

However, the presence of natural fractures and foliation in the test interval(s), as shown on image logs (e.g., Figure 3-34), support the possibility of fluid leakoff, although the actual amount of fluid leakoff into fractures and foliations is uncertain. Also, image logs obtained after the minifrac test in Station MF-2 (Figure 3-34) indicate that the length of induced fractures is small (approximately ~3 ft). As a result, the expected temperature correction might be between the estimated upper bound for high leakoff scenarios (~0.37 psi/ft) and lower bound for no leakoff scenario (~0.06 psi/ft).

**Table 3-11. Calculated thermal stress correction for Shmin using Equation 3-4.**

Station	Stress change using high leakoff assumption (psi)	Stress change using high leakoff assumption (psi/ft)	Stress change using no leakoff assumption (psi)	Stress change using no leakoff assumption (psi/ft)
MF-1	2067	0.37	330	0.06
MF-2	1885	0.34	308	0.06
MF-3	1826	0.35	297	0.06
MF-4	1912	0.32	360	0.06
MF-5	1821	0.31	344	0.06
MF-6	1795	0.32	339	0.06
MF-7	1695	0.3	320	0.06

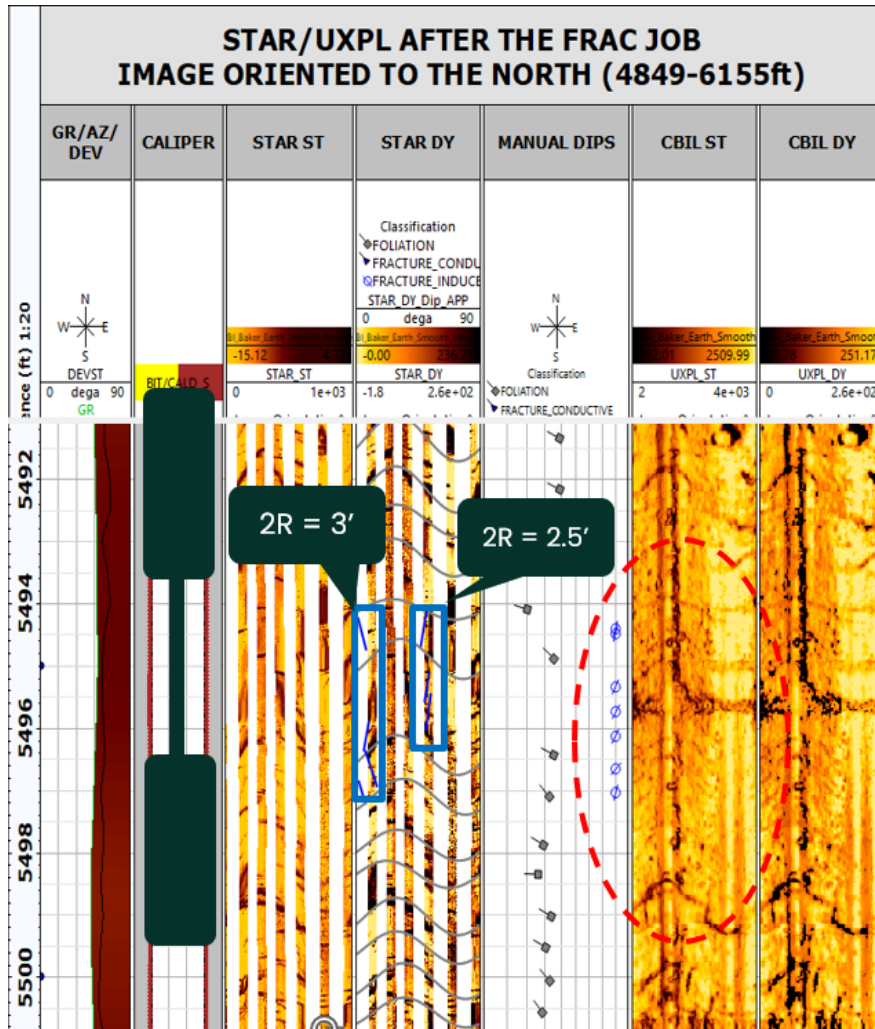


Figure 3-34. Image log after hydraulic fracture in Station MF-2 showing induced fractures, and presence of foliations in the test interval.

### 3.8.3 Shmin Results with Temperature Adjustment for Cooling prior to Testing

A Shmin value of 0.6 psi/ft, based on the analysis of MF-2, is considered to be a “representative” Shmin value (for the depth interval tested in the 16B(78)-32 borehole) unadjusted for the cooling effect on stress due to borehole fluid circulation during the minifrac testing. This value was adjusted to account for cooling using the calculated thermal stress adjustment factor for MF-2 (0.34 psi/ft; see Table 3-11), resulting in a “high” adjusted Shmin = 0.94 psi/ft. Recognizing the high uncertainty in the calculated thermal stress adjustment factors, an “intermediate” adjusted Shmin value of 0.8 psi/ft was calculated based on an intermediate thermal stress adjustment factor of 0.2 psi/ft. Thus, the Shmin values can be summarized as follows:

- Shmin = 0.6 psi/ft (no adjustment for cooling)
- Shmin = 0.94 psi/ft (high adjustment for cooling; 0.34 psi/ft)
- Shmin = 0.8 psi/ft (mid-range adjustment for cooling; 0.2 psi/ft)

In Section 4, SHmax magnitude is calculated for each of these Shmin values.

## 4 Maximum Horizontal Stress

The azimuth of SHmax was determined from analysis of image logs of DIFs in vertical section of borehole and a fracture created during the minifrac test at Station MF-2 (no other minifrac test stations had a detectable fracture on the post-test image logs). Shmin azimuth was determined assuming that it is perpendicular to the SHmax azimuth. The magnitude of SHmax was determined from analysis of minifrac tests MF-2 and MF-4 and DIFs in the 16B(78)-32 borehole.

### 4.1 SHmax Azimuth from Minifrac Tests

Image logs were obtained for all minifrac test stations before and after the minifrac tests to identify any fractures created by the minifrac tests. BH obtained two types of image logs (CBIL [UXPL] and STAR) before and after the minifrac testing. Of the seven minifrac stations where a test was conducted, a post minifrac test fracture was observed at only one station (MF-2). Detailed analysis of the image logs obtained before and after the MF-2 minifrac test identified a small number of individual thin induced fractures at the MF-2 station. These are represented as blue circles on the UXPL log in Figure 4-1. The tensile fracture(s) strike predominantly north-northeast/south-southwest at 30°/210° and ranging from 10° to 50°. Foliations are also striking northeast-southwest. This azimuth range is generally consistent with the azimuth of drilling-induced fractures shown in the next section.

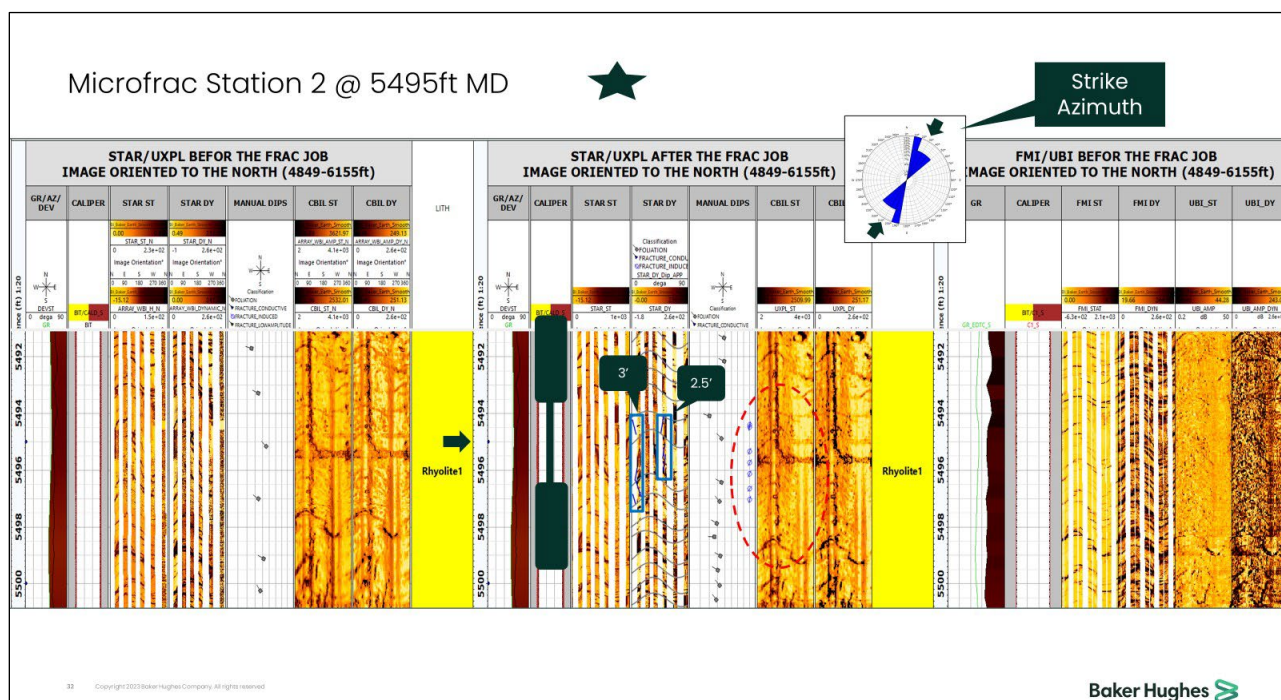


Figure 4-1. Image logs of minifrac test Station MF-2 before and after minifrac test (STAR and CBIL[UXPL] are Baker image logs; FMI and UBI are Schlumberger image logs. The STAR image after the minifrac test shows a stick and pull; therefore, affected portion of STAR image has limited usefulness for interpreting features.

## 4.2 SHmax Azimuth from Drilling Induced Fractures

In vertical wells, DIFs generally occur with a strike that corresponds to the direction of SHmax. If wellbore breakouts are present, they generally are oriented perpendicular to the drilling induced tensile fractures (DIFs), which corresponds to the direction of Shmin. In deviated boreholes, these features may not occur exactly in the SHmax and Shmin directions.

Image logs obtained prior to the minifrac testing were reviewed to identify DIFs. Figure 4-2 is an image log showing several DIFs (indicated by blue horizontal lines/rectangles in tracks 4 and 5 from the left in the strip chart) in the depth interval from 4844 to 6155 ft. The azimuth of the DIFs are plotted on a rose diagram shown in the figure. The predominant azimuth of the DIFs is 27° (northeast). No wellbore breakouts were observed in this interval. The strike of foliation features shows some variation through this interval but the predominant strike direction is ~25° (northeast) and their dip direction is ~292° (northwest). The foliation features are plotted on two rose diagrams in the figure. Three groups of natural fractures are indicated with average orientations of ~70° (northeast), ~10° (northeast), and ~340 to 350° (northwest).

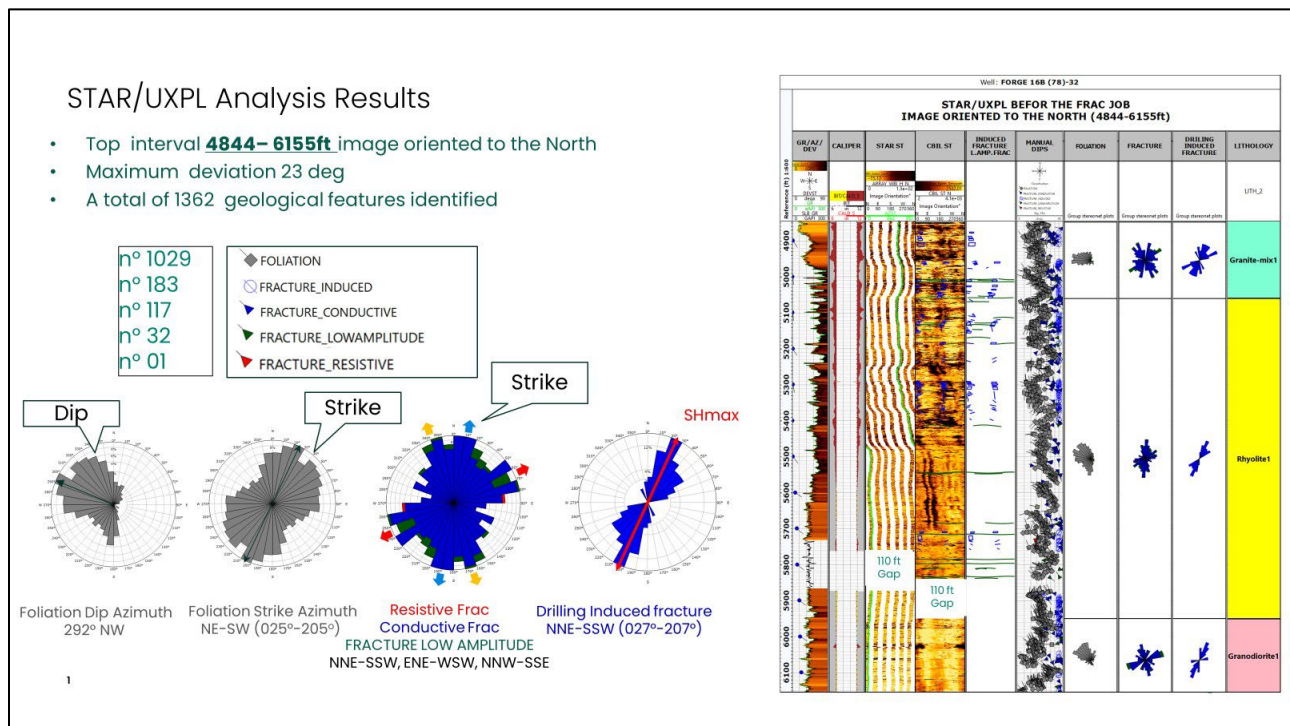
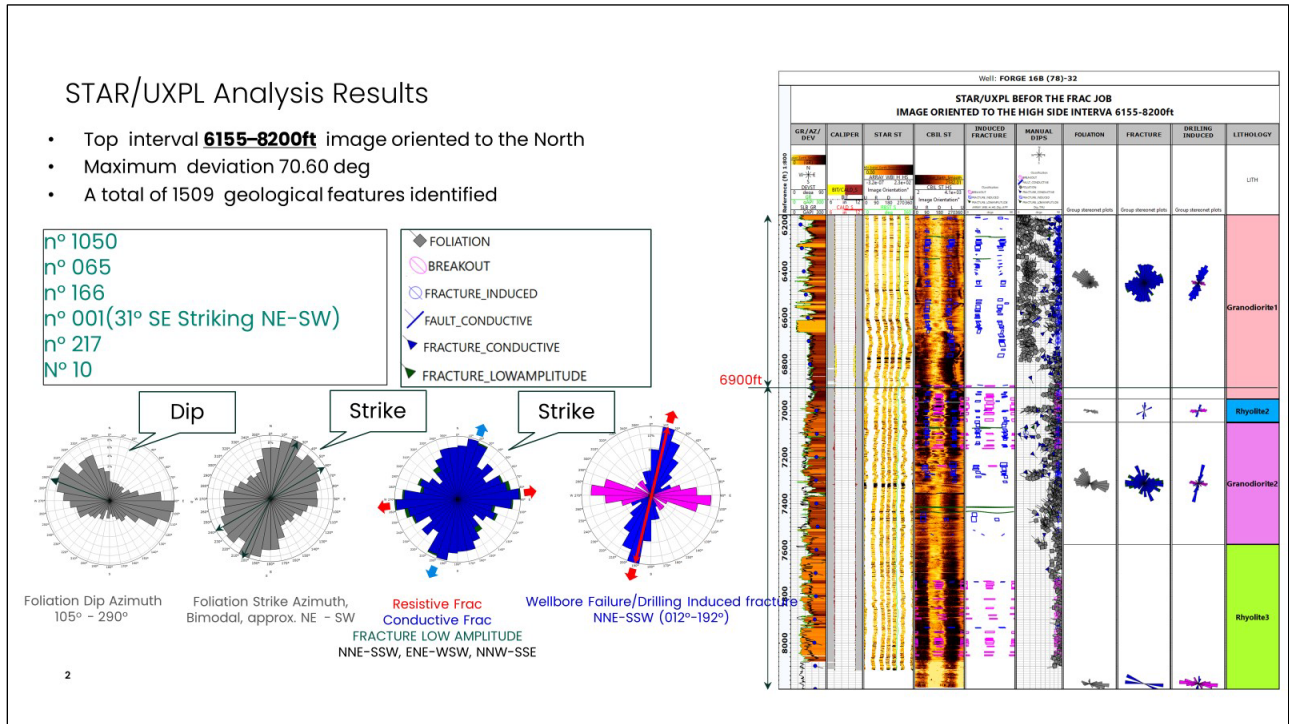


Figure 4-2. Image log for interval 4844 to 6155 ft showing orientation of DIFs, foliation features, and natural fractures.

Figure 4-3 is an image log showing several DIFs in the depth interval from 6155 to 8200 ft. The strike of the DIFs is predominantly ~12° (northeast). Note that because the depth interval is entirely below the kick-off point (5,638 ft MD) in the curve, the calculated DIF azimuth for this interval likely deviated from the true SHmax direction. Wellbore breakouts (shown by pink boxes in Figure 4-3, Track 5) were also observed in this depth interval, with a strike direction that is ~260° to 290° (west/northwest), which is roughly perpendicular to the strike of the DIFs. Foliation geometry shows greater variation throughout

this interval but mostly striking 20° to 60° (northeast) and with a predominant dip direction of ~290° (northwest). The natural fractures group into two modes, including one oriented 20° (northeast) and another oriented ~90° (east).



**Figure 4-3. Image log for interval 6155 to 8200 ft showing several DIFs (indicated by blue horizontal lines/rectangles in track 5 from the left).**

Xing et al. (2022) performed image log analysis of well 16A(78)-32 to estimate azimuth of SHmax using DIFs and breakout features. The azimuth of SHmax was determined as north-northeast/south-southwest direction. Interpreting DIF of image log in 58-32 well, Aljubran et al. (2021) estimated the azimuth of SHmax to be N25°E. In this study, the azimuth of SHmax was found to be predominantly N30°E based on the induced fracture(s) in the MF-2 test interval and predominantly N27°E based on several DIFs in the vertical section of well 16B(78)-32 which generally agrees with the previous studies.

### 4.3 SHmax Magnitude from Minifrac Tests MF-2 and MF-4

Different methods can be used to constrain SHmax magnitude, including using DIFs and/or breakout features (Zoback, 2010). However, using data from the minifrac tests is likely to provide a more accurate constraint on SHmax magnitude. This is because the pressure difference between the first injection cycle with breakdown and re-opening pressure in subsequent cycle(s) can provide a better estimate of tensile strength of the rock (important input to the stress polygon method) compared to core-based estimates of tensile strength.

SHmax magnitude was determined for MF-2 and MF-4 using the stress polygon model in BH's SFIB geomechanical stress modeling software. Figure 4-4 through Figure 4-6 show the stress polygon analysis for MF-2 for three values of Shmin (0.6, 0.8 and 0.94 psi/ft) and two tensile strength scenarios (T<sub>0</sub> = 0

and  $T_0 = UCS/10$ ). The  $SH_{max}$  is visually estimated at the point of intersection of  $Sh_{min}$  and the two tensile strength lines. For example, in Figure 4-4, the  $Sh_{min}$  line of 0.6 intersects the tensile strength line of  $T_0 = 0$  at  $SH_{max} > \sim 0.6$  psi/ft (actual value is likely slightly greater than  $Sh_{min}$ , but could not be determined by visual interpretation of the stress polygon analysis) and the  $T_0 = UCS/10 = 2000$  tensile strength line at  $SH_{max} = 0.76$  psi/ft. Values for other model input parameters used in the stress polygon analysis are shown in the stress polygon figures (for example,  $S_v = 1.08$  psi/ft). Because the interpretation of  $SH_{max}$  is done by visually inferring the intersection of  $Sh_{min}$  and the tensile strength lines, the method has some inherent uncertainty. Similar stress polygons are provided for  $Sh_{min} = 0.8$  psi/ft (Figure 4-5) and 0.94 psi/ft (Figure 4-6). For  $Sh_{min} = 0.8$  psi/ft,  $SH_{max}$  is 1.0 psi/ft for  $T_0 = 0$  and 1.4 psi/ft for  $T_0 = UCS/10$ . For  $Sh_{min} = 0.94$  psi/ft,  $SH_{max}$  is 1.37 for  $T_0 = 0$  and 1.77 psi/ft for  $T_0 = UCS/10$ .  $SH_{max}$  was determined for MF-4 using the same approach. Stress polygons for MF-4 are shown in Figure 4-7, Figure 4-8, and Figure 4-9, for  $Sh_{min}$  values of 0.6 psi/ft, 0.8 psi/ft, and 0.94 psi/ft, respectively. The calculated  $SH_{max}$  values for MF-2 and MF-4 based on the stress polygon analysis method are summarized in Table 4-1. Figure 4-10 and Figure 4-11 show bottom hole pressure during the MF-2 and MF4 mini-frac tests. By comparing fracture breakdown pressure in first cycle to the re-opening pressure in second cycle, in-situ tensile strength of the rock would be  $\sim 200$  psi or lower. This value shows that the assumption of  $T_0 = 0$  is more accurate to estimate  $SH_{max}$  compared to  $T_0 = UCS/10$ . By assuming  $Sh_{min} = 0.8$  psi/ft, the best estimate of  $SH_{max}$  would be 1-1.14 psi/ft according to Table 4-1.

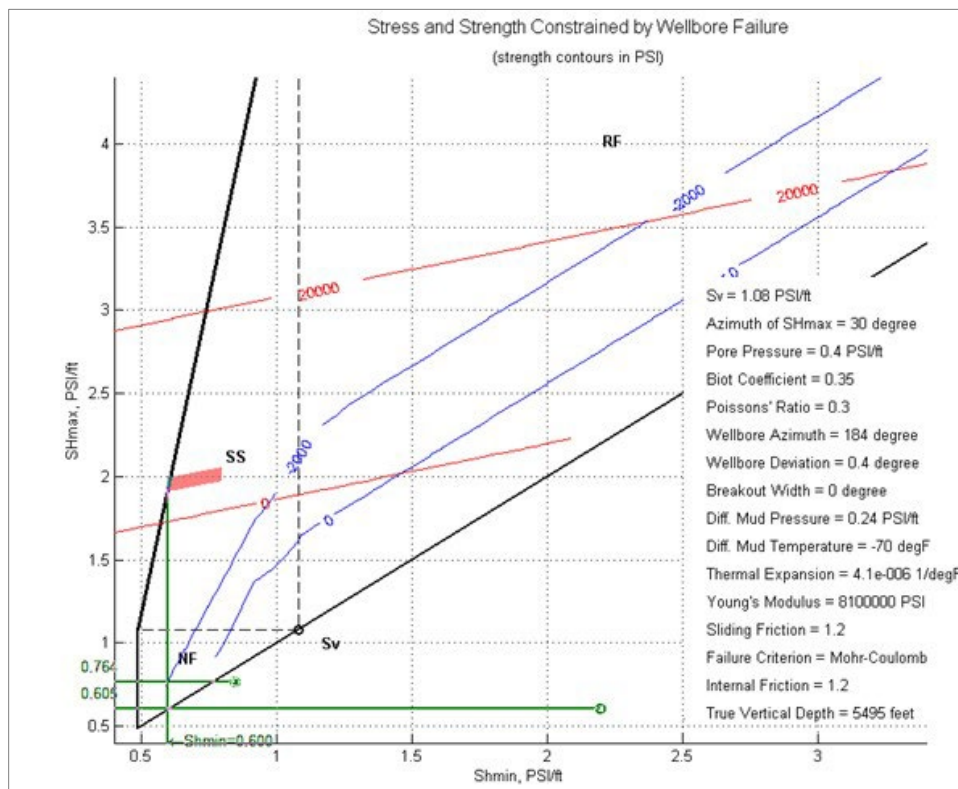


Figure 4-4. Stress Polygon for Determining  $SH_{max}$  magnitude for MF-2 at 5495 ft TVD for  $Sh_{min} = 0.6$  psi/ft and two tensile strength scenarios ( $T_0 = 0$  and  $T_0 = UCS/10 = 2000$  psi). This analysis

assumes differential drilling mud temperature of -70°F relative to the ambient formation temperature).

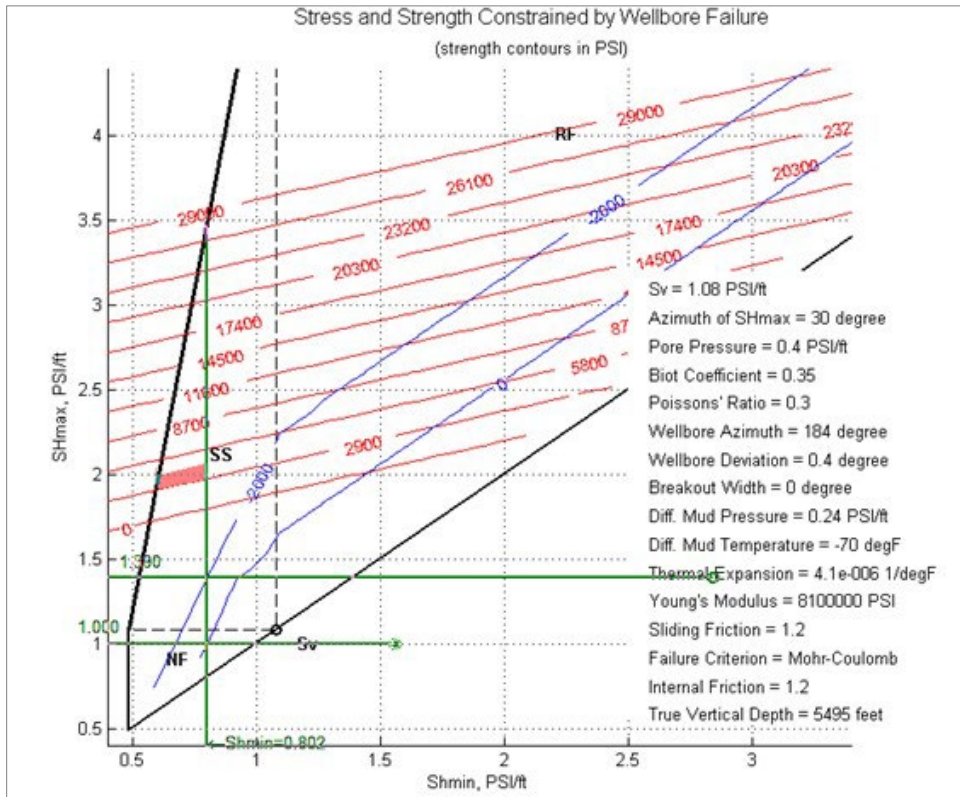


Figure 4-5. Stress Polygon for Determining SHmax magnitude for MF-2 at 5495 ft TVD for Shmin=0.8 psi/ft and two tensile strength scenarios (T<sub>0</sub>=0 and T<sub>0</sub>=UCS/10=2000 psi). This analysis assumes a differential drilling mud temperature of -70°F relative to the ambient formation temperature).

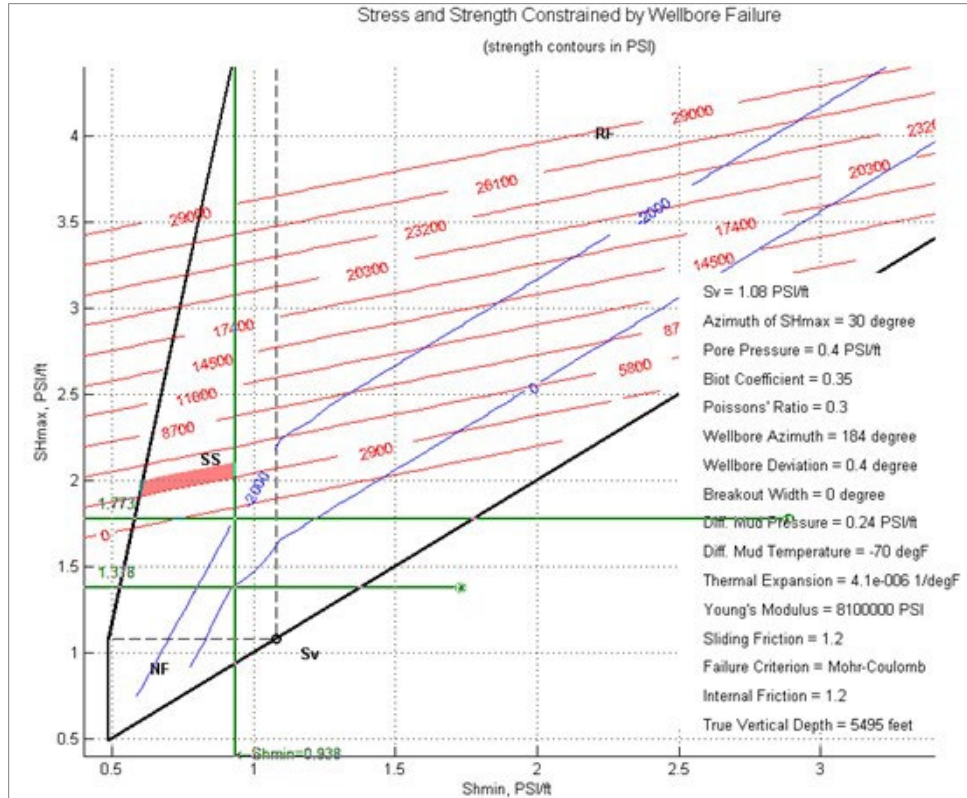


Figure 4-6. Stress Polygon for Determining SHmax magnitude for MF-2 at 5495 ft TVD for Shmin=0.94 psi/ft and two tensile strength scenarios ( $T_0=0$  and  $T_0=UCS/10=2000$  psi). This analysis assumes a differential drilling mud temperature of  $-70^\circ\text{F}$  relative to the ambient formation temperature).



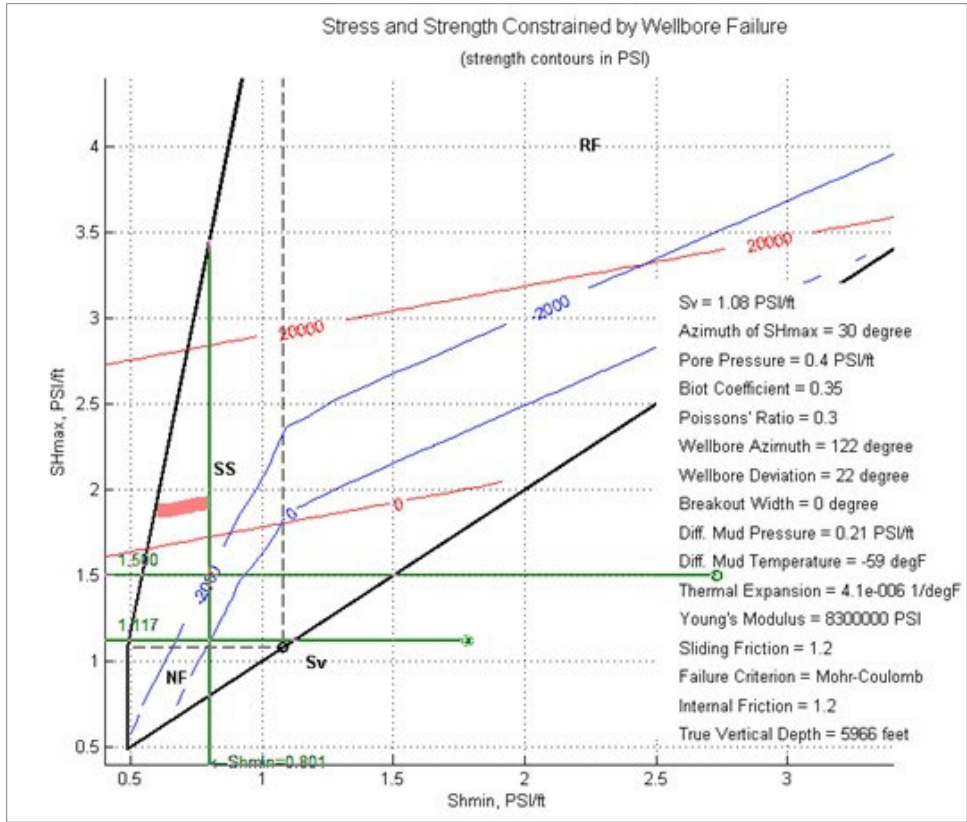


Figure 4-8. Stress Polygon for Determining SHmax magnitude for MF-4 at 5966 ft TVD for Shmin=0.8 psi/ft and two tensile strength scenarios ( $T_0=0$  and  $T_0=UCS/10=2000$  psi). This analysis assumes a differential drilling mud temperature of  $-59^{\circ}\text{F}$  relative to the ambient formation temperature).

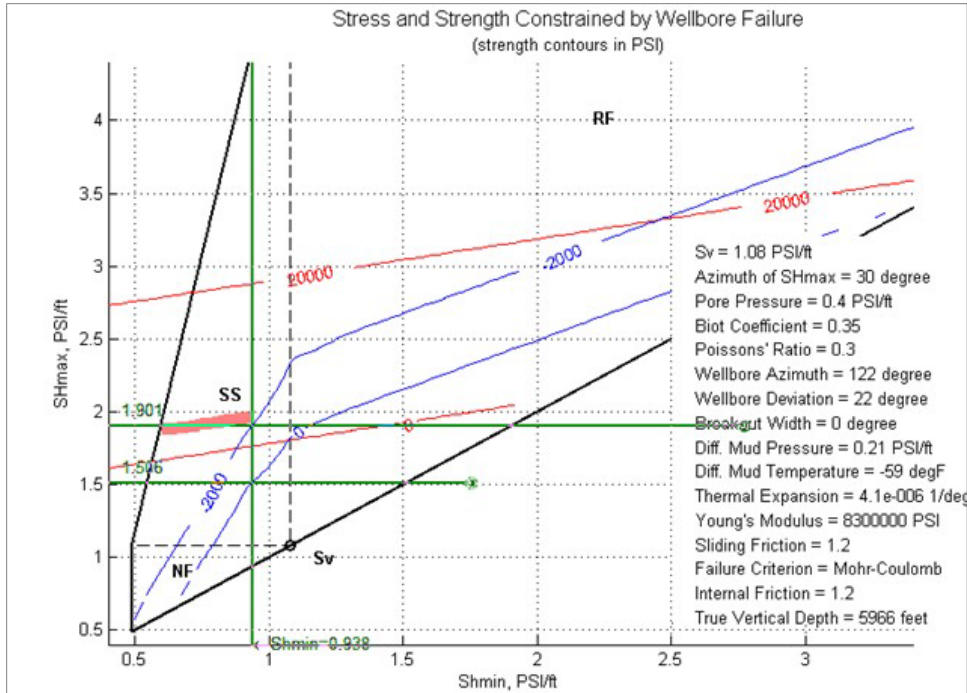


Figure 4-9. Stress Polygon for Determining SHmax magnitude for MF-4 at 5966 ft TVD for Shmin=0.94 psi/ft and two tensile strength scenarios ( $T_0=0$  and  $T_0=UCS/10=2000$  psi). This analysis assumes a differential drilling mud temperature of  $-59^{\circ}\text{F}$  relative to the ambient formation temperature).

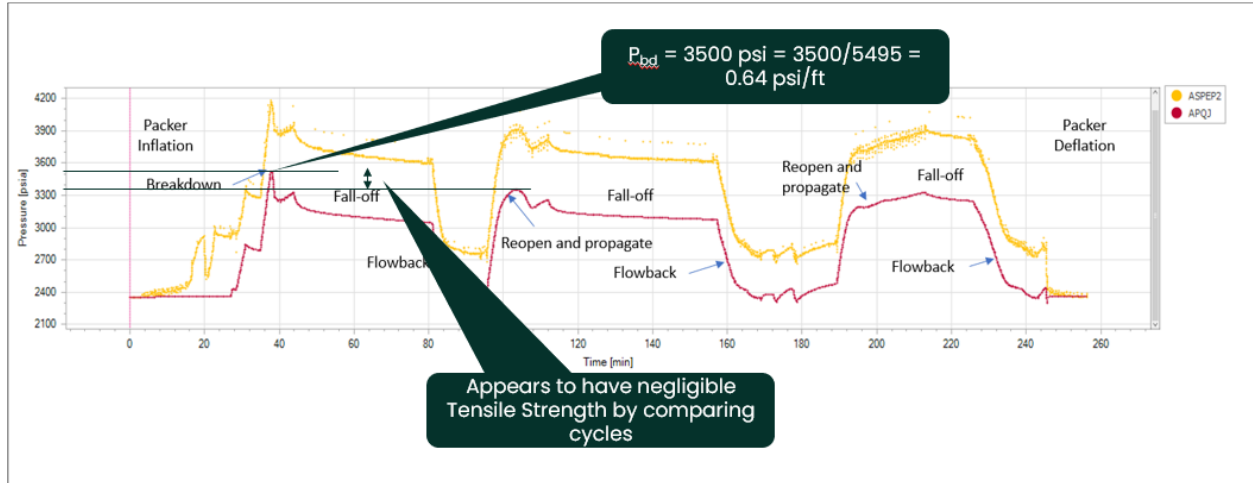


Figure 4-10. Bottom hole pressure (red) during MF-2 showing tensile strength estimate.

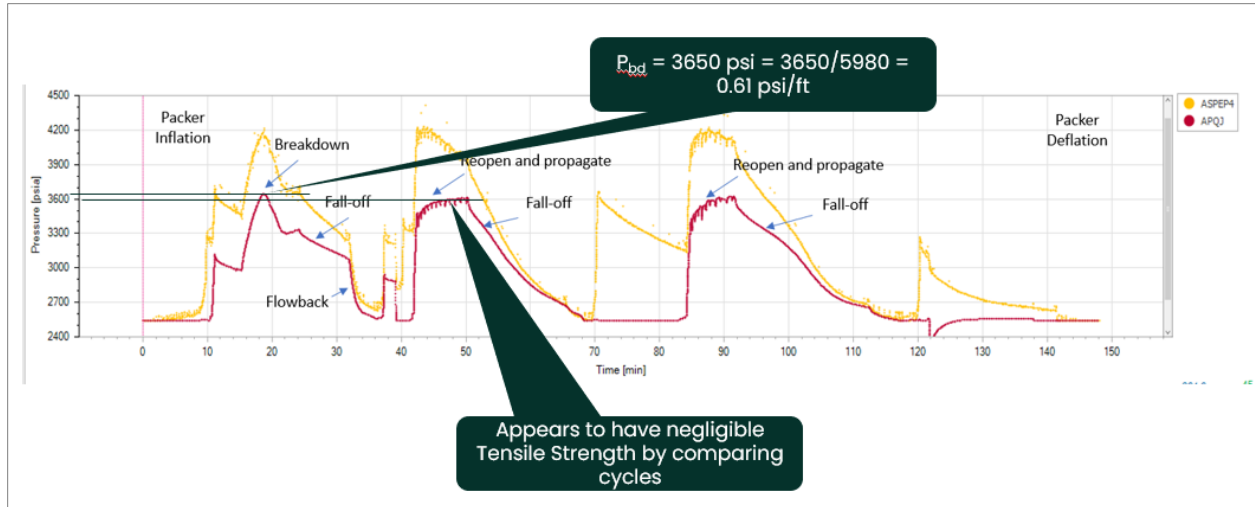


Figure 4-11. Bottom hole pressure (red) during MF-4 showing tensile strength estimate.

Table 4-1. SHmax magnitude determined for MF-2 and MF-4.

Shmin	MF-2 <sup>a</sup>		MF-4 <sup>b</sup>	
	T <sub>0</sub> =0	T <sub>0</sub> =UCS/10	T <sub>0</sub> =0	T <sub>0</sub> =UCS/10
0.6	>0.6 <sup>c</sup>	0.76	>0.6 <sup>c</sup>	0.92
0.8	1.0	1.4	1.11	1.50
0.94	1.37	1.77	1.50	1.90

- assumes differential drilling fluid temperature of -70° F (estimated from avg temp in MF-2 test interval (depth=5495ft) during minifrac test (232 °F) using bottomhole temperature gauge minus estimated background temp at this depth (302 °F)).
- assumes differential drilling fluid temperature of -59° F (estimated from avg temp in MF-4 test interval (depth=5980 ft) during minifrac test (263 °F) using bottomhole temperature gauge minus estimated background temp at this depth (322 °F)).
- actual value is likely slightly greater than Shmin, but could not be determined by visual interpretation of the stress polygon analysis

#### 4.4 SHmax Magnitude from Drilling Induced Fractures Using the Stress Polygon Method

According to Nadimi et al. (2020), DIFs were observed in well 58-32 even though the pressure (weight) of the drilling mud was only marginally above the hydrostatic pressure. Similarly, several DIFs were observed on image logs from the 16B(78)-32 borehole. Cooling during drilling (difference between mud temperature and formation temperature) could cause thermoelastic effects leading to DIFs. In this study, DIFs were analyzed to constrain SHmax using the stress polygon method, taking into account the impact of cooling during drilling.

The stress polygon method was used to estimate SHmax magnitude at selected discrete depths in the 16B(78)-32 borehole where DIFs were observed on the image log(s). Figure 4-12 shows examples of DIFs identified on the STAR and CBIL (UXPL) image logs (the DIFs are highlighted with blue rectangles and blue shading). Figure 4-13 (track 8) shows the calculated SHmax magnitude values determined with the stress polygon method for two values of tensile strength and assuming Shmin=0.8 psi/ft. The blue diamonds assume the tensile strength is equal to the UCS/10, whereas the green diamonds assume the tensile strength is equal to zero. Figure 4-13 also shows the value of key parameters used to calculate

SHmax magnitude, including: borehole azimuth, borehole inclination, delta-temp (temp difference between formation ambient temperature and drilling fluid temperature), static Young's modulus, static Poisson's Ratio, unconfined compressive strength, pore pressure, and vertical stress (Sv) magnitude. Figure 4-14 and Figure 4-15 provide the calculated SHmax values and corresponding input parameters for Shmin=0.6 psi/ft and Shmin=0.94 psi/ft. The calculated SHmax values based on DIFs are summarized in Table 4-2 for all three values of Shmin (0.6, 0.8 and 0.94). Note that in Table 4-2, SHmax is given for two temperature scenarios/assumptions: (1) drilling mud temperature was cooler than ambient formation temperature and (2) drilling mud temperature was equal to ambient formation temperature. Stress polygons for scenario (2) are not shown.

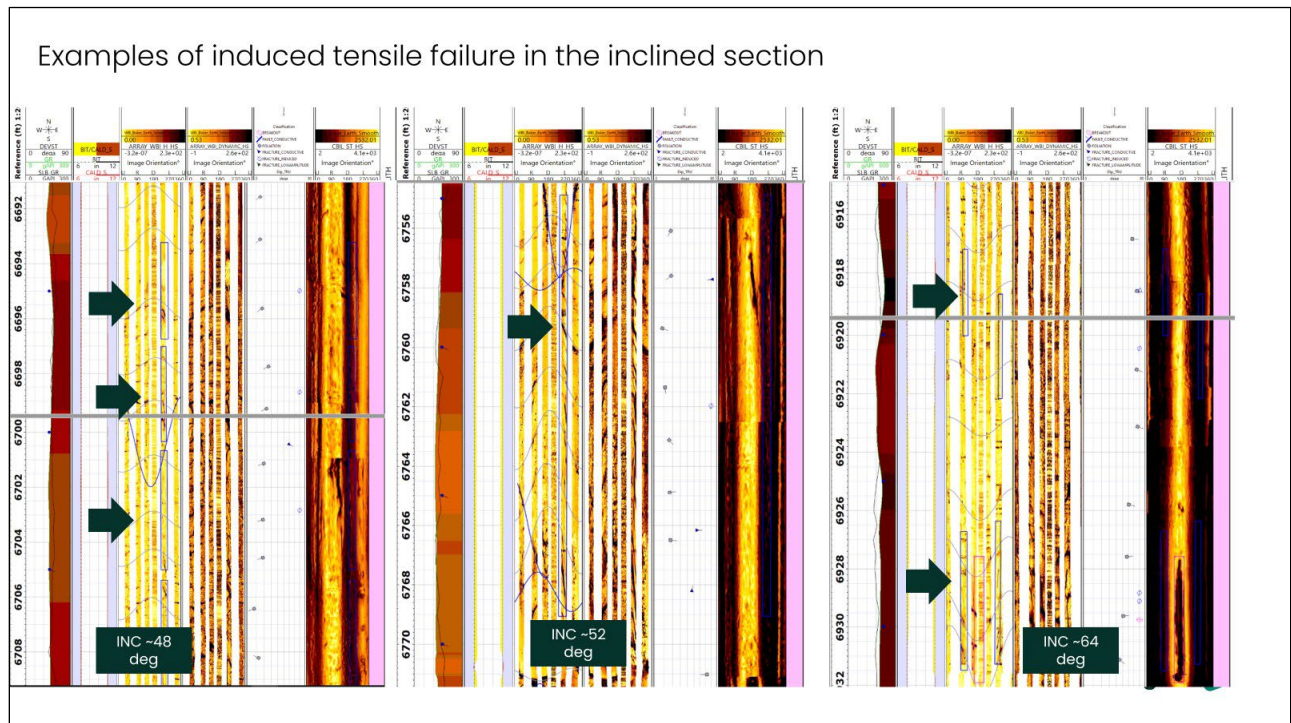


Figure 4-12. DIFs identified on STAR and CBIL (UXPL) image logs (highlighted with blue rectangles).

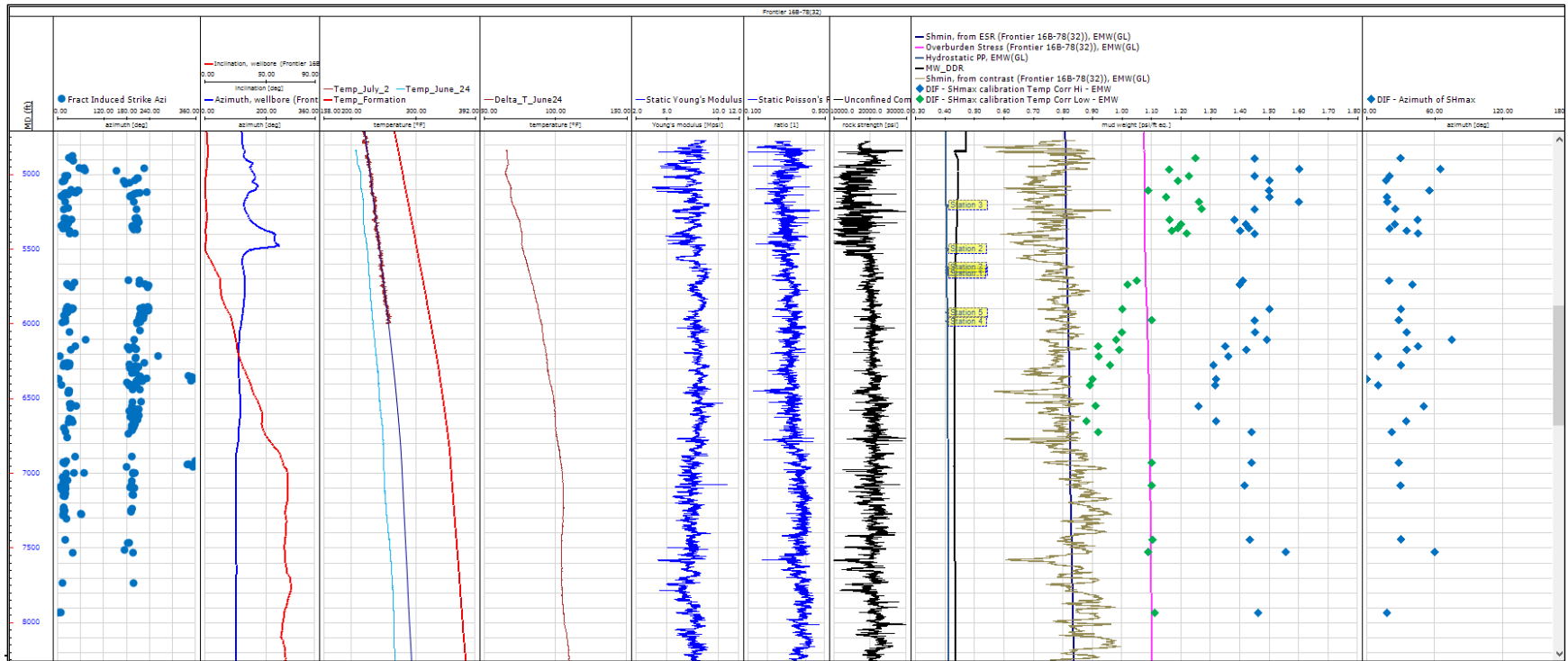


Figure 4-13. Calculated SHmax values (shown as green and blue diamonds in track 8) for Shmin=0.8 psi/ft and the two tensile strength scenarios and values of key input parameters used to calculate SHmax. In track 8, the blue diamonds assume the tensile strength is equal to the UCS/10; whereas the green diamonds assume the tensile strength is equal to zero.

# $S_{hmax}$ Estimation from Drilling Induced Fractures – $S_{hmin} = 0.6$ psi/ft

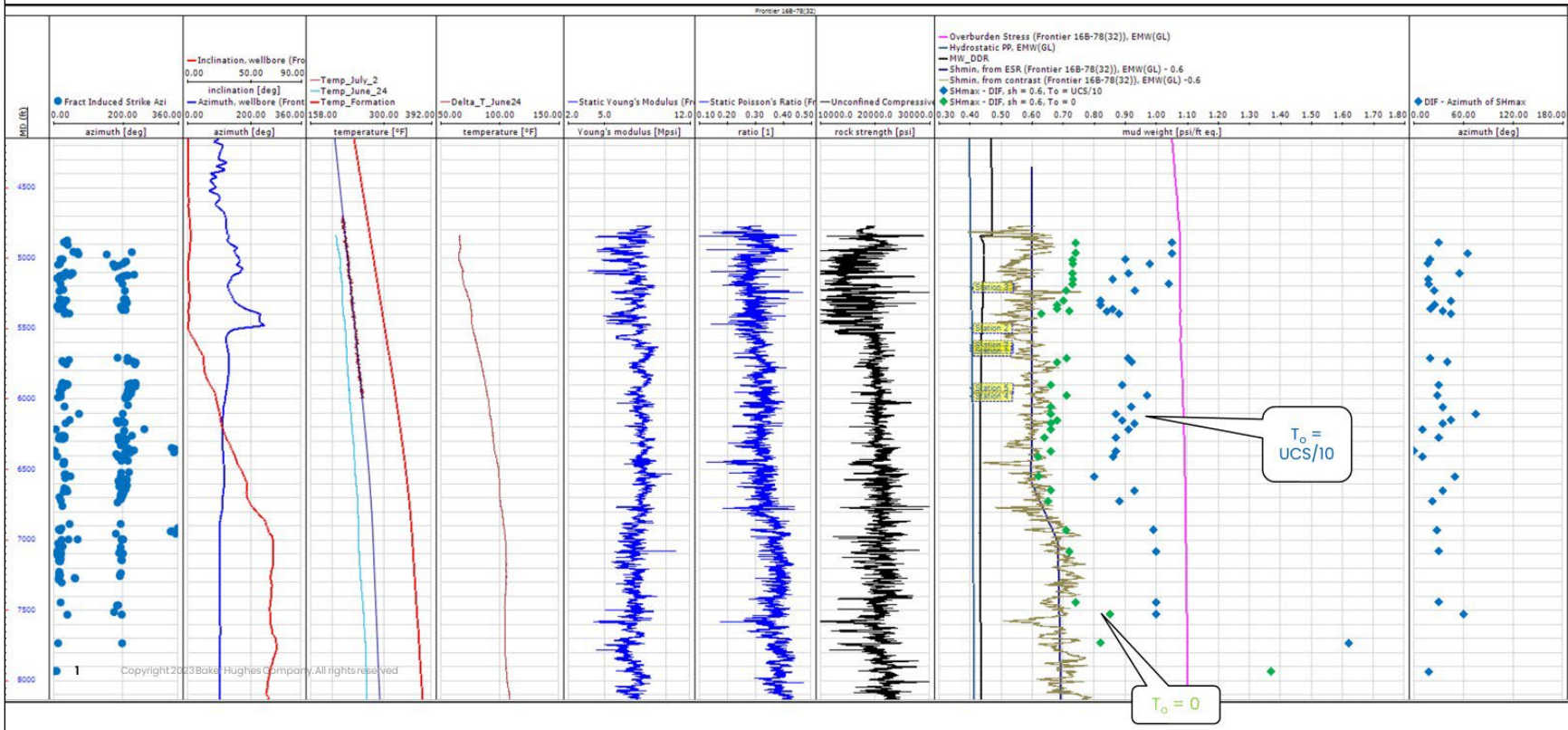


Figure 4-14. Calculated SHmax values (shown as green and blue diamonds in track 8) for  $S_{hmin}=0.6$  psi/ft and the two Tensile strength scenarios and values of key input parameters used to calculate SHmax. In track 8, the blue diamonds assume the tensile strength is equal to the UCS/10; whereas the green diamonds assume the tensile strength is equal to zero.

# $S_{hmax}$ Estimation from Drilling Induced Fractures – $S_{hmin} = 0.94$ psi/ft

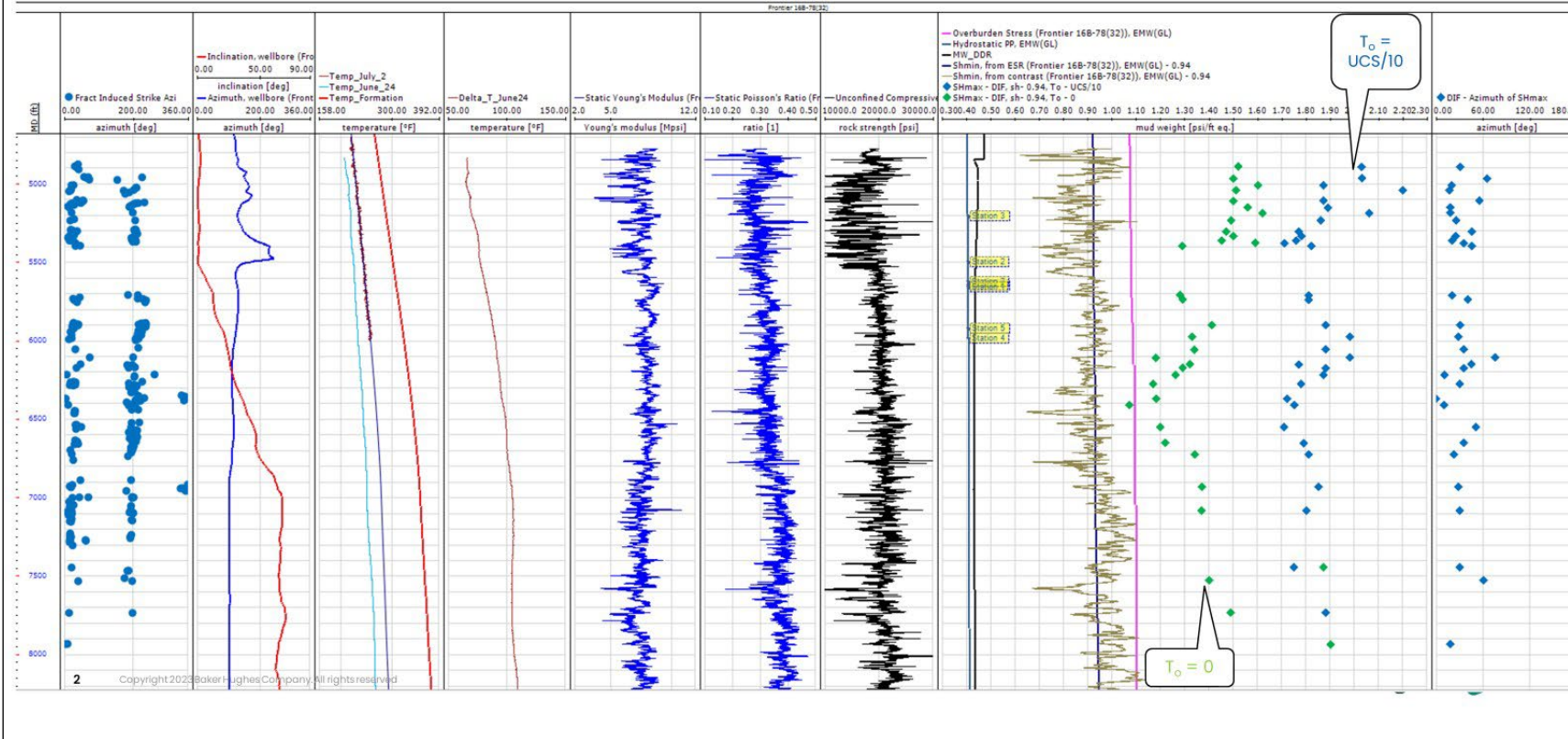


Figure 4-15. Calculated  $S_{hmax}$  values (shown as green and blue diamonds in track 8) for  $S_{hmin}=0.94$  psi/ft and the two Tensile strength scenarios and values of key input parameters used to calculate  $S_{hmax}$ . In track 8, the blue diamonds assume the tensile strength is equal to the UCS/10; whereas the green diamonds assume the tensile strength is equal to zero

**Table 4-2. Calculated Values of SHmax from DIFs at 33 depths.**

MD (ft)	TVD (ft)	UCS (kpsi)	SHmax_Azi (deg from North)	Cooling Considered	Delta T (Deg F)	YM (Mpsi)	PR	SHmax Grad (psi/ft) assuming Shmin = 0.6 (psi/ft) and T <sub>o</sub> = 0 (psi)	SHmax Grad (psi/ft) assuming Shmin = 0.6 (psi/ft) and T <sub>o</sub> = UCS/10 (psi)	SHmax Grad (psi/ft) assuming Shmin = 0.8 (psi/ft) and T <sub>o</sub> = 0 (psi)	SHmax Grad (psi/ft) assuming Shmin = 0.8 (psi/ft) and T <sub>o</sub> = UCS/10 (psi)	SHmax Grad (psi/ft) assuming Shmin = 0.94 (psi/ft) and T <sub>o</sub> = 0 (psi/ft)	SHmax Grad (psi/ft) assuming Shmin = 0.94 (psi/ft) and T <sub>o</sub> = UCS/10 (psi/ft)
4891	4890.2	21	30	Yes	-67	7.1	0.3	0.74	1.1	1.2	1.54	1.52	2.03
4891	4890.2	21	30	No	0	7.1	0.3	1.23	1.67	1.78	2.3	2.2	2.67
4965	4964.1	22	65	Yes	-67	7.1	0.3	0.74	1.2	1.16	1.6	1.5	2.03
4965	4964.1	22	65	No	0	7.1	0.3	1.23	1.69	1.65	2.09	2.1	2.6
5009	5008.1	12	20	Yes	-65	7.1	0.3	0.73	0.98	1.227	1.45	1.6	1.87
5009	5008.1	12	20	No	0	7.1	0.3	1.22	1.41	1.717	1.94	2.2	2.42
5040	5039.1	15	17	Yes	-66	7.1	0.3	0.73	0.98	1.19	1.5	1.51	2.2
5040	5039.1	15	17	No	0	7.1	0.3	1.22	1.62	1.77	2.08	2.21	2.55
5150	5149.1	12	18	Yes	-68	7.6	0.3	0.73	0.86	1.15	1.5	1.5	1.89
5150	5149.1	12	18	No	0	7.6	0.3	1.23	1.43	1.65	2	2.22	2.44
5184	5183.1	20	18	Yes	-69	7.1	0.3	0.73	1.14	1.261	1.6	1.56	2.06
5184	5183.1	20	18	No	0	7.1	0.3	1.28	1.68	1.811	2.15	2.19	2.67
5231	5230.1	11	25	Yes	-72	6.8	0.3	0.73	0.93	1.269	1.45	1.62	1.86
5231	5230.1	11	25	No	0	6.8	0.3	1.2	1.36	1.739	1.92	2.21	2.47
5303	5302	10	45	Yes	-74	7.4	0.3	0.71	0.82	1.16	1.38	1.49	1.77
5303	5302	10	45	No	0	7.4	0.3	1.22	1.35	1.67	1.89	2.18	2.4
5332	5331	13	25	Yes	-75	7.5	0.3	0.7	0.82	1.2	1.42	1.47	1.78
5332	5331	13	25	No	0	7.5	0.3	1.24	1.47	1.74	1.96	2.21	2.41
5361	5360	12	20	Yes	-75	7.4	0.3	0.68	0.86	1.19	1.43	1.5	1.76
5361	5360	12	20	No	0	7.4	0.3	1.24	1.46	1.75	1.99	2.21	2.43
5377	5376	11	35	Yes	-76	7.4	0.3	0.68	0.84	1.17	1.4	1.45	1.71
5377	5376	11	35	No	0	7.4	0.3	1.26	1.45	1.75	1.98	2.2	2.39
5395	5394	10	45	Yes	-76	6.5	0.3	0.72	0.88	1.22	1.45	1.59	1.82
5395	5394	10	45	No	0	6.5	0.3	1.22	1.41	1.72	1.95	2.22	2.4
5710	5707.1	20	20	Yes	-83	8.4	0.3	0.63	0.91	1.05	1.41	1.29	1.81
5710	5707.1	20	20	No	0	8.4	0.3	1.28	1.59	1.7	2.06	2.22	2.67
5737	5733.5	20	40	Yes	-83	8.4	0.3	0.71	0.92	1.02	1.4	1.28	1.81

**Table 4-2. Calculated Values of SHmax from DIFs at 33 depths. (Continued)**

MD (ft)	TVD (ft)	UCS (kpsi)	SHmax_Azi (deg from North)	Cooling Considered	Delta T (Deg F)	YM (Mpsi)	PR	SHmax Grad (psi/ft) assuming Shmin = 0.6 (psi/ft) and T <sub>o</sub> = 0 (psi)	SHmax Grad (psi/ft) assuming Shmin = 0.6 (psi/ft) and T <sub>o</sub> = UCS/10 (psi)	SHmax Grad (psi/ft) assuming Shmin = 0.8 (psi/ft) and T <sub>o</sub> = 0 (psi)	SHmax Grad (psi/ft) assuming Shmin = 0.8 (psi/ft) and T <sub>o</sub> = UCS/10 (psi)	SHmax Grad (psi/ft) assuming Shmin = 0.94 (psi/ft) and T <sub>o</sub> = 0 (psi/ft)	SHmax Grad (psi/ft) assuming Shmin = 0.94 (psi/ft) and T <sub>o</sub> = UCS/10 (psi/ft)
5737	5733.5	20	40	No	0	8.4	0.3	1.27	1.62	1.58	1.96	2.23	2.65
5900	5891.2	20	30	Yes	-88	7.8	0.3	0.68	0.89	1	1.5	1.29	1.88
5900	5891.2	20	30	No	0	7.8	0.3	1.2	1.68	1.52	2.02	2.18	2.66
5975	5961.6	18	28	Yes	-89	6.9	0.3	0.66	0.97	1.1	1.45	1.41	1.98
5975	5961.6	18	28	No	0	6.9	0.3	1.21	1.61	1.65	2	2.19	2.66
6056	6036	20	35	Yes	-91	7.4	0.3	0.71	0.92	1	1.45	1.33	1.88
6056	6036	20	35	No	0	7.4	0.3	1.27	1.64	1.56	2.01	2.21	2.66
6106	6081.3	20	75	Yes	-91	7.9	0.3	0.66	0.87	0.98	1.49	1.34	1.98
6106	6081.3	20	75	No	0	7.9	0.3	1.3	1.72	1.62	2.13	2.39	2.87
6150	6120.9	20	45	Yes	-93	8.5	0.3	0.66	0.89	0.92	1.35	1.18	1.77
6150	6120.9	20	45	No	0	8.5	0.3	1.229	1.69	1.489	1.919	2.25	1.72
6173	6141.4	20	35	Yes	-93	7.5	0.3	0.68	0.93	0.99	1.42	1.32	1.88
6173	6141.4	20	35	No	0	7.5	0.3	1.22	1.58	1.53	1.96	2.24	2.65
6217	6180.5	20	10	Yes	-94	7.5	0.3	0.66	0.91	0.92	1.36	1.29	1.87
6217	6180.5	20	10	No	0	7.5	0.3	1.24	1.69	1.5	1.94	2.23	2.65
6275	6231.1	20	30	Yes	-94	7.9	0.3	0.66	0.87	0.96	1.31	1.26	1.78
6275	6231.1	20	30	No	0	7.9	0.3	1.23	1.68	1.53	1.88	2.27	2.73
6369	6309.9	20	0	Yes	-96	8.3	0.3	0.64	0.87	0.9	1.32	1.17	1.72
6369	6309.9	20	0	No	0	8.3	0.3	1.24	1.68	1.5	1.92	2.27	2.75
6410	6342.7	20	10	Yes	-97	8.3	0.3	0.63	0.86	0.89	1.316	1.18	1.75
6410	6342.7	20	10	No	0	8.3	0.3	1.31	1.81	1.57	1.996	2.32	2.78
6550	6448.4	22	50	Yes	-99	9.1	0.3	0.62	0.7	0.91	1.26	1.07	1.71
6550	6448.4	22	50	No	0	9.1	0.3	1.37	1.84	1.66	2.01	1.37	1.84
6644	6448.4	20	35	Yes	-100	8.2	0.3	0.62	0.93	0.88	1.32	1.2	1.79
6644	6448.4	20	35	No	0	8.2	0.3	1.39	1.82	1.65	2.09	2.32	2.77
6720	6517.1	24	22	Yes	-100	8.1	0.3	0.6	0.88	0.92	1.44	1.22	1.81
6720	6517.1	24	22	No	0	8.1	0.3	1.38	1.86	1.69	2.21	2.26	2.76

**Table 4-2. Calculated Values of SHmax from DIFs at 33 depths. (Continued)**

MD (ft)	TVD (ft)	UCS (kpsi)	SHmax_Azi (deg from North)	Cooling Considered	Delta T (Deg F)	YM (Mpsi)	PR	SHmax Grad (psi/ft) assuming Shmin = 0.6 (psi/ft) and T <sub>o</sub> = 0 (psi)	SHmax Grad (psi/ft) assuming Shmin = 0.6 (psi/ft) and T <sub>o</sub> = UCS/10 (psi)	SHmax Grad (psi/ft) assuming Shmin = 0.8 (psi/ft) and T <sub>o</sub> = 0 (psi)	SHmax Grad (psi/ft) assuming Shmin = 0.8 (psi/ft) and T <sub>o</sub> = UCS/10 (psi)	SHmax Grad (psi/ft) assuming Shmin = 0.94 (psi/ft) and T <sub>o</sub> = 0 (psi/ft)	SHmax Grad (psi/ft) assuming Shmin = 0.94 (psi/ft) and T <sub>o</sub> = UCS/10 (psi/ft)
6930	6679.9	20	28	Yes	-104	7.7	0.3	0.62	0.99	1.1	1.44	1.34	1.85
6930	6679.9	20	28	No	0	7.7	0.3	1.71	2.62	2.19	2.53	2.61	3.09
7082	6739.4	20	30	Yes	-105	7.7	0.3	0.6	1	1.1	1.416	1.37	1.8
7082	6739.4	20	30	No	0	7.7	0.3	1.76	2.47	2.25	2.566	2.56	3.02
7443	6881.2	20	30	Yes	-105	7.7	0.3	0.6	1	1.104	1.433	1.37	1.75
7443	6881.2	20	30	No	0	7.7	0.3	1.7	2.32	2.194	2.523	2.49	2.91
7534	6916.2	20	60	Yes	-104	8	0.3	0.6	1	1.09	1.554	1.87	2.55
7534	6916.2	20	60	No	0	8	0.3	1.62	3.72	2.1	2.564	3.44	4.09
7736	6996.4	12	18	Yes	-107	7	0.3	0.85	1.26	1.11	1.46	1.4	1.88
7736	6996.4	12	18	No	0	7	0.3	1.72	2.28	1.98	2.33	2.39	2.85
7934	7070	22	10	Yes	-105	7	0.3	0.82	1.37	1.27	1.39	1.49	1.9
7934	7070	22	10	No	0	7	0.3	1.71	2.29	2.16	2.28	2.38	2.84

## 4.5 Summary SHmax Magnitude Calculated from Drilling Induced Fractures

The range of SHmax magnitude values for each Shmin and tensile strength scenario are summarized in Table 4-3 (all DIFs) and Table 4-4 (only DIFs in the vertical section of the borehole). All calculated SHmax values assume a drilling fluid that is cooler than the ambient formation temperature.

**Table 4-3. Summary of SHmax values determined with stress polygon method for 33 DIFs for two tensile strength scenarios and three values of Shmin (all 33 DIFs included).**

Shmin (psi/ft)	SHmax Range (T <sub>0</sub> =0) (psi/ft)	SHmax Range (T <sub>0</sub> =UCS/10) (psi/ft)
0.6	>0.6 <sup>a</sup> to 1.24	0.7 to 1.47
0.8	0.88 to 1.75	1.26 to 1.99
0.94	1.07 to 2.21	1.71 to 2.55

All calculated SHmax values assume a drilling fluid that is cooler than the ambient formation temperature. The orientation of SHmax inferred from DIFs falls ranges from 0 to 75° centered around 30°.

a. actual value is likely slightly greater than Shmin, but could not be determined by visual interpretation of the stress polygon analysis)

**Table 4-4. Summary of SHmax values determined with stress polygon method for 12 DIFs for two tensile strength scenarios and three values of Shmin (only DIFs in vertical section of borehole included [depth less than 5638 ft]).**

Shmin (psi/ft)	SHmax Range (T <sub>0</sub> =0) (psi/ft)	SHmax Range (T <sub>0</sub> =UCS/10) (psi/ft)
0.6	0.68 to 1.24	0.82 to 1.47
0.8	1.15 to 1.75	1.38 to 1.99
0.94	1.45 to 2.21	1.71 to 2.43

All calculated SHmax values assume a drilling fluid that is cooler than the ambient formation temperature. The orientation of SHmax inferred from DIFs ranges from 0 to 75° centered around 30°.

## 4.6 Verification of SHmax Magnitude Values from Stress Polygon

The SHmax values determined from the stress polygon method were checked using the equation below. It should be noted that this equation is valid only for the vertical section of the borehole.

$$SH_{max} = 3Sh_{min} - \alpha P_p - P_w + T_0 - \left( \frac{\alpha_{TC} \times E \times \Delta T}{1 - \nu} \right) \quad \text{Equation 4-1}$$

where:

Shmin is the minimum horizontal stress (psi),

$\alpha$  is the Biot coefficient (0.35),

Pw is the differential fluid pressure (mud pressure minus ambient pore fluid pressure (psi/ft)); the differential mud pressure in the DIFs stress polygons was calculated as mud weight minus the pore pressure gradient. It is assumed it was just the mud pressure creating the induced fractures during drilling (with borehole cooling). In the stress polygon analysis for MF-2 and MF-4, the differential mud pressure is the breakdown pressure gradient read from the pressure curves minus the pore pressure gradient. The borehole had to pressurize to induce a fracture during the test. The breakdown pressure gradient is 0.64 psi/ft for MF-2 and 0.61 psi/ft for MF-4.

Subtracting the pore pressure gradient (0.4 psi/ft) from these breakdown pressure gradients resulted in differential mud pressure of 0.24 and 0.21 psi/ft for MF-2 and MF-4, respectively.

$T_o$  is tensile strength (psi); two cases were considered to calculate a low estimate and a high estimate of SHmax:

$T_o=0$  (this scenario will produce the low value of SHmax)

$T_o = UCS/10$  (this scenario will produce the high value of SHmax)

$\alpha_{TC}$  is the thermal expansion linear coefficient of  $7.4 \times 10^{-6} \text{ 1/}^\circ\text{C}$  ( $4.11 \times 10^{-6} \text{ 1/}^\circ\text{F}$ ),

E is the Young's Modulus (psi),

$\Delta T$  is the temperature difference ( $^\circ\text{F}$ ) between the drilling fluid and the ambient temperature of the rock (i.e., borehole cooling due to drilling and circulating cold drilling mud/fluid). The temperature log from June 24 is considered the coolest the borehole has ever been – this log was used to estimate temperature difference to calculate SHmax.

$\nu$  is the Poisson's Ratio.

The calculated values of SHmax were determined to be within  $\pm 10\%$  of the values determined using the stress polygon method for the 12 DIFs that are in the vertical section of the borehole (DIFs in the deviated section of the borehole could not be validated with this equation). Note that there are 144 values of SHmax that were verified (i.e., 12 DIFs; three Shmin values, two tensile strength scenarios, two temperature scenarios).

## 5 CALCULATING SHMIN AND SHMAX DEPTH PROFILES

Shmin and SHmax calculated at discrete depth points (where DIFs were observed) were used to develop a “continuous” depth profile of Shmin and SHmax values for the 16B(78)-32 well.

Two curves are presented for both the Shmin and SHmax depth profiles (Figure 5-1), including:

1. An effective stress ratio (ESR) method derived (smooth) curve which was derived assuming a constant value for ESR (a different value of ESR was used to calculate Shmin and SHmax). The ESR is defined as  $ESR_{Shmin} = (Shmin - P_p)/(S_v - P_p)$  and  $ESR_{SHmax} = (SHmax - P_p)/(S_v - P_p)$ , which can be rearranged as follows to estimate Shmin and SHmax at any depth:

$$Shmin = ESR_{Shmin}(S_v - P_p) + P_p \quad \text{Equation 5-1}$$

$$SHmax = ESR_{SHmax}(S_v - P_p) + P_p \quad \text{Equation 5-2}$$

where:

Shmin = minimum horizontal stress gradient (psi/ft),

SHmax = maximum horizontal stress gradient (psi/ft),

Sv = vertical stress gradient (1.08 psi/ft),

Pp = Pore pressure (0.4 psi/ft)

2. A poroelastic (stress contrast) derived Shmin and SHmax curve described by the following equation (Zhang et al., 2023):

$$Shmin = \frac{\nu}{(1-\nu)}(\sigma_v - \alpha P_p) + \alpha P_p + \frac{E_{sta}}{(1-\nu^2)}(\epsilon_h + \nu\epsilon_H) \quad \text{Equation 5-3}$$

$$SHmax = \frac{\nu}{(1-\nu)}(\sigma_v - \alpha P_p) + \alpha P_p + \frac{E_{sta}}{(1-\nu^2)}(\epsilon_H + \nu\epsilon_{hH}) \quad \text{Equation 5-4}$$

where:

SHmax = maximum horizontal stress (psi),

Shmin = minimum horizontal stress (psi),

Pp = Pore pressure (psi),

E<sub>sta</sub> = static Young's Modulus (psi),

$\nu$  = static Poisson's Ratio,

$\epsilon_h$  = tectonic strain in the minimum horizontal stress direction,

$\epsilon_H$  = tectonic strain in the maximum horizontal stress direction, and

$\alpha$  = Biot's coefficient (0.35).

The analysis of Shmin in Section 3 determined that Shmin varies from 0.6 to 0.94 psi/ft depending on how the thermal effect of cooling during the min-frac tests was accounted for. These scenarios included:

- $Sh_{min}=0.6$  psi/ft (no adjustment for cooling)
- $Sh_{min}=-0.94$  psi/ft (high adjustment for cooling; 0.34 psi/ft)
- $Sh_{min} = 0.8$  psi/ft (mid-range adjustment for cooling; 0.2 psi/ft)

Therefore,  $Sh_{min}$  and  $SH_{max}$  depth profiles were developed for each of these three cases using the two methods described above. Input parameter values used to calculate the  $Sh_{min}$  and  $SH_{max}$  curves are summarized in Table 5-1. The resulting depth profiles are shown in Figure 5-1 (no adjustment for cooling), Figure 5-2 (high adjustment for cooling), and Figure 5-3 (mid range adjustment for cooling). It is noted that the methods used to calculate the depth profiles are approximation methods and are not universally accepted, therefore, the depth profiles for  $Sh_{min}$  and  $SH_{max}$  should be considered approximations.

**Table 5-1. Effective Stress Ratios and Tectonic Strains used to calculate  $Sh_{min}$  and  $SH_{max}$  Depth Profiles**

Shmin Case	Shmin ESR	Shmax ESR ( $T_0 = UCS/10$ )	Tectonic Strain $E_h$ ( $T_0 = UCS/10$ )	Tectonic Strain $E_H$ ( $T_0 = UCS/10$ )
0.6 psi/ft	0.3 (shallow) 0.43 (deep) <sup>a</sup>	0.8	0	0.0003
0.8 psi/ft	0.6	1.5	0.00002	0.0007
0.94 psi/ft	0.8	2.1	0	0.001

a. An ESR value of 0.3 for the shallow section was found to provide the best match to the two calibration points from MF-2 and MF-4, whereas an ESR of 0.43 was used for the deeper section to match the trend of the poroelastic curve and to honor the DFIT closure pressures from well 58-32.

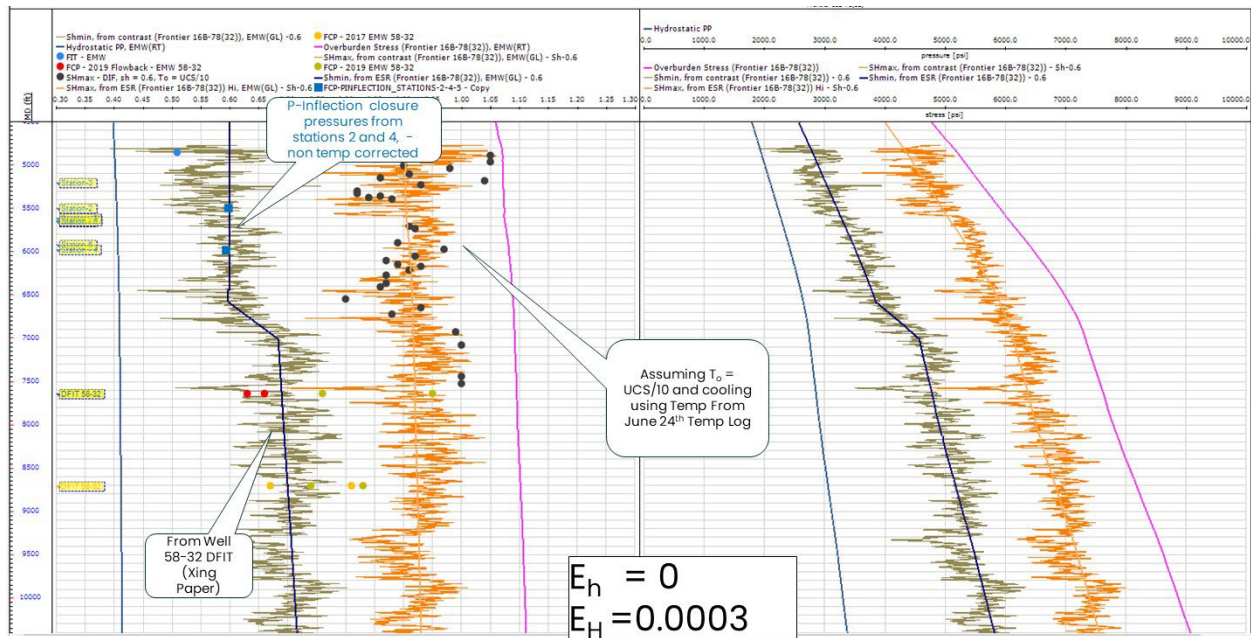


**Figure 5-1. A set of  $Sh_{min}$  and  $SH_{max}$  curves are presented with  $Sh_{min}$  calibrated to the non-temp adjusted closure pressures from the P-inflection method for Stations MF-2 and MF-4. The continuous blue  $Sh_{min}$  curve was constructed using an ESR of 0.3 in the shallower section and 0.43 in the deeper section to match the trend of the Poroelastic (green) curve and to honor the DFIT closure pressures from well 58-32 (shown by red dots). The black dots indicate the  $SH_{max}$  magnitudes calculated from DIFs given an  $Sh_{min}$  magnitude of 0.6 psi/ft and assuming cooling during drilling.**

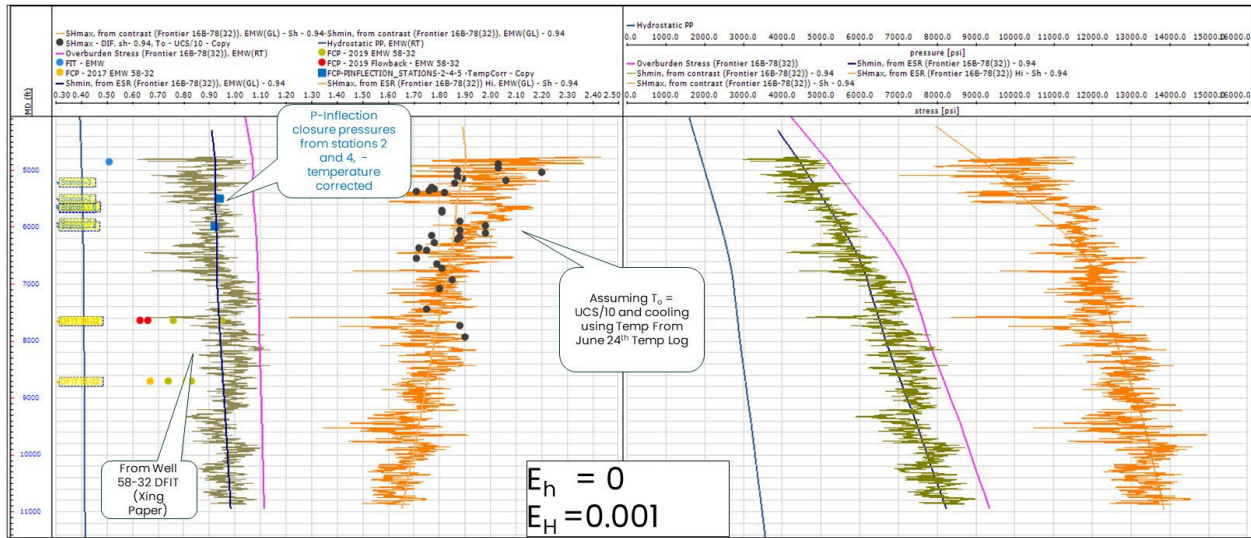


**Figure 5-2.** A different set of Shmin and SHmax depth curves are presented with Shmin being calibrated to only the temp adjusted (using the high end temperature adjustment) closure pressure from P-inflection method in Stations MF-2 and MF-4. The black dots indicate the SHmax magnitudes from the stress polygon analysis of DIFs given an Shmin magnitude of 0.94 psi/ft and assuming cooling during drilling. The resultant stress regime is strike slip. This scenario is considered less likely as the modeled wellbore failures do not match observations.

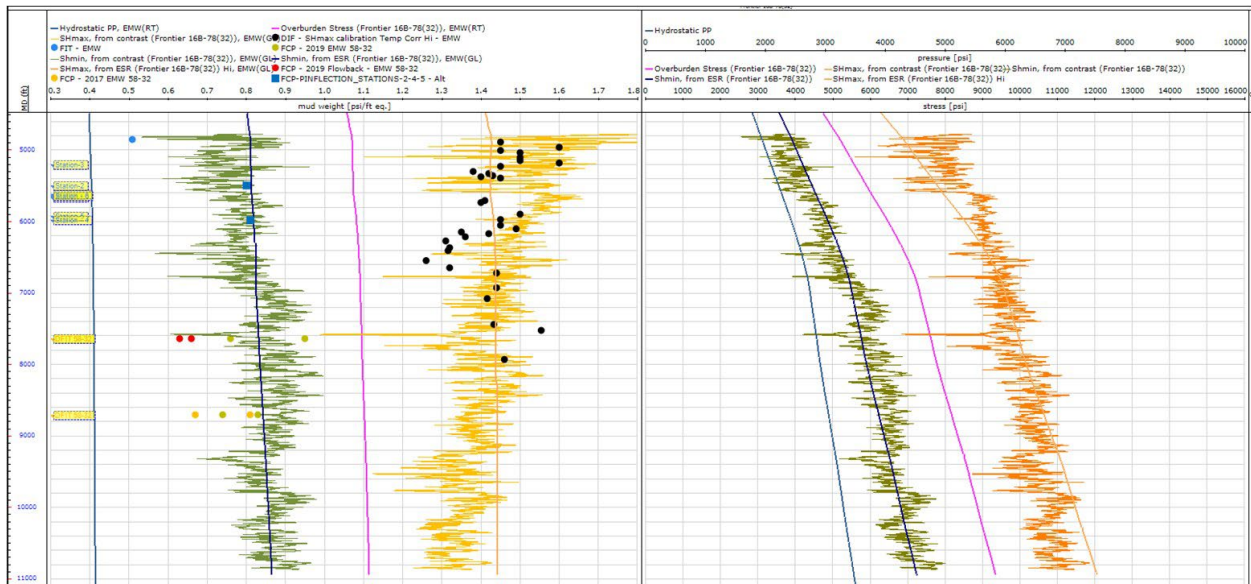


**Figure 5-3.** Shmin and SHmax depth curves with Shmin being calibrated to only the temp adjusted (using the mid value temperature adjustment) to closure pressure from P-inflection method in Stations MF-2 and MF-4. The black dots indicate the SHmax magnitudes from the stress polygon analysis of DIFs given an Shmin magnitude of 0.8 psi/ft and assuming cooling during drilling.

Based on [Figure 5-1](#) (no temperature adjustment to fracture closure pressure for cooling during minifrac tests), the  $S_{hmin}$  gradient is between  $\sim 0.6$  psi/ft in the shallower section and  $\sim 0.7$  to  $\sim 0.75$  psi/ft in the deeper section of the borehole. In this scenario, a normal faulting regime is indicated ( $S_v > S_{Hmax} > S_{hmin}$ ). Based on [Figure 5-2](#) (“high” temperature adjustment [0.94 psi/ft] to fracture closure pressure for cooling during minifrac tests), the  $S_{hmin}$  gradient is between  $\sim 0.9$  psi/ft and  $\sim 1.0$  psi/ft across the entire borehole section. In this scenario, a strike slip faulting regime is indicated ( $S_v > S_{Hmax} > S_{hmin}$ ). Based on [Figure 5-3](#) (“middle” temperature adjustment [0.8 psi/ft] to fracture closure pressure for cooling during minifrac tests), the  $S_{hmin}$  gradient is between  $\sim 0.8$  psi/ft and  $\sim 1.0$  psi/ft across the entire borehole section. Including the adjustment for cooling increases the values of  $S_{hmin}$  and  $S_{Hmax}$  such that they now bound the  $S_v$  curve, which changes the stress regime from normal to strike-slip ( $S_{Hmax} > S_v > S_{hmin}$ ).

## 6 DISCUSSION (SUPPLEMENTAL ANALYSES)

This section provides supplemental information from further analysis and interpretation of the minifrac test data, including:

- Analysis of stress regime ([Section 6.1](#))
- Analysis of flowback data for estimating fracture closure pressure ([Section 6.1.3](#))
- Analysis of re-opening pressure ([Section 6.2.2](#))
- Discussion of pressure response data during minifrac tests ([Section 6.4](#)).

### 6.1 Stress Regime

Additional analysis was performed to determine if a strikeslip regime or a normal stress regime can be explained/supported using DIFs and shearing of weak planes in well 16B(78)-32. This analysis is based on the deviated section of the well because the orientation of the wellbore and orientation of SHmax affect location of DIFs and shearing of the weak plane along the wellbore. On the other hand, in the vertical section, it is only orientation of SHmax which determines the location of DIFs and shearing of the weak plane. Different stress regimes cause the tensile fractures and shear fractures to form on different sides of the deviated borehole wall. Two scenarios were built using the Stress and Failure of Inclined Boreholes (SFIB) software (Baker Hughes) to predict tensile failure and shear failure at a wellbore for a normal and a strike slip stress regime. Table 6-1 shows parameters used for both models.

**Table 6-1. Parameters used for modeling DIFs.**

	<b>Model 1</b>	<b>Model 2</b>
<b>Stress Regime</b>	<b>Normal Stress Regime</b>	<b>Strike Slip Stress Regime</b>
Stress (Sh, SH, Sv) gradient (psi/ft)	0.6,0.9,1.1	0.8,1.5,1.1
Pore pressure gradient (psi/ft)	0.4	0.4
Well mud pressure (psi/ft)	0.404	0.404
Biot Coefficient	0.35	0.35
Well Azimuth (degrees relative to North)	103	103
Well Deviation (degrees from vertical)	70	70
Poisson Ratio	0.3	0.3
Young's Modulus (psi)	6.5e+6	6.5e+6
Thermal Coefficient (1/°F)	4.11e-6	4.11e-6
Cooling Temperature (°F)	100	100
SH azimuth (degrees relative to North)	30	30
Tensile Strength (psi)	0	0

#### 6.1.1 Tensile Failure Modeling

[Figure 6-1](#) and [Figure 6-2](#) show the expected location of a DIF using model 1 (normal stress regime), and model 2 (strike slip regime). DIFs were generated for a normal stress regime and a strike slip stress regime. The required tensile strength determines the locations in the borehole where fractures can be generated. The fractures develop within the regions in the wellbore with the required tensile strength (assigned as zero in both scenarios) or lower. As [Figure 6-1](#) shows, a DIF is likely to occur predominantly at the top and bottom (0 and 180°) location of the deviated borehole in a normal stress regime. On the other hand, DIFs are likely to occur on the sides (i.e., 90 and 270°) of the deviated borehole in a strike

slip regime (Figure 6-2). Note that fractures have a width (92° for normal stress regime, and 37° for strike slip case) so it is continuous along its center. The inclination of the fractures is the same in both cases (~70°). There is almost 45° difference in position of the center of the fractures around the wellbore (335° for normal case from top location of wellbore, and 289° for strike slip case from top location of wellbore).

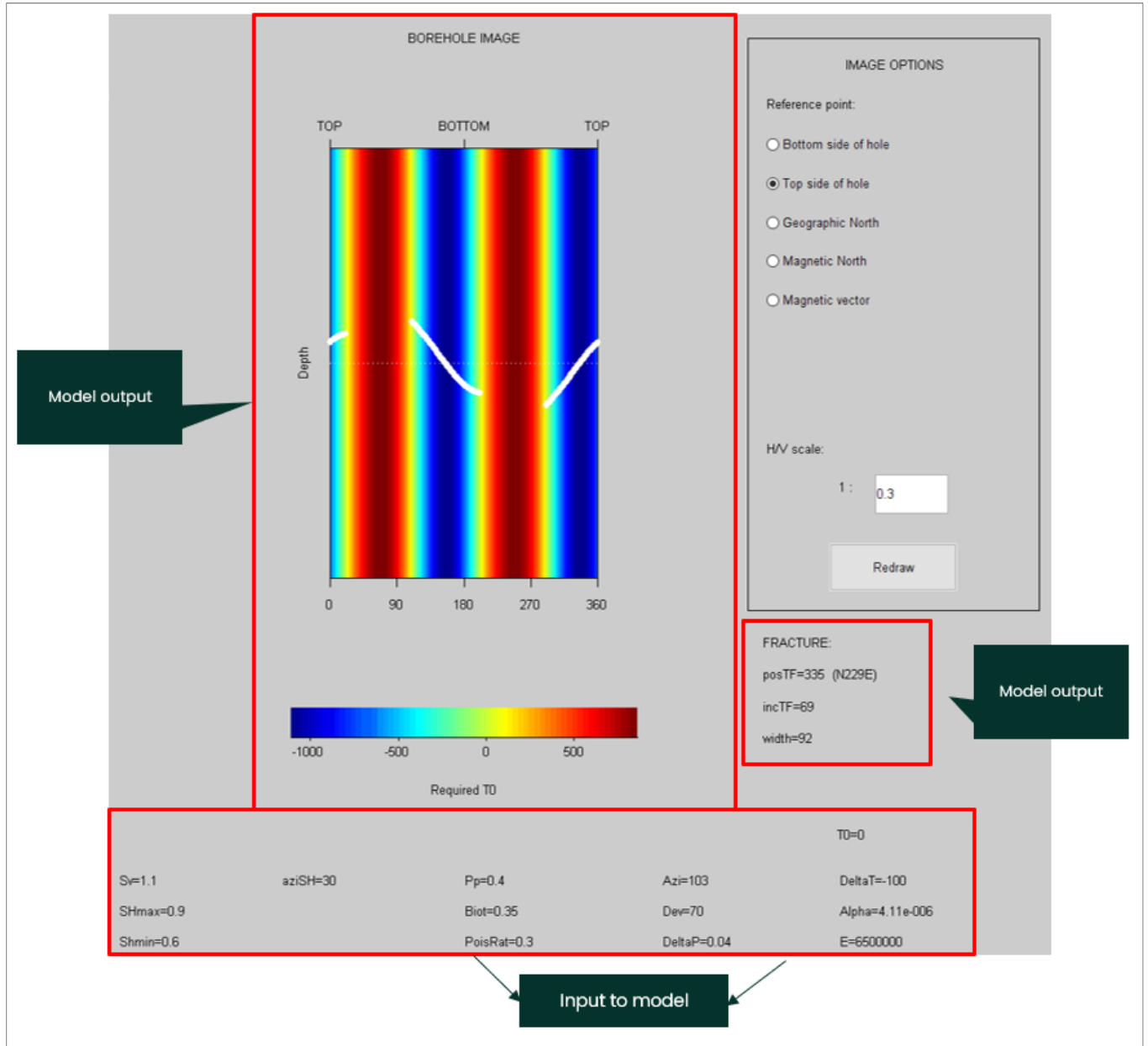
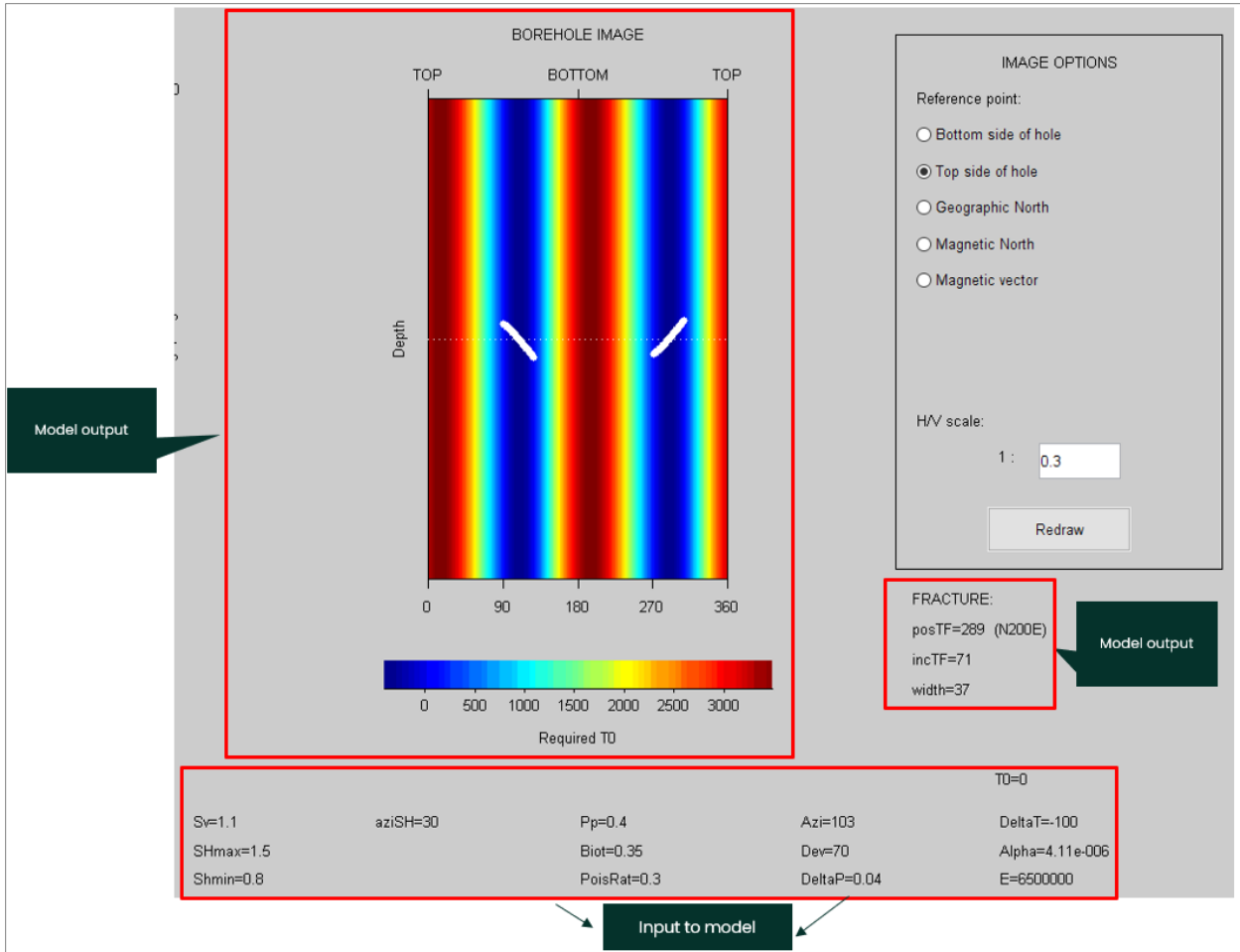


Figure 6-1. Predicted DIF location in deviated borehole for normal stress regime. White lines represent the DIF. DIF is likely to occur predominantly at the top and bottom (0 and 180°).



**Figure 6-2. Predicted DIF location in deviated borehole for strike slip stress regime. White lines represent the DIFs. DIF are likely to occur predominantly on the sides (90 and 270°) of the borehole.**

Figure 6-3 through Figure 6-5 are image logs for three deviated sections of the 16B(78)-32 well showing the occurrence of DIFs. The drilling induced tensile fractures are highlighted in blue rectangles (which is the focus of the analysis in this section). As shown in these figures, DIFs occur predominantly in the sides of the borehole (i.e., 90 and 270°), indicating, that a strike slip stress regime is more likely than a normal stress regime for 16B(78)-32.

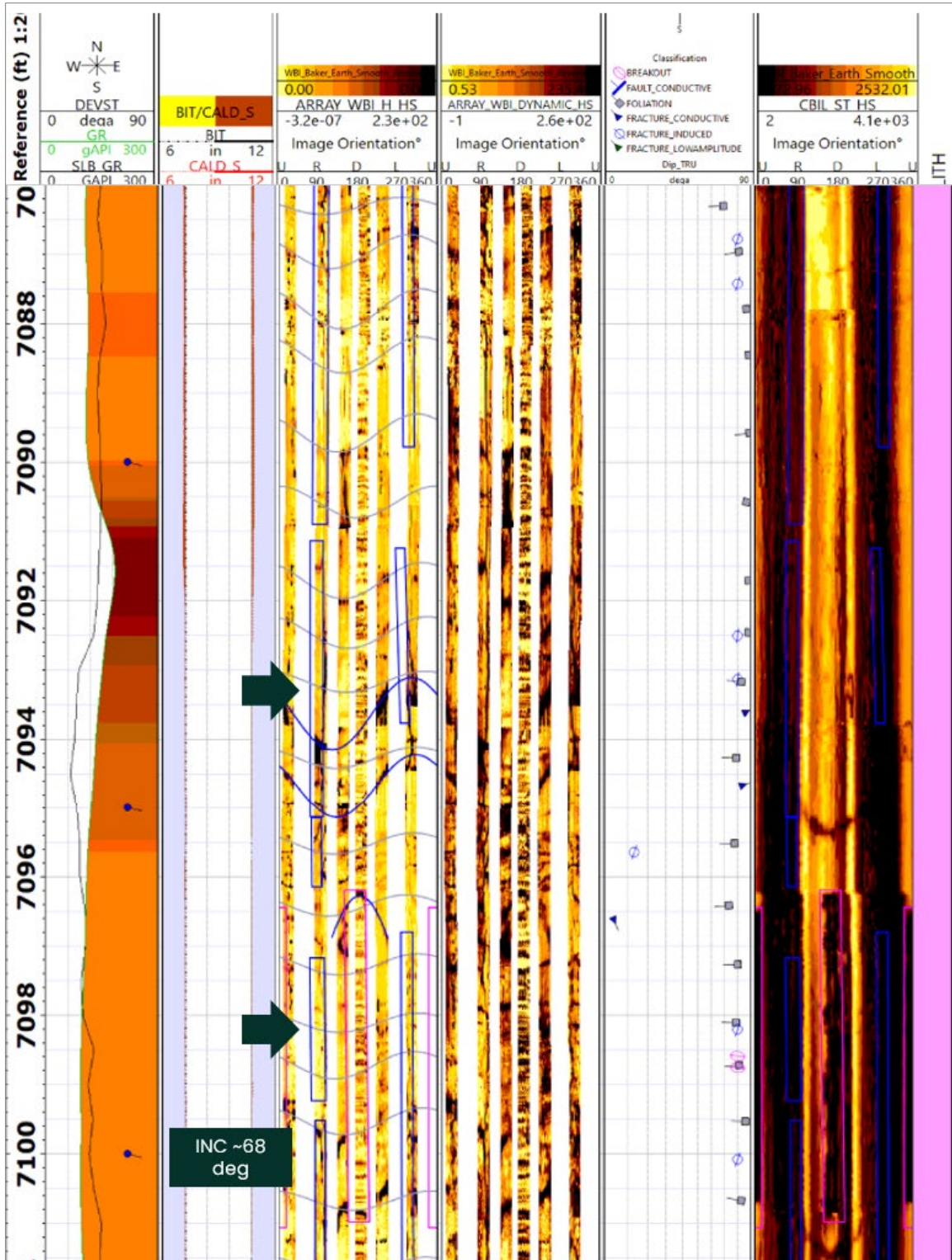


Figure 6-3. Image log for depth interval 7086 to 7101 ft of well 16B(78)-32, which is in the deviated section (inclination = 68°). Blue boxes show DIFs. All blue boxes are located on sides of the borehole.

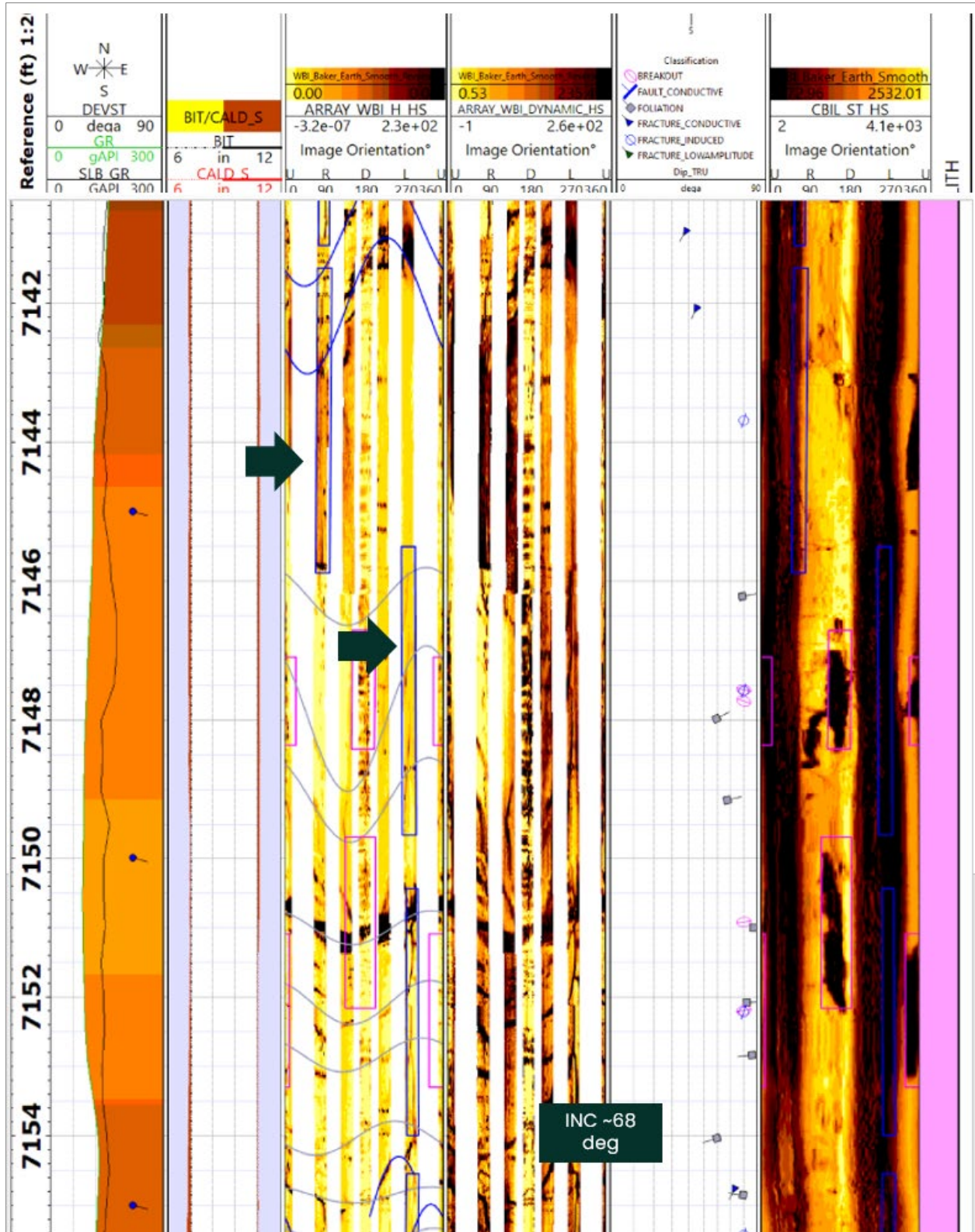


Figure 6-4. Image log for depth interval 7141 to 7155 ft of well 16B(78)-32, which is in the deviated section (inclination = 68°). In track 3, blue boxes show DIFs and pink boxes show breakouts. Blue boxes show DIFs. All blue boxes are located on sides of the borehole.

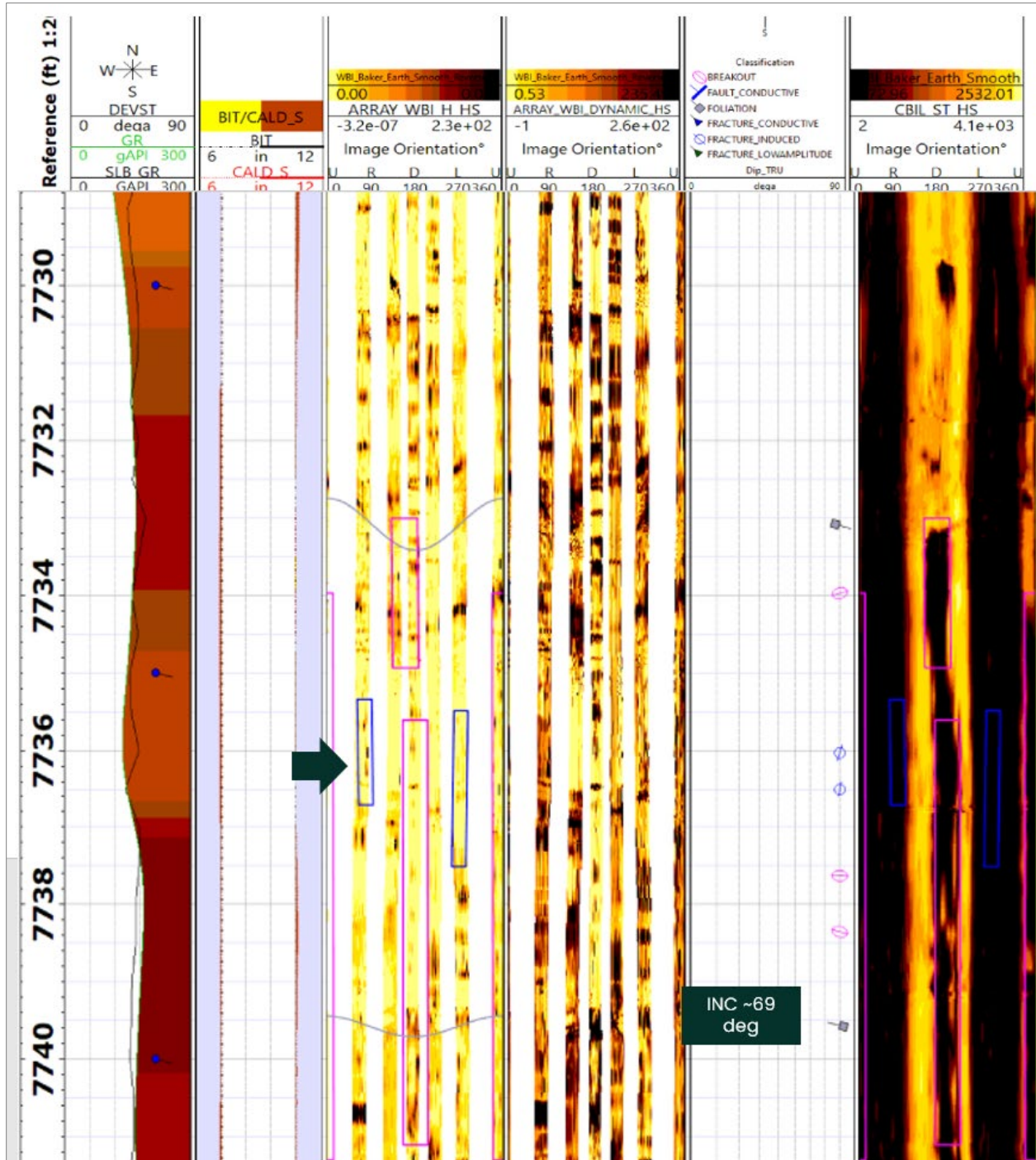


Figure 6-5. Image log for depth interval 7729 to 7741 ft of well 16B(78)-32, which is in the deviated section (inclination = 69°). In track 3, blue boxes show DIFs and pink boxes show breakouts. All blue boxes are located on sides of the borehole.

### 6.1.2 Shear Failure Modeling

Two models were built using the SFIB model to predict shear failures in a deviated borehole in a normal and a strike slip stress regime. Table 6-2 shows parameters used for both models.

**Table 6-2. Parameters used for modeling shear failure of a weak plane.**

Stress Regime	Model 1	Model 2
	Normal Stress Regime	Stike Slip Stress Regime
Stress (Sh, SH, Sv) gradient (psi/ft)	0.6,0.9,1.1	0.8,1.6,1.09
Pore pressure gradient (psi/ft)	0.4	0.4
Well mud pressure (psi/ft)	0.404	0.404
Biot Coefficient	0.35	0.35
Well Azimuth (degrees from North)	103	103
Well Deviation (degrees from vertical)	68	68
Poisson Ratio	0.3	0.3
friction coefficient of foliation	0.85	0.85
Cohesion of foliation	0	0
Foliation dip	60	77
Foliation azimuth	160	176
Friction coefficient of intact rock	0.85	0.85
Cohesion of intact rock	10000	10000

Figure 6-6 and Figure 6-7 show the expected location of shear fractures using model 1 (normal stress regime), and model 2 (strike slip regime). To model a weak plane, a planar feature (i.e., foliation in this work) and cohesion of zero for the foliation were assumed. Then, the shearing failure potential was predicted as well as its location along the plane using different stress regime assumptions. As Figure 6-6 and Figure 6-7 show, shear failure of a weak plane is likely to occur on the sides (90° and 270°) of the borehole in a normal regime, whereas a shear failure of a weak plane is likely to occur closer to the top and bottom of borehole in strike slip regime. Both models predict that the width of developed shear failure along weak bedding plane would be ~20°.

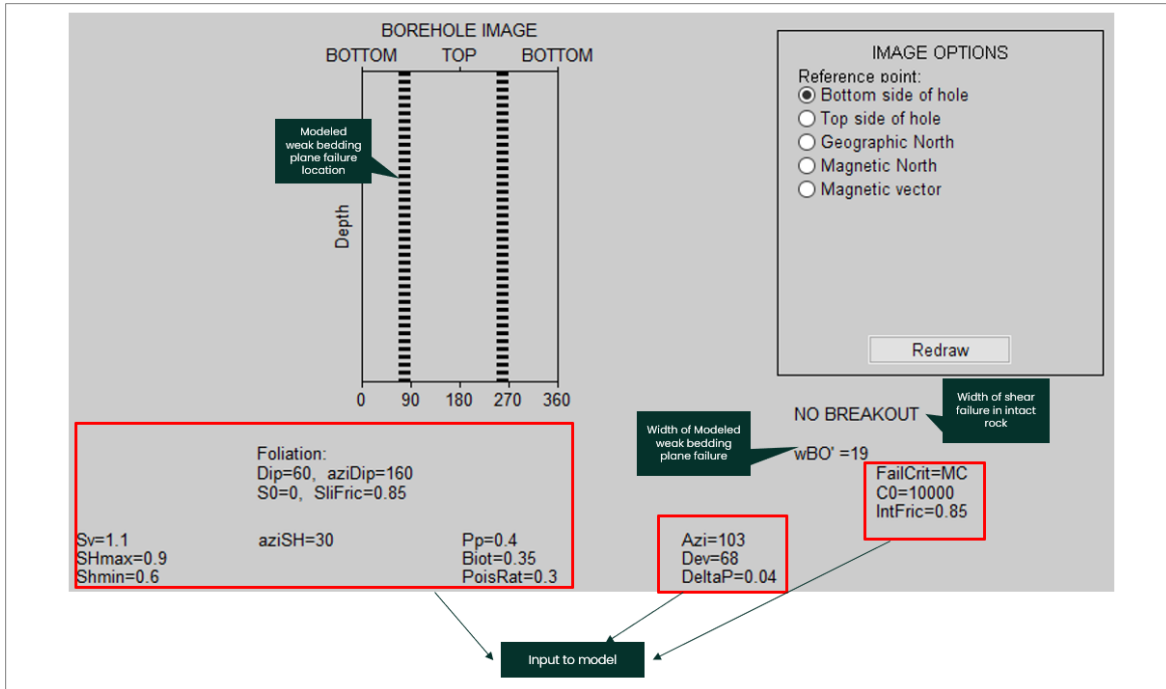
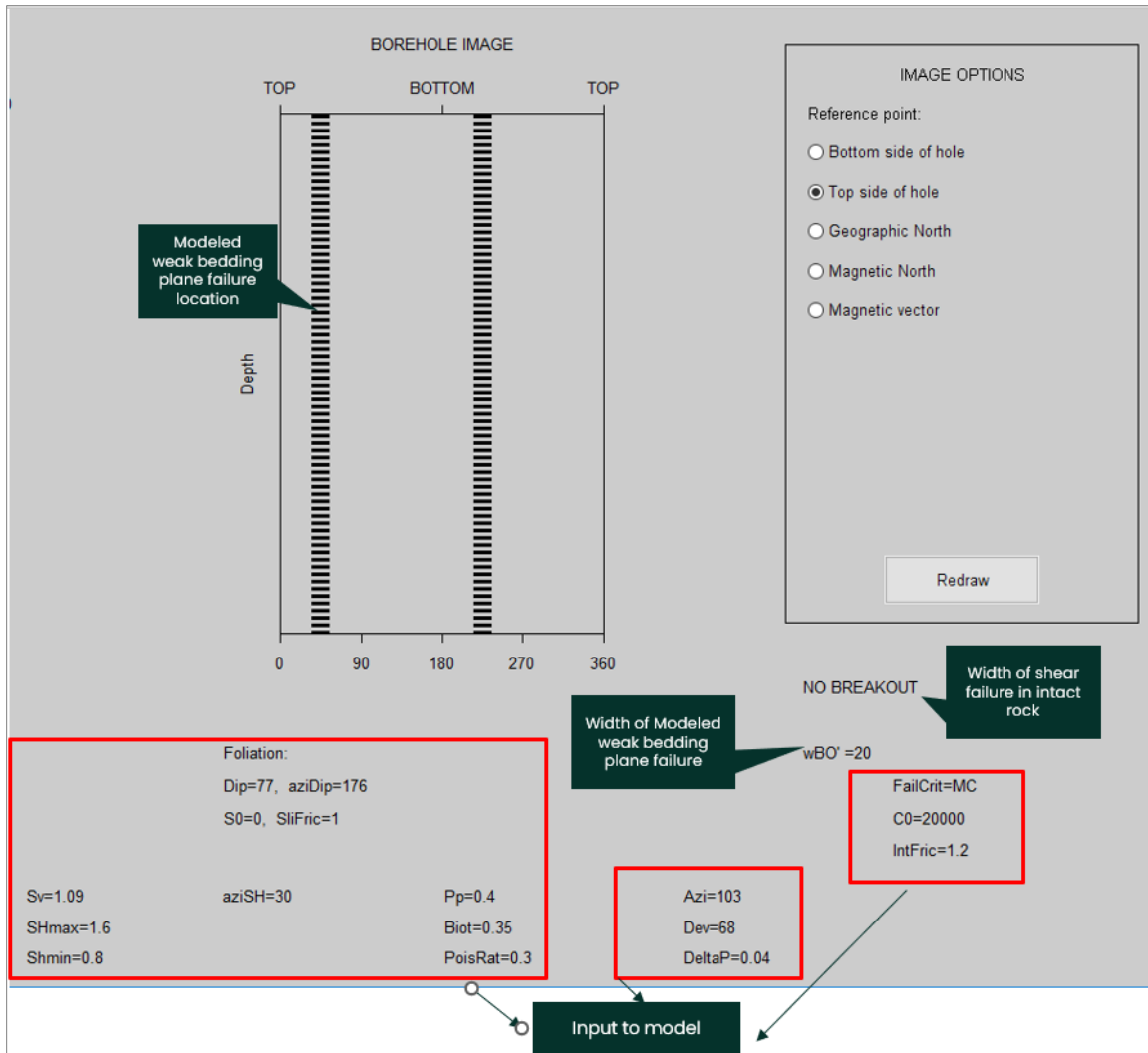


Figure 6-6. Predicted location of shear failure of a weak plane in a normal stress regime. Shear failure of a weak plane is likely to occur on the sides (90° and 270°) of the borehole in a normal regime.



**Figure 6-7. Predicted location of shear failure of a weak plane in a strike slip stress regime. Shear failure of a weak plane is likely to occur closer to the top and bottom) of the borehole in a strike slip regime.**

Figure 6-8 and Figure 6-9 are image logs showing a shear failure along a weak plane in the deviated section of the 16B(78)-32 well. The shear fractures are highlighted in blue rectangles. As Figure 6-8 and Figure 6-9 show, shear failures occur predominantly in the top and bottom of the borehole. As a result, this analysis indicates that the strike slip regime is more likely than the normal stress scenario.

Well Name: Forge 16B Log Date: Unknown  
Well Location: Utah Depth Range: 6,254.1 - 8,601.2 ft

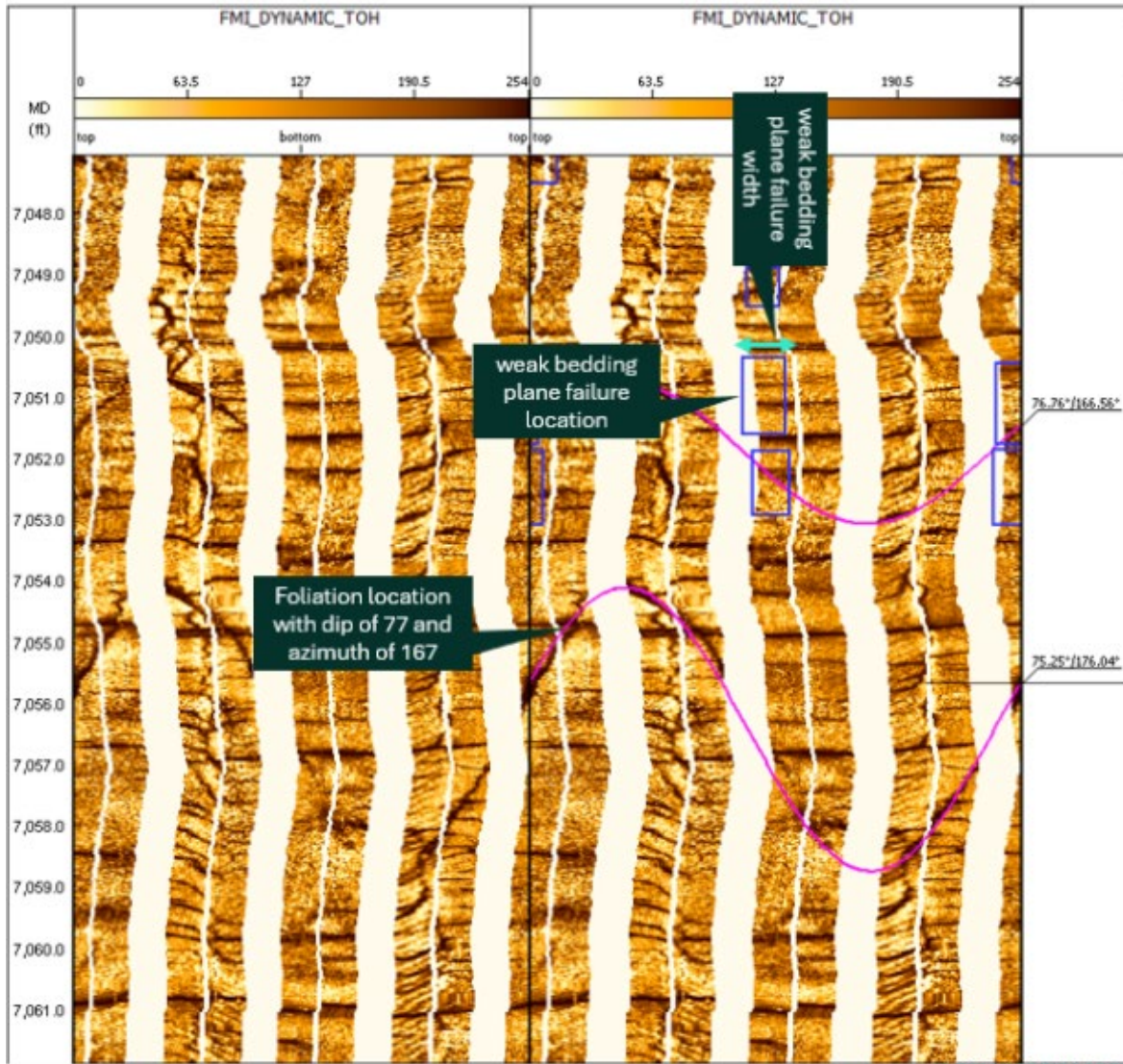


Figure 6-8. Image log of depth interval 7047 to 7062 ft in the 16B(78)-32 well. Blue boxes show rock shear failure along weak plane. Blue boxes are located on top/bottom of borehole. Pink curves show foliation locations. Note: additional foliations probably existed above/below two examples in image log ones (which is not depicted,) and weak bedding plane shear failure above two example foliations overlaying on them.

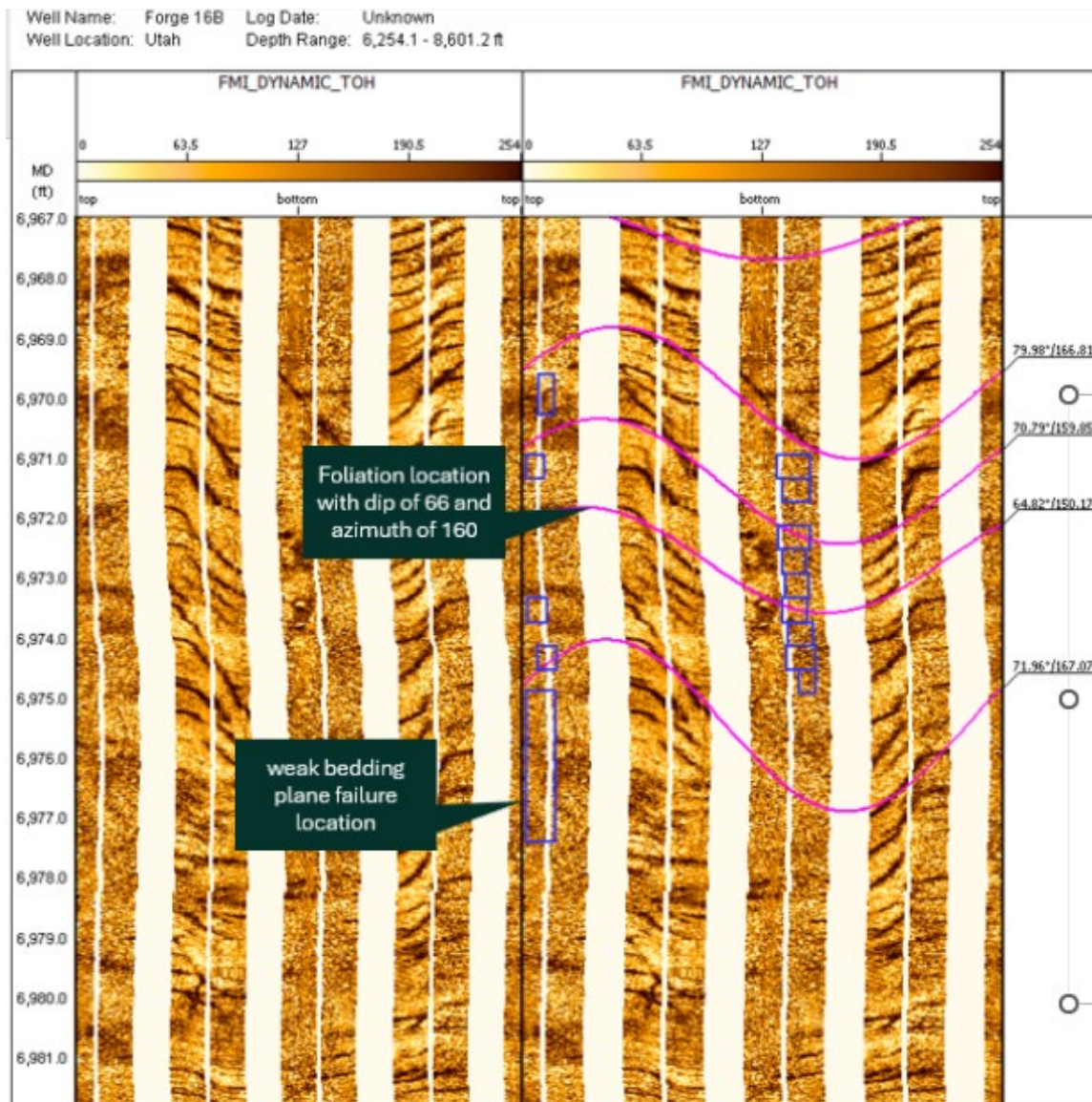


Figure 6-9. Image log of depth interval 6967 to 6981 f ft in the 16B(78)-32 borehole. Blue boxes show rock shear failure along weak plane. Blue boxes are located on top/bottom of borehole. Pink curves show foliation locations.

### 6.1.3 Stress Regime Summary

Different stress regimes cause tensile fractures and shear fractures along weak planes to form on different locations of the deviated borehole wall. Two scenarios were built using the BH SFIB model to study the impact of stress regime on the location of the tensile fractures and shear fractures along weak planes for a deviated section of the 16B(78)-32 borehole. Results show DIFs are more likely to occur on the sides of the deviated borehole (Figure 6-3 to Figure 6-5), whereas shear failure of weak bedding planes are more likely to occur at the top and bottom of the deviated borehole. The predicted locations of the tensile fractures (sides of borehole) and shear fractures along weak planes (top/bottom of borehole) are indicative of a strike slip stress regime. As a result, this analysis indicates that the strike slip regime is more likely than the normal stress regime.

According to Xing et al. (2022), the Utah FORGE site is located in the Basin and Range province, which is characterized as an extensional and normal faulting regime; however, strike-slip faulting is seen in the Sevier Valley region (Arabasz and Julander, 1986) and in the Escalante Valley (Whidden and Pankow, 2012), which are close to the Utah FORGE site. Xing et al. (2022) performed image log analysis of well 16A(78)-32 to constrain SHmax magnitude. Their results show the estimated magnitude of SHmax largely depends on the formation's compressive strength. Based on their breakouts analysis, both normal and strike-slip fault regimes are possible for the Utah FORGE site. Aljubran et al. (2021) conducted image log analysis and stress polygon analysis using image log data of well 58-32. Their stress polygon analysis shows normal and strike slip regimes are both possible. The stress polygon analysis in this study, based on minifrac results and DIFs, shows the stress regime is dependent on the magnitude of Shmin (whether 0.6, 0.8 or 0.94) and that normal and strike slip are both possible. As discussed in this section, the strike slip regime is more likely than the normal stress regime.

## 6.2 Flowback Analysis for Estimating Fracture Closure Pressure

Flowback tests are an alternative technique to estimate fracture closure pressure compared to methods that utilize fall-off data. Flowback tests are typically performed to reduce closure pressure measurement time when the fall-off period to estimate fracture closure pressure is long (Eltaleb and Soliman, 2023), for example in rocks with very low permeability. The system stiffness approach is the common way to interpret closure pressure during flowback tests (system stiffness increases when fracture closes [Raean and Brudy, 2001]). Using a constant and controlled flowback rate, pressure response is estimated by total compressibility of the system (both wellbore fluid and fracture). A characteristic change in the slope of the pressure versus return volume curve (increasingly negative slope) is expected during the flowback period when fracture closure occurs, as shown in Figure 6-10 (Savitski and Dudley, 2011). This is due to flow restriction that occurs when the fracture closes. Above point A, the slope of the curve represents stiffness of system when fracture is open. Below point C, the slope represents stiffness of only wellbore fluid since the fracture is closed. The fracture is closed during the transition between two slopes as shown in Figure 6-10 (Savitski and Dudley, 2011).

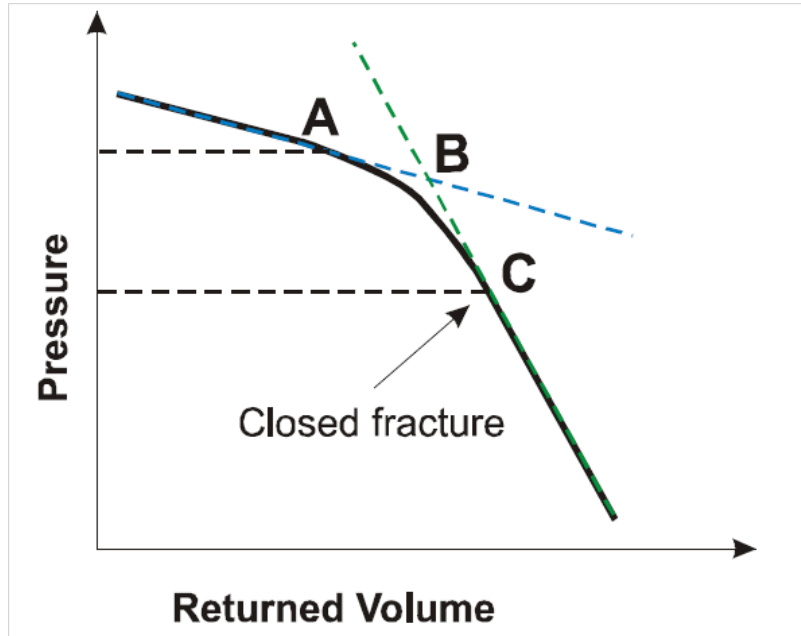


**Figure 6-10. A diagnostic plot of the flowback test showing characteristic increasingly negative slope (Savitski and Dudley, 2011).**

Xing et al. (2020b) performed flowback tests as a part of a diagnostic fracture injection test (DFIT) in well 58-32 at the Utah FORGE site to estimate fracture closure pressure. Note that not all of the flowback tests performed during DFIT tests for well 58-32 were used for closure pressure analysis. This was due to (1) flowback analysis not being started soon enough after shut-in (i.e., fracture closed before flowback period), and (2) issues related to volumetric flowback rate. When flowback starts late after shut-in, the corresponding pressure will be lower than true closure pressure thus preventing inference of closure pressure. For example, in one test performed by Xing et al. (2020b), the estimated closure pressure using flowback analysis (~ 2175 psi) was much lower than closure pressure estimated from an extended shut-in period (~2806 psi) using DFIT tests. The lower estimated closure pressure using flowback analysis could be due to (1) picking artificial gradient if flowback started after fracture already began to close during shut-in period; or (2) impact of natural fractures where there is tortuous connection between wellbore and natural fractures (Xing et al., 2020a). If flowback is longer than the natural fall-off shut-in period, flowback analysis could minimize the impact of natural fractures. As a result, flowback analysis can give a better estimate of closure pressure in natural fractured intervals of a formation (Xing et al., 2020a).

Xing et al. (2020b) performed flowback tests as a part of a diagnostic fracture injection test (DFIT) in well 58-32 at the Utah FORGE site to estimate fracture closure pressure. Note that not all of the flowback tests performed during DFIT tests for well 58-32 were used for closure pressure analysis. This was due to (1) flowback analysis not being started soon enough after shut-in (i.e., fracture closed before flowback period), and (2) issues related to volumetric flowback rate. When flowback starts late after shut-in, the corresponding pressure will be lower than true closure pressure thus preventing inference of closure pressure. For example, in one test performed by Xing et al. (2020b), the estimated closure pressure using flowback analysis (~ 2175 psi) was much lower than closure pressure estimated from an extended shut-in period (~2806 psi) using DFIT tests. The lower estimated closure pressure using flowback analysis could be due to (1) picking artificial gradient if flowback started after fracture already began to close during shut-in period; or (2) impact of natural fractures where there is tortuous connection between

wellbore and natural fractures (Xing et al., 2020a). If flowback is longer than the natural fall-off shut-in period, flowback analysis could minimize the impact of natural fractures. As a result, flowback analysis can give a better estimate of closure pressure in natural fractured intervals of a formation (Xing et al., 2020a).

### 6.2.1 Flowback Analysis for Minifrac Tests Conducted in This Study

Flowback analysis was attempted for multiple cycles of the seven minifrac tests performed in the 16B(78)-32 well. Two criteria were used to perform the flowback analysis and ensure the results are reliable. First, the slope of the P versus V curve during flowback should become increasingly negative (steeper), similar to what is shown by the pressure versus return volume curve in [Figure 6-10](#). Second, measured stiffnesses ( $dp/dv$ ) during the injection period and after closure during the flowback period should be similar (e.g., within 25 % of each other). Three of the seven minifrac tests provided useable data for the flowback method; these include MF-1 cycle 1, MF-5 cycle 1, and MF-6 cycle 1. The other four tests were not interpretable with the flowback method. This might be due to the following reasons: (1) a constant pumping (withdrawal) rate was not used in many cycles due to flowback pump limitations; and (2) several flowback tests were performed after a period of fall-off. As a result, the main closure might have occurred before flowback started. The flowback analysis of the three tests that meet the two criteria are discussed below.

[Figure 6-11](#) shows the bottom hole pressure versus flowback volume of cycle 1 of Station MF-1. As [Figure 6-11](#) shows, the slope increases, which could be a signature of fracture closure. The estimated closure pressure using this flowback analysis would be 3902 psi ([Figure 6-11](#)). Note that this cycle shows signature of closure using the ISIP and bi-linear methods (see [Section 3](#)) but did not show signature of fracture closure using the other fall-off analysis methods including G-Function plot, SRT method and log-log pressure derivative method. As a result, it is possible the fracture did not close completely during natural fall-off, and it finally closed during flowback time. The FCP estimate (3902) for cycle 1 of the MF-1 minifrac test is lower than the fracture closure pressure estimated using the ISIP estimated closure pressure from cycle 1 (4536 psi). Stiffness of the system (in this case mainly stiffness of wellbore fluid between straddle packers) during injection is 0.781 (psi/cc), and after fracture closure is very similar to 0.77 (psi/cc), which supports the claim that a fracture closed. Stiffness is calculated using the slope of pressure versus cumulative volume during the injection period and during the flowback period. Also, as [Figure 6-12](#) shows, the flowback rate is not constant in the test which might add uncertainty in results interpretation.

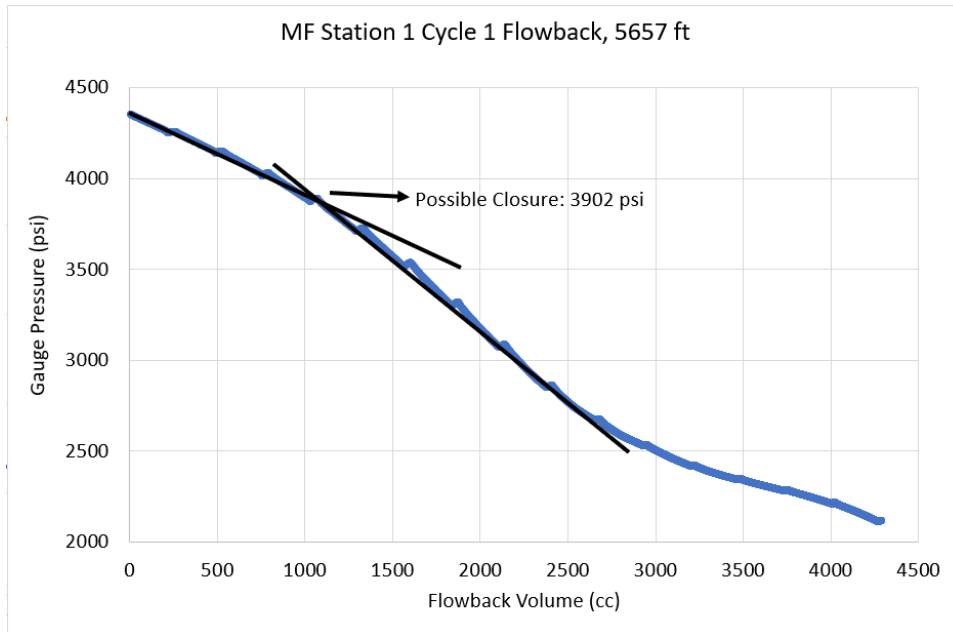


Figure 6-11. Pressure versus flowback volume curve for cycle 1 of Station MF-1.

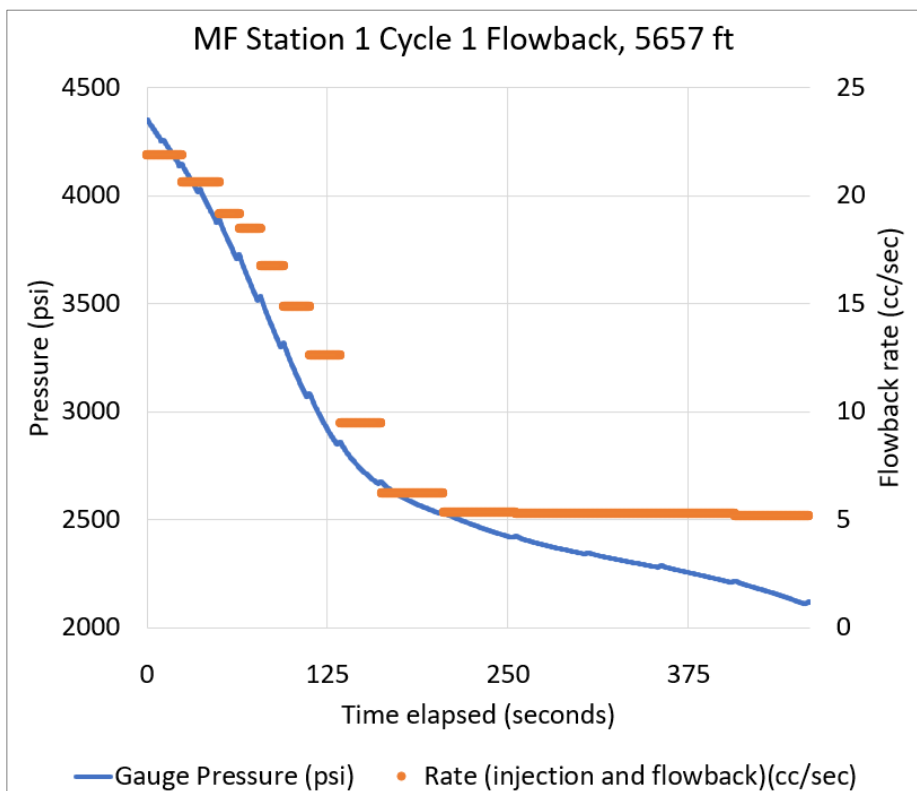


Figure 6-12. Pressure and flowback rate versus time for cycle 1 of Station MF-1.

Figure 6-13 shows the bottom hole pressure versus flowback volume of cycle 1 of Station MF-5. As Figure 6-13 shows, the slope of the pressure versus return volume becomes increasingly negative (steeper), which could be a signature of fracture closure. The estimated closure pressure using the flowback analysis method is 2932 psi (Figure 6-13). This cycle (similar to cycle 1 of Station MF-1) shows signature of closure using the ISIP and bi-linear methods but did not show signature of closure using the other fall-off analysis methods including G-Function plot, SRT method and log-log pressure derivative method. As a result, it is possible the fracture did not close completely during natural fall-off, and it finally closed during flowback time. Using flowback analysis, the estimated closure pressure (2932 psi) is lower than the ISIP estimated closure pressure from cycle 1 (3262 psi) and lower than the bi-linear closure pressure (3250 psi). Also, stiffness of the system during injection is 0.86 (psi/cc), and after fracture closure is 0.76 psi/cc. These stiffness values are considered to be sufficiently similar to meet the second criteria for fracture closure (although they are not as consistent as cycle 1 of Station MF-1, which may indicate that a fracture closed). Also, as Figure 6-14 shows, the flowback rate is not constant and it is noisy in the test which might add uncertainty in results interpretation.

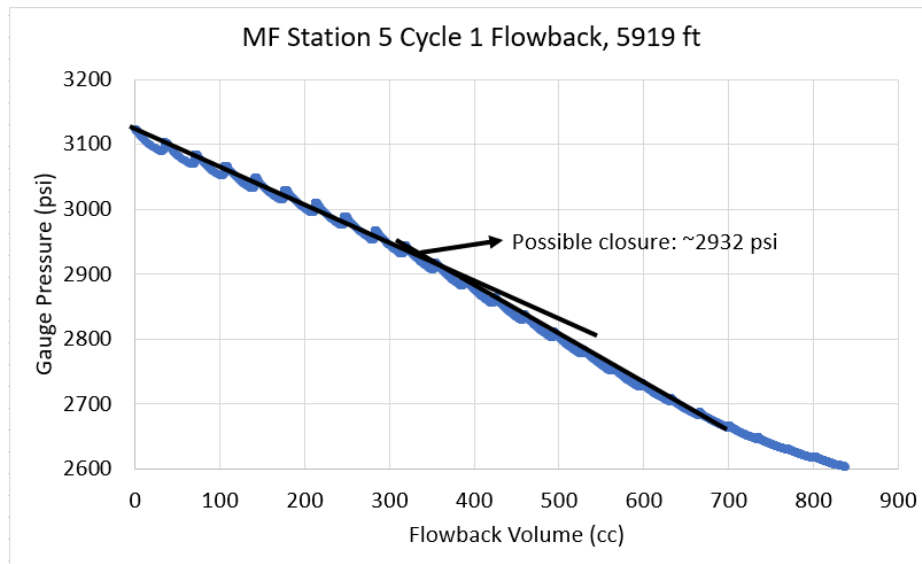
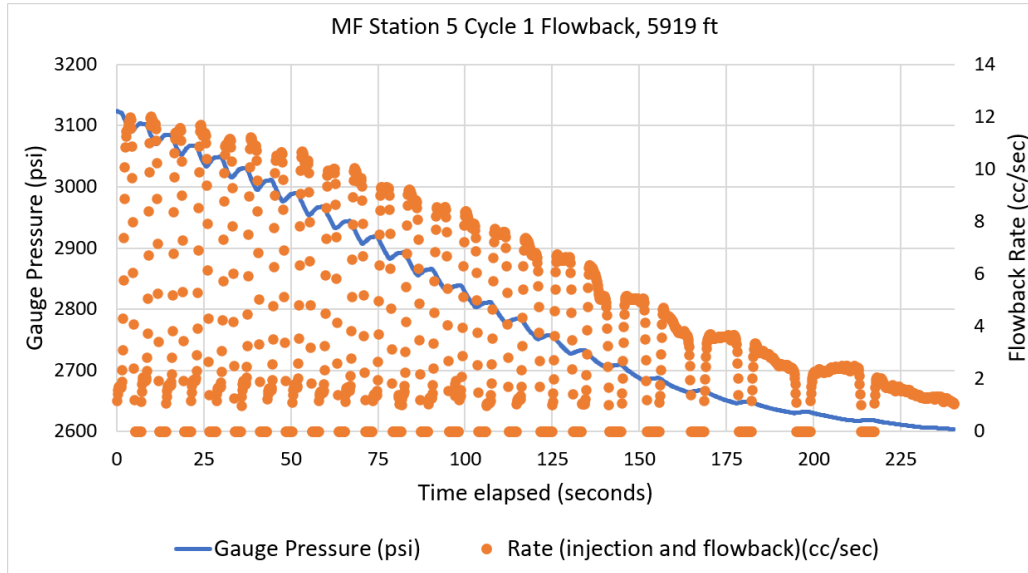


Figure 6-13. Pressure versus flowback volume curve for cycle 1 of Station MF-5.



**Figure 6-14. Pressure and flowback rate versus time for cycle 1 of Station MF-5.**

Figure 6-15 shows the bottom hole pressure versus flowback volume of cycle 1 of Station MF-6. As Figure 6-15 shows, the slope of pressure versus return volume becomes increasingly negative (steeper) which could be a signature of fracture closure. The estimated closure pressure using a flowback analysis would be 3231 psi. Note that this cycle (unlike cycle 1 of Station MF-1 and cycle 1 of Station MF-5) shows signature of closure using fall-off analysis methods including G-Function plot (3456, 3433, and 3419 psi), SRT method (3434 psi) and log-log derivative method (3462 psi). The estimated closure pressure using the flowback analysis method (3231 psi) is lower than the ISIP estimated closure pressure form cycle 1 (3476 psi) and the bi-linear closure pressure (3473 psi). Stiffness of the system during injection is 0.58 (psi/cc) is similar to the stiffness after fracture closure is 0.7 (psi/cc) (although they are not as consistent as cycle 1 of Station MF-1), which may indicate that fracture closed. Also, as Figure 6-16 shows, the flowback rate is not constant in the test which might add uncertainty in results interpretation.

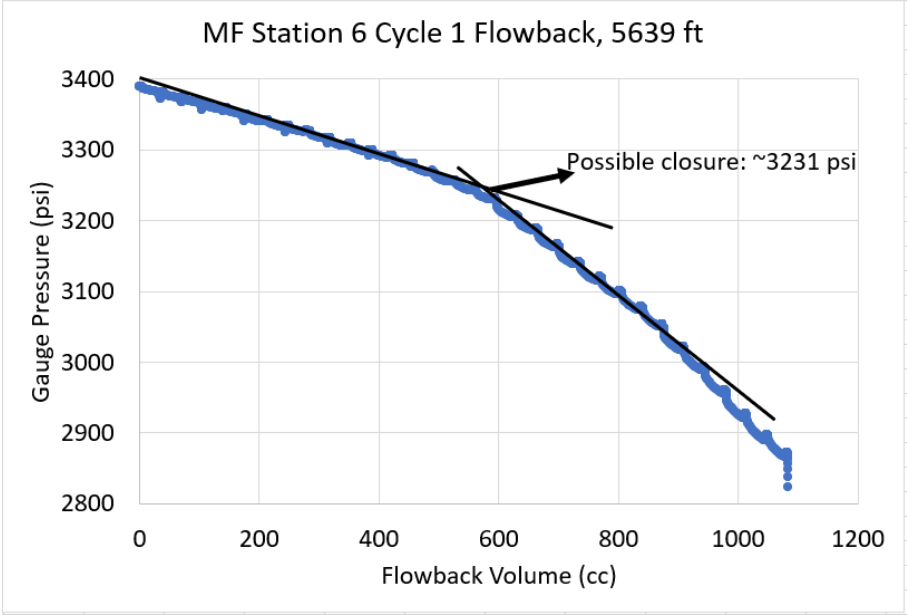


Figure 6-15. Pressure versus flowback volume curve for cycle 1 of Station MF-6.

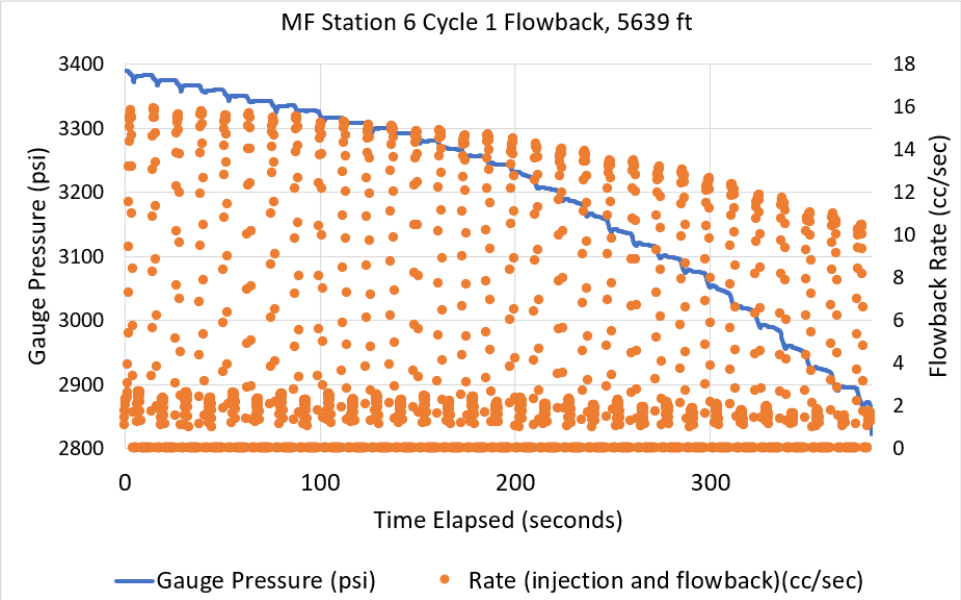


Figure 6-16. Pressure and flowback rate versus time for cycle 1 of Station MF-6

## 6.2.2 Flowback Summary

Flowback tests were performed as a part of the minifrac tests of well 16B(78)-32 at the Utah FORGE site. Analysis of flowback data for three tests were used to estimate fracture closure pressure, while the flowback data for the other tests were not interpretable using the flowback analysis method. This was due to not meeting one or both criteria for flowback analysis including (1) an increasing slope observed during flowback (i.e., lower to steeper trend) and (2) consistent and/or similar values for measured stiffness during injection period and after closure during flowback. Another challenge in test interpretation was variable flowback rates for many cycles.

The estimated fracture closure pressure determined with the flowback analysis method for the three tests found to be interpretable (MF-1 cycle 1, MF-5 cycle 1, and MF-6 cycle 1) was lower than fracture closure pressure estimated during the fall-off period (specifically ISIP). Similar results were observed for flowback analysis of DFIT for well 58-32. This could be due to the fact that flowback started after the fracture already began to close during the shut-in period. Considering the injection rate was low during minifrac testing performed in well 16B(78)-32 (compared to DFIT test), results from ISIP analysis should provide more reliable results for fracture closure and  $Sh_{min}$  compared to fall-off and/or flowback section (Hickman and Davatzes, 2010). Table 6-3 compares fracture closure pressure from analysis of flowback data and analysis of fall-off data for the three minifrac tests found to be interpretable using the flowback analysis method (i.e., MF-1, MF-5, and MF-6).

**Table 6-3. Comparison of fracture closure pressure from analysis of flowback data and analysis of fall-off data.**

Test and Cycle	Fracture closure pressure (psi) and gradient (psi/ft) from Flowback Analysis	Fracture closure pressure (psi) and gradient (psi/ft) from analysis of fall-off data
MF-1 Cycle 1	3902/0.69	4536/0.8 <sup>a</sup>
MF-5 Cycle 1	2932/0.5	3262/0.55 <sup>a</sup>
MF-6 Cycle 1	3231/0.57	3476/0.62 <sup>a</sup> 3473/0.62 <sup>b</sup> 3434/0.61 <sup>c</sup> 3462/0.61 <sup>d</sup> 3432/0.61 <sup>e</sup> ; 3417/0.61 <sup>e</sup> 3456/0.61 <sup>f</sup> 3433/0.61 <sup>g</sup> ; 3419/0.61 <sup>g</sup>

- a. Fracture closure pressure equal to ISIP; b. bi-linear method; c. SRT; d.e. log-log Pressure deriv.; f.g. G-function Plot analysis.

## 6.3 Re-opening Pressure Estimation with Pressure versus Injected Volume Plots

Bröker and Ma (2022) demonstrated that a plot of pressure versus injected fluid volume can sometimes be used to estimate fracture re-opening pressure (it should be noted that fracture re-opening pressure is not equal to fracture closure pressure and therefore is not equal to  $Sh_{min}$ ). Before fracture re-opening, a linear relationship is expected between pressure and injected volume. After fracture re-opening, a deviation from linearity due to fracture connection to the hydraulic system would be expected. Consequently, system stiffness ( $dP/dV$ ) decreases when re-opening occurs.

This technique was used to estimate re-opening pressure for the seven minifrac tests conducted in this study. The results are discussed below.

### 6.3.1 Re-Opening Pressure Results

Figure 6-17 shows the pressure versus injected volume for a repeat cycle (after first cycle) of the Station MF-1 minifrac test. There is no sharp change in pressure versus injected volume for cycle 2 of Station MF-1. As a result, an exact re-opening pressure cannot be definitively determined with this method. Note that a pressure of 3751 psi is highlighted in the plot in Figure 6-17 because there is a small deviation from straight line at this pressure, which could be due to a fracture re-opening. However, because the deviation is small, there is high uncertainty as to whether a fracture re-opened at this pressure.

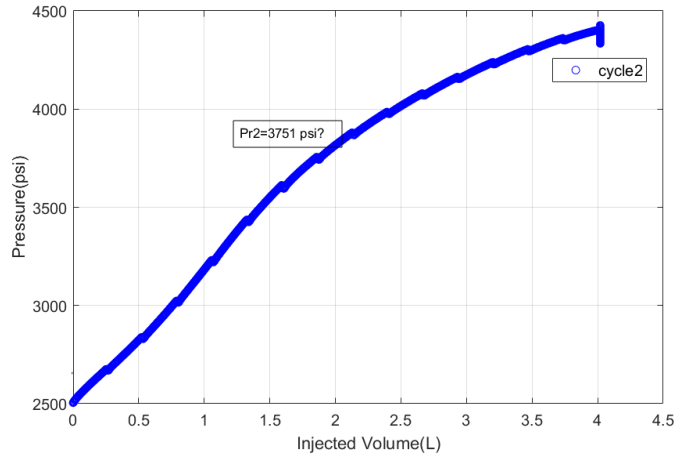


Figure 6-17. Pressure versus injected volume for repeat cycle 2 of Station MF-1.

Figure 6-18 shows the pressure versus injected volume for repeat cycles 2 and 3 of the Station MF-2 minifrac test. There is a distinct change in pressure versus injected volume for both cycles 2 and 3 of Station MF-2. In both cycles, pressure is not constant/stable after re-opening. Re-opening pressure is lower in cycle 3 (3116 psi) compared to cycle 2 (3194 psi). By repeating cycles, fracture length is increased which causes a more gradual re-opening and a decrease in re-opening pressure. This trend is also observed in previous minifrac studies (Bröker and Ma, 2022).

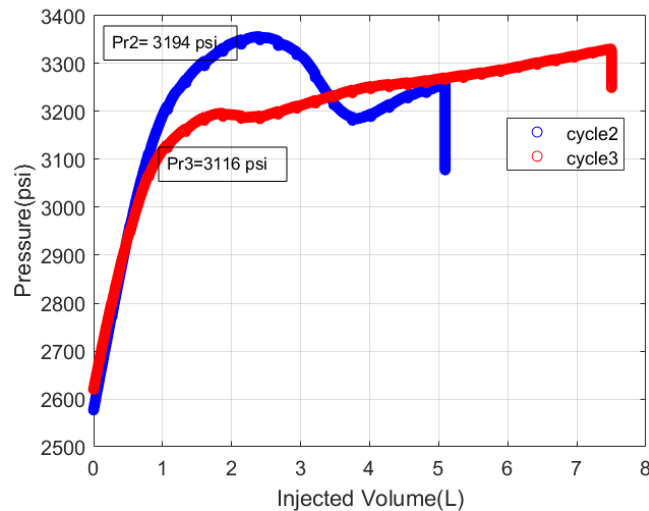


Figure 6-18. Pressure versus injected volume for repeat cycles 2 and 3 of Station MF-2.

Figure 6-19 shows the pressure versus injected volume for repeat cycle 2 of the Station MF-3 minifrac test. There is no sharp change in pressure versus injected volume for this cycle, but a small deviation from a straight line occurs at 2625 psi, which could be due to a fracture re-opening. However, because the deviation is small, there is high uncertainty as to whether a fracture re-opened at this pressure.

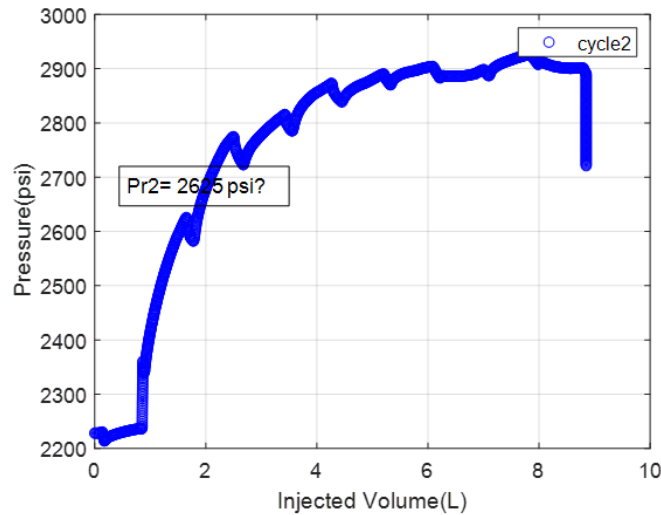


Figure 6-19. Pressure versus injected volume for repeat cycle 2 of Station MF-3.

Figure 6-20 shows the pressure versus injected volume for repeat cycles 2 and 3 of the Station MF-4 minifrac test. There is a distinct change in pressure versus injected volume at 3475 psi for cycle 2 and at 3432 psi for cycle 3. In both cycles, propagation pressure increases slightly after fracture re-opening but flattens with increasing volume injected. Re-opening pressure is slightly lower in cycle 2 compared to cycle 3. This is expected because fracture length increases with repeated cycles, which causes a decrease in re-opening pressure.

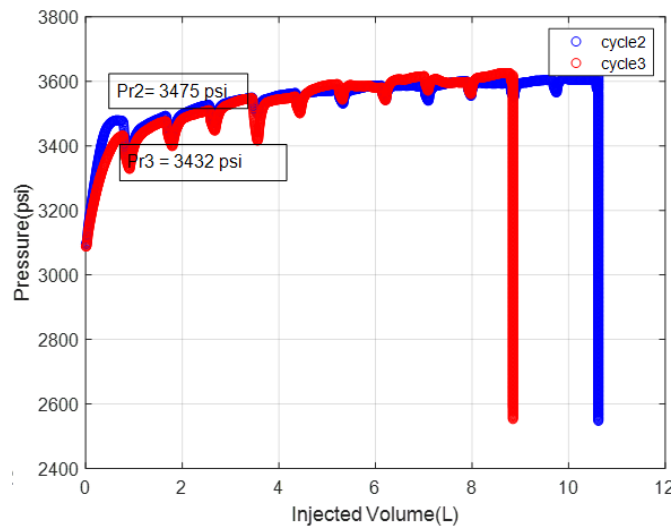
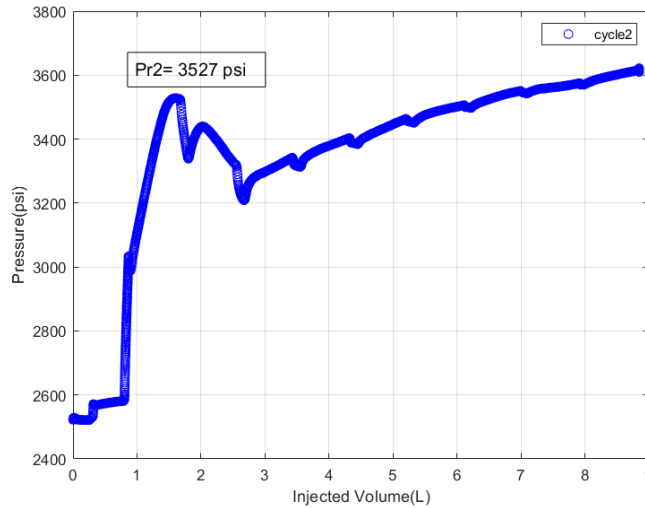


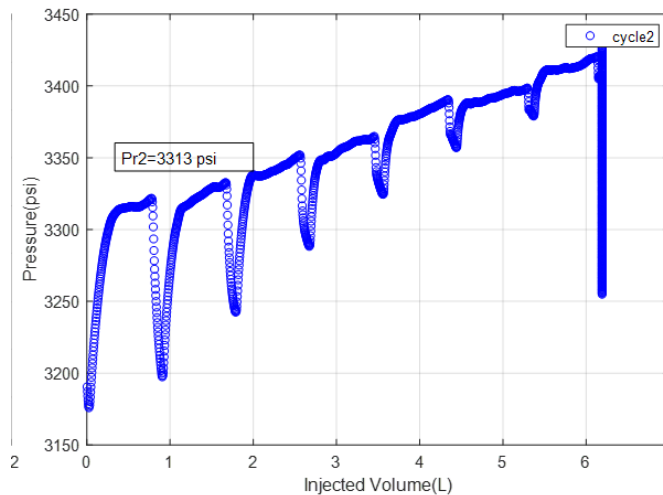
Figure 6-20. Pressure versus injected volume for recycles of Station MF-4.

Figure 6-21 shows the pressure versus injected volume for repeat cycle 2 of the Station MF-5 minifrac test. There is a distinct change in pressure versus injected volume at 3527 psi. Also, there is minor change in stiffness (slope) at pressure  $\sim$  3000 psi. After re-opening, the pressure continues to increase during propagation. Multiple mechanisms, including for example tortuosity around the wellbore and impact of small natural fractures and cracks, can contribute to an increase in propagation pressure. Such an increase in treatment pressure during fracture propagation was also observed during some DFIT tests (some cycles) performed in well 58-32 at the FORGE site (Xing et al., 2020a).



**Figure 6-21. Pressure versus injected volume for repeat cycle 2 of Station MF-5.**

Figure 6-22 shows the pressure versus injected volume for repeat cycle 2 of the Station MF-6 minifrac test. There is a distinct change in pressure versus injected volume at 3313 psi for cycle 2. As observed in other tests, the pressure continues to increase during propagation after re-opening.



**Figure 6-22. Pressure versus injected volume for cycle 2 of Station MF-6.**

Figure 6-23 shows the pressure versus injected volume for cycles 2 and 3 of the Station MF-7 minifrac test. There is no sharp change in pressure versus injected volume for either cycles 2 or 3. A small deviation from straight line occurs in cycles 2 and 3 at 2933 psi. This could be due to a fracture re-opening, however because the deviation is small, there is high uncertainty as to whether a fracture re-opened at this pressure.

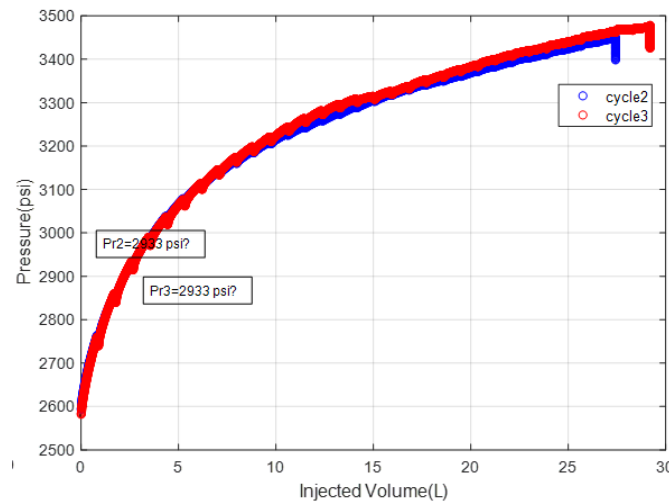


Figure 6-23. Pressure versus injected volume for recycles of Station MF-7.

### 6.3.2 Re-Opening Pressure Summary

Plotting pressure versus cumulative injected fluid volume was useful for estimating fracture re-opening pressure for minifrac tests 2, 4, 5, and 6. In other stations, the pressure versus injected fluid volume plot shows the stiffness deviated only slightly from linearity. However, the change of slope is not significant enough to conclude that a fracture re-opened in these tests. As a result, re-opening pressure cannot be exactly identified. In repeat cycles of Stations MF-2 and MF-4, a decrease in re-opening pressure was observed in the subsequent cycle, which could be due to increase in fracture length.

## 6.4 Observations Regarding Pressure Behavior during Minifrac Tests

This section provides additional information about the nature of the pressure response data from the minifrac tests and potential implications on the interpretation of fracture closure pressure (Shmin).

**The interpretation of the pressure response data for some minifrac tests may be complicated by the use of a non-constant injection rate**

Zoback and Haimson (1982) recommend that hydraulic fracturing tests include multiple cycles of fluid injection and falloff (including flowback to allow for drainage of excess fluid pressure from hydraulic fracture). They recommend using the same constant injection rate for all cycles. The seven minifrac tests performed in this study included multiple cycles (2 to 4 cycles); however, a constant injection rate was achieved (due to limitations of the pump in the BH RCX straddle packer tool) for only two tests (MF-1 and MF-2) (Figure 6-24). The non-constant injection rate used in the other tests may adversely affect closure pressure interpretation.

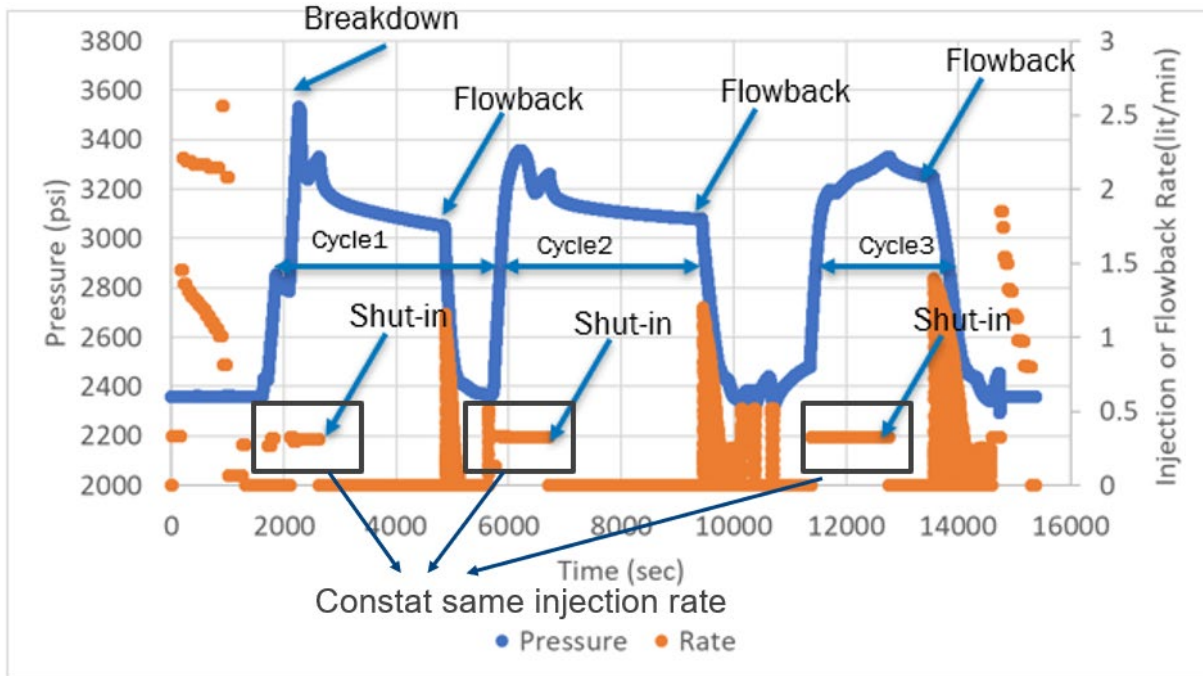


**Figure 6-24. Constant injection rate in multiple cycles of Station MF-2.**

**Higher injection rate/volume often gives a higher propagation pressure and closure pressure**

Xing et al. (2020) observed that a higher injection rate/volume often gives a higher closure pressure. By increasing injection rate, the back pressure would also increase, causing an increase in closure pressure. The back pressure increase is likely due to natural fracture slippage and dilation causing total stress increase in the injection region.

For multiple minifrac tests performed in the 16B(78)-32 well in this study, a higher injection rate was typical for the second and third cycles compared to the first cycle. For example, at Station MF-3 the injection rate was 5.47 cc/sec for the first cycle and 18 cc/sec for the second cycle. Also, in Station MF-4, the injection rate was 5.10 cc/sec during the first cycle and 20 cc/sec in the second cycle. Due to the increase in injection rate, higher propagation and closure pressure were observed in the repeat cycles of those stations. Figure 6-25 shows pressure increase in second cycle compared to first cycle at station MF-3.

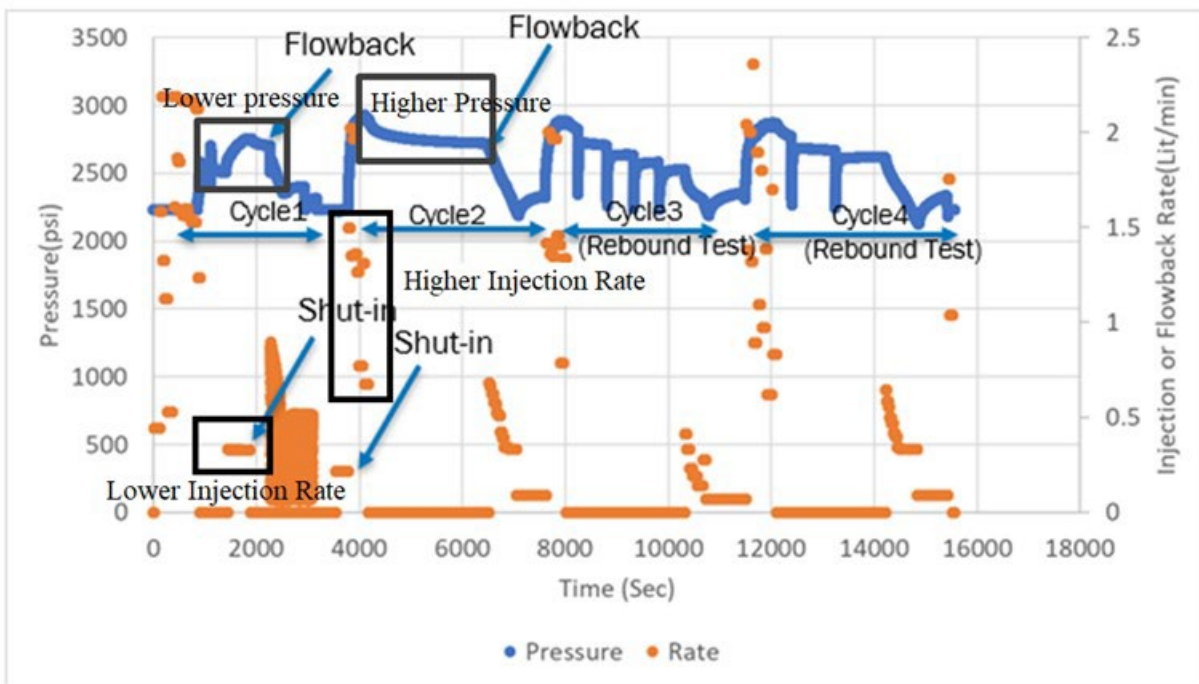
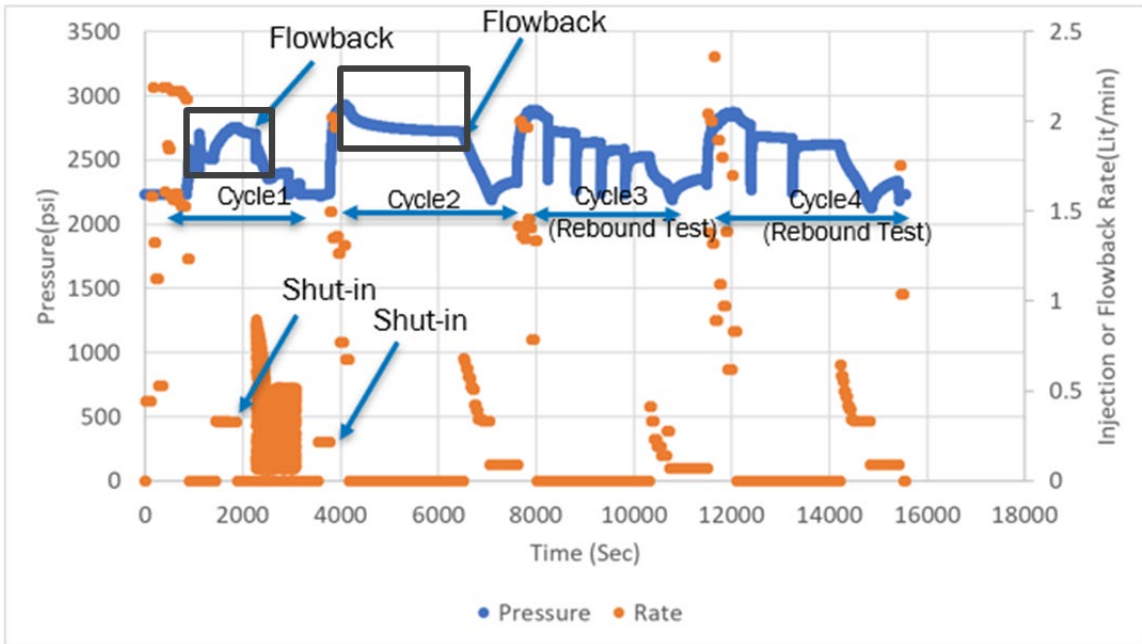


Figure 6-25. Example of pressure increase in cycle 2 compared to cycle 1 of Station MF-3.

**ISIP is recommended to estimate  $Sh_{min}$  when injection rate is low**

Fracture closure pressure is defined as the in-fracture fluid pressure at fracture closure associated with minimum principal in-situ stress (Xing et al., 2020). Various methods can be used to estimate closure pressure, including ISIP, bi-linear, G-function, SRT, and pressure derivative during fall-off, and pressure versus return volume analysis during flowback. The injection rate used in the test may determine which analysis method is most appropriate for estimating  $Sh_{min}$ . For example, Hickman and

Zoback (1983) state that ISIP can be used to estimate  $Sh_{min}$  for low injection rate hydraulic fracture tests. Hickman and Davatzes (2010) estimated  $Sh_{min}$  using ISIP from a hydraulic fracture test using a flow rate of 2 bbl/min (5300 cc/sec). The magnitude of  $Sh_{min}$  was determined from a stable ISIP value obtained from multiple fracture propagation cycles (where ISIP was defined as the pressure at which the pressure-time curve departs from an initial linear pressure drop immediately after injection is stopped and the well is shut-in). Xing et al. (2020) also state that ISIP and re-opening pressure could be used to represent  $Sh_{min}$  when the injection rate is low (they mention an injection rates of 1000 to 5200 cc/s for minifrac tests and 13000 cc/sec to 39000 cc/s for DFIT tests),

The injection rate used for the seven minifrac tests in this study was in the range of 5 cc/sec to 40 cc/sec, which is much lower than the “low” rates used in the above-mentioned tests. Zoback and Haimson (1981) state that ISIP can be a better estimate of the fracture closure pressure when injection rate is “extremely low”.

### **Lack of breakdown could indicate the presence of fractures**

Lack of breakdown in the first cycle of a minifrac test could indicate the presence of natural or DIFs (Aljubran et al., 2021). DIFs, if present, might re-open during a minifrac test. Among the seven minifrac tests performed in this study, Stations MF-1, MF-3, MF-6, and MF-7 do not show a clear breakdown during the first cycle. In station MF-1, there is evidence that a conductive fracture was present at the time of the test (Figure 6-26). Figure 6-27 shows the pressure-time history for Station MF-1 minifrac test and there is no breakdown observed in the first cycle. In other stations, there was no evidence of the presence of natural fractures in image logs, however there were multiple structural features (foliations) present that might explain why breakdown was not observed. For example, Figure 6-28 shows the presence of foliations in Station MF-3 test interval.

Note that depending on the orientation of natural fractures compared to stress status, the closure pressure might be higher or lower as a result of interaction between the natural fractures and the induced hydraulic fracture(s) compared to the case with no natural fractures (Kamali et al., 2019; Nadimi et al., 2020). If natural fractures are connected to the wellbore and not optimally oriented, the hydraulic fracture could propagate initially along natural fractures, resulting in higher closure pressure compared to the case in which no natural fractures existed (Xing et al., 2020). Similarly, shearing (reactivation) of an optimally oriented natural fracture intersecting the wellbore could lead to a lower fracture closure pressure compared to the case with no natural fracture(s) present (Nadimi et al., 2020).

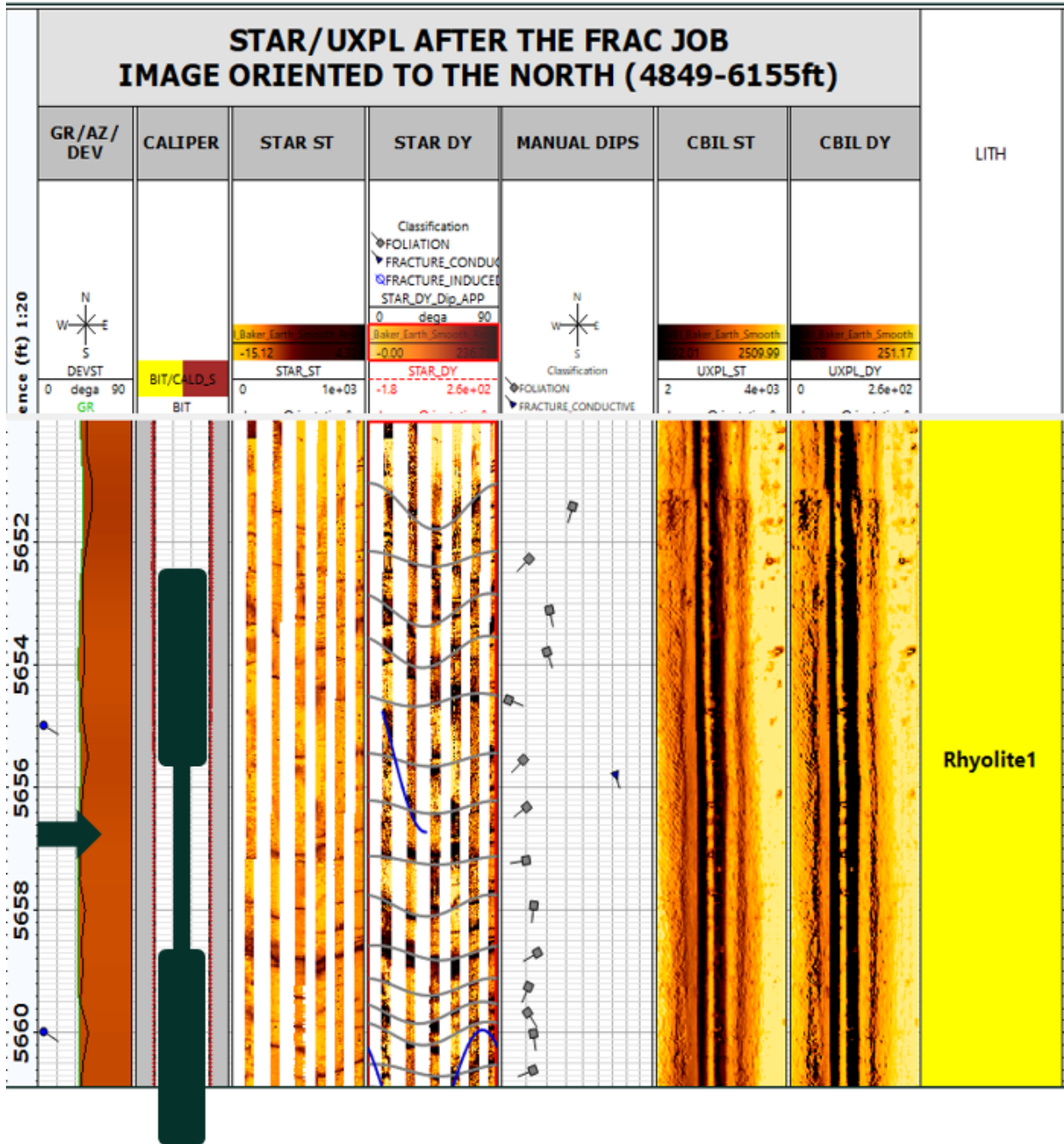


Figure 6-26. Possible conductive natural fracture in the Station MF-1 test interval (shown by blue line at ~5655 to 5657 ft).

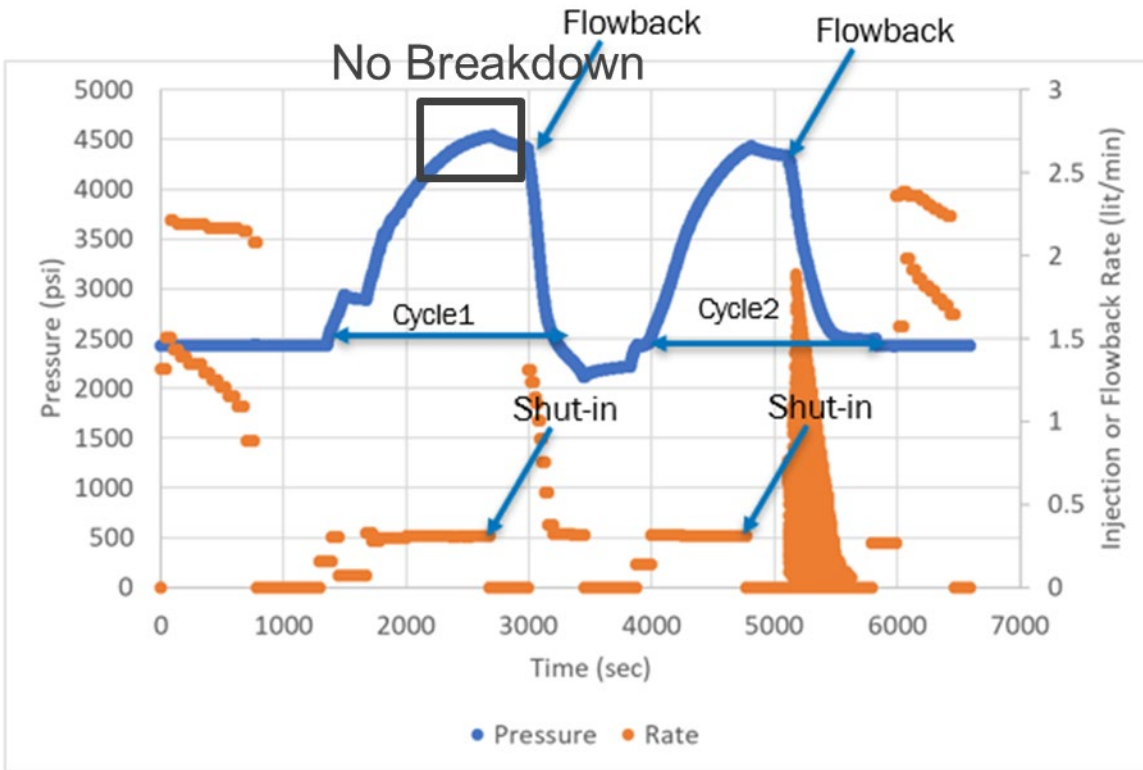


Figure 6-27. Station MF-1 pressure time record (no indication of breakdown), possibly due to the presence of fractures.

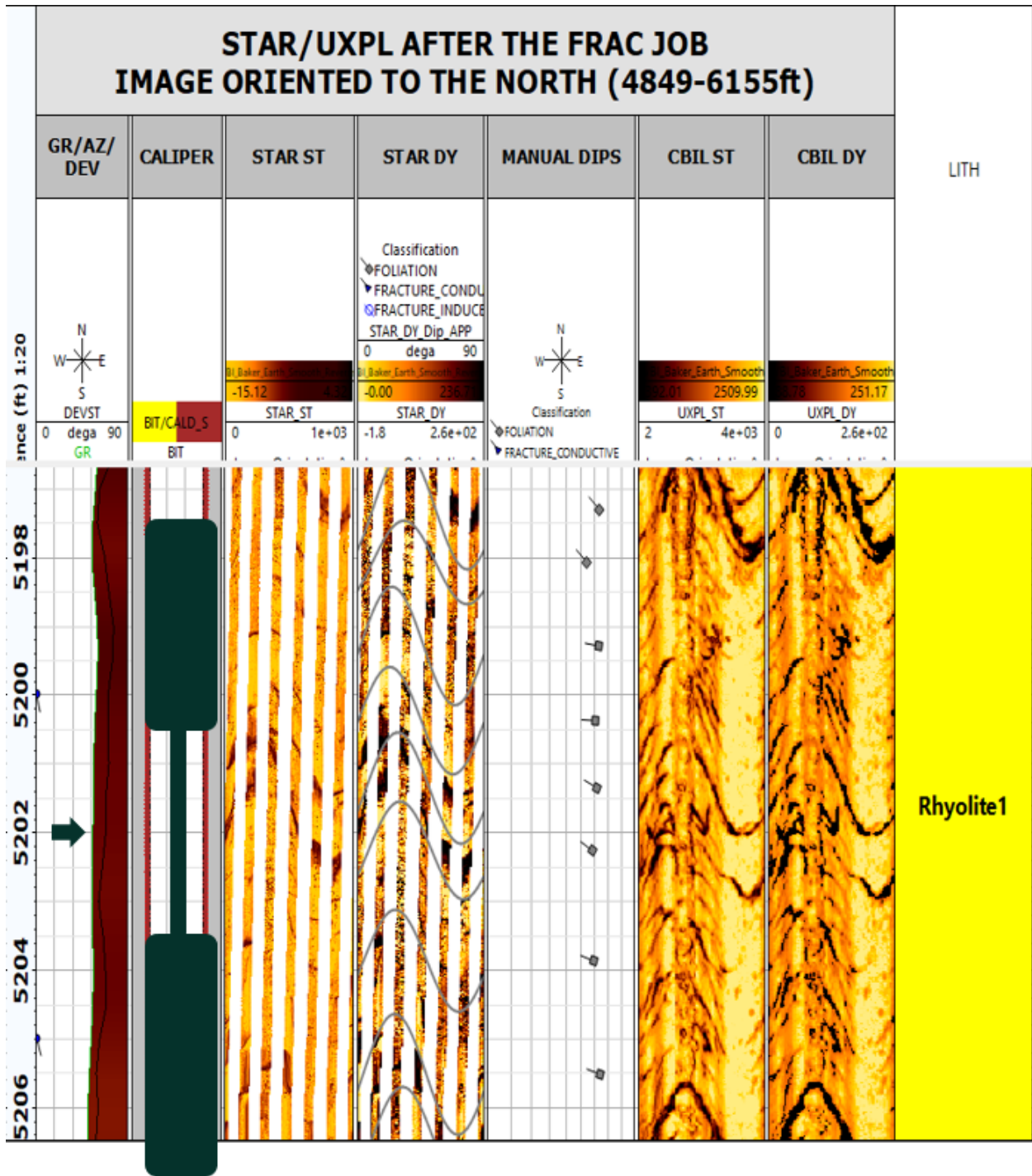


Figure 6-28. Presence of foliations in Station MF-3 interval (shown by square symbol on a stick in Track 5).

### Closure of multiple fractures may complicate interpretation of closure pressure

If multiple natural fractures are present in the same test interval, multiple fractures can close during a test, which can be observed by multiple signatures of fracture closure in the G-Function plot and derivative plots as multiple humps. This may cause difficulties in determining the correct value for  $Sh_{min}$ . This phenomenon was observed in the G-Function plot and the derivative plot for multiple DFIT tests conducted in well 58-32 at the Utah FORGE site (Xing et al., 2020; Nadimi et al., 2020). Figure 6-29 and Figure 6-30 are G-Function plots for cycle 2 of Station MF-2 and cycle 1 of Station MF-3 conducted in this study both showing multiple humps. On these G-Function plots, the closure was picked at the departure of the semi-log derivative of pressure from a straight line (Tangent method).

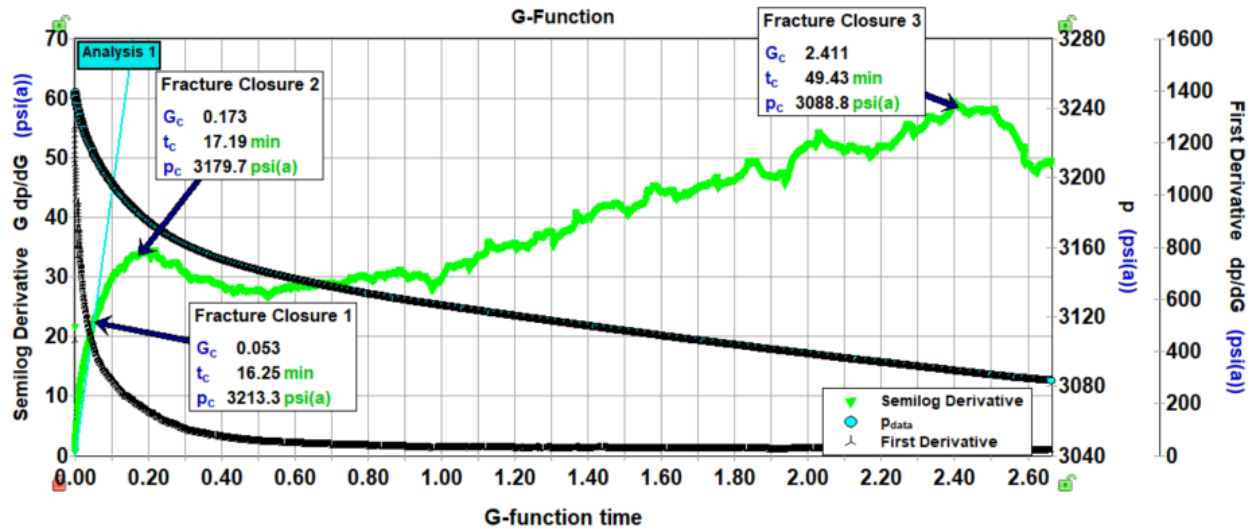


Figure 6-29. G-Function plot showing multiple humps for cycle 2 of Station MF-2.

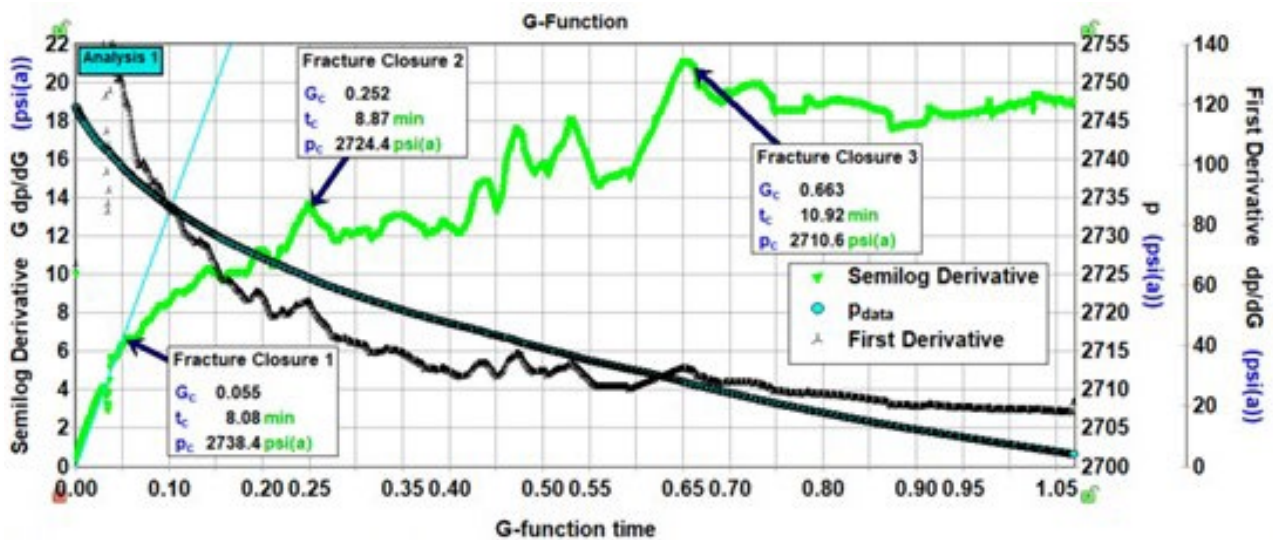
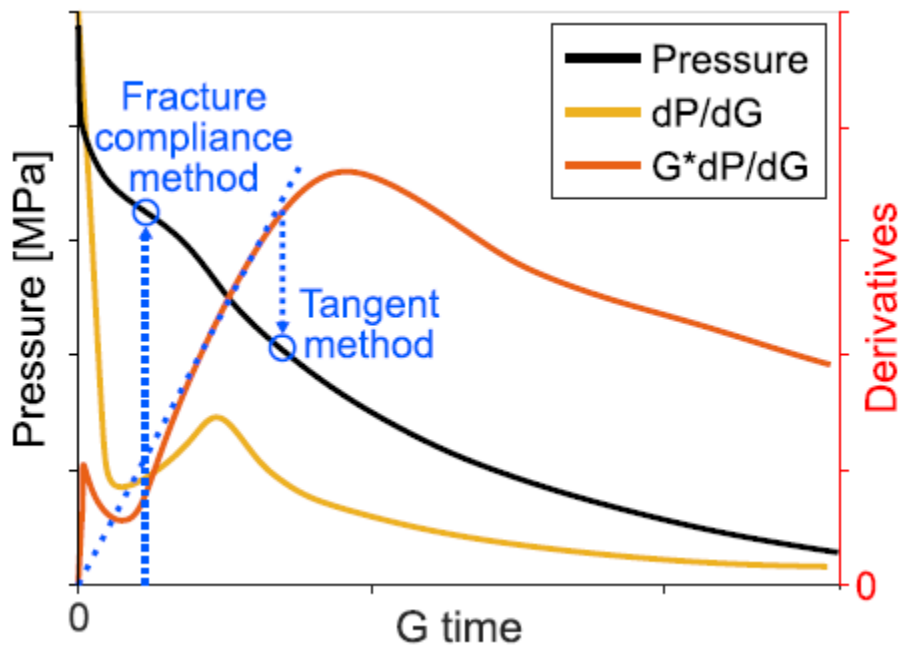


Figure 6-30. G-Function plot showing multiple humps for cycle 1 of Station MF-3).

### Tangent and compliance method to estimate closure pressure

The tangent and compliance methods can be used to estimate fracture closure pressure with a G-Function plot. Both methods are illustrated in Figure 6-31. Using the tangent method, a straight line drawn from the plot origin to the tangent to the semi-log derivative on a G-Function plot ( $Gdp/dG$ ) leads to closure pressure at the departure or downward curvature from a straight line (Barree et al., 2007). Using the tangent method can underestimate minimum horizontal stress, especially in low permeability formations (McClure et al., 2019). The compliance method is an alternate method for picking the onset of fracture closure to estimate  $Sh_{min}$ . When the fracture walls first come into contact, this causes a decrease compliance of the system (McClure et al., 2019). Using this method, the contact pressure is picked when the semi-log derivative begins to curve upward. McClure et al. (2019) recommend picking contact pressure from  $dp/dG$  after the curve begins to increase from the minimum).



**Figure 6-31. Comparison of the Tangent and Compliance methods for estimating fracture closure pressure on a G-Function plot (Broker and Ma, 2022).**

Picking of contact pressure using  $dp/dG$  plot requires good separation between minimum and maximum values of  $dp/dG$  (McClure et al., 2019). In some tests, a clear pick cannot be made. McClure et al. (2022) discuss a case where there is adequate evidence to indicate closure versus a case with no clear indication of closure. Also, they discuss the significance of a monotonic decrease in  $dp/dG$  (McClure et al., 2019), which could be due to injecting into a preexisting hydraulic fracture, injecting into a highly conductive natural fracture, a hydraulic fracture intersecting a highly conductive natural fracture, or a severe pressure drop at the wellbore interface. In the case of a monotonic decrease in  $dp/dG$ , ISIP could be the best estimate of  $Sh_{min}$  (McClure et al., 2019).

Figure 6-32 through Figure 6-34 show G-Function plots for Station MF-2 cycle 3, Station MF-1 cycle 1, and Station MF-3 cycle 1.  $dG/dp$  is shown by the black curve. As shown in Figure 6-32 through Figure 6-34, there is a monotonic decrease in  $dp/dG$ . As mentioned above, this could be due to injection into a highly conductive natural fracture or into an induced hydraulic fracture intersecting a highly conductive

natural fracture (McClure et al., 2019). All three cycles have an inflection in the  $dp/dG$  curve in early G-time, but there might not be adequate separation between inflection points to pick a closure pressure.

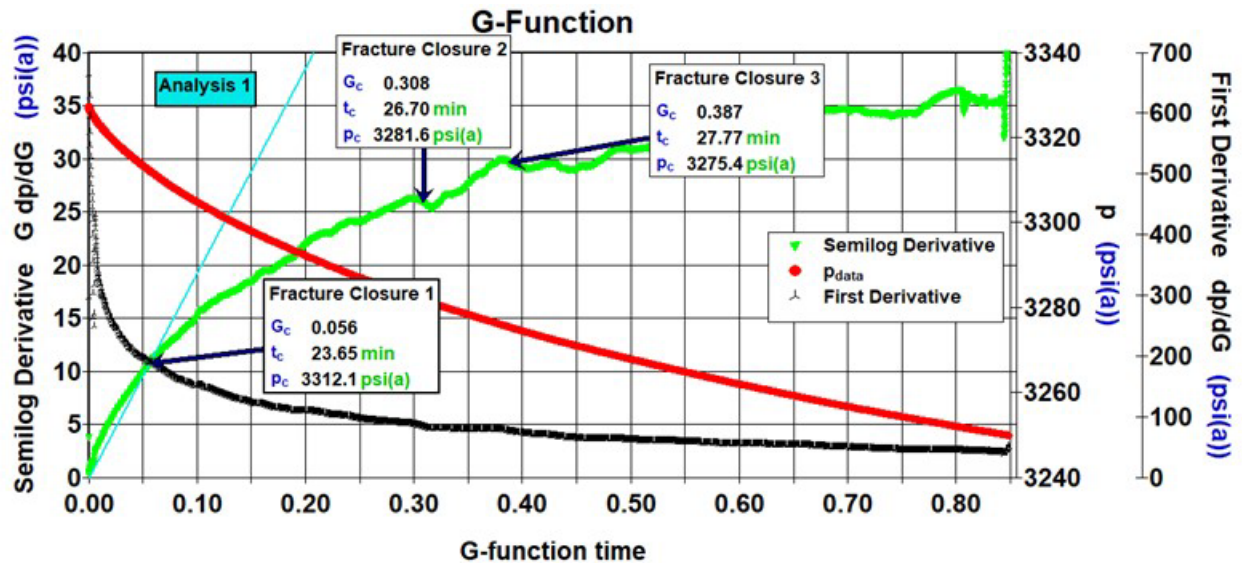


Figure 6-32. G-Function plot for MF-2 cycle 3.

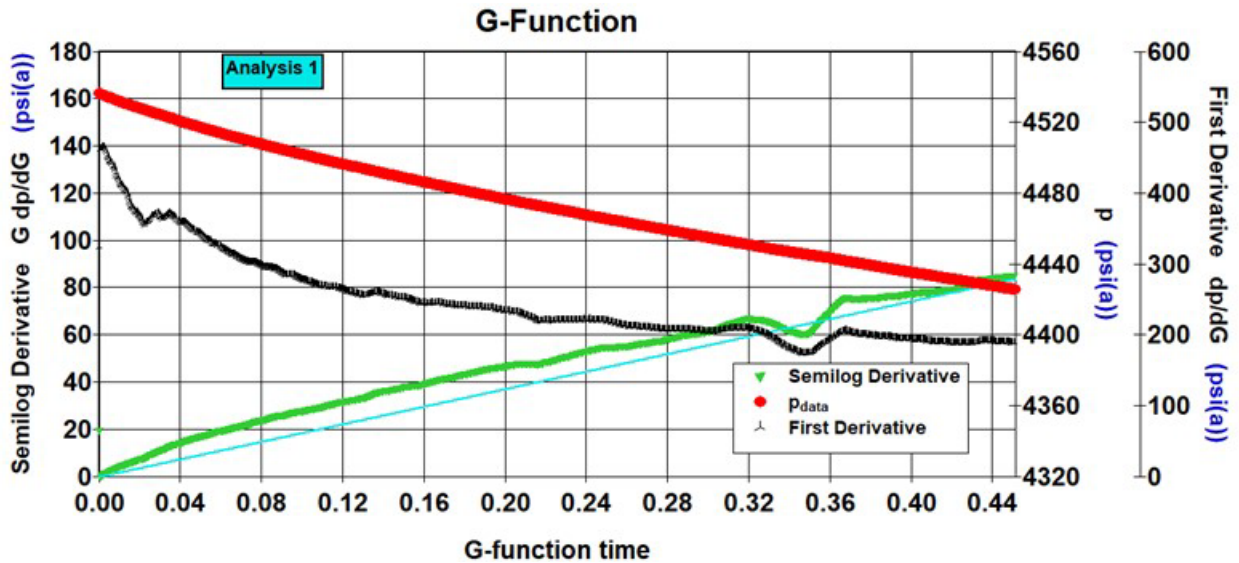


Figure 6-33. G-Function plot for MF-1 cycle 1.

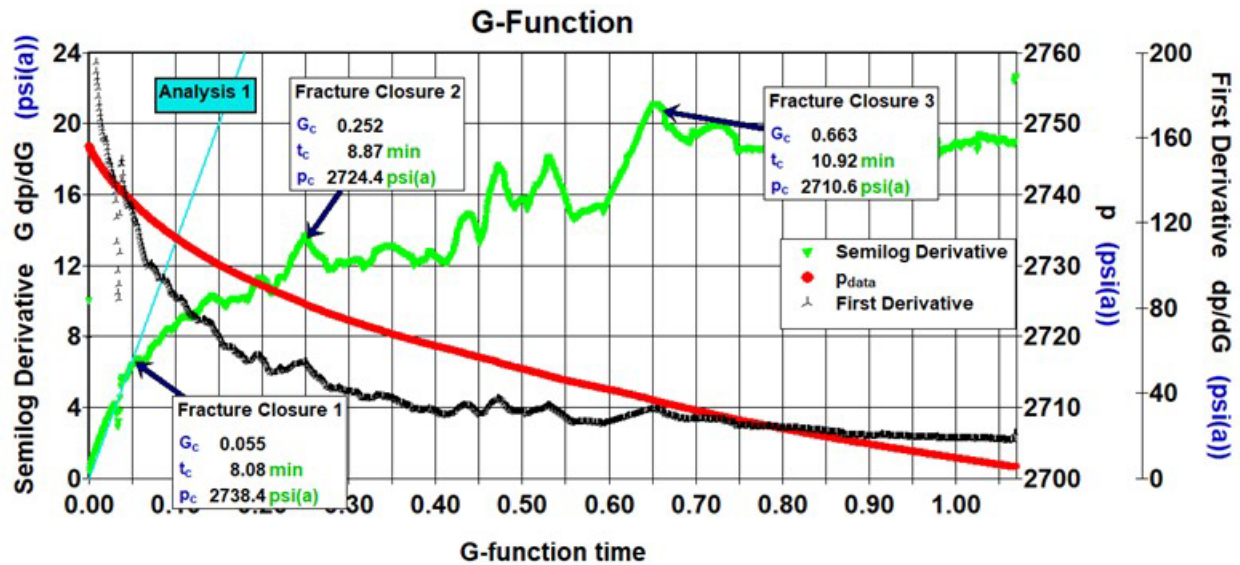


Figure 6-34. G-Function plot for MF-3 cycle 1.

In this study, the ISIP from MF-2 may be the best estimate of  $Sh_{min}$ .

Among the seven minifrac tests performed in this study, the MF-2 test shows the clearest signature (based on pressure response) of an induced fracture occurring during the minifrac test. At Station MF-2, breakdown occurs during the first cycle, and a post-test image log shows evidence of a newly developed tensile fracture with strike of N25°E, which is consistent with other estimates  $SH_{max}$  at the site. Also, there is a distinct change in the stiffness of the system (based on the pressure versus injected volume analysis method, which provides evidence of re-opening of the fracture (see Figure 6-18). In addition, the injection rate was constant during all three cycles of the MF-2 test. The ISIP is very similar in all three cycles (0.6 psi/ft, 0.59 psi/ft, 0.61 psi/ft), and could be the best estimate for  $Sh_{min}$ .

For stations MF-4 and MF-5, the pressure data indicate that breakdown occurred during the first cycle, however, the post-test image log does not show evidence of a newly developed tensile fracture. Also, there is a distinct change in stiffness of the system using pressure versus injected volume (specifically in station MF-4 cycle 2) which provides evidence of re-opening of a fracture (see Figure 6-20). The ISIP determined for station MF-4 second and third cycle (0.6 psi/ft) is another point to represent minimum horizontal stress. However, because the injection rate is changing in this station, the result is not as reliable as station MF-2.

**The values of  $Sh_{min}$  determined in this study are comparable to the low end of the range of values from previous studies.**

Xing et al. (2020a, 2000b) analyzed pressure response data for DFIT tests conducted in 2017 and 2019 in well 58-32 at the Utah FORGE site. The estimated closure pressure gradient was in the range of 0.65 psi/ft to 0.95 psi/ft, based on different analysis methods used, including ISIP, G-function, pressure derivative, and SRT. Nadimi et al. (2020) reported a fracture closure range of 0.58 psi/ft to 0.73 psi/ft using the G-function analysis and derivative analysis of a 2017 DFIT test in well 58-32. Aljubran et al. (2021) performed multiple analyses including G-Function plot and ISIP for a DFIT test in well 58-32 and reported a  $Sh_{min}$  value of ~0.75 psi/ft. The predicted value of  $Sh_{min}$  from this study is ~0.6 psi/ft based primarily on the ISIP observed for station MF-2 and station MF-4). So, although the value of  $Sh_{min}$  in this study is comparable to previous studies but it is in the lower end of the range unless adjusted for close

to borehole temperature effect. The thermoelastic effect due to cooling prior to the minifrac tests adds uncertainty to the estimated  $S_{hmin}$  for well 16B(78)-32. As discussed in section 3 of this report, cooling could lead to a range of  $S_{hmin}$  of 0.6 psi/ft to 0.94 psi/ft with a mid value of  $\sim 0.8$  psi/ft. [Table 6-4](#) provides a summary of  $S_{hmin}$  values estimated from different tests at the Utah FORGE site.

**Table 6-4. Comparison of  $S_{hmin}$  values from different tests at the Utah FORGE site.**

<b>Authors</b>	<b>Type of Test</b>	<b><math>S_{hmin}</math> (psi/ft)</b>
Xing et al. (2020a, 2000b)	Analysis of DFIT tests conducted in 2017 and 2019 in well 58-32 based on different analysis methods, including ISIP, G-Function, pressure derivative, and SRT.	0.65 to 0.95
Nadimi et al. (2020)	G-Function and pressure derivate analysis of a 2017 DFIT test in well 58-32	0.58 to 0.73
Aljubran et al. (2021)	G-Function plot and ISIP for a DFIT test in well 58-32	$\sim 0.75$ psi/ft
This study	Analysis of minifrac tests (MF-2 and MF-4) conducted in the 16B(78)-32 wellbore based on ISIP method,	0.6 psi/ft without temperature adjustment; 0.8 psi/ft to 0.94 psi/ft with “mid” and “high” temperature adjustment values

## 7 REFERENCES

- Aljubran, M., R. Horne, and M. Zoback. 2021. "Utah Forge Injection Test Interpretation," *Proceeding World Geothermal Congress*, Iceland.
- Allis, R., M. Gwynn, C. Hardwick, W. Hurlbut, and J. Moore. 2018. "Thermal Characteristics of the FORGE Site, Milford, Utah," *Geothermal Resources Council Transactions*, Vol. 42, 15.
- Baker Hughes. 2023. "Microfrac Analysis and Interpretation Report," FORGE 16B(78)-32 Microfrac Analysis, GEM.230 REPORT, Prepared by Greg Schlachter, Umesh Prasad, Steve Smith.
- Barree, R.D., V.L. Barree, and D.P. Craig. 2007. April. "Holistic Fracture Diagnostics," In *SPE Rocky Mountain Petroleum Technology Conference/Low-Permeability Reservoirs Symposium* (pp. SPE-107877). SPE.
- Bröker, Kai and Ma Xiaodong .2022. "Estimating the Least Principal Stress in a Granitic Rock Mass: Systematic Minifrac Tests and Elaborated Pressure Transient Analysis." *Rock Mechanics and Rock Engineering* 55, no. 4: pgs. 1931-1954.
- Economides, Michael J., and Kenneth G. Nolte. 1989. *Reservoir Stimulation*. Vol. 2. Englewood Cliffs, NJ: Prentice Hall.
- Eltaleb, I. and M.Y. Soliman. 2023. "New Pump-In Flowback Model Verification with In-Situ Strain Measurements and Numerical Simulation," *Energies*, 16(4), 1970.
- Hickman, S.H. and N.C. Davatze. 2010. In-Situ Stress and Fracture Characterization for Planning of an EGS Stimulation in the Desert Peak Geothermal Field, Nevada.
- Hickman, S.H., and M.D. Zoback. 1981, December. "The Interpretation of Hydraulic Fracturing Pressure-time Data for In Situ Stress Determinations," In *Proc. Workshop on Hydraulic Fracturing Rock Stress Measurements*, pp. 103-127.
- Kamali, A., A. Ghassemi, J. McLennan, and J. Moore. 2019. "Analysis of FORGE DFIT Considering Hydraulic and Natural Fracture Interactions: In *Proceedings of the 44th Workshop on Geothermal Reservoir Engineering*.
- McClure, M., G. Fowler, and M. Picone. 2022, January. "Best Practices in DFIT Interpretation: Comparative Analysis of 62 DFITs from Nine Different Shale Plays," In *SPE International Hydraulic Fracturing Technology Conference and Exhibition* (p. D031S011R001). SPE.
- Nadimi, S., B. Forbes, J. Moore, and J.D. McLennan. 2020. "Effect of Natural Fractures on Determining Closure Pressure," *Journal of Petroleum Exploration and Production Technology*, Vol. 10, pgs. 711-728.
- Raaen, A.M. and M. Brudy. 2001. "Pump-in/flowback Tests Reduce the Estimate of Horizontal In-situ Stress Significantly," In *SPE Annual Technical Conference and Exhibition?* (pgs. SPE-71367). SPE.
- Savitski, A.A. and J.W. Dudley. 2011. "Revisiting Microfrac In-situ Stress Measurement via Flow Back-A New Protocol," In *SPE Annual Technical Conference and Exhibition*. OnePetro.
- Xing, P., J. McLennan, and J. Moore. 2020a. "In-situ Stress Measurements at the Utah Frontier Observatory for Research in Geothermal Energy (Forge) Site," *Energies*, 13(21), pg. 5842.

Xing, P., A. Goncharov, D. Winkler, B. Rickard, B. Barker, A. Finnilla, and McLennan, J. 2020b. Flowback data evaluation at FORGE. In *ARMA US Rock Mechanics/Geomechanics Symposium* (pp. ARMA-2020). ARMA.

Zhang, J., Fan, X., Huang, Z., Liu, Z., Fan, Z., and Liu, L. 2023. In situ stress determination in isotropic and anisotropic rocks and its application to a naturally fractured reservoir. *Geomechanics and Geophysics for Geo-Energy and Geo-Resources*, 9(1), 51.

Zoback, Mark D. 2010. *Reservoir geomechanics*. Cambridge university press.

Zoback, M.D., C.A. Barton, M. Brudy, D.A. Castillo, T. Finkbeiner, B.R. Grollmund, D.B. Moos, P. Peska, C. D. Ward, D.J. Wiprut. 2003. Determination of stress orientation and magnitude in deep wells. *International Journal of Rock Mechanics and Mining Sciences*, Volume 40, Issues 7-8, Pages 955-1276.

Zoback, M. D., and Haimson, B. C. 1982. Status of the hydraulic fracturing method for in-situ stress measurements. In *ARMA US Rock Mechanics/Geomechanics Symposium* (pp. ARMA-82). ARMA.

**APPENDIX A MINIFRAC FIELD-TESTING SUMMARY REPORT**

The field testing program for Utah FORGE Project 2439 was conducted on site at the 16B(78)-32 well from June 22 through July 3, 2023. Field activities are summarized in [Table A-1](#). Companies on the wellsite included Frontier Drilling (rig operator), Battelle (Project 2439 lead), and Baker Hughes (well service company), among other wellsite consultants and University of Utah personnel. Prior to beginning the field-testing program, the wellbore was reamed and a gyro(scope) survey was run by Scientific Drilling. After the gyro survey was completed, the drillpipe was tripped in to approximately 9,100 ft MD to circulate and cool the wellbore ahead of the planned well logging run to 9,000 ft MD.

**Table A-1. Field activities associated with the minifrac testing program.**

Date(s)	Activity	Start	Stop	Hours
6/22-6/23	First circulation (before baseline logging run)	8:40 PM (6/22)	12:45 PM (6/23)	16.1
6/23	Trip out drill pipe	12:45 PM (6/23)	6:30 PM (6/23)	5.75
6/23	Safety meeting, prep for baseline run	6:30 PM (6/23)	8:00 PM (6/23)	1.5
6/23-6/25	Baseline logging run incl. troubleshooting issues	8:00 PM (6/23)	2:30 PM (6/25)	42.5
6/25	Trip in drill pipe while waiting for replacement WL truck	2:30 PM (6/25)	6:00 PM (6/25)	3.5
6/25-6/27	Circulate while waiting for replacement WL truck (2 <sup>nd</sup> circulation event)	6:00 PM (6/25)	9:45 AM (6/27)	39.75
6/27	Trip out drill pipe	9:45 AM (6/27)	1:30 PM (6/27)	3.75
6/27-6/28	TIH with RCX tools to vertical section	1:30 PM (6/27)	3:15 AM (6/28)	13.75
6/28	Conduct MF tests 1, 2, 3 in vertical section	3:15 AM (6/28)	5:45 PM (6/28)	14.5
6/28	POOH with RCX tools	5:45 PM (6/28)	11:10 PM (6/28)	5.4
6/28-6/29	Trip in drill pipe for cooling deviated section	11:10 PM (6/28)	3:45 AM (6/29)	4.6
6/29	Cooling for 16 hours (3 <sup>rd</sup> circulation event)	3:45 AM (6/29)	7:45 PM (6/29)	16
6/29	Trip out drill pipe	7:45 PM (6/29)	12:00 AM (6/29)	4.2
6/30	Trip in RCX tools for deviated section MF tests (PC)	12:00 AM (6/30)	2:00 PM (6/30)	14
6/30	Attempt to conduct MF test in deviated section, tool failed/no tests completed	2:00 PM (6/30)	8:00 PM (6/30)	6
6/30-7/1	Trip out RCX tool	8:00 PM (6/30)	3:00 AM (7/1)	7
7/1	Trip in RCX tool; running only on wireline	3:00 AM (7/1)	8:00 AM (7/1)	5
7/1	Conduct MF tests 4, 5, 6 in vertical section	8:00 AM (7/1)	8:30 PM (7/1)	12.5
7/1	Trip out RCX tool to diagnose packer inflation problem	8:30 PM (7/1)	12:00 AM (7/1)	3.5
7/2	Trip in RCX tool on wireline	12:00 AM (7/2)	5:45 AM (7/2)	5.8

**Table A-1. Field activities associated with the minifrac testing program. (Continued)**

Date(s)	Activity	Start	Stop	Hours
7/2	Finish MF6, conduct MF7 in vertical section (WL); further testing precluded due to tool issues.	5:45 AM (7/2)	12:45 PM (7/2)	7
7/2	Trip out RCX tools	12:45 PM (7/2)	3:30 PM (7/2)	2.75
7/2-7/3	Rig up logging tools, repeat logging run, rig down (WL)	3:30 PM (7/2)	1:00 AM (7/3)	9.5
Total Time (hrs)				244.35

Circulation/cooling event #1

Based on suggested circulation times from modeling by DrillCool, circulation continued for 16 hours to ensure that the wellbore was cool enough to run the Baker Hughes well log tools within their temperature ratings. Fluid temperature upstream and downstream of the chillers and circulation pump rate were continuously recorded during each circulation event. This is shown in Figure A-1, with the “Before Chiller” blue line indicating the temperature of the fluid coming out of the wellbore and “After Chiller” orange line indicating temperature after the wellbore fluid went into the surface chillers before entering the wellbore again. During the first circulation period, the average pump rate was 845 gallons per minute, with average temperature before chiller at 124.6°F and average temperature after chillers at 108°F. After the 16-hour circulation concluded at 12:45 PM on June 23, the drillpipe was tripped out of hole and the reamer BHA was disassembled.

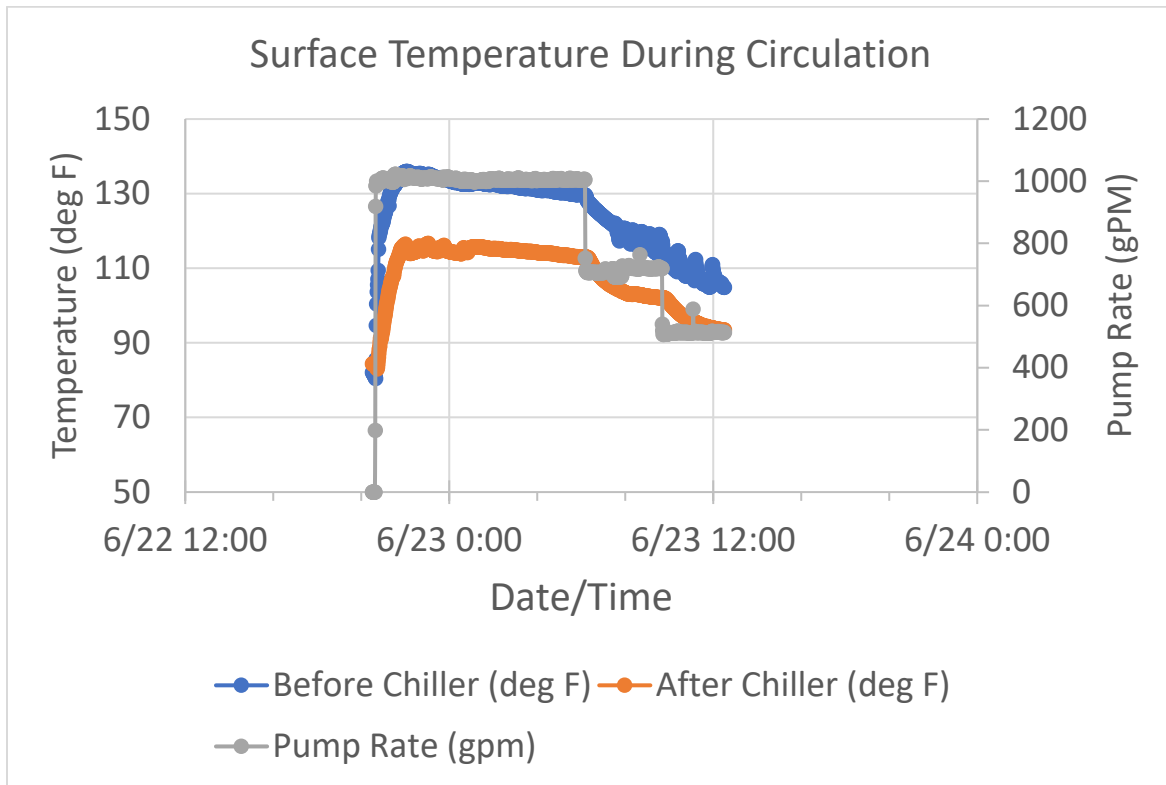


**Figure A-1. Surface temperature before and after wellbore fluid entered the chillers, and circulation pump rate in gallons per minute for the first circulation period. Data courtesy of Pason.**

### Baseline logging run (PCL)

At 6:30 PM on June 23, Baker Hughes began to rig up the image and multi-pole sonic logging tools for the baseline logging run ([Figure A-2](#)). A pre-job safety meeting was held at this time to discuss job hazards and mitigation measures. The tool string also contained a temperature, tension, and mud resistivity (TTRM) tool, which allowed for continuous monitoring while the tools were downhole.

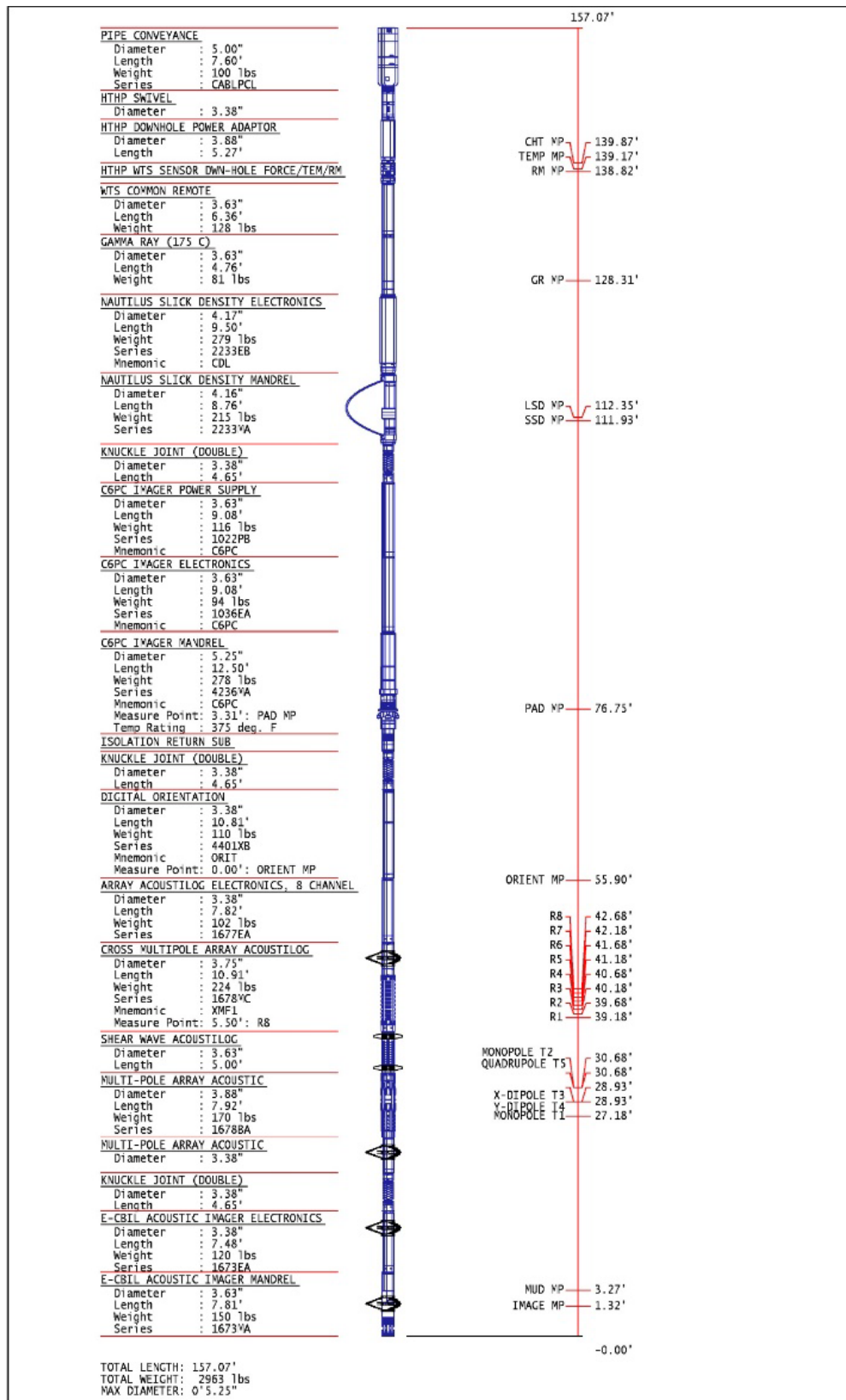


**Figure A-2. Tool string for logging events, which includes Baker Hughes' ZDL, STAR, XMAC and UXPL logging tools.**

**Table A-2. Description of Logging Tool String**

Description	Series	Length (ft)	Weight (lbs)
PCL Simphor assembly w/ 4-1/2" I.F. box top connection	3983LF	7.60	100
HTHP Swivel	4422XA	3.55	68
HTHP Downhole Power Adapter	4431XA	5.27	128
WTS DWN-HOLE FORCE/TEMP/RM sensor	2890XB	2.67	80
HTHP WTS Telemetry	3590XA	9.17	270
HTHP Digital Spectralog	1390XA	9.50	282
STAR Imager power supply	1022PB	9.08	116
STAR Imager electronics	1036EB	9.08	94
STAR Imager mandrel	4236MA	12.50	278
Isolation sub	3992XA	2.08	45
HTHP Digital Orientation	4490XA	10.00	294
HTHP XMAC electronics	1690EA	10.0	270
HTHP XMAC acoustic RX	1690MC	13.79	348
HTHP XMAC acoustic isolator	1690PA	5.0	134
HTHP XMAC acoustic TX	1690BA	7.92	162
HTHP XMAC TX power supply	1690FA	7.00	186
HTHP double knuckle	4421XA	4.58	104
UXPL acoustic imager electronics	1673EA	7.48	120
UXPL acoustic imager mandrel	1673MA	7.81	150
ATLAS Bullplug		0.34	41
		144.43	3256

The baseline logging run was done with the pipe-conveyed logging method to minimize the potential for stuck tools in the deviated section of the wellbore. With this method, the movement of wireline and drillpipe down the wellbore must be coordinated and in sync to ensure the tools are moving at the same rate as the drillpipe. It is also critical to keep tension on the wireline so that it does not tangle. A side entry sub, which is part of the tool string, allows the wireline to latch onto the drillpipe at a specified depth. Starting at 10:45 PM on June 23, the drillpipe and logging tool string was tripped into the hole, with the stabilizer and side entry sub added to the string at 4:45 AM on June 24. Concurrently, this is the time the latch point was reached at 4,837 ft MD. Tripping into hole continued until 10:00 AM on June 24, when the total depth planned for the logging run of 9,158 ft MD was reached. The descent into the well included recording of temperature continuously from the TTRM tool. The maximum temperature recorded during this descent was 282°F (Figure A-3).

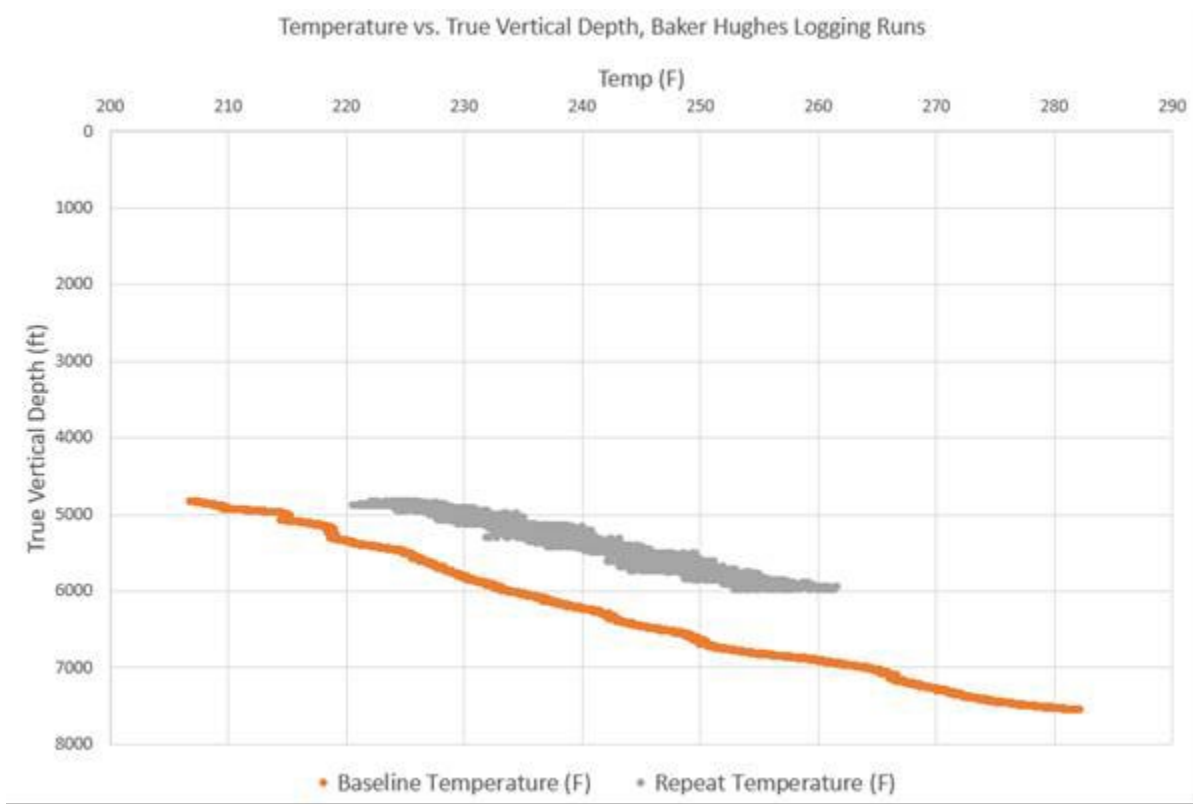
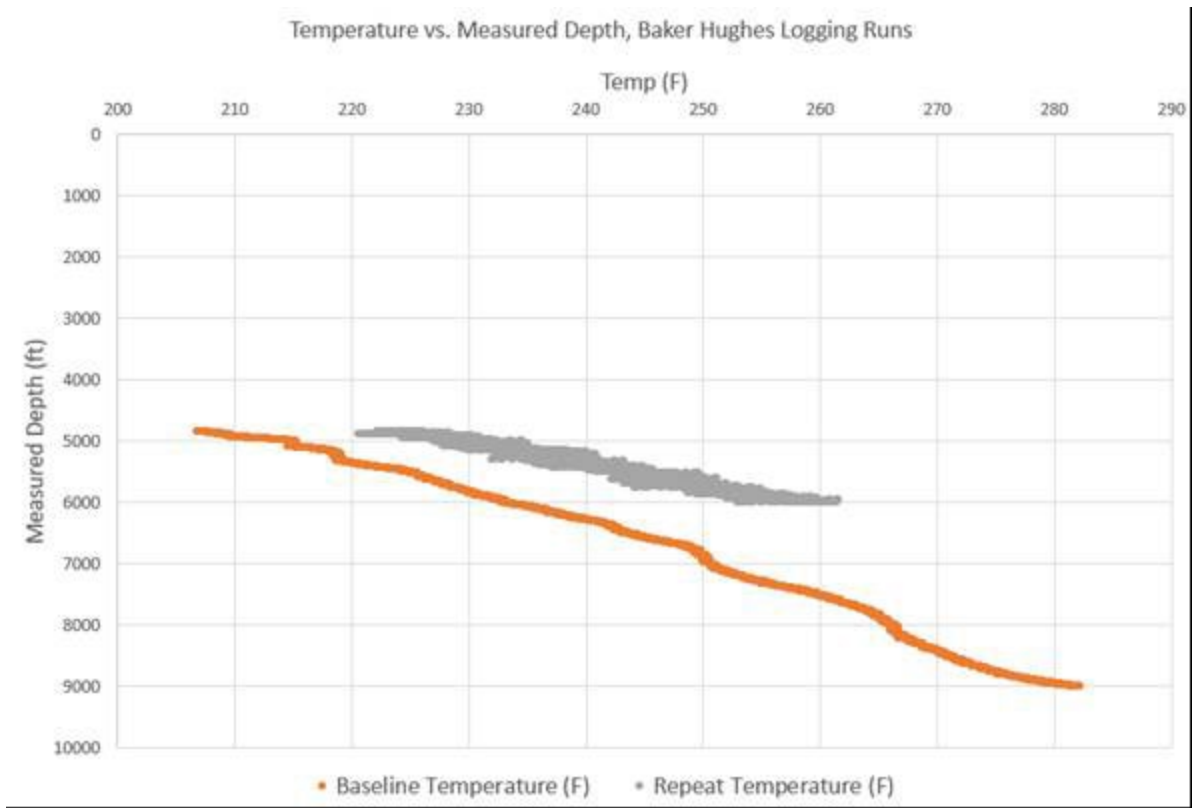


Figure A-3. Continuous temperature recorded descending into the well by the Baker Hughes TTRM tool (Measured Depth [top] and Total Vertical Depth [bottom]).

After reaching the target depth of 9,158 ft MD, tripping out the tool string began. The string stayed at the target depth for 10 minutes, and data collection began at this point. Initially, the logging tool string was pulled out of the well at approximately 6 feet per minute. At 6:30 PM on June 24, it was discovered that the logger's depth did not match the pipe tally. Additionally, there were telemetry issues and data were not being transmitted properly back to the Baker Hughes wireline truck.

Logging up continued to the side entry sub, when it was discovered at 1:30 AM on June 25 that the wireline was wrapped around the outside of the drillpipe. This can be attributed to the previously described mismatch in pipe tally and wireline depth. In other words, there was too much slack on the wireline which caused it to tangle around the drillpipe and drag it. Poor communication on the rigsite between the rig floor and wireline operators contributed to the Baker Hughes field engineers being seven stands off in their count of the drillpipe tally. Because of these errors, some data from the deeper sections of the baseline logging run were rendered unusable, as the data was off-depth (>~6,900 ft MD). Additionally, there are missing log sections from 5,763 and 5,873 feet on the resistivity-based image log tool, and 5,839 to 5,948 on the multi-pole acoustic tool (Figure A-4). Furthermore, the wireline had to be cut from the drillpipe and a new wireline truck had to be called to the site to continue operations (Figure A-5).

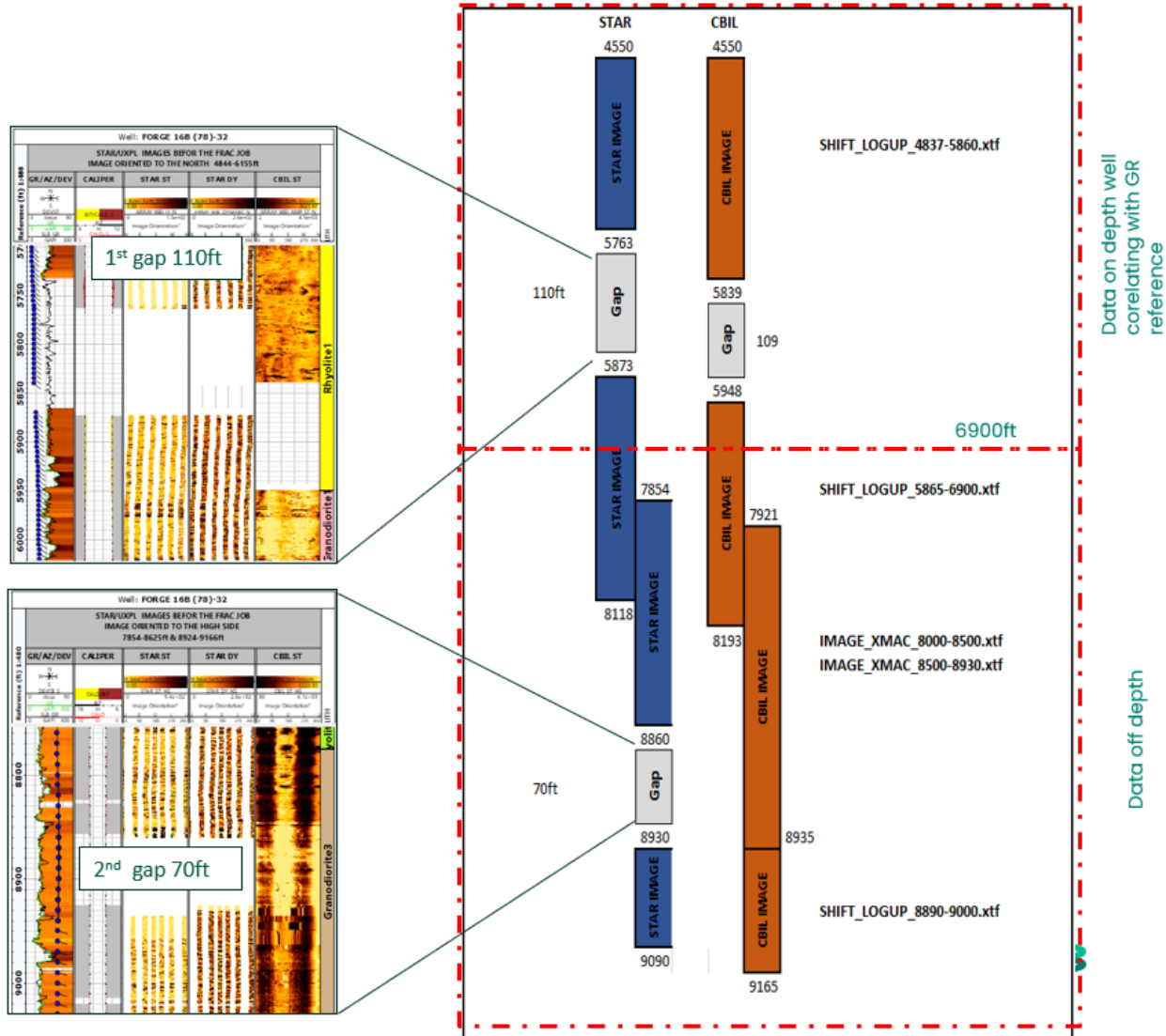
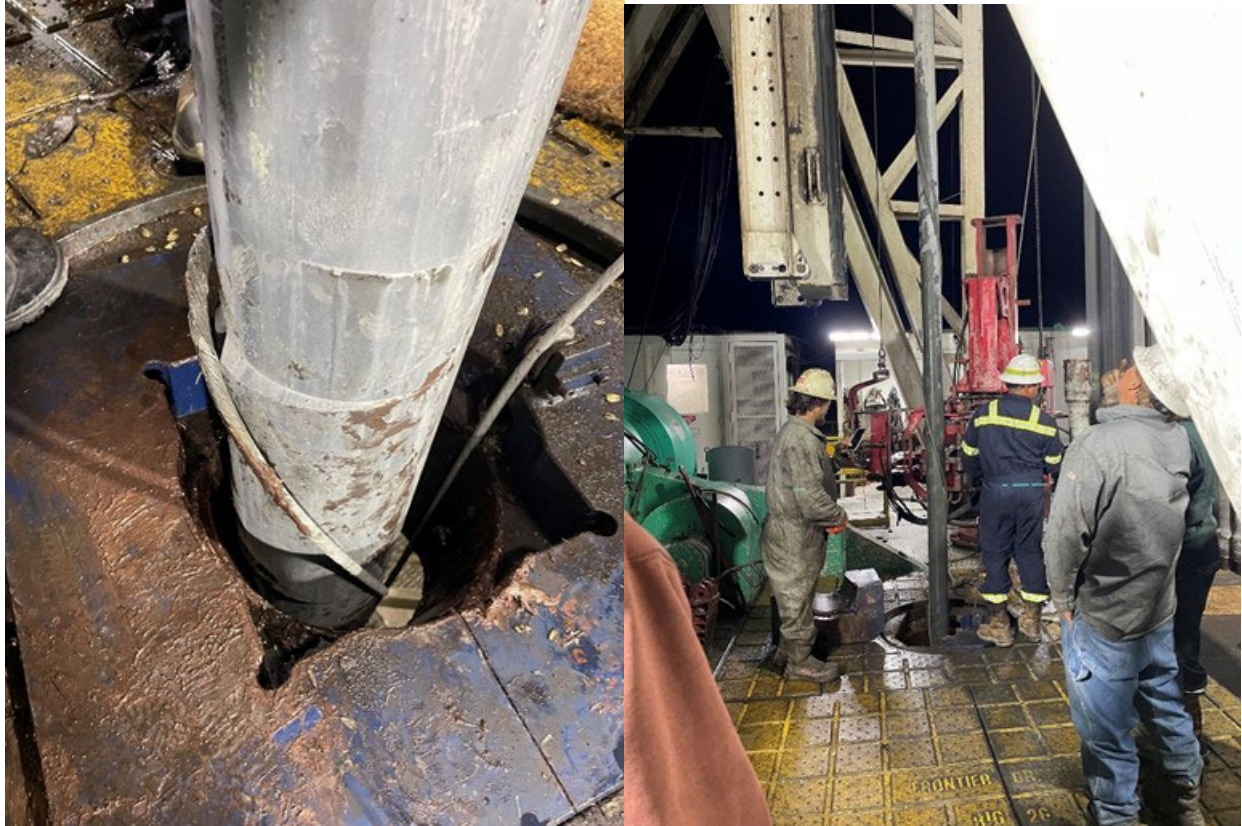


Figure A-4. Description of well sections that have missing data. Courtesy of Baker Hughes.



**Figure A-5. Slack wireline around drillpipe during baseline logging run operations.**

#### Circulation/cooling event #2

At 12:30 PM on June 25, 2023 the wireline was cut from the drillpipe and coordination for sending a new wireline truck began. While waiting for the new wireline truck to arrive on site, the decision was made to begin circulating fluid to cool the wellbore ahead of the first set of minifrac tests. The first set of minifrac tests (MF-1, MF-2, and MF-3) were to be conducted in the shallow vertical section of the wellbore (above kick-off point of is 5,638 ft ft); therefore, the rig crew tripped to a depth of 5,863 ft MD and began circulating at 6 PM. On June 26, an all hands meeting between Battelle, Baker Hughes, and rig personnel was held in the company trailer to discuss errors in communication and decide a new path to continue the project.

Circulation continued through June 27 until the new Baker Hughes wireline truck arrived at approximately 10 AM. This circulation period lasted for approximately 36 hours, allowing ample time for the wellbore to be cooled (Figure A-6). Average pump rate during this circulation period was 381 gallons per minute, with average temperature before chillers at 89.6°F and average temperature after chillers at 83.3°F. At noon on June 27, the drillpipe was out of the hole and the circulation period was over to prepare the Baker Hughes minifrac tools for testing at surface and downhole, confirming communication between the tools and packer integrity (seal test).

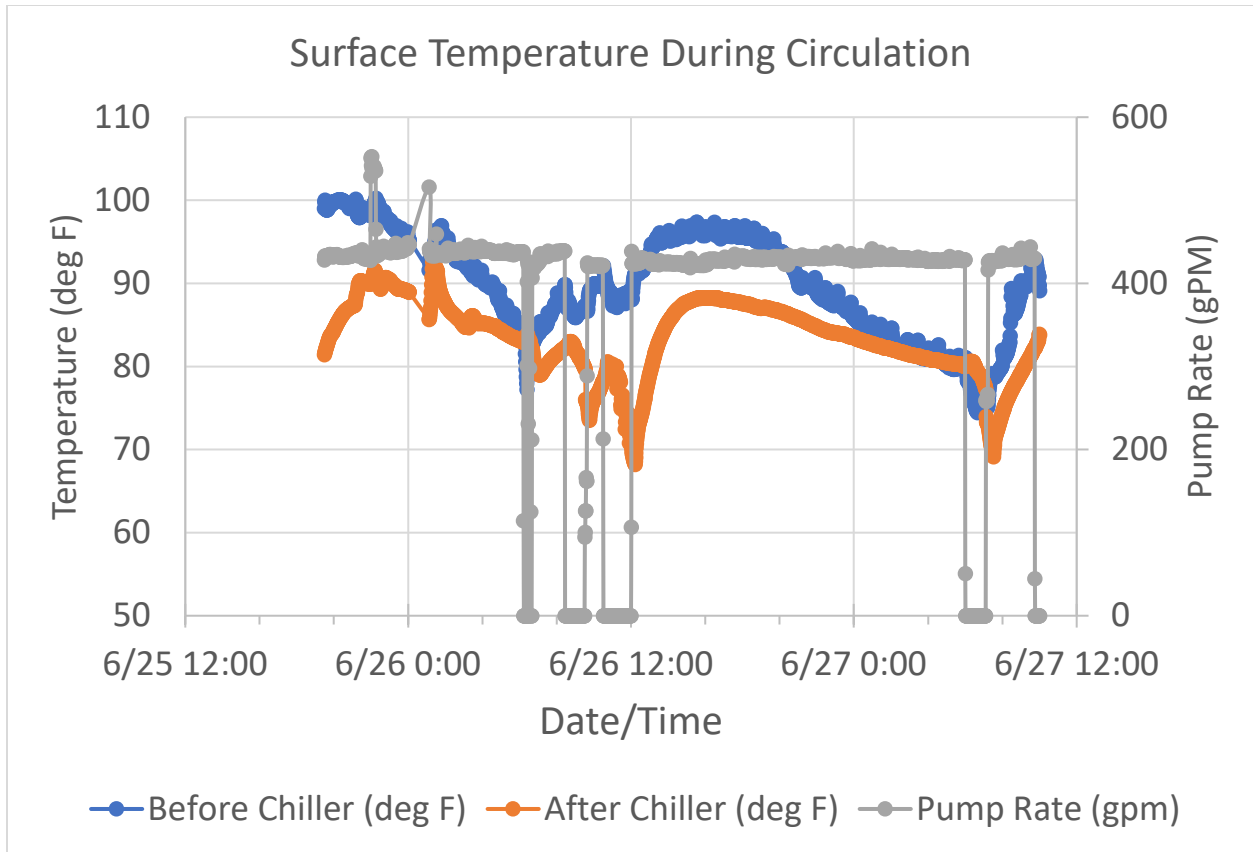


**Figure A-6. Surface temperature before and after wellbore fluid entered the chillers, and circulation pump rate in gallons per minute for the second circulation period. Data courtesy of Pason.**

Minifrac deployment #1 (5,800 ft) June 28

The RCX (straddle packer) tool and sleeve packer tool were run into hole at 10 PM on June 27 until reaching the first test depth of 5657.31 ft MD (MF-1). The sleeve packer was included on the string in case tested sections could not reach breakdown with the straddle packer. Due to the sleeve packer's higher max pressure that can be achieved, it was included on the string as a backup testing option. A schematic of the minifrac tool string can be seen in [Figure A-7](#).

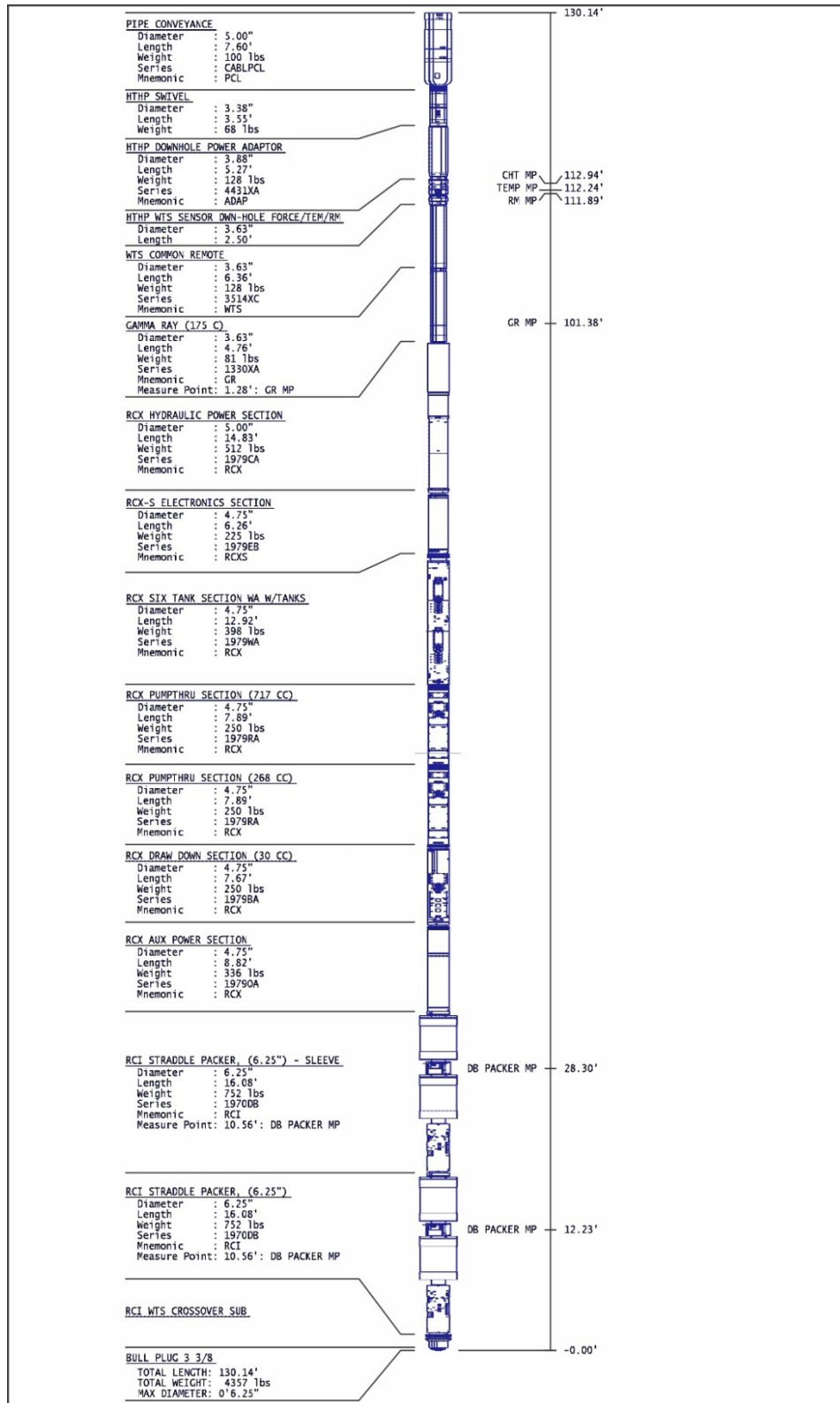


Figure A-7. Tool diagram of the Baker Hughes RCI/RCX Packer Tool String with Sleeve Packer.

**Table A-3. Description of RCI/RCX Tool Diagram**

Description	Series	Length (ft)	Weight (lbf)
PCL Simphor assembly w/ 4-1/2" I.F. box top connection	3983LF	7.60	100
HTHP Swivel	4422XA	3.55	68
HTHP Downhole Power Adapter	4431XA	5.27	128
WTS DWN-HOLE FORCE/TEMP/RM sensor	2890XB	2.67	80
HTHP WTS Telemetry	3590XA	9.17	270
RCX Hydraulic	1979CA	14.83	512
RCX Electronic	1979EA	6.26	225
RCX Tank Carrier	1979WA	12.92	398
RCX Large Pump 885cc	1979RA	7.89	250
RCX High Pressure pump 268cc	1979RA	7.89	250
RCX Power Supply	1979OA	8.82	336
RCX Drawdown pump 36cc	1979BA	7.67	250
RCX Straddle Packer	1970DC	16.08	752
RCX Sleeve Frac Packer	1970DC	16.08	752
RCX WTS XO	1972XA	1.33	45
HTHP Digital Spectralog	1390XA	9.50	282
WTS Bullplug		0.34	68
		<b>137.87</b>	<b>4766</b>

This first set of minifrac tests was conducted using the pipe conveyed logging method that was also used on the baseline logging run. At this depth, the straddle packers were set and there were two minifrac injection/flowback cycles as part of the test. MF-1 testing began at 4:30 AM and concluded at 7 AM on June 28. Pressure response at this interval did not behave like a typical minifrac test, with a “roll-over” effect in the pressure response curves, indicating that there were potentially existing fractures at this depth.

After completion of MF-1, the tool was pulled up to 5494.6 ft MD for the second test on this run (MF-2). MF-2 involved three cycles of injection/flowback from approximately 7 AM to noon on June 28. After completion of MF-2 the, tool was pulled up to 5201.6 ft MD for the final minifrac test on this descent into the well. MF-3 began at approximately 1:30 PM through 5:45 PM on June 28. There were four injection and flowback cycles as part of the test. At the conclusion of MF-3, the tools were pulled out of hole to begin the next circulation period ahead of the deep minifrac tests (8,000-9,000 ft MD). The first set of minifrac tests were operationally smooth, with no issues encountered.

Circulation/cooling event #3 (prior to PCL 8,500 ft minifrac deployment)

At 10 PM on June 28, the Baker Hughes tools were out of hole and tripping into the well to 9,100 ft MD for circulation continued until 3:45 AM on June 29. Circulation continued for the duration of June 29, with drillpipe out of hole at midnight on June 30. Average pump rate during this circulation period was 392.4 gallons per minute, with average temperature into the chillers at 99.3°F, and average temperature out of the chillers at 89.4°F.

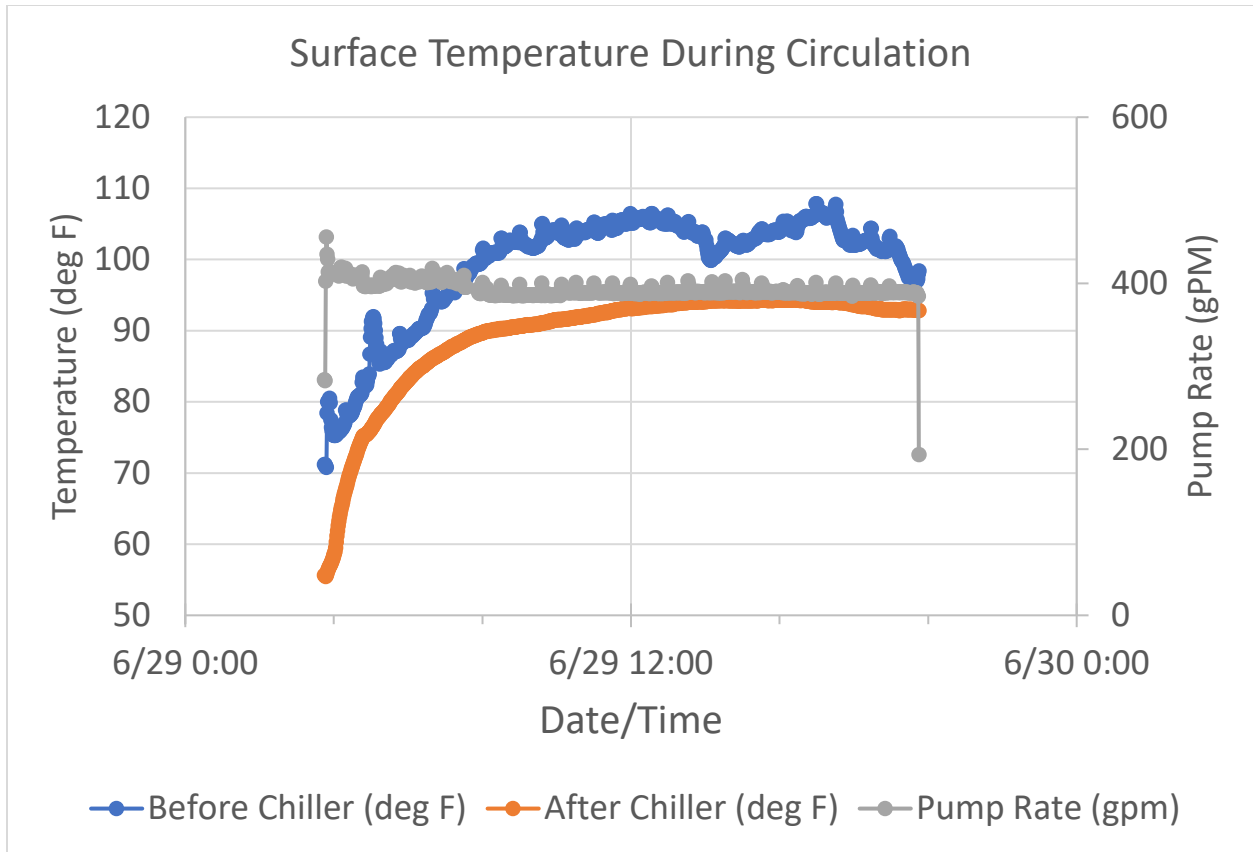


**Figure A-8. Surface temperature before and after wellbore fluid entered the chillers, and circulation pump rate in gallons per minute for the third circulation period. Data courtesy of Pason. 8,500 ft minifrac deployment with SP#1**

At this time, the Baker Hughes crew started to rig up the RCX tool string in preparation for the next minifrac tests in the deeper section of the wellbore. After rigging up the tools, drillpipe was tripped into hole to 5400 ft MD when the wireline truck lost power. The Baker Hughes team began troubleshooting the loss of power, and once resolved, continued tripping and running into hole to the first test depth of 8474 ft MD. At this depth, the truck again lost power and the tools were not in communication with the truck likely due to a short-circuiting issue. Therefore, the tools were slowly pulled up to several shallower depths and again tested to see if communication could be reestablished. When this failed, the decision was made to abandon testing in the deep deviated interval and pull the tools out of hole.

The RCX tools reached surface at midnight on July 1 and were rigged down. At this point, the sleeve packer tool was tested and was determined to be passing too much current, rendering it inoperable. As a piece of the tool string containing the straddle packer, the sleeve packer had to be removed to prevent further electrical issues and allow current to pass through the other tools. Rather than continuing with pipe-conveyed logging, the decision was made to run the RCX tool string on wireline in the vertical/slightly-deviated section of the wellbore due to the time limit to complete testing.

Minifrac deployment #3 (#2 in vertical section) July 1 – Wireline conveyed

The RCX tool was run into hole to 5980 ft MD starting at 5:30 AM on July 1 to begin testing minifrac station MF-4. Testing at MF-4 occurred from 8 AM on July 1 to 11 AM. There were three injection and flowback cycles at this station. After deflating the packers, the tool was moved to 5918 ft MD for MF-5

which occurred from 11 AM to 3 PM over four injection and flowback cycles. MF-6 (cycle 1 only) occurred from 3 PM to 6:30 PM at 5639 ft MD, with three total attempted injection and flowback cycles. The packer began to lose its seal during this test, particularly on cycle 2.

The tools were pulled out of hole and laid down on the rig floor at 8:30 PM on July 1. It was determined that the straddle packer was damaged and unable to be inflated, therefore the backup straddle packer on site was installed and deployed for further minifrac testing.

Minifrac deployment #4 (#3 in vertical section) July 2

At 4 AM on July 2, the new straddle packer tool was run in hole to continue the minifrac test at MF-6, depth 5639 ft MD. After this test was completed, the tool was moved to 5616 ft MD for MF-7, the final test of the program. There were continued difficulties building pressure in this test due to poor packer seal, and the three cycles in this test concluded at noon on July 2. An additional test was attempted at depth of 5469 ft MD, although the packers failed to inflate, and it was decided to pull out of hole and prepare for the repeat logging run. At surface, it was apparent that there were punctures in the packer tools that prevented them from inflating, likely due to rough borehole conditions (Figure A-9).



**Figure A-9. Punctures in the straddle packer tool prevented effective pressure buildup during later tests.**

### Repeat Wireline logging run to 6,120 ft MD

The repeat logging run of image and multi-pole sonic logs began at 6 PM on July 2. Since the tools were to be run on wireline and cover sections where minifrac tests had been conducted, the total logging depth was 6,130 ft MD. The logging run commenced at 7 PM on July 2 and continued until midnight. The logs cover the casing shoe (~4,800 ft MD) to 6,130 ft MD. At the conclusion of this run, the tools were laid down at the surface and Baker Hughes rigged down to complete the work at the site. [Figure A-10](#) provides an overview of temperature data from all Baker Hughes logging runs and stationary minifrac test intervals, in addition to SLB's previous logging runs into the FORGE 16B (78)-32 well.

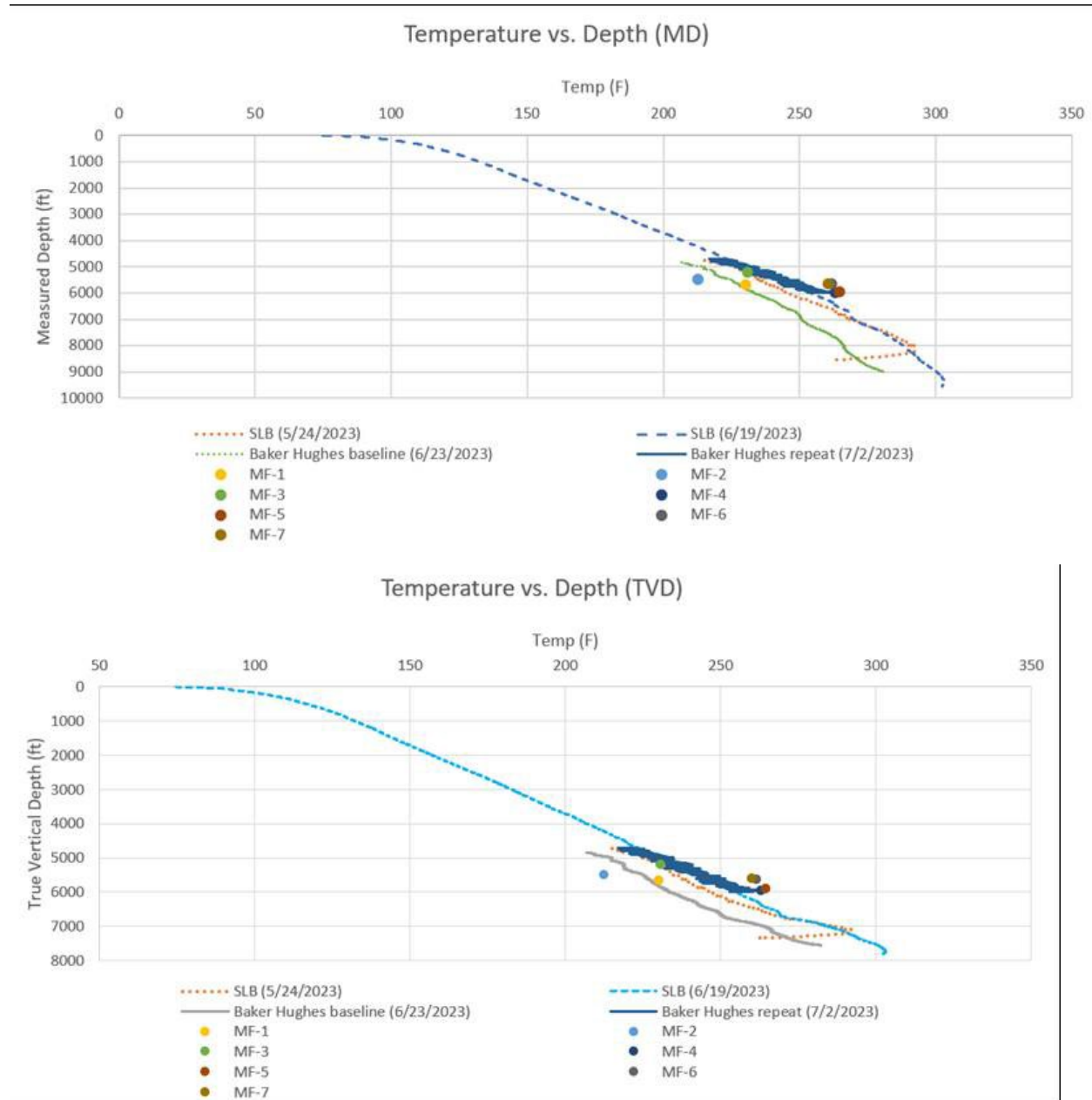


**Figure A-10. Summary of temperature data for the FORGE 16B (78)-32 well from SLB's logging runs, Baker Hughes logging runs, and stationary minifrac test intervals (Measured Depth [top] and Total Vertical Depth [bottom]).**